From the holdings of the Department of Special Collections , Princeton University Library, Princeton, NJ

These documents are either in the public domain, or can only be used for educational and research purposes (Fair use) as per U.S. Copyright law (text below). By accessing this file, all users agree that their use falls in the public domain or within fair use as defined by the copyrightlaw. We do not charge any permission or usage fees for the publication of images of material inour collections, including those provided by Princeton University Library, via our website, catalog, or directly from staff.For more information regarding copyright, credit, and citation please review the information onthe Copyright, Credit and Citation Guidelines page of our website.
https://library.princeton.edu/special-collections/policies/copyright-credit-and-citation-guidelines. If you have any questions, including how to order higher-quality images from the collection, contact Special Collections Public Services via our Ask Us! Form. https://library.princeton.edu/special-collections/ask-us

Doctoral Dissertations, 2011-2026 | Public and International Affairs

2023

EVALUATING LOW-CARBON TECHNOLOGY DEPLOYMENT POLICIES TO ACCELERATE THE DECARBONIZATION OF CHINA'S ENERGY SYSTEM

Peng, Liqun

Princeton, NJ : Princeton University

http://arks.princeton.edu/ark:/88435/dsp01xd07gw92c

U.S. Copyright law: The copyright law of the United States (Title 17, §108, United States Code) governs the making of photocopies or other reproductions of copyrighted material. Under certain conditions specified in the law, libraries and archives are authorized to furnish a photocopy or other reproduction. One of these specified conditions is that the photocopy or reproduction is not to be used for any purpose other than private study, scholarship, or research. If a user makes a request for, or later uses, a photocopy or reproduction for purposes in excess of fair use that user may be liable for copyright infringement. This institution reserves the right to refuse to accept a copying order if, in its judgment, fulfillment of the order would involve a violation of copyright law. https://www.copyright.gov/title17/title17.pdf

EVALUATING LOW-CARBON TECHNOLOGY DEPLOYMENT POLICIES TO ACCELERATE THE DECARBONIZATION OF CHINA'S ENERGY SYSTEM

Liqun Peng

A DISSERTATION

PRESENTED TO THE FACULTY

OF PRINCETON UNIVERSITY

IN CANDIDACY FOR THE DEGREE

OF DOCTOR OF PHILOSOPHY

RECOMMENDED FOR ACCEPTANCE BY

THE PRINCETON SCHOOL OF

PUBLIC AND INTERNATIONAL AFFAIRS

Adviser: Denise L. Mauzerall

January 2023

© Copyright by Liqun Peng, 2023.
All rights reserved.

Abstract

China's rapid economic growth has been fueled by the fossil-fuel dominated energy system. China is the world's top carbon emitter, and it also suffers from serious air pollution. A large-scale energy transition toward significantly less coal and other fossil fuel consumption is necessary for tackling both GHG mitigation and regional air pollution simultaneously in China. To achieve a large-scale and low-carbon energy transition in China, it is critical that the Chinese government strengthens its commitment to policies that increase the share of renewable and clean energy sources in its energy mix, as well as foster the development of a diversified portfolio of clean energy technologies. My dissertation focuses on a variety of low-carbon technology deployment polices in China and examines potential synergies and tradeoffs between air quality, carbon emission mitigation and economic costs in the decarbonization of China's energy system. It includes three analytical chapters.

Chapter 2 estimates the climate, air quality and health co-benefits of alternative energy vehicles (AEVs, e.g., electric vehicles and hydrogen fuel cell vehicles). I find that co-benefits increase dramatically as the electricity grid decarbonizes and hydrogen is produced from non-fossil fuels (i.e., green hydrogen). Relative to 2015, a conversion to AEVs using largely non-fossil power can reduce air pollution and associated premature mortalities and years of life lost by 329,000 persons/year and 1,611,000 life years/year. Thus, maximizing climate, air quality, and health benefits of AEV deployment in China requires rapid decarbonization of the power system.

Chapter 3 evaluates heterogeneous effects of battery storage deployment strategies on

decarbonization of provincial power systems in China. I find that battery deployment strategies will affect national electricity transmission and provincial coal-fired power generation and CO_2 emissions. We then allow each province to deploy any of the three battery strategies and find that intra- and inter-provincial heterogeneity in battery deployment results in lowest system costs. System costs are minimized when provinces with abundant (limited) renewable resources relative to their electricity demand directly couple batteries to renewable generation (deploy demand side batteries). Provinces with intermediate renewable generation minimize costs when batteries are directly connected to the grid.

Chapter 4 analyzes the tradeoffs between subsidies and life cycle GHG emissions in electrolytic hydrogen production. I find that financial subsidies are necessary to accelerate electrolytic hydrogen development. Electrolytic hydrogen will become cost-competitive with brown or grey hydrogen after 2040. However, subsidizing grid-based electrolytic hydrogen can't effectively reduce GHG emissions from 2025-2030 because of the low level of decarbonized power system. Higher subsidies in renewable-based hydrogen result in lower costs for CO_2 emission reductions. Transporting hydrogen with pipelines leads to a 12-20% drop in $LCOH_2$ within individual provinces and a 24-31% increase in life cycle GHG emissions due to higher emissions from low H_2 production cost provinces that use high coal grid electricity and H_2 leakage.

Acknowledgements

The journey to accomplish my dissertation has been long but meaningful. I am grateful to have the help and support from so many professors, colleagues, friends, and family, who guide me to be here.

First, I would like to express my deepest appreciation to my advisor, Prof. Denise Mauzerall. She has been an incredible advisor who guides me through my academic challenges and gives her insightful suggestions on both academic research and personal life. I am so grateful that she spent so much time working with me and help me improve my research questions and manuscripts. She is always responsive and supportive when I need her guidance and suggestions. I feel so lucky of being her student. Without her guidance and persistent help, this dissertation would not have been possible.

I would like to gratefully acknowledge the guidance, support, and encouragement of my Ph.D. committee members. I am especially indebted to Prof. Gang He for his continued collaboration and mentorship. Gang is extremely supportive and responsive. When I felt disappointed with my research results, he always told me not to give up. I am very grateful for his understanding and encouragement for every small step I make. I am thankful to Prof. Qiang Zhang who supervised my master's thesis and guided me to start my research journey when I was in Tsinghua University. His passion for research inspired me and motivated me to pursue a doctoral degree at Princeton. He continues to support my research at Princeton and provides his insights on my research questions. I'd like to thank Prof. Jesse Jenkins. I learned the power system modeling from Jesse and his classes. His class is one of the best classes I've taken at Princeton. Jesse has an open mind in many

aspects, and I learned tremendously from the enlightening conversations with him. Thank Prof. Valerie Karplus, I also learned a lot from her expertise on China's energy policies. Thank Prof. Jiang Lin for spending a lot of time to read my thesis and provided many insightful suggestions and questions.

This dissertation has also benefited from interactions with many professors and scholars from various fields and places. I would thank my general examiners: Prof. Steve Davis, Prof. Ines Azevedo and Dr. Eric Larson. I really appreciate for their valuable guidance and feedback on my research ideas at the early stage of my PhD. I also learned tremendously from the enlightening conversations with Prof. Machel Davison, Prof. Michael Oppenheimer, Prof. Jacques DE Chalendar, Dr. Chris Greig, and Dr. Micah S Ziegler.

I would like to thank my English tutor Lynne Fagles, who helps to practice my English when I came to Princeton. She is so kind and considerate. We have very close relationship. I treat her like my grandma.

I deeply appreciate the interactions with Dr. Mi Zhou, Dr. Juannan Yang, Dr. Yang Guo, Dr. Hongxun Liu, Dr. Mi Zhou, Dr. Feiqi Liu and Dr. Chuan Zhang, who provided me with valuable suggestions on my research projects and career development.

I was so honored to join Princeton Energy and Climate Scholars (PECS) group, I learned a lot from discussions with other group members.

I am deeply thankful to Princeton University, CPREE and PIIRS for the financial support.

I also thank the intellectual interactions and genuine support from our group

members and my friends in the Science, Technology and Environmental Policy (STEP) community: Prof. Wei Peng, Prof. Yue Qin, Dr. Juannan Yang, Dr. Yixin Guo, Dr, Xu Chen, Dr. Yiheng Tao, Dr. Zhongshu Li, Dr. Da Pan, Xiangwen Fu, Shangwei Liu, Malini Nambiar, Rohit Gupta, Dr. Jing Liang, Dr. Yuanyu Xie, Rachel Young, Pooja Ramamurthi, Yujie Wu, Glen Chua, Jieyi Lu, Ned Downie, Melissa Tier… Thank my cohort-mate Nic Choquette-Levy, who gave me many insightful suggestions on my papers and writings. I cheer for the five and half years' friendship with him.

I am grateful to many other Princeton staff who have also helped me tremendously throughout these years: Charles Crosby, Keely Swan, Ann Lengyel, Karen McGuiness, Jimmy Wang, and the computational science and engineering support team. I want to extend my special gratitude to Chuck Crosby for always preparing the most delicious food and making C-PREE my second home at Princeton.

I also appreciate the accompany and support from my friends at Princeton: Dr. Chris Crawford, Dr. Helene Benveniste, Ziyao Tian, Paul Nix, Zhuqi Li, Dr. Tingyin Xiao, Yinuo Zhang, Dr. Weitao Shuai, Fan Chen, Qingshi Wang, Dr. Liye Chen, Dr. Xinwei Yu, Jinyuan Qi, Jing Qian, Hanruo Zhang, Zheng Guan …. We share many special and meaningful memories together. I sincerely cherish our friendship and appreciate everything you have done for me.

Most importantly, I need to thank you my parents Shanxia Jin and Xiangbin Peng, who unconditionally support me the whole process. I absolutely would not have gotten to this stage without their love and encouragement. I haven't seen them in person for more than three years due to the pandemic. I miss them so much and so do they.

Finally, I wish to thank my loving husband, Desmond, who provides incredible support and inspiration. Thank you for always staying with me and helping me get back to the right way when I feel anxious about my research. But most of all, thank you for making me better in all aspects and sharing your life with me. I feel so powerful when I have your accompany and support.

This dissertation is dedicated to my parents and my husband.

Table of Contents

Chapter 1: Introduction _____ *1*

Chapter 2: Alternative-energy-vehicle deployment delivers climate, air quality and health co-benefits when coupled with decarbonizing power generation in China _____ *11*

1. Introduction _____ 11

2. Results _____ 15

2.1 Total air pollutant and CO_{2e} emission changes _____ 15

2.2 Spatial distribution of air pollutant and CO_{2e} emissions _____ 16

2.3 Air pollutant and CO_{2e} tailpipe emission reductions _____ 17

2.4 Air pollutant and CO2e power sector and upstream emission increases _____ 18

2.5 Impacts on surface air pollutant concentrations _____ 20

2.6 Human health and economic benefits _____ 22

3. Discussion _____ 24

4. Materials and Methods _____ 31

4.1 Scenario design _____ 31

4.2 Air pollutant and GHG emission estimation _____ 32

4.3 Air quality simulations _____ 35

4.4 Analysis of health impacts associated with air pollution _____ 37

4.5 Evaluation of economic benefits of improved health and GHG mitigation _____ 39

Chapter 3: Heterogeneous effects of battery storage deployment strategies on decarbonization of provincial power systems in China _____ *58*

1. Introduction _____ 58

2. Results _____ 62

2.1 National transmitted power and transmission costs _____ 62

2.2 Trade-offs between national carbon emissions and power system costs _____ 63

2.3 Effects of battery storage deployment strategies depend on provincial resources

64
2.4 Provincial heterogeneous battery storage deployment strategies 67
2.5 High carbon prices can drive decarbonization of China's power system 69
2.6 The effect of battery storage cost reduction trajectories on national installed battery storage capacity and CO_2 emissions 70
3. Discussion 71
4. Methods 75
4.1 SWITCH-China model 75
4.2 Objective function 76
4.3 Scenario design 78
Chapter 4: Subsidizing grid-based electrolytic hydrogen could increase GHG emissions 99
1. Introduction 99
2. Results 104
2.1 National analysis of levelized costs of hydrogen ($LCOH_2$) by generation technology 104
2.2 National analysis of life cycle GHG emissions 105
2.3 Trade-offs between subsidies and GHG emissions in provincial electrolytic hydrogen production 106
2.4 Potential hydrogen pipeline network and impacts on subsidies and life cycle GHG emissions of electrolytic hydrogen 108
2.5 Trade-offs between $LCOH_2$ and GHG emissions across four scenarios from 2025-2040 109
3. Discussion and policy implications 110
4. Methods 117
4.1 Scenario design 117
4.2 Levelized Cost of Hydrogen Production 118
4.3 Life cycle GHG emission estimation 120

4.4 SWITCH-China model _____ 122
4.5 Hydrogen pipeline network selection model _____ 123
Chapter 5: Conclusion _____ *140*
Appendix for Chapter 2 _____ *145*
Appendix for Chapter 3 _____ *191*
Appendix for Chapter 4 _____ *210*

Chapter 1: Introduction

China's rapid economic growth has been fueled by its fossil-fuel dominated energy system. In 2020, China accounted for 26% of global energy consumption and 31% of global carbon dioxide (CO_2) emissions (Statistical Review of World Energy, 2021), making it the largest energy consumer and CO_2 emitter in the world (IEA, 2021a and IEA, 2021b.). Coal still dominates China's energy consumption, although the share of coal consumption in primary energy had decreased from 70% to 57% from 2010 to 2020 (China national bureau of Statistics). The use of coal and other fossil fuels not only contributes to CO_2 emissions, but also worsens the ambient air quality. In 2017, about one million premature mortalities in China were attributed to ambient $PM_{2.5}$ and O_3 pollution (Yin et al., 2020).

Facing domestic and international pressure to reduce CO_2 emissions, China has announced an ambitious goal to peak CO_2 emissions by 2030 and achieve carbon neutrality by 2060. The pace of China's emission reduction over the coming decades will be important in determining whether the world would succeed in preventing global warming from exceeding 2 C. In addition to the climate goal, China is also ambitious to improve air quality and protect public health. Large-scale decarbonization in the energy sector is necessary to simultaneously tackle greenhouse gas (GHG) emissions and regional air pollution in China. To achieve a large-scale and low-carbon energy transition, it is critical that the Chinese government strengthen its commitment to policies that increase the share of renewable and clean energy sources in its energy mix, as well as foster the development of a diversified portfolio of clean energy technologies.

The Chinese government has designed and implemented various policies to support its clean energy transition, including financial subsidies for solar and wind energy, deployment of electric vehicles, promoting energy efficiency, and reducing coal use. In its 14th Five-Year Plan (2021-2025), the Chinese government set the goal to raise the non-fossil fuel share of total energy consumption to 20% by 2025 (from ~16% in 2020), and to achieve a 18% reduction in CO_2 intensity and a 13.5% reduction in energy intensity during 2021-2025.

China's carbon neutrality commitment and relevant renewable energy policies will speed up the decarbonization in the power sector, which accounts for 48% of total CO_2 emissions in China (IEA, 2021b). The direct use of low-emission electricity in place of fossil fuels is one of the most important drivers of emission reduction in the net zero emissions. Currently, China is the world's largest producer of wind and solar energy (Organization for Economic Cooperation and Development), and the largest domestic and outbound investor in renewable energy (Jaeger et al., 2017). In the past decade, solar and wind power generation have increased rapidly in China, largely due to the cost reduction of solar and wind power. Solar and wind power generation increased from 2TWh to 306TWh and from 72TWh to 566.7TWh from 2011-2021, respectively (CREO, 2019; IEA, 2022). The Chinese government also stresses efforts to advance the large-scale and high-quality development of wind and solar power generation. Future policy initiatives focus on tax breaks and low-interest loans to low-carbon project developers, power market reforms, and grid improvement.

Electrification is also key to decarbonize the transport and residential sectors. China

has the largest electric vehicle stock (4.8 million) in the world, accounting for 40% of the global total electric vehicle stock (Global EV outlook 2021). China has set a goal to have new energy vehicles (include electric vehicle and hybrid vehicles) to take 40 percent of all car sales by 2030 and 95% of all car sales by 2035 (China-SAE, 2020). Also, the government aims to promote the replacement of public service vehicles with electric vehicles and the use of heavy cargo trucks fueled by electricity, hydrogen fuel, and liquefied natural gas (NDRC, 2021). In the meantime, efficiency improvements and electrification would drive the most of emission reductions in the industrial sector in the short term. (IEA, An energy sector roadmap to carbon neutrality in China. 2021). However, electrification alone cannot fulfill the goal.

To fully decarbonize energy sectors, emerging innovative technologies, such as clean hydrogen, are necessary. Clean hydrogen could provide long-term energy storage and offer ways to support clean energy transition in a range of sectors and industries that are difficult or expensive to be electrified, such as long-haul transport. Hydrogen can transport energy from renewables over long distances – from regions with abundant solar and wind resources, to regions with high demand and limited renewable resources thousands of kilometers away. Ambitious, targeted, and near-term action is needed to further overcome barriers and reduce costs of clean energy hydrogen production.

Although studies have demonstrated China's success in deploying various policies to develop clean energy technologies and to facilitate the decarbonization of energy system (Zheng et al., 2017; Zhang 2019, Guo et al., 2020; Shi et al., 2022, Tang et al., 2022), few studies tried to quantify the economic costs and evaluate the effects of those policies on

air quality improvement and GHG emissions mitigation. For example, to decarbonize the power sector, one big challenge is that China must ensure electricity security and meet growing electricity demand while simultaneously cutting emissions. The significant increase in renewables and electrification of end-users plays a central role in clean energy transitions. However, due to the intermittency of solar and wind power, a secure and decarbonized power sector requires other flexible resources on a much larger scale than what currently exists today. These include low-carbon dispatchable power plants, energy storage, demand response, and transmission expansion. The availability and cost of these technologies depend on local conditions, social acceptance, and policies (IEA, 2021c). Other challenges include 1) the development of low-carbon hydrogen, which can be applied for both power sector and other hard-to-abate sectors such as long-haul transport and industry; 2) a major expansion of the energy supply infrastructure, such as ultra-high voltage long-distance transmission lines, charging station, hydrogen storage and pipelines, which are necessary for displacing amounts of fossil fuels with clean energy such as electricity and hydrogen. This implies not just massive investments but also concerted and coordinated efforts across many stakeholders, including duly addressing leakage and safety risks related to the handling of hydrogen.

This dissertation aims to advance the understanding of the synergies and tradeoffs between air quality, decarbonization goals and economic costs in China's low-carbon technology deployment strategies, focusing on alternative-energy-vehicles, battery storage deployment, and electrolytic hydrogen production. I applied a variety of analytical tools, including air quality modeling, capacity expansion power system

modeling, health impact assessment and optimization, to address the three knowledge gaps identified above. Chapter 2 estimates the climate, air quality and health co-benefits of alternative energy vehicles (i.e. electric vehicles and hydrogen fuel cell vehicles), Chapter 3 evaluates various battery storage deployment strategies to maximize decarbonization of China's power system, and Chapter 4 analyzes various incentive policies to accelerate a transition to green hydrogen production.

Chapter 2 analyzes the air quality, health, carbon emission, and economic benefits of replacing internal combustion engine vehicles with various alternative energy vehicles (AEVs). Alternative energy vehicles (AEVs) including electric, hydrogen fuel cell, and natural gas vehicles, can reduce carbon emissions and improve air quality. However, climate, air quality, and health benefits of AEVs powered with deeply decarbonized power generation are poorly quantified. In this chapter, I estimate the air pollutant and greenhouse gas (GHG) emission changes in 2050 of various penetration rates of alternative energy vehicles combined with various carbon intensities of the electric power grid. I use an atmospheric chemistry model to simulate the air quality impacts of AEV deployment in China and estimate the avoided premature deaths attributed to reduced ambient $PM_{2.5}$ and ozone exposure, I then evaluate the economic benefits of avoided premature deaths and reduced GHG emissions. I find the co-benefits increase dramatically as the electricity grid decarbonizes and hydrogen is produced from non-fossil fuels (i.e. green hydrogen). A conversion to AEVs using largely non-fossil power (91%) can reduce 5.7ug/m3 $PM_{2.5}$ and 4.9 ppb maximum daily 8 h average (MDA8) O_3 concentration compared with the 2015 base case. This will also reduce associated

premature mortalities and years of life lost by 329,000 persons/year and 1,611,000 life years/year. Thus, maximizing climate, air quality, and health benefits of AEV deployment in China requires rapid decarbonization of the power system.

Chapter 3 examines the effects of various nationally uniform and heterogenous battery deployment strategies with varying battery costs and carbon prices on provincial carbon emissions and power system costs in China between 2025 and 2050. I improve a high-resolution power system model, SWITCH-China, to study the effects of battery storage deployment strategies on provincial carbon emissions and power system costs in China. I find that nationally uniform battery deployment, where batteries are charged only with co-located renewable energy, will effectively smooth peak electricity transmission and decrease (increase) coal power generation in provinces with abundant (limited) renewable resources compared with batteries directly connected to the grid. In contrast, demand side batteries that discharge only to local distribution grids will increase power transmission and increase coal power generation in provinces with abundant renewable resources. I further find that intra- and inter-provincial heterogeneity in battery deployment results in the lowest system costs. System costs are minimized when provinces with abundant (limited) renewable resources relative to their electricity demand directly couple batteries to renewable generation (deploy demand side batteries). Battery storage will play an important role in low-carbon power systems, but how to match battery storage deployment with renewable resources, the availability of transmission, and the characteristics of demand while minimizing costs are key to maximizing its potential to decarbonize power systems.

Chapter 4 evaluates the best option to accelerate the development of cost-competitive electrolytic hydrogen which minimizes GHG emissions per kg H_2 in China. I first estimate the $LCOH_2$ and life cycle GHG emissions from all hydrogen production technology from 2025-2050. I then quantify the difference of levelized costs and GHG emissions between coal-based hydrogen and electrolytic hydrogen using both grid electricity and renewably generated electricity for each year. Further, I evaluate the trade-offs between subsidies and life cycle GHG emissions in accelerating the development of cost-competitive electrolytic hydrogen. In addition, I test the impacts of hydrogen pipelines on $LCOH_2$ and life cycle GHG emissions. I find that financial subsidies are necessary and critical to accelerate electrolytic hydrogen development. Electrolytic hydrogen will become cost-competitive with fossil-based hydrogen after 2040. However, subsidizing grid-based electrolytic hydrogen could increase life cycle GHG emissions from 2025-2030 because electricity from power grid remains heavily dependent on coal power. Larger subsidies for renewable- rather than grid-based electrolytic hydrogen result in lower costs for CO_2 emission reductions. Moreover, although transporting hydrogen with pipelines leads to a national 12-21% drop in $LCOH_2$, it increases national life cycle GHG emissions by 20-38% due to higher emissions from low hydrogen production cost provinces that use high coal grid electricity and increased hydrogen leakage.

Chapter 5 is the concluding chapter. I first summarize the findings in Chapter 2-4 about the effects of low-carbon technology deployment polices on air quality, carbon emissions and economic costs in China. I then propose some suggestions on future research for

policy makers to evaluate the benefits and trade-offs of low carbon technology deployment to facilitate energy transition and achieve carbon neutrality by 2060.

Reference

Statistical Review of World Energy 2021. https://www.bp.com/content/dam/bp/business-sites/en/global/corporate/pdfs/energy-economics/statistical-review/bp-stats-review-2021-full-report.pdf

NDRC. National Development and Reform Commission. 2021. Action plan for carbon dioxide peaking before 2030. https://en.ndrc.gov.cn/policies/202110/t20211027_1301020.html

Organization for Economic Cooperation and Development, "Energy—Renewable energy," https://data.oecd.org/energy/renewable-energy.htm.

Joel Jaeger, Paul Joffe, and Ranping Song, "China Is Leaving the U.S. Behind on Clean Energy Investment," World Resources Institute, January 6, 2017, http://www.wri.org/blog/2017/01/china-leaving-us-behind-clean-energy-investment.

China-SAE, China Society of Automotive Engineers. 2020. Technology Roadmap 2.0 for Energy-Saving and New Energy Vehicles.

Guo, Y. et al. Air quality, nitrogen use efficiency and food security in China are improved by cost-effective agricultural nitrogen management. Nat Food 1, 648–658 (2020).

IEA. 2021a. Global Energy Review: CO2 Emissions in 2020. https://www.iea.org/articles/global-energy-review-co2-emissions-in-2020

IEA, 2021b. An Energy Sector Roadmap to Carbon Neutrality in China. https://iea.blob.core.windows.net/assets/6689062e-43fc-40c8-9659-

01cf96150318/AnenergysectorroadmaptocarbonneutralityinChina.pdf

IEA, 2021c. The Role of Low-Carbon Fuels in the Clean Energy Transitions of the Power Sector. https://iea.blob.core.windows.net/assets/01ca16c8-e493-475c-81c4-04ac5d3b9882/Theroleoflow-carbonfuelsinthecleanenergytransitionsofthepowersector.pdf

NEA. National Energy Administration. 2022. Construction and operation of photovoltaic power generation in 2021. http://www.nea.gov.cn/2022-03/09/c_1310508114.htm

Shi, Q. et al. Co-benefits of CO2 emission reduction from China's clean air actions between 2013-2020. Nat Commun 13, 5061 (2022).

Tang, R. et al. Air quality and health co-benefits of China's carbon dioxide emissions peaking before 2030. Nat Commun 13, 1008 (2022).

Yin, P. et al. The effect of air pollution on deaths, disease burden, and life expectancy across China and its provinces, 1990–2017: an analysis for the Global Burden of Disease Study 2017. The Lancet Planetary Health 4, e386–e398 (2020).

Zheng, Y. et al. Air quality improvements and health benefits from China's clean air action since 2013. Environ. Res. Lett. 12, 114020 (2017).

Zhang, Q. et al. Drivers of improved PM2.5 air quality in China from 2013 to 2017. Proceedings of the National Academy of Sciences 116, 24463–24469 (2019).

Chapter 2: Alternative-energy-vehicle deployment delivers climate, air quality and health co-benefits when coupled with decarbonizing power generation in China

1. Introduction

To meet the goal of the Paris Agreement, to limit global warming to 1.5°C above pre-industrial temperatures, global CO_2 emissions must approach net zero around 2050 (IPCC, 2018). As the world's top carbon emitter, China has faced both domestic and international pressure to reduce CO_2 emissions. China now aims to peak CO_2 emissions by 2030 and achieve carbon neutrality by 2060. Rapid industrialization has resulted in extreme levels of air pollution and China has declared a 'war on air pollution' to improve air quality and protect public health. About one million premature mortalities in China were attributed to ambient $PM_{2.5}$ and O_3 pollution in 2017[1]. The decarbonization of the on-road transport sector offers opportunities to simultaneously reduce emissions of air pollutants and greenhouse gases (GHG) and obtain climate, air quality and human health benefits.

China's rapid economic growth has led to a dramatic increase in vehicle numbers which are a growing source of air pollutant and CO_2 emissions. Vehicle ownership in China grew from ~172 million vehicles in 2015 to 260 million vehicles in 2020[2]. According to the Multi-resolution Emissions In China (MEIC)[3] inventory, in 2015 on-road vehicle-emissions accounted for 23%, 27%, 18%, and 9% of national NO_x, VOC, CO and CO_2 emissions, respectively. Although heavy duty trucks (HDTs) only accounted for 2.4% of total vehicle numbers (Table S2.6), they contributed approximately half of on-road NO_x

and $PM_{2.5}$ emissions and one-third of on-road CO_2 emissions in 2015. Conversely, although the stock of on-road light-duty passenger vehicles (LDPVs, e.g. private cars, taxies) accounted for more than 50% of total vehicle numbers, their share of vehicle NO_x and $PM_{2.5}$ emissions are only 4% and 6% while their emissions of CO_2 are ~30% of total vehicle fleet emissions.[3]

Starting in 2012, China made an ambitious commitment to develop five million new energy vehicles by 2020, including plug-in hybrid electric vehicles (PHEVs), battery electric vehicles (BEVs) and hydrogen fuel cell electric vehicles (HFCVs)[4]. In addition, between 2011 and 2019, the development of both compressed natural gas/liquid natural gas (CNG/LNG) vehicles and CNG/LNG fueling stations increased rapidly. Four factors motivate China's policy promotion of clean energy vehicles: (1) Mitigation of air pollutant emissions from the transport sector and associated health benefits; (2) Decarbonization of the vehicle sector to facilitate achievement of peak CO_2 emissions before 2030 and carbon neutrality before 2060; (3) Improved alternative energy vehicles will provide a competitive advantage to Chinese vehicle manufacturers and allow them to increase market share in the global transportation market; (4) Increased penetration of AEVs will increase domestic energy security by reducing national dependence on oil imports.

Many findings[5,6,7,8,9,10,11,12] demonstrate that replacing internal combustion engine vehicles (ICEVs) with EVs can effectively improve air quality and public health, while mitigating GHG emissions. However, the magnitude of these benefits depends on the level of electricity decarbonization and the efficiency of the chosen vehicles. Additional

studies[13,14,15] estimate the life-cycle emissions from HFCVs. Schnell et al (2021)[16] illustrate that the potential of electric vehicles (EVs) to ameliorate extreme air pollution events in winter is limited and that the air quality and climate co-benefits of EVs depend on the emissions from power generation. Most previous studies focus on target years 2025 or 2030, which does not allow time to deeply decarbonize the power sector and hydrogen supply. They also focus only on either EVs or HFCVs. China's EV market is growing fast with 1.1 million EVs sales in 2019[17]. While EVs certainly have the edge in today's passenger vehicle market due to their lower price and increasingly available charging infrastructure, HFCVs likely have their place in the future of mobility particularly in medium and heavy-duty trucks. HFCVs are good options for long distance travel of heavy-duty vehicles because of their good energy efficiency, fast refueling, and their relatively high-density energy source compared to current batteries. Thus, we consider both EVs and HFCVs when examining AEV replacement of ICEVs to achieve climate, air quality and health benefits.

Our study goes beyond previous work by including all types of AEVs (EVs, electric motorcycles (EMCs), HFCVs and CNG/LNG vehicles powered with a variety of electricity sources. (See Note S1. Alternative energy vehicles and Table S2.5). We provide the first comprehensive examination of how to maximize potential co-benefits for climate, air quality and health of increased penetration of all types of AEVs and the importance of decarbonizing the power system to maximize these co-benefits. We begin with scenario development of various AEV penetrations and power sector energy mixes in China. (See Experimental Procedure, Scenario design). Scenarios are described in Table 2.1 with

analysis focused on those in bold. We estimate the reduced air pollutant and equivalent CO_2 (CO_{2e}) emissions from replacing ICEVs with AEVs as well as the increased emissions from electricity generation and upstream emissions. (See Experimental Procedure, Air pollutant and GHG emission estimation). We then employ an atmospheric chemistry transport model (WRF-Chem v3.6.1) to simulate improvements in annual average air quality and summer O_3 concentrations over China from deployment of these AEVs using a variety of energy sources. (See Experimental Procedure, Air quality simulations). Finally, we estimate the co-benefits of AEV utilization for air quality, health and climate and calculate the economic benefits of AEV penetration with various levels of electricity decarbonization in China. (See Experimental Procedure). We find that climate, air quality and human health co-benefits increase with increasing AEV penetration in the on-road transport sector with benefits increasing as electricity is increasingly decarbonized (at least 55% decarbonization is necessary to reduce emissions). In the most aggressive scenario (MP-HR), in which we assume all vehicles are replaced by AEVs using a 91% non-fossil fuel penetration, annual population-weighted $PM_{2.5}$ and summer maximum daily 8 h average (MDA8) O_3 concentrations decrease by 5.7ug/m^3 and 4.9ppb, representing 9.1% and 7.8% reductions compared to the 2015 base case, respectively. Calculated avoided premature mortalities due to reduced exposure to ambient $PM_{2.5}$ and O_3 in the MP-HR scenario are 329,000 (95% CI: 254,200-383,100). Our results illustrate the importance of simultaneously decarbonizing the power system while transforming the transport sector from ICEVs to AEVs.

2. Results

2.1 Total air pollutant and CO_{2e} emission changes

Total air pollutant and CO_{2e} emissions will change as the penetration rate of alternative energy vehicles and the level of grid decarbonization changes. Figure 2.1 shows the net change in total and percent of air pollutant emissions of NO_x, VOC, $PM_{2.5}$, SO_2 and CO_{2e} from vehicle tailpipes and energy sources for each scenario relative to the 2015 Base case. Air pollutant (e.g. SO_2 and $PM_{2.5}$) and CO_{2e} emissions will increase if we increase the penetration of AEVs more rapidly than the electricity grid decarbonizes. We find the deployment of AEVs will result in reductions of all air pollutants and CO_{2e} emissions when the penetration of renewable power is above 40% (low renewable penetration scenario). Figure 2.2 separates the changes in emissions from vehicle tailpipes, the additional power generation required by the added AEVs, and upstream emissions from hydrogen and natural gas for each scenario. Emissions of all air pollutants and CO_{2e} decrease when AEV penetration and decarbonized power increase simultaneously. For all scenarios, the deployment of AEVs results in net reductions of NO_x and VOCs. However, in the 2015 power mix scenarios, which rely heavily on coal power, electrifying passenger vehicles and trucks increases total SO_2, $PM_{2.5}$ and carbon dioxide equivalent (CO_{2e}, GWP100) emissions (Figure 2.1 and Table S2.7). When maximum penetration of AEVs is paired with high renewable electricity penetration (MP-HR scenario) the largest emission reductions are obtained. In the MP-HR scenario, emissions from vehicle tailpipes and power sector together are reduced by ~41% of NO_x, 84% of VOC, 15% of $PM_{2.5}$, 5% of SO_2 and 17% of CO_{2e} of emissions in the 2015 base case. The provincial

distribution of emission changes for each scenario is shown in Figure S2.1.

2.2 Spatial distribution of air pollutant and CO_{2e} emissions

AEVs deployed in regions with clean electricity bring high emission reductions while AEVs deployed in regions with dirty coal power result in increased emissions of air pollutants and CO_{2e}. In 2015, more than 85% of electricity in the north and northeast power girds came from coal-fired power plants[18]. Power grid details are shown in Figure S2.4. In 2015 the proportion of coal-fired electricity was between 60%-70% in the northwest, east, and central grids[18]. The south grid was the nation's cleanest regional grid and was the only one using less than 50% coal-fired electricity. Hydroelectricity is the largest source of power in the south grid.

Figure 2.3(A) shows the change of air pollutant and CO_{2e} emissions when ICEVs are replaced with AEVs under the HP-2015 scenario compared to the 2015 base case. Although tailpipe emissions decrease, AEV deployment increases total SO_2 emissions for all provinces due to increased SO_2 emissions from the power sector that result. In addition, increases in $PM_{2.5}$ as well as CO_{2e} emissions occur in most provinces due to increased emissions from the 2015 power grid. However, high penetration of AEVs with the 2015 power mix still reduces NO_x and VOC emissions for all provinces, because the NO_x and VOC emissions from electricity needed for the AEVs is much less than their emissions from vehicles. Figure 2.3(B) shows the net change of air pollutant and CO_{2e} emissions when ICEVs are replaced with AEVs under the HP-HR scenario compared to the base case. In this scenario, AEV deployment significantly decreases emissions of NO_x, VOC, $PM_{2.5}$ and CO_{2e}, especially for the provinces with large vehicle populations and

dirty electricity supply, such as Shandong, Jiangsu and Guangdong, as decarbonized power replaces an additional 27% of coal power generation. Figure 2.3 (C) shows the emission reductions attributable to decreases from the power sector when the 2015 power mix is replaced with 91% decarbonized electricity and hydrogen to AEVs. The differences of $PM_{2.5}$, SO_2 and CO_{2e} emissions between the 2015 power mix and 91% non-fossil grid are substantial, due to the high emission factors of $PM_{2.5}$, SO_2 and CO_{2e} for 2015 coal-fired power plants. Thus, a decarbonized power supply results in enormous air quality and CO_{2e} mitigation benefits from vehicles when AEVs are widely deployed.

2.3 Air pollutant and CO_{2e} tailpipe emission reductions

Tailpipe emissions dominate the emission reductions resulting from a replacement of ICEVs with AEVs. We analyze the change in tailpipe emissions that result across our four AEV scenarios. National tailpipe air pollutant emission reductions range from 10% to 100% for NO_x, 12% to 100% for $PM_{2.5}$, 14% to 100% for VOC and 12% to 100% for CO_{2e} across our scenarios (see Figure S2.5).

Replacing all ICEVs with AEVs (MP scenario) results in the largest reductions in primary $PM_{2.5}$, NO_x, VOC and CO_2 tailpipe emissions. Emission reductions in the MP scenario (100%) are much higher than in the HP scenario (~50-60%), because complete replacement of light-, medium- and heavy-duty trucks with electric trucks and HFCVs occurs in the MP scenario. Replacement of trucks contribute more to air pollutant and CO_2 emission mitigation than replacing the LDPVs with AEVs, especially for NO_x and $PM_{2.5}$ emission reductions. This is because most trucks use diesel engines and both NO_x and $PM_{2.5}$ emission standards are weaker for diesel engines than gasoline engines[19].

Total tailpipe emission reductions for each AEV technology type vary due to the extent of their uptake. Figure 2.4 shows the contribution of various AEV types to total on-road vehicle emission mitigation. Among AEVs, EVs and EMCs reduce emissions of all pollutants the most because EVs become the dominant type of AEV. For example, in Figure 2.4(D), the MP scenario, 100% of private passenger vehicles, 100% of commercial passenger vehicles (e.g. buses and taxies), 100% of motorcycles and 50% of trucks are electrified while 50% of trucks are replaced with HFCVs. NO_x emission reductions from HFCVs are nearly as large as EVs+EMCs in the MP scenario, due to the large contribution of ICE trucks to NO_x emissions in the on-road transport sector.

2.4 Air pollutant and CO2e power sector and upstream emission increases

The adoption of EVs and EMCs increase electricity demand and, in turn, increase electricity production and resulting air pollutant and CO_{2e} emissions. Depending on the decarbonization level of the power grid this increased electricity demand offsets some of the benefits of tailpipe reductions from EVs. We estimate the increased electricity consumption from electric vehicles in the transport sector based on the vehicle kilometers travelled (VKT) and electricity consumption per unit distance travelled (Figure S2.6). The increased electricity consumption is small compared to total electricity generation in China. For example, in the MP scenario, the increased electricity consumption is only 7% of total electricity generation in 2015 (NESY, 2016). In our four primary scenarios, private passenger vehicles dominate increases in electricity consumption because the electrification ratio of private passenger vehicles is higher than trucks and the stock of private passenger vehicles is much larger than commercial passenger vehicles. We

compare the increased emissions from the electricity needed to charge electric vehicles in various scenarios in Figure S2.7. We find that emissions increase when the 2015 power mix is used and increasingly decrease when 45% non-fossil and 91% non-fossil fuel power is used. (See Figure 2.4). In this analysis we neglect emissions associated with coal mining and hence may slightly underestimate emission reductions resulting from non-fossil electricity generation.

Since CO_{2e} emissions of hydrogen production from methane reforming is ~ ten times higher than form electrolysis of water powered by renewable electricity[20]. We set up a sensitivity analysis which assumes 10%, 50%, 70% and 90% of hydrogen production from renewable energy in LP, IP, HP, and MP scenarios, respectively. Detailed descriptions of hydrogen source scenarios can be found in Table S2.5.

The adoption of natural gas vehicles (NGVs) and HFCVs increase the consumption of natural gas and hydrogen and further increase upstream emissions from the production and leakage of hydrogen and natural gas, which includes pre-production & gathering, processing, transmission & storage and distribution (Figure S2.8). However, the increased upstream emissions have only tiny impacts on emissions compared with the other changes in the transport system, accounting for less than 0.03%-3% increase of the 2015 vehicle emissions by switching to NGVs and HFCVs. Light-duty trucks (LDTs) are the main contributor to upstream emissions from both hydrogen and natural gas, followed by heavy-duty trucks (HDTs) and medium-duty trucks (MDTs). LDTs and HDTs are responsible for almost 80% of total hydrogen and natural gas upstream emissions in all scenarios (Figure S2.8).

The absolute increase in $PM_{2.5}$ and CO_{2e} emissions from power generation and upstream natural gas and hydrogen production only account for 2%, 0.6%, 0.6% and 0.1%, 0.2%, 0.2% of net reductions in $PM_{2.5}$ and CO_{2e} emissions from AEVs deployment in LP-LR, HP-HR and MP-HR scenarios, respectively. This indicates that with high penetration of low-carbon electricity, using AEVs can greatly mitigate, and nearly eliminate, both air pollutant and CO_{2e} emissions.

2.5 Impacts on surface air pollutant concentrations

We simulate China's 2015 base case surface air quality for January, May, July and September using the WRF-Chem v 3.61 regional atmospheric chemistry transport model. We analyze reductions in NO_2, $PM_{2.5}$ and O_3 across China. Modeled $PM_{2.5}$ and ozone (O_3) concentrations are in good agreement with observations (Figure S2.11).

We find that replacement of ICEVs with AEVs in our scenarios will deliver an increasing reduction in annual average NO_2, $PM_{2.5}$ and O_3 concentrations nationwide (Figure 2.5 and Figure S2.12) relative to the 2015 base case. The highest NO_2 reductions will occur in the most highly populated cities. The annual national population-weighted NO_2 reductions are $6.3 ug/m^3$ in the MP-HR scenario due primarily to decreasing tailpipe emissions.

The air quality simulation results indicate that national annual average population-weighted $PM_{2.5}$ (from January and July simulations) would decrease by $0.6 \mu g m^{-3}$, $2.1 \mu g m^{-3}$ and $5.7 \mu g m^{-3}$ in the LP-LR, HP-HR and MP-HR scenarios, respectively, compared to the base case. The reduction of population-weighted $PM_{2.5}$ concentrations represents 1.0%, 3.4% and 9.1% of base case $PM_{2.5}$ concentrations, respectively. The

national annual average decreases in population-weighted $PM_{2.5}$ are largely from tailpipe emission reductions (Figure 2.2) suggesting that higher proportions of AEV penetration can readily lead to greater reductions in ambient $PM_{2.5}$ concentrations as long as the grid decarbonizes. The annual $PM_{2.5}$ reductions can reach 6.8 and 4.5$\mu g m^{-3}$ in the MP-HR scenario in Beijing and Shanghai. These reductions are 5-8 times larger than the annual average $PM_{2.5}$ concentration reduction (0.8$\mu g m^{-3}$) achieved nationally. This indicates that AEV deployment can result in significant air quality benefits in traffic-dense metropolitan urban areas. Our simulation results show that inorganic aerosols (nitrate, sulfate, and ammonium) account for 71% of $PM_{2.5}$ concentration reductions, with nitrate contributing 48% and sulfate contributing 7% (Figure S2.14A). Although NH_3 emissions remain constant, nitrate reduction contributes to lower ammonium aerosol concentrations.

Reductions in $PM_{2.5}$ concentrations have significant seasonal variations due to seasonally varying rates of secondary inorganic aerosol formation. Replacing ICEVs with AEVs decreases $PM_{2.5}$ concentrations in January more than in July (Figure S2.13) due to differences in temperature, humidity and meteorology between summer and winter. For the MP-HR scenario, average population-weighted $PM_{2.5}$ concentrations decrease 7.5$\mu g/m^3$ and 3.9$\mu g/m^3$ in January and July, respectively. Based on our simulation results (Figure S2.14A and S2.14B), inorganic aerosol (nitrate, sulfate and ammonium), BC and OC concentrations also decrease more in January than in July. Average population-weighted nitrate, sulfate and ammonium concentrations decrease 3.1$\mu g/m^3$, 0.5$\mu g/m^3$ and 1.1$\mu g/m^3$ in January; 2.3$\mu g/m^3$, 0.3$\mu g/m^3$ and 0.8 $\mu g/m^3$ in July, respectively.

We find the adoption of AEVs results in widespread decreases of ground-level MDA8

O_3 concentrations in summer (May, July and September simulations) in most areas of China due to the large resulting reductions in NO_x and VOCs. We find that summer MDA8 population-weighted O_3 concentrations over China decrease by 0.5ppb, 2.8ppb and 4.9ppb in the LP-LR, HP-HR and MP-HR scenarios, respectively, representing 0.9%, 4.4% and 7.8% reductions compared to the 2015 base case (Figure 2.5). The impacts on winter O_3 concentrations are more diverse (Figure S2.15) with slight decreases in regional O_3 concentrations and significant increases in most urban areas. Compared to the decreases in summer averages of MDA8 O_3, decreases in monthly averages of 24 h O_3 are smaller (Figure S2.16).

The change in monthly average 24 h O_3 is determined by whether the O_3 formation is in a VOC-limited or NO_x-limited regime. We use the ratio of the product of formaldehyde (HCHO) and hydrogen peroxide (H_2O_2) to nitrogen dioxide (NO_2) ($HCHO*H_2O_2/NO_2$) at the surface as a regime indicator, and use regime thresholds identified by Xing et al[21] over East Asia (a ratio <1 being VOC-limited and >1 being NO_x-limited). Figure S2.17 shows that most areas in China are in a VOC-limited regime in winter, where O_3 increases when NO_x decreases. In comparison, the NO_x-limited areas, where O_3 decreases as NO_x decreases, are larger outside of winter. Although the North China Plain is in a VOC-limited regime even in July, the simultaneous reduction of NO_x and VOC emissions in that area result in a monthly average decrease in 24 h O_3 in July as well.

2.6 Human health and economic benefits

We observe significant human health benefits of increased penetration of AEVs and increasing benefits as the power sector decarbonizes, primarily due to resulting

reductions in annual ambient $PM_{2.5}$ and O_3 concentrations across China. We estimate that annually approximately 40,200 (95% CI: 30,000-63,000), 224,700 (95% CI:187,400-279, 400) and 329,000 (95% CI: 254,200-383,100) premature deaths are avoided in LP-LR, HP-HR and MP-HR scenarios due to reduced long-term exposure to annual $PM_{2.5}$ and O_3 concentrations. Gridded and provincial avoided premature mortalities in LP-LR, HP-HR and MP-HR scenarios are shown in Figure S2.18 and Table S2.11-2.12. The premature mortalities and years of life lost (YLL) attributed to ambient $PM_{2.5}$ and O_3 exposure in 2050 are shown in Table S2.13-2.14 by age group for the above three scenarios. Although total population changes little between 2015 and 2050, the population ages over those 35 years. The aging of the population results in larger numbers of premature mortalities and YLL by 2050 than if the age distribution had remained unchanged over that interval (see as Table S2.13-2.16).

We further compare the monetary benefits of human health improvements and CO_{2e} emission reductions (Figure 2.6). A variety of methods are used to monetize air quality and climate benefits (Experimental Procedures). We estimate the economic benefits based on various baseline studies of value of statistical life (VSL)[22, 23, 24, 25, 26, 27] and social cost of carbon (SCC)[28, 29, 30, 31, 32]. The economic benefits of combining health benefits and GHG emission reductions due to ICEVs replacement with AEVs and increasing use of decarbonized power are US2015$6-187 billion, US2015$33-1102 billion and US2015$49-1588 billion in LP-LR, HP-HR and MP-HR scenarios, respectively. Between 2010 and 2018, average US VSL values ($18.9 million) were more than one order of magnitude higher than average Chinese VSL ($0.5 million) values. Despite relatively low VSL values

for China, our results highlight enormous economic benefits of improving China's air quality and associated human health while mitigating GHG emissions by switching from traditional engine vehicles to AEVs across the country.

3. Discussion

China is the largest emitter of CO_2 in the world. China's CO_2 emissions reached 10.2 Gt in 2019, accounting for 31% of global fossil fuel CO_2 emissions. To meet the Paris Agreement's target to limit global temperature increase to below 2 ℃ above pre-industrial levels, net global CO_2 emissions must be carbon neutral by around mid-century[33, 34]. In 2020, China pledged to reach net carbon neutrality by 2060. Carbon-neutrality of the on-road transport sector is critical to achieve this goal. The rapid decarbonization of the electricity generated to power electric vehicles is a critical component of achieving carbon neutrality of the transport sector as is the uptake of HFCVs using green hydrogen derived from non-fossil electricity to power heavy duty trucks. At the same time, China is suffering from severe air pollution due to rapid industrialization. Exposure to ambient air pollution is estimated to have resulted in one million premature mortalities in 2017[1]. Conversion of internal combustion engines to EV and HFC vehicles will eliminate tail pipe emissions of air pollutants and if powered with renewable electricity will also eliminate most air pollutant emissions from power generation. Despite the large opportunities from a transformation of the transport and power sector to non-fossil power, no prior systematic quantification of the benefits for GHG mitigation, air quality and public health improvements of deep decarbonization has been made for China. Our study fills this gap by including passenger vehicles,

motorcycles, heavy duty trucks and the power sector (100% non-fossil energy for vehicles and 91% non-fossil energy for electricity and hydrogen).

We develop an integrated assessment framework to evaluate the implications of AEV penetration levels with various power system supply designs in China on GHG mitigation, air quality, and premature deaths. To evaluate the benefits of decarbonizing the transport sector, including both passenger vehicles, motorcycles, and trucks, and eliminate emissions of air pollutants, we simultaneously evaluate the adoption of various AEVs, suited for a variety of applications (e.g., EVs and EMCs as replacements for passenger cars and motorcycles, respectively, and HFCVs as a replacement for diesel trucks and buses) and consider the implications of a variety of energy sources for these AEVs. We find that increased AEV penetration alone increases $PM_{2.5}$, SO_2 and CO_{2e} emissions, when AEVs are powered using electricity generated with the mix of technologies utilized in 2015 and hydrogen is derived from coal or natural gas rather than via water electrolysis using non-fossil electricity. We find that for AEVs to yield air quality, health and climate benefits, their uptake must be coupled with decarbonization of the power sector and the greater the level of decarbonization, the larger the benefits are for all three factors. For instance, if AEVs are powered primarily with fossil electricity (28% non-fossil energy), annual CO_{2e} emissions increase by 149Tg. However, if AEVs are powered primarily with non-fossil energy (91% non-fossil energy), annual CO_{2e} emissions decrease by 420Tg. Our findings indicate that simultaneously increase uptake of AEVs while rapidly decarbonizing the power sector and hydrogen production will yield the largest co-benefits. Decarbonization of the power sector is of utmost

importance in maximizing the benefits of increasing AEV penetration.

China's government recently announced a development plan for the new energy vehicle industry (EVs and HFCVs) [35]. This plan states that as of 2035, 50% of new cars sold in the country will be either electric, plug-in hybrid, or fuel cell vehicles, and 50% of new cars will be conventional hybrids, which still run entirely on gasoline but have improved fuel efficiency compared with ICEVs. Sales of new pure ICEVs (non-hybrid gas powered vehicles) will be banned starting in 2035. Although starting in 2021 EV adopters receive fewer monetary incentives than before, new supportive policy will focus on HFCVs to improve the industry's supply chain and technologies[36]. Municipal governments are now being encouraged to align environmental and industrial interests to incentivize AEV deployment in China. Current AEV policy puts China on a path for reduced air pollutant and carbon emissions from the vehicle sector if rapid decarbonization of power generation takes place simultaneously.

Currently, 69% hydrogen production comes from fossil fuel (55% for coal gasification and 14% for stream methane reforming) while the rest is a byproduct of industrial processes[20]. In comparison, water electrolysis using renewably generated electricity ("green hydrogen") only accounted for 3% of hydrogen production in 2020[20]. However, based on the White Paper on China's Hydrogen Energy and Fuel Cell Industry[37], hydrogen production from renewable energy water electrolysis in 2050 will reach 70%, while the share of hydrogen from fossil fuel will drop to 20%. In our study, we set up a sensitivity analysis (Table S2.6) to estimate the potential emission mitigation from hydrogen production if non-fossil generated electricity with water electrolysis replaces

fossil production of hydrogen. The results indicate that total air pollutant and CO_{2e} emissions from HFCVs would decrease by 73% if green hydrogen penetration increases from 10% to 90%.

In order to address the urgency of climate change and explore the potential of further improving air quality via AEV deployment, our study considered a variety of decarbonization levels for electricity generation and includes more AEV types than Liang et al (2019)[11] or Schnell et al (2021)[16]. Liang et al (2019)[11] estimated the air quality and health benefits of projected electric passenger vehicle penetration in 2030, given current policies, and found 17,456 (95% CI: 10,656-22,160) avoided annual premature deaths nationally due to reduced $PM_{2.5}$ and O_3 concentrations in China. We find that in our scenarios the avoided premature deaths due to an expansion of the AEV fleet including EVs, EMCs, HFCVs and NGVs powered with over 90% decarbonized electricity could be as large as ~329,000 persons (95% CI: 254,200-383,100). Schnell et al (2021)[16] found that the deployment of passenger and light-duty truck EVs ameliorate several wintertime air pollution episodes, bring health benefits and reduce CO_2 emissions when the marginal electricity generation is 50% emission-free. However, summer O_3 pollution is also detrimental to human health. Rather than analyzing air pollution episodes in a single season, we simulate changes in annual average air pollution levels for $PM_{2.5}$ and summer MDA8 O_3 concentrations as well as CO_2 emission reductions for each of our scenarios. We find summer MDA8 O_3 will decrease in all of our scenarios leading to a reduction in premature deaths of 31,300 (10% of the ~329,000 total avoided premature mortalities). A key difference between our work and both previous studies is that we consider higher

penetration rates of AEVs powered with an 85% renewable electricity mix (91% decarbonized power including nuclear) and in addition to EVs we also include EMCs, HFCVs and NGVs. In our MP-HR scenario, NO_x, VOC, $PM_{2.5}$, SO_2 and CO_{2e} emissions from on-road vehicles only account for 0.3%, 1.2%, 1.1%, 7.0% and 7.0% of the emissions of on-road vehicles in 2015. Our analysis also extends beyond previous studies to include changes in annual air pollution concentrations, resulting premature mortalities and years of life lost. A conversion to AEVs using largely non-fossil power can reduce air pollution and associated YLL by ~ 1,611,000 life years per year compared to the 2015 base case.

Increased electricity demand will bring challenges and opportunities to the power grid system. In our study, we assume that the increased electricity demand for charging electric vehicles is derived from newly built power plants. In addition, we assume that the power grid will be updated with increased power capacity, transmission, and distribution capacity, to support the increased demands resulting from AEV growth. However, future research on how to best meet the increased electricity demand while reducing emissions via incorporation of variable renewable generation, increased storage and transmission is crucial.

Our results are subject to several uncertainties and limitations. First, we chose 2015 as the base year in this study as it was the most recent year for which we had access to complete data. Considering China's decreasing transport and power sector air pollutant emissions in recent years[38], the environmental and health benefits in each scenario may be smaller than we estimated. Second, our scenarios are sensitivity analyses to investigate the implications of various alternative energy vehicles powered with a variety of energy

sources that the literature indicates are possible by 2050. However, because emissions from other sectors are kept at 2015 levels, these analyses do not represent actual 2050 air pollution concentrations which may affect the health benefit estimates we made. Third, we did not include emissions from the off-road vehicle sector (e.g., agricultural machines and construction equipment). These emissions are substantial, and their elimination is needed to further improve air quality and achieve carbon neutrality. EV and HFCV technology could likely be used in these off-road applications. Future research on the co-benefits of replacing traditional agricultural and construction equipment with electric and hydrogen fuel cell engines is needed. Fourth, emissions from mining, transport and distribution of fossil fuels used in the power sector, as well as emissions from the construction and disposal of power generation technology are not included in our study.

In addition to the factors discussed above, the MEIC emission inventory we use assumes a perfect implementation of emission standards. However, due to limited inspection and maintenance in China MEIC underestimates actual air pollutant and CO_2 emissions from the transport sector [39]. We use MEIC to quantify the change of air pollutant (primary $PM_{2.5}$, NO_x, SO_2, VOC, BC, OC) and CO_2 emissions resulting from various AEV scenarios. Anenberg et al.[39] shows that actual NO_x emission factors for passenger cars, heavy-duty trucks and buses in China are 50%-330% higher than permitted by emission standards if they were perfectly enforced. Furthermore, MEIC was developed assuming that traffic volumes are homogeneous within provinces[40]. However, significant nonlocal truck traffic is not reflected in static registration data. Yang et al.[41] developed a link-level emission inventory based on multiple datasets extracted

from the extensive road traffic monitoring network in Beijing and argued that previous conventional emission inventories underestimated the emissions of both NO_x and $PM_{2.5}$ by ~45% primarily due to missing contributions from nonlocal HDTs. As a result of these factors, our findings underestimate the benefits of conversion from ICEVs to AEVs.

In conclusion, we find that high AEV penetration must be coupled with deeply decarbonized electricity to maximize co-benefits for air quality, health and GHG mitigation. If AEV penetration increases rapidly and is powered with the 2015 power mix (72% fossil fuel), $PM_{2.5}$, SO_2 and CO_{2e} emissions will increase. Decreasing fossil fuel used in the power sector to 45% (low renewable penetration scenario) decreases both air pollutant and CO_{2e} emissions from AEV deployment relative to the vehicle fleet emissions in 2015 (base case). High AEV penetration powered with 91% non-fossil fuel electricity (MP-HR, maximum penetration of AEVs with high renewable electricity scenario) maximizes air quality, health, and climate co-benefits. In this most aggressive scenario, national annual population-weighted $PM_{2.5,}$ summer MDA8 O_3 concentrations and CO_{2e} emissions decrease by 5.7ug/m^3 (~9%), 4.9ppb (~8%), and 708Tg (~7%), respectively, of China's 2015 population weighted concentrations and emissions. Calculated annual avoided premature mortalities and YLL due to reduced exposure to ambient $PM_{2.5}$ and O_3 in the MP-HR scenario are 329,000 (95% CI: 254,200-383,100) persons and ~1,611,000 (1,425,000 – 1,739, 200) years of life lost. Thus, we find that increased penetration of AEVs that use non-fossil generated electricity and hydrogen to replace highly polluting internal combustion engines will be a critical component of China's efforts to improve air quality while reaching net zero carbon emissions by 2060.

4. Materials and Methods

4.1 Scenario design

We set up various levels of AEV penetration and decarbonization levels for the power sector to present variability in the benefits resulting from future AEV penetration levels depending on possible penetration levels of various vehicle types and power sector electricity mixes (Figure S2.2 and S2.3) for 2050. The alternative energy vehicle penetration for passenger vehicles and trucks includes Low Penetration (LP), Intermediate Penetration (IP), High Penetration (HP) as well as an idealized Maximum Penetration (MP) scenario. The power generation mixes include low renewable (LR) and high renewable (HR) scenarios. The national total projections for low, intermediate and high penetration of alternative energy vehicles in the transport sector, and low and high renewable power generation scenarios are based on the uncertainty ranges of the 2050 projections by the Rocky Mountain Institute[42] (Reference Scenario and Reinventing Fire China Scenario, 2017) and the Chinese Energy Research Institute[43] (Stated policies and Below two degree Scenario in the China Renewable Energy Outlook 2018). In the aggressive alternative energy vehicle scenario (MP scenario) we assume that 100% of internal combustion engine vehicles (ICEVs) are replaced by alternative energy vehicles.

The LP, IP and HP scenarios describe the EV penetration ranges for passenger vehicles (7.5-80%) and trucks (2-9%), CNG/LNG penetration ranges for trucks (3-6%), and hydrogen fuel cell vehicle penetration for trucks (2-18%) from the literature[42,43]. Table S2.3 provides specific penetration rates for each type of alternative vehicle for each scenario and Table S2.4 provides scenarios of power generation mixes in 2050.

4.2 Air pollutant and GHG emission estimation

We adopt a counterfactual method to evaluate the air quality, CO_2 mitigation and health benefits of increasing penetration of AEVs with varying penetrations of decarbonized electricity. We use 2015 air pollutant emissions as our base case. For each scenario we keep all emissions outside the vehicle and power sectors the same as in our base case while changing emissions from the vehicle and power sectors. The changes reflect varying penetration rates of AEVs, as well as changes in emissions from the power sector for the electricity used to power the AEVs or generate hydrogen (e.g. reduced emission factors for coal and gas power plants, and two penetration levels for decarbonized electricity).

We use the bottom-up Multi-Resolution Emission Inventory of China (MEIC) developed by Tsinghua University in 2015 as our base case[38]. The MEIC inventory is a high-resolution anthropogenic air pollutant and carbon dioxide emission inventory for China. MEIC has a three-dimension matrix, which includes time, location, and emissions of each species (SO_2, NO_x, CO, NMVOC, NH_3, BC, OC, $PM_{2.5}$, PM_{10}, and CO_2). It includes ~800 anthropogenic sources, aggregated to five main sectors: power, industry, residential, transport and agriculture. The emissions of a particular species are estimated by the following equation[44]:

$$E_i = \sum_j \sum_k A_{i,j,k} \left[\sum_m X_{i,j,k,m} EF_{j,k,m} (1 - \eta_n) \right] \quad (1)$$

Where i represents the province; j represents the sectors; k represents the fuel or product types; m represents the technology type for combustion and industrial process; n

represent a specific control technology; A is the activity rate, such as fuel consumption; X is the fraction of fuel or production for a sector that is consumed by a specific technology; EF is the emission factor; η_n is the removal efficiency of control technology n.

We calculate both downstream emissions associated with end-use fuel (i.e., gasoline or diesel) combustion and, upstream emissions associated with additional electricity generation, production, processing, transmission and distribution of hydrogen and nature gas in each scenario.

We estimate the emission changes in a particular species of air pollutants and CO_2 emissions resulting from an AEV scenario in the transport sector as follows:

$$\Delta E_{i,T} = P_{i,j} \times E_{i,j} \quad (2)$$

Here, ΔE represents change of emissions relative to the base case, T represents the transport sector; i represents province, P represents penetration of AEVs for each vehicle type j. Vehicle types include commercial passenger vehicles (including buses, taxies, and others), private passenger vehicles, trucks, and motorcycles. The proportion of BEVs and PHEVs in various vehicle fleet under LP, IP, HP, and MP scenario is shown in Table S2.5 (see Note S2.2 Electric vehicle deployment strategy in Supplemental information for a more detailed description)).

It's worth noting that there are no commercial vehicle emissions in MEIC. Commercial vehicle emissions are included in the passenger vehicle category. Therefore, we separate the emissions of buses and taxies from passenger vehicles in MEIC using the 2015 population of buses and taxies[45], 2015 vehicle kilometers travelled[45]and emission factors[46].

$$E_{i,CV} = Pop_{i,T} \times VKT_{i,T} \times EF_{i,T} + Pop_{i,B} \times VKT_{i,B} \times EF_{i,B} \quad (3)$$

Here, E represents emissions of an air pollutant, i represents province, CV represents commercial vehicles, Pop represents the population of each vehicle type, VKT represents annual vehicle kilometers of each vehicle type, EF represent the emission factor, T and B represent taxies and bus vehicle types, respectively.

We estimate the emission changes in a particular species of air pollutants and CO_2 emissions in the power sector as follows:

$$\Delta E_{i,P} = Pop_{i,j} \times VKT_{i,j} \times ELE_{i,j} \times EF_{i,j} \quad (4)$$

Here, ΔE is change of emissions of a pollutant from the power sector relative to the base case; P represents power sector; i and j represent provinces and vehicle types; Pop represents population of electrified vehicles for each vehicle type, VKT represents 2015 annual vehicle kilometers travelled (Table S2.8), ELE represents electricity consumption of electrified vehicles per kilometer (Table S2.8) and EF is the emission factor of air pollutants and CO_{2e} emissions from electricity generation used for the AEVs. Emission factors are derived from the existing literature (Table S2.9). We adopt the emission factors of coal and natural gas power plants in 2030 because we assume new power plants will be built to provide electricity for the new AEVs and that the emission control technologies for fossil fuel combustion by 2030 will be mature and will not decline significantly after 2030. We estimate annual vehicle kilometers traveled based on the average of lifetime vehicle miles traveled in typical cities in China in 2015 [47]. Lifetime vehicle miles traveled is 165,000km (102,525 mi) (assuming annual mileage of approximately 11000 km (6835 mi annual mileage) and a 15-year average vehicle lifetime (Ministry of Commerce of The

People's Republic of China)).

We estimate annual upstream emissions from production, processing, transmission and distribution of hydrogen and natural gas as follows:

$$E_{i,UP} = Pop_{i,n} \times VKT_{i,j,n} \times EF_{i,j,n} + Pop_{i,h} \times VKT_{i,j,h} \times EF_{i,j,h} \quad (5)$$

Here, E is the increased emissions from natural gas and hydrogen; UP represents upstream emissions, i and j represent provinces and vehicle types; n and h represents natural gas and hydrogen fuel cell vehicles; Pop represents population of natural gas or hydrogen fuel cell vehicles, VKT represents annual vehicle kilometers travelled of natural gas or hydrogen fuel cell vehicles, EF represents the emission factor of air pollutants and CO_{2e} emissions from production, processing, transmission and distribution of hydrogen or natural gas[48, 49, 50].

Lastly, we calculate the total emission changes in the transport and power sector for each scenario, using the same temporal and spatial distribution as MEIC 2015, and create monthly gridded emissions for each counterfactual scenario.

4.3 Air quality simulations

We simulate the ambient concentration changes of $PM_{2.5}$, O_3 and NO_2 for January, May, July and September for the 2015 base case, LP-LR, HP-HR and MP-HR scenarios using WRF-Chem v3.6.1 (https://www2.acom.ucar.edu/wrf-chem). The model resolution is 27 km by 27 km, with the domain covering China and parts of other Asian countries (9 N to 58 N, 60 E to 156 E). The model has 37 vertical layers from the surface (32m) to 50 hPa. 2015 initial and lateral meteorological boundary conditions are provided by the National Centers for Environmental Prediction (NCEP) FNL (Final) Operational Global Analysis

data (https://rda.ucar.edu/datasets/ds083.2/index.html) at 1 1 resolution. Chemical initial and boundary conditions are derived from The Community Atmosphere Model with Chemistry (CAM-Chem v4)[51].

The physical and chemical schemes used in WRF-Chem are as follows: the RRTM scheme for longwave radiation[52], the Goddard shortwave scheme[53], the Morrison aerosol microphysics scheme[54], the Noah land surface scheme[55], the Yonsei University PBL scheme[56], the model for simulating aerosol interactions and chemistry (MOSAIC) for aerosol[57], and CBMZ[58] for gas-phase chemistry. Biogenic emissions are calculated online using the Model of Emission of Gases and Aerosols from Nature (MEGAN) coupled with WRF-Chem[59]. Natural dust emissions are calculated by the modified GOCART scheme[60]. We apply an improved scheme that better represents the formation of secondary inorganic aerosols[61].

Because our simulations are only for 2015, we compare the meteorology during the winter (January) and summer (May, July and September) of 2011, 2013, 2015, 2017 and 2019 with the average of 2011-2020 by using climate reanalysis data from the European Centre for Medium-Range Weather Forecasts (ECMWF, https://www.ecmwf.int/). We find that in January, May, July, and September of 2015 the mean boundary layer height is within 15%, the wind speed at 925hPa is with 20% and the precipitation is within 50% of the ten-year average over most regions of China (Figure S2.9 and S2.10). We find that the meteorology for other years with which we compare diverges from the 10-year average by more than 2015, making us comfortable using 2015 for our analysis as others have done[62, 63]. The modeled meteorological parameters (i.e., 2-m air temperature, dewpoint

temperature, 10-m wind speed, and sea level pressure) are compared with observations from the National Climate Data Center (NCDC) (Table S2.10). In Figure S2.11 we compare $PM_{2.5}$ dry mass concentrations and summer MDA8 O_3 concentrations in the base case with observations from the Ministry of Ecological Environment (MEE). We obtain good model agreement with observations across China in the months we simulate.

4.4 Analysis of health impacts associated with air pollution

We calculate the avoided premature mortalities attributed to the reduced ambient $PM_{2.5}$ and O_3 concentrations. Assessment of the ambient $PM_{2.5}$ associated premature mortality from noncommunicable diseases and lower respiratory infections (NCD +LRIs) is based on epidemiological cohort studies of long-term exposure to $PM_{2.5}$[64]. The reduction in premature deaths in each scenario is estimated as follow:

$$\Delta \mathrm{Mort}_{\mathrm{i,p}} = \mathrm{POP}_{\mathrm{j,p}} \times \mathrm{B_i} \times \left(\frac{1}{\mathrm{RR_i(C_S)}} - \frac{1}{\mathrm{RR_i(C_{BASE})}}\right) \quad (6)$$

Here, $\Delta \mathrm{Mort}_{\mathrm{i,P}}$ is the change of premature mortality between base case and AEV scenarios in WRF-Chem grid p from disease i, $\mathrm{POP}_{\mathrm{j,p}}$ represents the number of population with age group j in grid p. B_i is the national base case mortality rate for each disease i. RR is the relative risk for disease i at the $PM_{2.5}$ concentration (C). Cs is the $PM_{2.5}$ concentration in various AEV scenarios. C_{BASE} is the $PM_{2.5}$ concentration in the base case. The RR for each disease is calculated from the exposure response function for a particular concentration of $PM_{2.5}$ based on the Global Exposure Mortality Model (GEMM)[64].

According to GEMM, relative risks (RR) of NCDs and LRIs associated with $PM_{2.5}$ exposure is calculated for adults (≥25 y old) using age groups with 5-year intervals from 25 to older than 85 as follows:

$$RR(c) = e^{\frac{\theta * \log\left(\frac{c}{\alpha+1}\right)}{1+e^{-\frac{c-\mu}{v}}}}, c = \max(0, c - 2.4) \quad (7)$$

Here c is long-term ambient $PM_{2.5}$ concentration; $\theta, \sigma, \mu, and\ v$ are parameters that determine the shape of RR in GEMM and are specified for each age group. The values for $\sigma, \mu, and\ v$ are constant across all age groups for NCD+LRI while θ *varies by age group*. In our study, we perturb the value of θ based on its mean and standard error described in Burnett et al. (2018)[64] , and generate 10,000 shapes of RR for each age interval. We further calculate the mean and 95% confidence intervals of avoided premature deaths and potential years of life lost (YLL) for each age interval in each AEV scenario.

Avoided premature deaths due to reduced ambient O_3 concentration are estimated from:

$$\Delta Mort_{i,p} = POP_{j,p} \times B_{i,p} \times \left(1 - \frac{1}{RR_i}\right) \quad (8)$$

We use a log-linear concentration-response function (CRF) between change in O_3 concentration and RR:

$$RR = \exp(-\beta \Delta c) \quad (9)$$

Here, $\Delta Mort_{i,p}$is the change in mortality attributable to long-term O_3 exposure, POP is the population of adults older than 30 years, Δc is the change in O_3 concentration between various AEV scenarios and the base case, and β is the CRF slope calculated from a recent estimate of RR per 10ppb increase in annual mean MDA8 O_3 of 1.02 (95% CI: 1.01–1.04) for all diseases[65]. We use the average MDA8 O_3 concentration for Jan, May, July, and September as the annual mean MDA8 O_3 concentration.

Age-specific mortality rates were calculated by dividing the number of deaths in each age group by the total deaths of all ages. The function for estimating YLL, which proposed by Romeder and McWhinnie in 1977[66] is as follows:

$$YLL = \sum_{i=1}(Age_{limit} - j - 0.5) * d_i \quad (10)$$

Here, YLL is the summation of all age-specific YLLs; Age_{limit} is the upper limit of age, which we choose 80 years based on the existing literature[67]; j is the mid-point of the class interval of each age group. For example, the mid-point of the class interval of 25–29 years is 27. 0.5 is a constant; d_i is the number of premature deaths due to $PM_{2.5}$ and O_3 exposure in each class interval.

Because our AEV scenarios were developed to reflect possible penetration rates by 2050, we project 2050 population to better represent the health benefits of each scenario. Gridded population in 2050 is derived by scaling gridded population data in 2015 from the Global Population for the World (GPW) dataset[68], based on population projections by country and by age group in 2050 from the United Nations World Population Prospects 2019 revision under a medium fertility scenario[69] assuming that the spatial distribution of population in each country in 2050 is the same as that in 2015. We find population changes between 2015 and 2050 are very slight but the age distribution is older which will affect the number of premature mortalities and potential YLL due to exposure to air pollutants. Base case mortality rates for each disease are obtained from the Global Burden of Diseases (GBD) study (http://ghdx.healthdata.org/). We assume base mortality rates are unchanged across the scenarios.

4.5 Evaluation of economic benefits of improved health and GHG mitigation

Monetizing air quality and climate benefits is controversial and is often based on the value of a statistical life (VSL, a measure of people's willingness to pay to reduce their mortality risk) and the social cost of carbon (SCC, the marginal global societal cost of emitting an additional ton of carbon), respectively. VSL estimates vary substantially across countries, age groups and income groups[70]. Studies on the value of a statistical life (VSL) have been widely conducted in the developed world, but few such studies can be found for developing countries. He and Wang et al. [22], Xie et al.[23] and Lei, et al.[24] publish VSL estimates from survey studies for China (low and high estimates $90,000 and

$250,000). The baseline VSL based on the US is US$1.6 million(2005), US$9.6 million (2015) and US$7.7 million (2007) in West et al.[25] and Viscusi et al.[26] and Li et al.[27]. We estimate the air quality and climate benefits based on various baseline studies and present the results in Figure 2.6A. The VSL is estimated as follows:

$$\mathrm{VSL} = \mathrm{VSL}_{\mathrm{base}} \times \left(\frac{\mathrm{pcGDP2015}_{\mathrm{China}}}{\mathrm{pcGDP}_{\mathrm{Base}}}\right)^{\eta} \quad (11)$$

Here, $\mathrm{VSL}_{\mathrm{base}}$ is the VSL in the year identified in the original manuscript, η is the income elasticity, income elasticity is set to be 0.4 in this study[71]. $\mathrm{pcGDP2015}_{\mathrm{China}}$ and $\mathrm{pcGDP}_{\mathrm{Base}}$represent per capita GDP in 2015 for China and baseline GDP from the country of each study.

Most published estimates of the SCC have been derived from integrated assessment models (IAMs) that combine economic growth, climate processes, human health, policies and feedbacks. Despite the inherent uncertainties in models such as these, they are the best tools currently available for estimating SCC. SCC estimates range from $20 to higher than $ 200/tons CO_2[28, 29,30, 31, 32]. We estimate the uncertainty range of climate benefits based on these SCC estimates.

Table 2.1: Alternative Energy Vehicle (AEV) scenarios[1]

Cases	Transport sector	Electricity for AEVs
Base case	**2015 on-road transport**	**2015 power mix (25%; 3%)**
LP-2015	Low AEV penetration (2-50%)	2015 power mix (25%; 3%)
LP-LR	**Low AEV penetration (2-50%)**	**Low renewable penetration (40%; 15%)**
LP-HR	Low AEV penetration (2-50%)	High renewable penetration (85%; 6%)
IP-2015	Intermediate AEV penetration (5-80%)	2015 power mix (25%; 3%)
IP-LR	Intermediate AEV penetration (5-80%)	Low renewable penetration (40%; 15%)
IP-HR	Intermediate AEV penetration (5-80%)	High renewable penetration (85%; 6%)
HP-2015	High AEV penetration (9-100%)	2015 power mix (25%; 3%)
HP-LP	High AEV penetration (9-100%)	Low renewable penetration (40%; 15%)
HP-HR	**High AEV penetration (9-100%)**	**High renewable penetration (85%; 6%)**
MP-HR	**Maximum AEV penetration (50-100%)**	**High renewable penetration (85%; 6%)**

[1] Details of the scenarios are provided in Experimental Procedures and Tables S3, S4 and S5. Scenarios in bold are those for which we simulate air quality. The percentages in brackets under the transport sector indicate the penetration of various types of AEVs. The first number indicates the penetration of EVs for trucks, and the second number indicates the penetration of EVs for buses and taxis. Penetration of passenger vehicles fall within the range of these two numbers. The first number in AEV electricity percentages represent the penetration of renewable energy for power generation and the second indicates the penetration of nuclear power. In all renewable penetration scenarios, the emission factor for coal and gas power plants are adjusted to expected 2030 levels. For all scenarios, electricity utilized in other sectors continues to use 2015 emission factors.

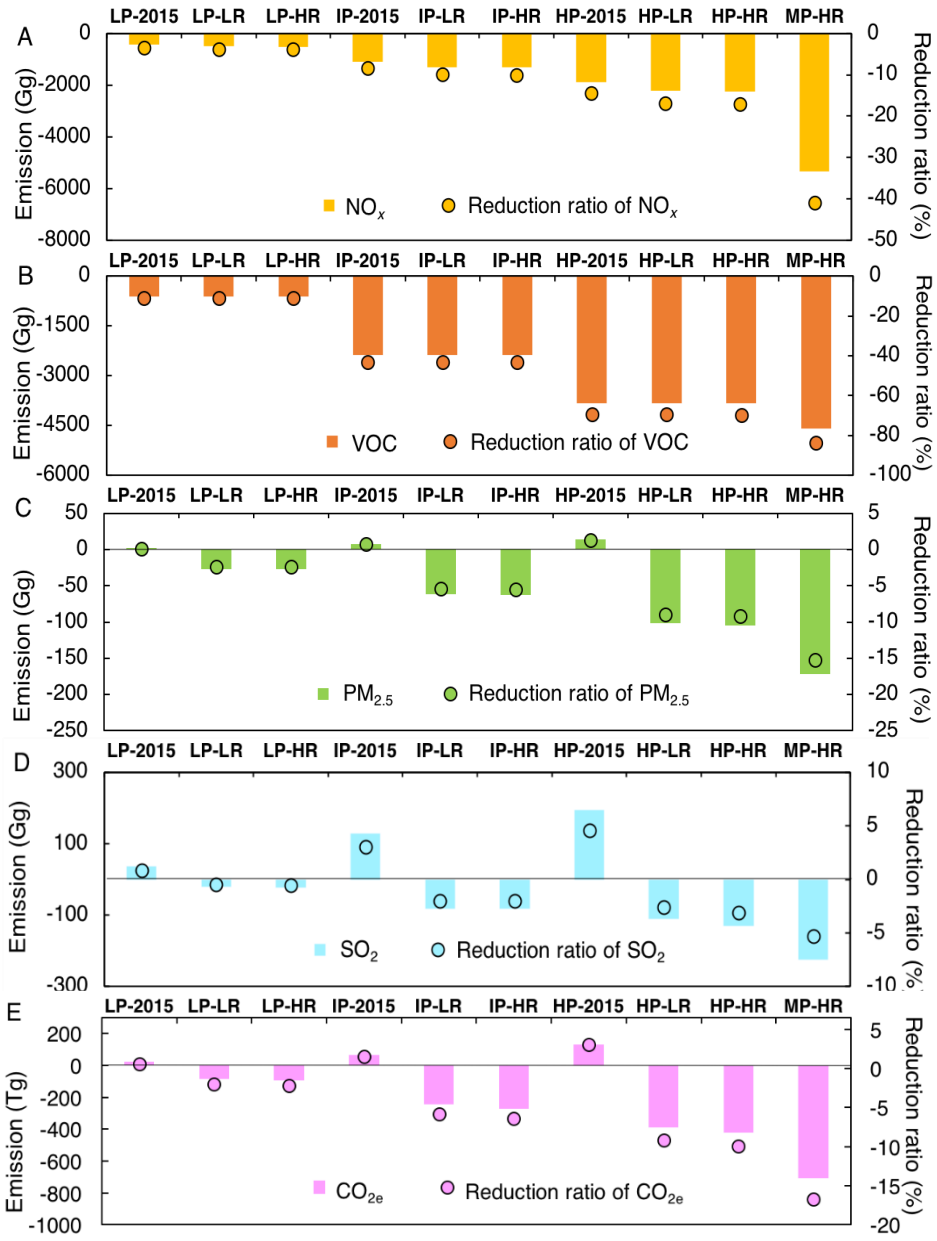

Figure 2.1. Changes in total and percent of air pollutant and CO_{2e} emissions under each scenario

Changes in (A) NO_x, (B) VOC, (C) $PM_{2.5}$, (D) SO_2 and (E) CO_{2e} emissions from both vehicle tailpipes and energy sources for each scenario relative to the base case. Bars indicate the total emission changes compared to the base case. Dots indicate the percent reduction of emissions relative to the base case.

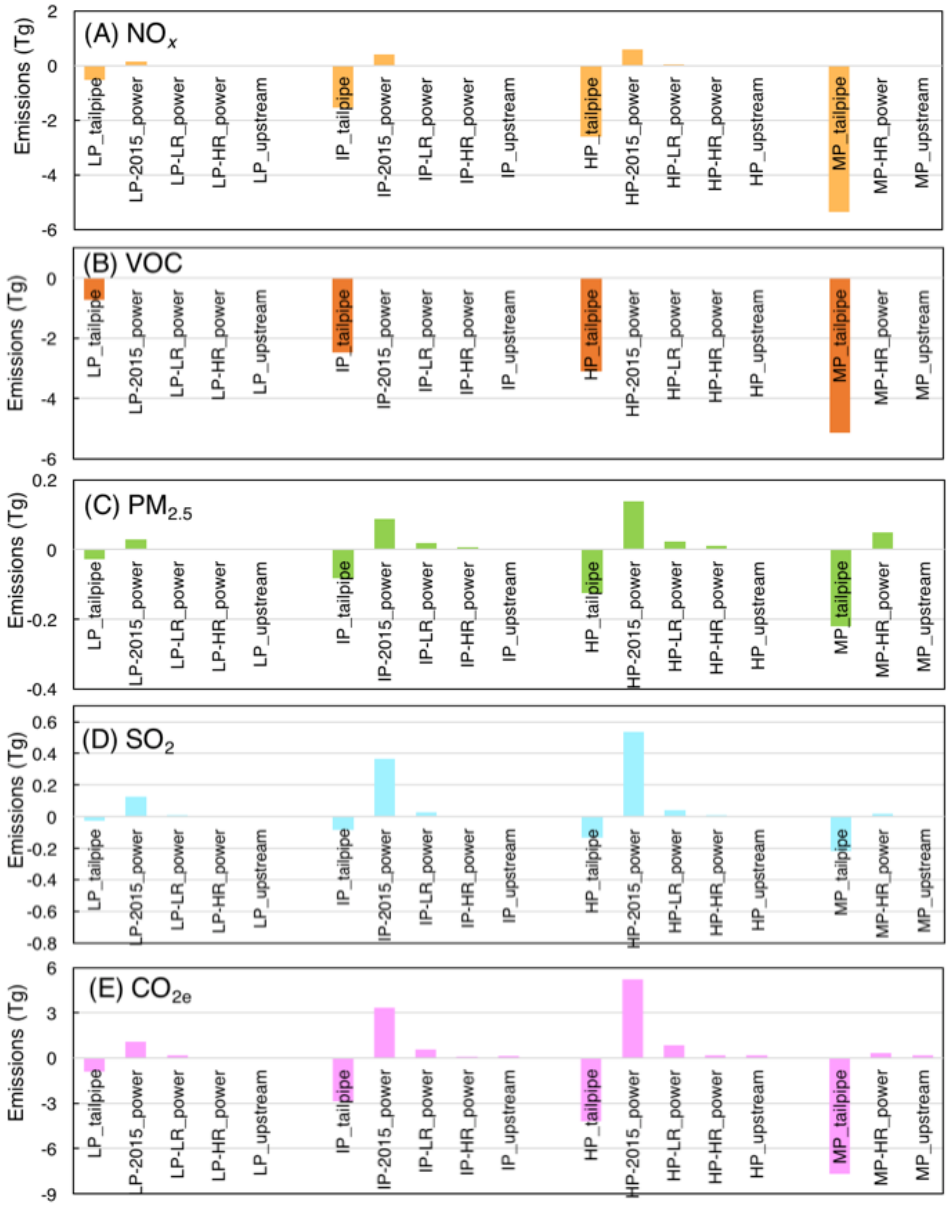

Figure 2.2. Changes in emissions from vehicle tailpipes, power generation, and upstream emissions from hydrogen and natural gas for each scenario. Emission changes of (A) NO_x, (B)VOC, (C) $PM_{2.5}$, (D) SO_2 and (E) CO_{2e}. For each pollutant we include emissions changes from conversion from the 2015 base case to each scenario. For each scenario we include 1) tailpipe emissions, 2) power generation emissions and 3) upstream emissions. Scenarios include combinations of vehicle sector emissions (LP, IP, HP, and MP) powered by 2015, low and high renewable penetration (LP and HR) electricity. Please see Table S6 for description of hydrogen production associated with each power scenario.

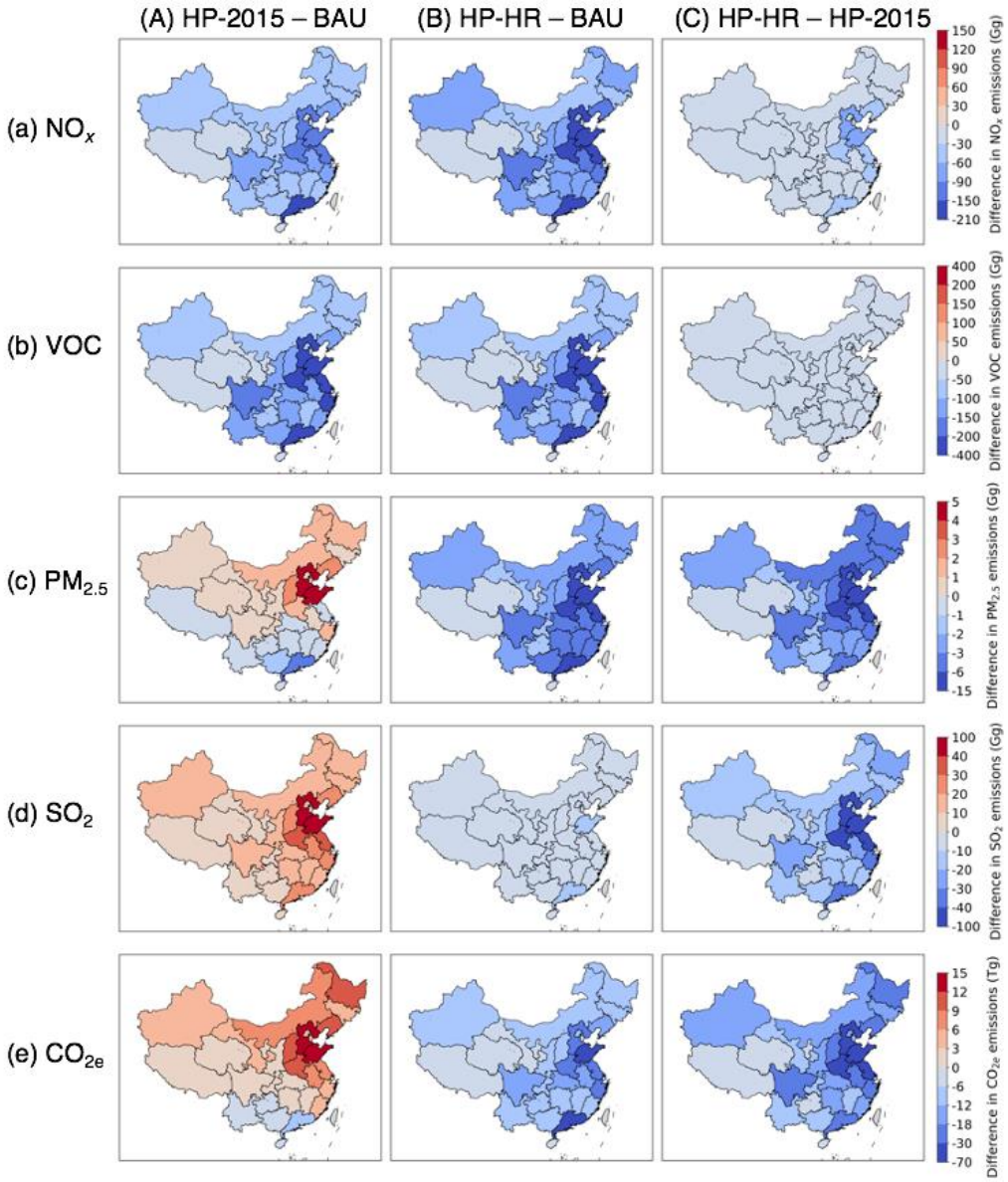

Figure 2.3. Comparison of provincial air pollutant and CO_{2e} emission changes from various AEV deployments and power sector decarbonization levels.

Provincial changes in (a) NO_x, (b) VOC, (c) $PM_{2.5}$, (d) SO_2 and (e) CO_{2e} emissions under (A) HP-2015 scenario (high AEV penetration with 2015 power mix) compared to the base case (2015 on-road transport with 2015 power mix); (B) HP-HR scenario (high AEV penetration with high renewable penetration) compared to the base case; and (C) Difference in air pollutants (a-d) and (e) CO_{2e} emissions between HP-HR scenario and HP-2015 scenario.

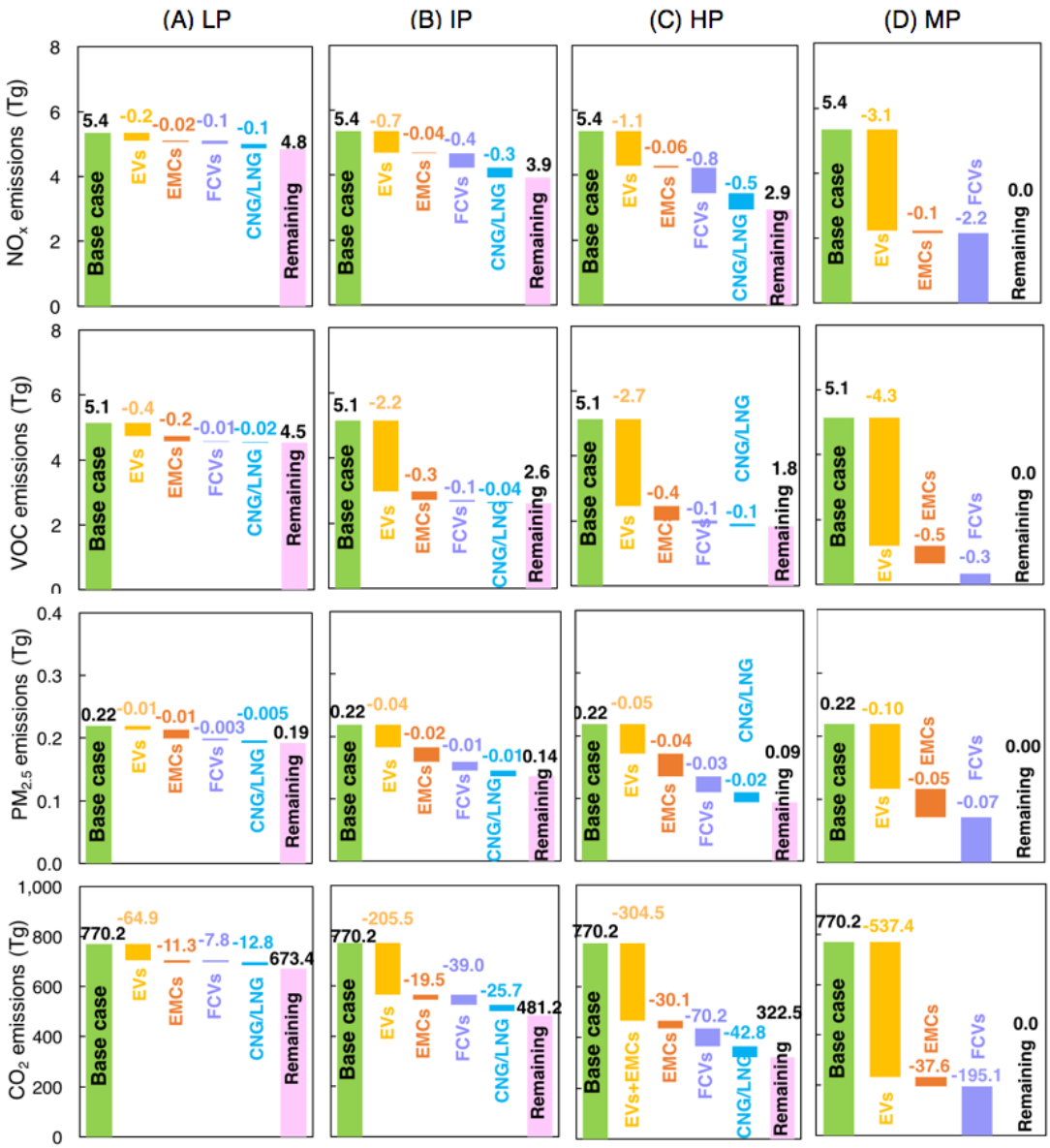

Figure 2.4. Contribution of EVs, EMCs, FCVs and CNG/LNG vehicles to total tailpipe emission reductions from on-road vehicles.

Yellow, purple, and blue bars and numbers indicate the reduced air pollutant and CO_{2e} emissions from EVs, EMCs, FCVs and CNG/LNG vehicles under (A) Low penetration (LP), (B) Intermediate penetration (IP), (C) High penetration (HP) and (D) Maximum penetration (MP) scenarios. The right pink bar in A-D represents the remaining tailpipe emissions from on-road vehicles. In (D) MP scenario, tailpipe emissions have been eliminated.

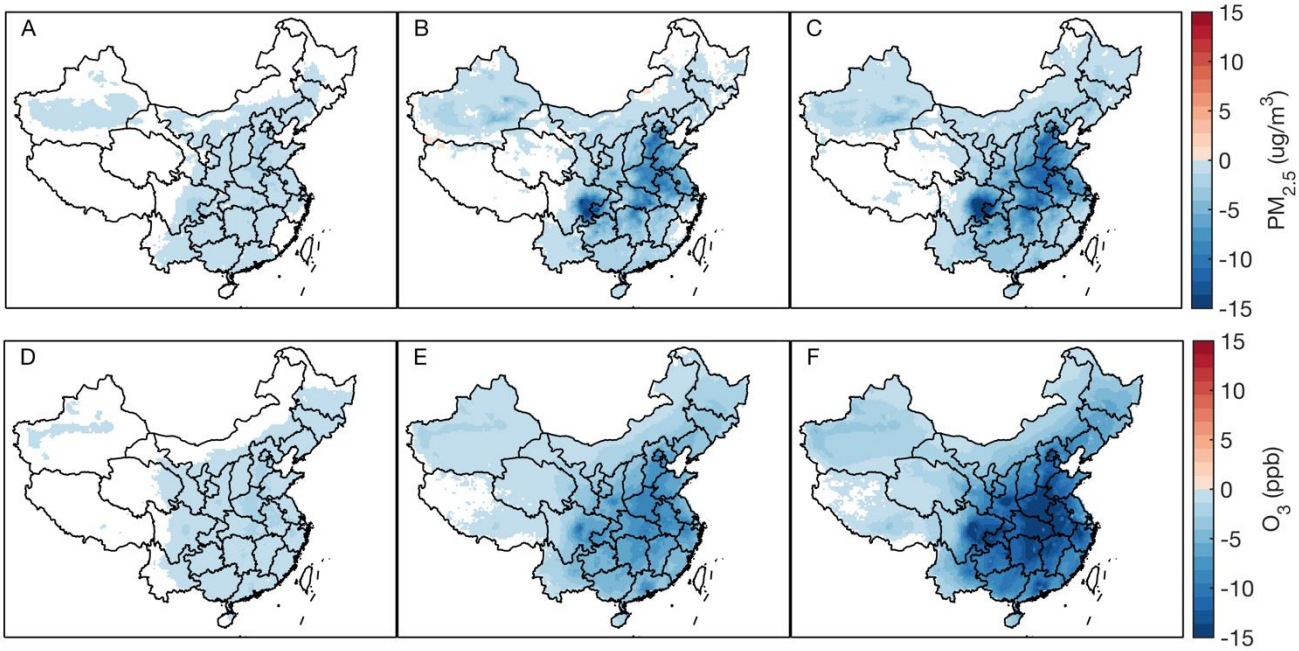

Figure 2.5. Reductions in simulated annual $PM_{2.5}$ and summer MDA8 O_3 concentrations. Reduced annual $PM_{2.5}$ concentrations from the (A) LP-LR, (B) HP-HR, and (C) MP-HR scenarios, respectively, compared to the base case. Reduced summer (May, July and September) MDA8 O_3 concentration from the (D) LP-LR, (E) HP-HR, and (F) MP-HR scenarios, respectively, compared to the base case. See Figure. S2.14 for MDA 8 O_3 concentration in January.

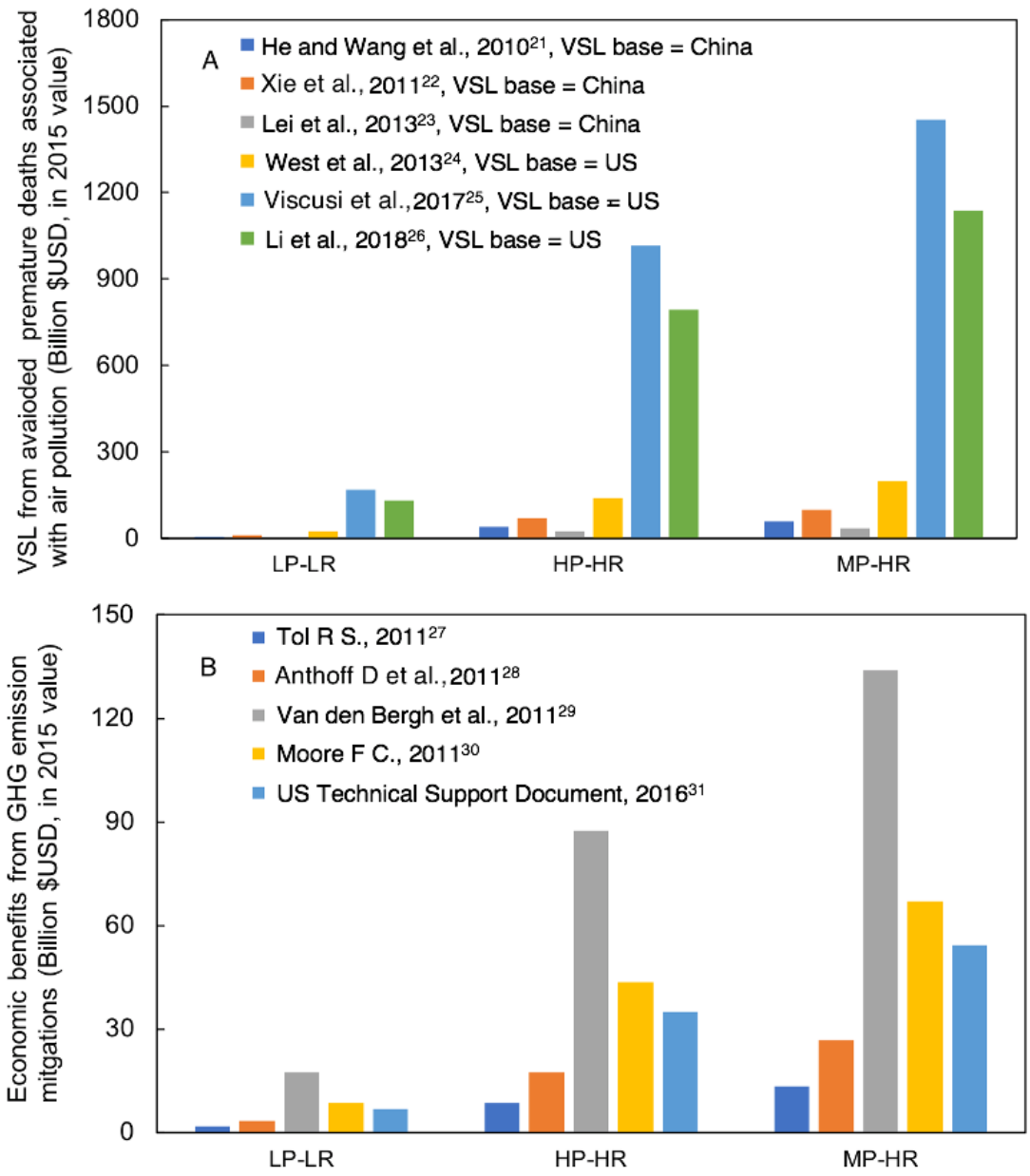

Figure 2.6. Comparison of economic benefits using valuations from various previous analyses

Data are shown for (A) VSL from avoided premature deaths and (B) economic benefits from reduced GHG emissions under LP-LR, HP-HR and MP-HR scenario, respectively. Colors indicate the data sources of VSL and SCC estimates.

Acknowledgements

This chapter is published as "Alternative energy vehicle deployment delivers climate, air quality and health co-benefits when coupled with decarbonizing power generation in China", co-authored by Feiqi Liu, Mi Zhou, Mingwei Li, Qiang Zhang, Denise L. Mauzerall, on One Earth, Aug 2021, 4: 1127-1140; DOI:10.1016/j.oneear.2021.07.007.

Reference

1. Yin, P., Brauer, M., Cohen, A.J., Wang, H., Li, J., Burnett, R.T., Stanaway, J.D., Causey, K., Larson, S., Godwin, W., et al. (2020). The effect of air pollution on deaths, disease burden, and life expectancy across China and its provinces, 1990–2017: an analysis for the Global Burden of Disease Study 2017. The Lancet Planetary Health 4, e386–e398.

2. Qiao, Q., and Lee, H. (2019). The Role of Electric Vehicles in Decarbonizing China's Transportation Sector.

3. MEIC, the Multi0resolution Emissions In China. http://www.meicmodel.org/.

4. Millikin, M. (2012). China publishes plan to boost fuel-efficient and new energy vehicles and domestic auto industry; targeting 500K PHEVs and EVs in 2015, rising to 2M by 2020. Green Car Congress.

5. Tessum, C.M., Hill, J.D., and Marshall, J. (2014). Life cycle air quality impacts of conventional and alternative light-duty transportation in the United States. PROC. NAT. ACAD. OF SCI. (U.S.A.) 111, 18490–18495.

6. Huo, H., Cai, H., Zhang, Q., Liu, F., and He, K. (2015). Life-cycle assessment of greenhouse gas and air emissions of electric vehicles: A comparison between China and the U.S. Atmospheric Environment 108, 107–116.

7. Tamayao, M.-A.M., Michalek, J.J., Hendrickson, C., and Azevedo, I.M.L. (2015). Regional Variability and Uncertainty of Electric Vehicle Life Cycle CO2 Emissions across the United States. Environ. Sci. Technol. 49, 8844–8855.

8. Yuksel, T., Tamayao, M.-A.M., Hendrickson, C., Azevedo, I.M.L., and Michalek, J.J. (2016). Effect of regional grid mix, driving patterns and climate on the comparative

carbon footprint of gasoline and plug-in electric vehicles in the United States. Environ. Res. Lett. 11, 044007.

9. Peng, W., Yang, J., Lu, X., and Mauzerall, D.L. (2018). Potential co-benefits of electrification for air quality, health, and CO2 mitigation in 2030 China. Applied Energy 218, 511–519.

10. Schnell, J.L., Naik, V., Horowitz, L.W., Paulot, F., Ginoux, P., Zhao, M., and Horton, D.E. (2019). Air quality impacts from the electrification of light-duty passenger vehicles in the United States. Atmospheric Environment 208, 95–102.

11. Liang, X., Zhang, S., Wu, Y., Xing, J., He, X., Zhang, K.M., Wang, S., and Hao, J. (2019). Air quality and health benefits from fleet electrification in China. Nature Sustainability 2, 962–971.

12. Peters, D.R., Schnell, J.L., Kinney, P.L., Naik, V., and Horton, D.E. (2020). Public Health and Climate Benefits and Trade-Offs of U.S. Vehicle Electrification. GeoHealth 4, e2020GH000275.

13. Granovskii, M., Dincer, I., and Rosen, M.A. (2006). Life cycle assessment of hydrogen fuel cell and gasoline vehicles. International Journal of Hydrogen Energy 31, 337–352.

14. Hao, H., Mu, Z., Liu, Z., and Zhao, F. (2018). Abating transport GHG emissions by hydrogen fuel cell vehicles: Chances for the developing world. Front. Energy 12, 466–480.

15. Chen, Y., Hu, X., and Liu, J. (2019). Life Cycle Assessment of Fuel Cell Vehicles Considering the Detailed Vehicle Components: Comparison and Scenario Analysis in China Based on Different Hydrogen Production Schemes. Energies 12, 1–24.

16. Schnell, J.L., Peters, D.R., Wong, D.C., Lu, X., Guo, H., Zhang, H., Kinney, P.L., and

Horton, D.E. (2021). Potential for Electric Vehicle Adoption to Mitigate Extreme Air Quality Events in China. Earth's Future 9, e2020EF001788.

17. Global EV Outlook 2020 (2020). 276.

18. Shen, W., Han, W., Wallington, T.J., and Winkler, S.L. (2019). China Electricity Generation Greenhouse Gas Emission Intensity in 2030: Implications for Electric Vehicles. Environ. Sci. Technol. 53, 6063–6072.

19. Wu, Y., Zhang, S., Hao, J., Liu, H., Wu, X., Hu, J., Walsh, M.P., Wallington, T.J., Zhang, K.M., and Stevanovic, S. (2017). On-road vehicle emissions and their control in China: A review and outlook. Science of The Total Environment 574, 332–349.

20. Liu, F., Mauzerall, D.L., Zhao, F., and Hao, H. (2021). Deployment of fuel cell vehicles in China: Greenhouse gas emission reductions from converting the heavy-duty truck fleet from diesel and natural gas to hydrogen. International Journal of Hydrogen Energy 46, 17982–17997.

21. Xing, J., Ding, D., Wang, S., Dong, Z., Kelly, J.T., Jang, C., Zhu, Y., and Hao, J. (2019). Development and application of observable response indicators for design of an effective ozone and fine-particle pollution control strategy in China. Atmos. Chem. Phys. 19, 13627–13646.

22. He, J., and Wang, H. (2010). The value of statistical life: a contingent investigation in China (The World Bank).

23. Xie, X. (2011). The value of health: method for environmental impact assessment and strategis for urban air pollution control.

24. Lei Y, and Ho M S (2013). The Valuation of Health Damages, in Clearer Skies Over

China: Reconciling Air Quality, Climate, and Economic Goals (London: The MIT Press).

25. West, J.J., Smith, S.J., Silva, R.A., Naik, V., Zhang, Y., Adelman, Z., Fry, M.M., Anenberg, S., Horowitz, L.W., and Lamarque, J.-F. (2013). Co-benefits of mitigating global greenhouse gas emissions for future air quality and human health. Nature Climate Change 3, 885–889.

26. Viscusi, W.K., and Masterman, C.J. (2017). Income Elasticities and Global Values of a Statistical Life. J. Benefit Cost Anal. 8, 226–250.

27. Li, M., Zhang, D., Li, C.-T., Mulvaney, K.M., Selin, N.E., and Karplus, V.J. (2018). Air quality co-benefits of carbon pricing in China. Nature Climate Change 8, 398–403.

28. Tol, R. (2011). The Social Cost of Carbon. Annual Review of Resource Economics 3, 419–443.

29. Anthoff, D., Rose, S., Tol, R.S.J., and Waldhoff, S.T. (2011). Regional and Sectoral Estimates of the Social Cost of Carbon: An Application of Fund. SSRN Journal.

30. van den Bergh, J.C.J.M., and Botzen, W.J.W. (2014). A lower bound to the social cost of CO2 emissions. Nature Clim Change 4, 253–258.

31. Moore, F.C., and Diaz, D.B. (2015). Temperature impacts on economic growth warrant stringent mitigation policy. Nature Climate Change 5, 127–131.

32. Technical Support Document: Technical Update of the Social Cost of Carbon for Regulatory Impact Analysis Under Executive Order 12866 (Interagency Working Group on Social Cost of Greenhouse Gases, US Government, 2016).

33. Millar, R.J., Fuglestvedt, J.S., Friedlingstein, P., Rogelj, J., Grubb, M.J., Matthews, H.D., Skeie, R.B., Forster, P.M., Frame, D.J., and Allen, M.R. (2017). Emission budgets and

pathways consistent with limiting warming to 1.5 C. Nature Geosci 10, 741–747.

34. Tokarska, K.B., and Gillett, N.P. (2018). Cumulative carbon emissions budgets consistent with 1.5 C global warming. Nature Climate Change 8, 296–299.

35. Office of the State Council (2020). The development plan of new energy vehicle industry from 2021-2035. http://www.gov.cn/zhengce/content/2020-11/02/content_5556716.htm.

36. China's subsideies to fast-track development of fuel cell vehicles. https://asia.nikkei.com/Business/Automobiles/China-s-subsidies-to-fast-track-development-of-fuel-cell-vehicles (2020).

37. China Hydrogen Alliance. White paper on China's hydrogen energy and fuel cell industry. (2019). (2019).

38. Zheng, B., Tong, D., Li, M., Liu, F., Hong, C., Geng, G., Li, H., Li, X., Peng, L., Qi, J., et al. (2018). Trends in China's anthropogenic emissions since 2010 as the consequence of clean air actions. Atmospheric Chemistry and Physics 18, 14095–14111.

39. Anenberg, S.C., Miller, J., Minjares, R., Du, L., Henze, D.K., Lacey, F., Malley, C.S., Emberson, L., Franco, V., Klimont, Z., et al. (2017). Impacts and mitigation of excess diesel-related NO x emissions in 11 major vehicle markets. Nature 545, 467–471.

40. Li, M., Liu, H., Geng, G., Hong, C., Liu, F., Song, Y., Tong, D., Zheng, B., Cui, H., Man, H., et al. (2017). Anthropogenic emission inventories in China: a review. National Science Review 4, 834–866.

41. Yang, D., Zhang, S., Niu, T., Wang, Y., Xu, H., Zhang, K.M., and Wu, Y. (2019). High-resolution mapping of vehicle emissions of atmospheric pollutants based on large-scale,

real-world traffic datasets. Atmos. Chem. Phys. 19, 8831–8843.

42. Reinventing Fire: China. A roadmap for China's Revolution in Energy Consumption and Production to 2050. (2019).

43. China National Renewable Energy Centre (2018). China Renewable Energy Outlook 2018.

44. Zhang, Q., Streets, D.G., Carmichael, G.R., He, K.B., Huo, H., Kannari, A., Klimont, Z., Park, I.S., Reddy, S., Fu, J.S., et al. (2009). Asian emissions in 2006 for the NASA INTEX-B mission. Atmos. Chem. Phys. 9, 5131–5153.

45. Chen, X., Zhang, H., Xu, Z., Nielsen, C.P., McElroy, M.B., and Lv, J. (2018). Impacts of fleet types and charging modes for electric vehicles on emissions under different penetrations of wind power. Nature Energy 3, 413–421.

46. Zhang, S., Niu, T., Wu, Y., Zhang, K.M., Wallington, T.J., Xie, Q., Wu, X., and Xu, H. (2018). Fine-grained vehicle emission management using intelligent transportation system data. Environmental Pollution 241, 1027–1037.

47. Innovation Center for Energy and Transportation (2018). 2018 New Data Analysis on Real-world Driving and Fuel Consumption for Passenger Cars in China. https://cdn.xiaoxiongyouhao.com/partner/icet/icet_xxyh_2018.pdf.

48. Tong, F., Jaramillo, P., and Azevedo, I.M.L. (2015). Comparison of Life Cycle Greenhouse Gases from Natural Gas Pathways for Medium and Heavy-Duty Vehicles. Environ. Sci. Technol. 49, 7123–7133.

49. Qin, Y., Höglund-Isaksson, L., Byers, E., Feng, K., Wagner, F., Peng, W., and Mauzerall, D.L. (2018). Air quality–carbon–water synergies and trade-offs in China's natural gas

industry. Nature Sustainability 1, 505.

50. Guo, Y., Tian, J., and Chen, L. (2020). Managing energy infrastructure to decarbonize industrial parks in China. Nature Communications 11, 981.

51. Lamarque, J.-F., Emmons, L.K., Hess, P.G., Kinnison, D.E., Tilmes, S., Vitt, F., Heald, C.L., Holland, E.A., Lauritzen, P.H., Neu, J., et al. (2012). CAM-chem: description and evaluation of interactive atmospheric chemistry in the Community Earth System Model. Geoscientific Model Development 5, 369–411.

52. Mlawer, E.J., Taubman, S.J., Brown, P.D., Iacono, M.J., and Clough, S.A. (1997). Radiative transfer for inhomogeneous atmospheres: RRTM, a validated correlated-k model for the longwave. Journal of Geophysical Research: Atmospheres 102, 16663–16682.

53. Chou, M.-D., and Suarez, M.J. (1994). An Efficient Thermal Infrared Radiation Parameterization For Use In General Circulation Models.

54. Morrison, H., and Pinto, J.O. (2005). Mesoscale Modeling of Springtime Arctic Mixed-Phase Stratiform Clouds Using a New Two-Moment Bulk Microphysics Scheme. J. Atmos. Sci. 62, 3683–3704.

55. Chen, F., and Dudhia, J. (2001). Coupling an Advanced Land Surface–Hydrology Model with the Penn State–NCAR MM5 Modeling System. Part I: Model Implementation and Sensitivity. Mon. Wea. Rev. 129, 569–585.

56. Hong, S.-Y., Noh, Y., and Dudhia, J. (2006). A New Vertical Diffusion Package with an Explicit Treatment of Entrainment Processes. Mon. Wea. Rev. 134, 2318–2341.

57. Zaveri, R.A., Easter, R.C., Fast, J.D., and Peters, L.K. (2008). Model for Simulating Aerosol Interactions and Chemistry (MOSAIC). Journal of Geophysical Research. D.

(Atmospheres), 113(D13):Art. No. D13204 113.

58. Zaveri, R.A., and Peters, L.K. (1999). A new lumped structure photochemical mechanism for large-scale applications. Journal of Geophysical Research 104, 30.

59. Guenther, A., Karl, T., Harley, P., Wiedinmyer, C., Palmer, P.I., and Geron, C. (2006). Estimates of global terrestrial isoprene emissions using MEGAN (Model of Emissions of Gases and Aerosols from Nature). Atmos. Chem. Phys., 30.

60. Jones, S.L., Adams-Selin, R., Hunt, E.D., Creighton, G.A., and Cetola, J.D. (2012). Update on modifications to WRF-CHEM GOCART for fine-scale dust forecasting at AFWA. AGU Fall Meeting Abstracts 33, A33D-0188.

61. Chen, D., Liu, Z., Fast, J., and Ban, J. (2016). Simulations of sulfate–nitrate–ammonium (SNA) aerosols during the extreme haze events over northern China in October 2014. Atmospheric Chemistry and Physics 16, 10707–10724.

62. Xing, J., Lu, X., Wang, S., Wang, T., Ding, D., Yu, S., Shindell, D., Ou, Y., Morawska, L., Li, S., et al. (2020). The quest for improved air quality may push China to continue its CO2 reduction beyond the Paris Commitment. PNAS 117, 29535–29542.

63. Liu, M., Huang, X., Song, Y., Tang, J., Cao, J., Zhang, X., Zhang, Q., Wang, S., Xu, T., Kang, L., et al. Ammonia emission control in China would mitigate haze pollution and nitrogen deposition, but worsen acid rain. 6.

64. Burnett, R., Chen, H., Szyszkowicz, M., Fann, N., Hubbell, B., Pope, C.A., Apte, J.S., Brauer, M., Cohen, A., Weichenthal, S., et al. (2018). Global estimates of mortality associated with long-term exposure to outdoor fine particulate matter. PNAS 115, 9592–9597.

65. Turner, M.C., Jerrett, M., Pope, 3rd CA, Krewski, D., Gapstur, S.M., Diver, W.R., Beckerman, B.S., Marshall, J.D., Su, J., Crouse, D.L., et al. (2016). Long-Term Ozone Exposure and Mortality in a Large Prospective Study. Am J Respir Crit Care Med 193, 1134–1142.

66. Romeder, J.M., and McWhinnie, J.R. (1977). Potential years of life lost between ages 1 and 70: an indicator of premature mortality for health planning. Int J Epidemiol 6, 143–151.

67. Life expectancy at birth, total (years). United Nations World Population Prospects. https://data.worldbank.org/indicator/SP.DYN.LE00.IN?view=chart

68. Center for International Earth Science Information Network - CIESIN Columbia University, Gridded Population of the World, Version 4 (GPWv4): Population Count Adjusted to Match 2015 Revision of UN WPP Country Totals. (2016).

69. United Nations Department of Economic and Social Affairs, Population Division 2019 World Population Prospects: the 2019 Revision (https://esa.un.org/unpd/wpp/Download/ Standard/Population/) (Accessed: 19 AUG 2020).

70. Viscusi, W.K., and Aldy, J.E. (2003). The Value of a Statistical Life: A Critical Review of Market Estimates Throughout the World. Journal of Risk and Uncertainty 27, 5–76.

71. Hammitt, J.K., and Robinson, L.A. (2011). The Income Elasticity of the Value per Statistical Life: Transferring Estimates between High and Low Income Populations. Journal of Benefit-Cost Analysis 2, 1–29.

Chapter 3: Heterogeneous effects of battery storage deployment strategies on decarbonization of provincial power systems in China

1. Introduction

The carbon dioxide (CO_2) emissions from China's power sector reached ~5030Tg in 2020 (IEA, 2021), accounting for more than 40% of China's energy-related CO_2 emissions or 14% of global energy-related CO_2 emissions (IEA, 2021). Decarbonizing China's power sector is essential for decarbonization of China's economy and critical to keep the global temperature increase below 2 C. In 2020, China has pledged to peak its CO_2 emissions by 2030 and achieve carbon neutrality by 2060. The deep decarbonization of electricity generation plays a very significant role in achieving this goal.

To achieve China's decarbonization goal while meeting its increasing electricity demand, renewable energy must be deployed and replace coal-fired power generations. One of the main challenges of an increasing role for wind and solar generation in the power system is that they are variable – the energy depends on the weather and time of day. There are various technologies that can smooth the fluctuations of wind and solar power, with energy storage being most promising. Many studies (de Sisternes, et al., 2016; Arbabzadeh, et al., 2019; Ziegler, et al., 2019, He et al., 2020, Dowling et al., 2020, Bistline et al., 2020 and Sepulveda et al., 2021) have found that energy storage could play an important role in decarbonizing the power system by offering a new, carbon-free source of operational flexibility and facilitating the integration of variable renewable energy sources. Battery storage has fast response, large energy capacity and can be deployed

flexibly. What is more, the cost of battery storage has decreased very quickly in recent years, which makes it economically feasible for large-scale deployment. Thus, in this study we focus on battery storage as the main source of energy storage for balancing variable renewable generation to achieve decarbonization goals.

While the benefits of battery storage are clear, there are multiple ways to deploy batteries. Knowledge of the advantages and disadvantages as well as the impacts and costs of these strategies are necessary to allow policy makers to identify the best options. Intuition might indicate that if more renewables and batteries are used in the power system, the system cost will increase due to the high cost of renewables and batteries, and CO_2 emissions will decrease, since the power system will be cleaner. However, the effect of battery storage deployment on CO_2 emissions is more complicated. Craig et al. (2018) showed that deploying battery storage would enable a shift of generation from gas-fired to coal-fired power and therefore increase CO_2 emissions in the power system in the Electricity Reliability Council of Texas (ERCOT). Hittinger et al (2017) illustrated that total CO_2 emissions are lower when storage must be charged from collocated wind than when it is charged directly from the grid. These studies focus on either small local regions or a short period of time in the U.S. The effects of different storage deployment strategies on CO_2 emissions at the national/provincial level in China and at multi-year scales is underexplored in the literature.

China's government has encouraged various battery storage deployment strategies. Since 2021, local governments and power grid enterprises put forward "centralized renewable energy + energy storage" development incentive policies (NDRC, 2021; NDRC,

2022). These batteries are referred to as 'Renewable-connected' batteries since they are co-located with renewable generation and charged only from co-located renewables (wind or solar). China's government also set a goal of increasing 'Grid-connected' and 'Demand-side' battery storage to achieve a flexible and robust grid system. Demand-side battery storage is deployed in local power grids and is connected to demand loads, such as industrial factories or commercial buildings, usually to act as an emergency energy source and to achieve power arbitrage. For instance, electric vehicles could provide mobile battery storage and be connected to commercial buildings or residential apartments as Demand-side batteries. Due to safety concerns and power line deployment, the distribution power grid cannot transmit power back to the transmission power grid in China, so that the energy stored in demand side batteries can only meet local demands. Grid-connected battery storage is the most flexible type of storage as it is connected to the central grid. Electricity used to charge Grid-connected storage could be from either fossil fuels or non-fossil fuels, such as wind, solar and nuclear power, and the stored energy can be discharged back to the central grid.

To understand how different types of battery storage configurations affect power system decarbonization, our research first explores the effects of battery storage deployment strategies on China's power system costs and CO_2 emissions. We begin with scenario development of three nationally uniform battery storage deployment strategies, two carbon prices and three battery cost trajectories (Table 3.1A) (See "Scenario design" in the Methods). Figure 3.1 depicts the three nationally uniform battery storage deployment strategies. Carbon prices and battery cost trajectories are described in Table

3.1A. We mainly analyze the scenarios in bold. For each scenario, our method chooses the optimal installed power, battery capacity, power generation and interprovincial transmission that minimize system costs through an improved capacity expansion power system model (SWITCH-China) (See Methods). In other words, our results provide policy makers with the best location, timing, and scale of installing renewable generators and battery storage for every scenario in China within the next 30 years. To further understand the effect of various battery storage deployment strategies on different provinces, we examine a "Mixed" option that allows each province to install all three types of battery storage – RE-connected, Grid-connected, and Demand-side batteries (Table 3.1B). We combine the mixed strategy with both low and high carbon prices as well as a rapid battery cost decrease to set up two additional scenarios – Mixed-Low-R and Mixed-High-R. These scenarios allow each province to utilize all three battery deployment scenarios differ from the scenarios that require each province to utilize only one type of battery storage. We then compare the system cost and CO_2 emissions of the optimal solutions at national/provincial levels across scenarios.

The results indicate that national electricity transmission capacities and costs, as well as provincial coal-fired power generation vary depending on the battery deployment strategies. RE-connected batteries require the lowest transmission capacity among the three battery strategies from 2025-2050, which result in the lowest transmission costs. Also, RE-connected batteries will decrease coal-fired power generation in provinces with abundant renewable resources by up to 9% compared with Grid-connected batteries. However, RE-connected batteries will increase coal-fired power generation by up to 69%

in provinces with limited renewable resources compared with Grid-connected batteries. Demand-side and RE-connected batteries have opposite effects on provincial coal-fired power generation and national transmission when each are compared with Grid-connected batteries. Our results identify renewable resources, the availability of transmission, and the characteristics of demand that determine the system costs and CO_2 emission of provincial heterogeneous battery storage deployment strategies.

2. Results

2.1 National transmitted power and transmission costs

Large-scale deployment of battery storage will require greater electricity transmission capacity. However, depending on the chosen battery deployment strategy, necessary transmission capacity and costs will vary. At the national level between 2025-2050, we find RE-connected batteries reduce the most needed transmission capacity of the three battery deployment strategies (Figure 3.2 A). This is because the locally generated renewable power meets a larger portion of the local demand compared with the other strategies so that less power is transmitted. We also find that peak transmitted power from RE generation is reduced the most (Figure 3.2 B) resulting in the lowest transmission costs each year (Figure 3.2 D).

The Demand-side battery strategy requires the highest transmission capacity (Figure 3.2 A) which results in the highest transmission costs in each studied year (Figure 3.2 D). Figure 1B shows the transmission power profile in an example of two days in 2050. We find that the Demand-side battery strategy has the largest peak transmission and largest variation, indicating its need for the largest transmission capacity, which can be verified

from Figure 3.2A. The areas under the curves in Figure 2B represent transmitted electricity and the Demand-side battery strategy transmits less electricity than the Grid-connected battery strategy, even though its peak transmission is higher. Figure 3.2 C also shows that the Grid-connected battery strategy has the highest total transmitted electricity in both 2045 and 2050.

2.2 Trade-offs between national carbon emissions and power system costs

In general, trade-offs between carbon emissions and electricity costs occur in the three battery storage deployment strategies. With both uniform low carbon prices and rapid battery storage cost decreases across deployment strategies, Figure 3 shows the annual national average CO_2 emissions and electricity costs per MWh of the three battery storage deployment strategies. The electricity cost of each strategy is calculated as the annual system costs divided by the annual generated electricity. For all three strategies, as decarbonization rates increase over the years, CO_2 emissions decrease rapidly, and electricity costs decrease due to the decreased costs of renewable energy. Comparing the three strategies, CO_2 emissions are similar, but electricity costs decrease rapidly from 2035 to 2050. Electricity costs of the RE-connected battery strategy and the Grid-connected strategy remain similar, while the Demand-side battery strategy costs are much higher. In 2050, system costs of the Demand-side battery strategy are ~13% higher than Grid-connected or RE-connected battery strategies (Figure 3.3). The total carbon emissions and power system costs are shown in Table S3.2 and S3.3. We also find that high carbon prices and rapid decrease of battery storage costs play key roles in large-scale battery deployment and a rapid decarbonization of the power system (See Supplementary Note

3.3 and 3.4).

2.3 Effects of battery storage deployment strategies depend on provincial resources

The results show that nationally uniform strategies have varying effects on individual provinces. We use the Grid-connected strategy as the baseline scenario since battery storage in this strategy can be flexibly used on either the supply or demand side. We find that the effects of the RE-connected and Demand-side battery strategies mainly depend on the characteristics of provincial energy generation and demand. We observe that certain provinces' total local power generation exceeds their total demand; we refer to these provinces as supply provinces. Their optimal local coal-fired power generation increases under the RE-connected battery strategy and decreases under the Demand-side battery strategy, relative to the Grid-connected strategy. On the other hand, we call provinces where local power generation is less than total demand, demand provinces, and the optimal local coal-fired power generation decreases with a RE-connected battery strategy and increases with a Demand-side battery. Figure S3.9 shows distribution of supply and demand provinces under most situations. We explain the reasons for these observations in the following paragraphs using an energy balance.

Each province balances energy as shown in Equation (1) and (2), which is the key to explaining the effects of battery storage deployment strategies on power generation and CO_2 emissions. In equation (2), the left-hand side consists of local dispatched electricity, battery charge and discharge as well as net transmitted electricity into the province. The sum of these three terms must balance the demand of the province in each time step from 2025 to 2050, and thus the energy balance holds on an annual scale. Analyzing the

annual energy balance provides insight into the effects of battery storage deployment strategies.

$$Dispatched\ electricity = Generated\ electricity - Curtailed\ electricity \quad (1)$$

$$Dispatched\ electricity + (Battery\ discharge - battery\ charge) + Net\ transmitted\ electricity = Demand \quad (2)$$

We choose Chongqing and western Inner Mongolia as a typical demand and supply province, respectively, in 2040, a time of considerable difference between these two provinces. Figure 3.3 shows the annual dispatched power of Chongqing and western Inner Mongolia in 2040. In 2040, the electricity demand of Chongqing is more than twice its power generation. The lack of power generation is fulfilled by power transmitted from other provinces. At this time, the power generation of western Inner Mongolia is around 6-8 times its electricity demand. The excess power generation is transmitted to other provinces through transmission lines. As the demand of a province is the same across the three battery strategies and power balancing must be satisfied, the strategies can only affect power generation, battery charge and discharge, and net transmitted power on the left-hand side of Equation (1).

The Grid-connected strategy results in supply province batteries being charged by power generated in the supply province. Depending on the province, this power generation could be dominated by fossil or non-fossil generation. In a demand province, batteries will be charged with a power mix that is a combination of power generated locally and power transmitted from other provinces.

Unlike the Grid-connected strategy, the RE-connected battery strategy includes the constraint that batteries can only be charged by local renewable generators. This

constraint leads to a reduction in installed batteries as well as a reduction in net transmitted power to demand provinces, as they cannot rely on transmitted power to charge their batteries. Thus, we observe that in Chongqing province, battery discharge in the year 2040 decreases from 23TWh in the Grid-connected strategy to 3TWh in the RE-connected strategy, and net transmitted power decreases from 79TWh to 48TWh, as the RE-connected constraint is added (Figure 3.3). To balance the demand, the local fossil power generation increases from 72TWh to 95TWh. As coal is the cheapest option, coal-fired power generation increases from 32TWh to 54TWh, accounting for 96% of the power generation increase. As demand provinces require less transmitted power from supply provinces, transmission from supply provinces decreases. In fact, we observe that while western Inner Mongolia supplies 2952TWh in the Grid-connected strategy, it only supplies 2540TWh in the RE-connected battery strategy. In order to achieve power balance in western Inner Mongolia, fewer batteries and less power generation are needed as the additional constraint is added.

The effect of the Demand-side battery strategy on supply and demand provinces is opposite to that of the RE-connected battery strategy. Relative to the Grid-connected strategy, in the Demand-side strategy batteries continue to be charged from the grid but we add a demand side constraint that battery storage can only be discharged to local distribution power grids. As supply provinces cannot discharge battery power to the central grid in this strategy, we expect a decrease in their optimal battery storage. In fact, in Figure 3.4, we observe a decrease from 105TWh to 76TWh in western Inner Mongolia as the demand side constraint is added. This decreased battery discharge has two effects. First, RE needs to be transmitted immediately to demand provinces rather than stored in

batteries, which will increase the need for additional electricity transmission to serve peak generation periods. Second, during periods of low generation in supply provinces and high demand in demand provinces both RE power generation and battery discharge decrease, so more fossil fuel power generation is required to balance the demand. Therefore, we observe an increase in coal power generation in western Inner Mongolia from 958TWh to 1206TWh as the demand side constraint is added. As for demand provinces like Chongqing, as more power is transmitted from supply provinces (from 154TWh to 164TWh), more batteries are needed to store this energy, and thus the local power generation will decrease (from 72TWh to 65TWh).

Figure 3.5 shows the annual coal-fired power generation and power discharged from battery storage from 2025-2050. Over each time step analyzed, the RE-connected battery strategy decreases coal power generation in the supply province western Inner Mongolia and increases it in a demand province Chongqing, while the Demand-side battery strategy has the opposite effect. The Grid-connected battery strategy typically falls between the RE-connected and Demand-side battery strategies. Our results also indicate that as carbon prices increase over time, coal-fired generation decreases and battery storage increases, as expected (Table S3.1). Dispatched power and load profiles from 2025 to 2050 for Chongqing and western Inner Mongolia under three battery deployment strategies are shown in Figure S.3.10 and S.3.11.

2.4 Provincial heterogeneous battery storage deployment strategies

By comparing the total costs of various battery deployment strategies, we observe that the Mixed strategy has the lowest total cost. This is expected since the Mixed strategy

allows all three types of battery deployment strategies so that the optimized solutions of allowing only RE-connected, Grid-connected, or Demand-side batteries are feasible solutions in the optimization problem of the mixed strategy. As this is a minimization problem with the total cost as the objective, the optimized solution of the Mixed strategy would have a total cost not greater than any of the feasible solutions. Thus, the result of the Mixed strategy has the lowest total cost as compared to the results of constraining the provinces to each strategy.

The Mixed strategy reconfirms our observation in the previous section – the optimal battery deployment strategy in each province depends on the characteristics of provincial energy generation and demand, as well as renewable resources within the province. By allowing each province to utilize the battery deployment strategy of their choice via cost minimization, we gain insights from the deployment strategy portfolio of each province – the portions of each type of batteries in the optimized solution (Figure 3.6 and Figure S.3.13). We find that Chongqing, a typical demand province, installs 100% Demand-side batteries in both Mixed-Low-R and Mixed-High-R. This is consistent with Figure 3.4B which explored battery deployment choices under a uniform national strategy. In the nationally uniform strategy Chongqing also installs far more Demand-side than Grid-connected or RE-connected batteries. In western Inner Mongolia, a typical supply province, a majority of the installed batteries are RE-connected batteries – 62% in Mixed-Low-R and 79 % in Mixed-High-R. In both scenarios, only 3% of the installed batteries are Demand-side batteries. This result indicates that the most cost-effective portfolio for supply provinces is to have more RE-connected batteries and less Demand-side batteries. This is also consistent with Figure 3.4B. In the uniform national strategies for western

Inner Mongolia, the installed RE-connected batteries have the largest battery power discharge whereas the Demand-side batteries have the least.

2.5 High carbon prices can drive decarbonization of China's power system

Decarbonization of the power system can be driven by regulatory actions (e.g., requiring the closure of old inefficient power plants) or by market mechanisms like emission trading and carbon prices. In our model, the decarbonization rates are driven by carbon prices. Figure 3.7 presents the effect of low and high carbon prices that both increase over time on annual CO_2 emissions, optimal power capacity and generation, battery storage and system costs. The optimal system is one which minimizes total costs. Total costs equal the physical system costs plus CO_2 emissions weighted by carbon price.

Here, we highlight several observations from Figure 3.7. First, we find that in each year, higher carbon prices indeed result in higher penetration of renewables (rapid decarbonization rates) than lower carbon prices with particularly rapid growth in solar generation because the capital costs of solar are lower than those of wind (Figure 3.7 A and 3.7 B). To balance the increased variable renewable generation, more battery storage must be installed (Figure 3.7 E) thus leading to greater battery storage deployment under high and rapidly increasing carbon prices. Second, Figure 3.7 E shows that for both low and high carbon prices, the deployment of 4-hour battery storage is favored over 1-hour and 10-hour battery storage. This is because long duration energy storage is needed to better utilize intermittent renewable energy, but storage in 10-hour batteries is more costly than in 4-hour batteries per kW. Nevertheless, the capacity of long duration battery storage (10h) increases more when carbon prices are high than when they are low, except

in 2050. Third, high carbon prices will accelerate the decarbonization of the power system (Figure 3.7A and 3.7 B) while only marginally increasing system costs (Figure 3.7 F).

However, battery storage plays an increasingly important role over time as renewable generation increases (Figure S3.7 and S3.8) and CO_2 prices increase (Fig 3.7 A). In 2030, few batteries are available to store excess solar and wind electricity. By 2050 grid-connected batteries store around half the power generated by renewables and discharge the stored power to the grid primarily during the evening peak period (after 4pm) as shown in Figure 3.8.

2.6 The effect of battery storage cost reduction trajectories on national installed battery storage capacity and CO_2 emissions

At each time step, the evolution of battery costs has significant impacts on installed capacity of battery storage, CO_2 emissions, and electricity costs. Other than the three cost trajectories specified in our scenarios (Base case, Moderate decrease of battery storage costs and Rapid decrease of battery storage costs), we also examine an extreme no-storage scenario where we assume the cost of battery storage is prohibitively expensive, and thus no battery storage is built in the power system. From Figure 3.9, we observe that both CO_2 emissions and electricity costs under the no-battery storage scenario are the highest of all battery storage scenarios. The cost trajectories with the lowest prices (R) results in the highest installed capacity of battery storage, lowest CO_2 emissions, electricity costs and vice versa under both low and high carbon prices. This indicates that success in decreasing battery production costs will have valuable benefits for both CO_2 mitigation and electricity cost reductions. We conclude that the cost trajectories with the lowest

(rapid cost decrease) storage price along with high carbon prices achieve the lowest CO_2 emissions across all eight scenarios shown in Figure 3.9.

3. Discussion

Batteries will play a key role in the rapid decarbonization of the power system. With increasing penetration of renewables, batteries can balance short-term electricity supply and demand while providing load shifting to fill gaps during peak demand while improving grid stability and providing consistent current. Batteries rapidly decreasing costs provide opportunities for rapid scale-up. However, how to best deploy battery storage at the sub-national level remains an open question.

Our results indicate that the effects of battery deployment strategies on national electricity transmission and provincial coal-fired power generation varies by province. Compared to nationally uniform Grid-connected batteries, we find that optimally deployed RE-connected batteries effectively reduce peak and total electricity transmission with annual transmission costs reduced by ~9%. Also, coal-fired power generation decreases by ~9% in provinces with abundant renewable resources. This occurs because provinces with abundant renewable energy using renewable connected batteries transmit less locally generated electricity to other provinces than they would under the grid connected scenario. Less transmission leads to less local coal power generation because less local power generation is required. However, coal-fired power generation is increased by up to 69% in provinces with limited renewable resources. This is because these provinces rely on electricity transmitted from other provinces and less transmission requires more local power generation to balance the demand. As renewable

resources are limited and coal-fired electricity is the cheapest alternative, an increase in coal-fired power generation is observed in these provinces.

Nationally uniform Demand-side and RE-connected batteries have opposite effects on provincial coal-fired power generation and national transmission when they are compared with optimally deployed Grid-connected batteries (Figure 3.2). Coal-fired power generation is increased by up to 26% in provinces with abundant renewable resources that use demand side batteries. This is because fewer batteries are installed as they are connected to the local grid and cannot discharge to the central grid. With fewer batteries to smooth the intermittency of the renewable generation, more coal-fired electricity is required to meet local demand. However, coal-fired power generation is decreased by up to 22% in provinces with limited renewable resources since more power is transmitted into these provinces and less local power generation is needed.

A rapid decrease of battery storage costs will significantly increase the scale of battery deployment and correspondingly reduce CO_2 emissions. We also find that high carbon prices will accelerate decarbonization levels while only marginally increasing system costs. With high carbon prices, carbon neutrality of the power sector can be achieved by 2050 if battery costs decrease moderately to rapidly.

In this study, we use carbon price as a driver to accelerate the decarbonization levels of China's power system. In order to verify the rationality of our carbon price assumptions, we compare the CO_2 emissions from our two scenarios Grid-Low-R and Grid-High-R with other modeling results of CO_2 emissions in China's power system (Energy Foundation, China's New Growth Pathway, 2020). Figure 3.10 shows that the CO_2 emissions in our study are within the ranges of other studies, except for higher CO_2

emissions in 2025 under Grid-Low-R. Unlike the other studies, we assume CO_2 emissions will continue to increase until 2025 before decreasing. Our assumption is based on President Xi's announcement in the Leader Summit on Climate, 2021, that China will strictly limit the increase in coal consumption over the 14th five-year plan period (2020-2025) and only begin to phase down coal power projects in the 15th five-year plan period (2025-2030). We therefore assume that coal-fired power generation will continue to increase from 2020-2025 before decreasing after 2025.

We observe that RE generated electricity in the RE-connected battery strategy is lower than that in the Gird-connected battery strategy in western Inner Mongolia. It might be tempting to think that with the RE-connected strategy, renewables will be utilized more efficiently, so that more renewables should be build. However, this is not true for provinces like western Inner Mongolia. In the Grid-connected strategy, the installed batteries in western Inner Mongolia are already acting as "RE-connected batteries" because installed renewable capacities largely exceed the capacity of installed batteries. In other words, the RE-connected constraint is already satisfied (or it's satisfied almost all the time). Thus, changing these batteries to RE-connected batteries won't change what is charging these batteries much if we look at this province alone. What causes RE generated electricity to decrease is that other demand provinces with relatively little RE cannot charge their batteries directly from the grid. Thus, they cannot utilize RE from other provinces and thus require less transmitted power in their provinces to charge their batteries because their batteries can only be charged by local RE. Therefore, overall, it appears that RE connected batteries leads to a similar outcome as the Grid connected battery scenario. However, there are large provincial differences in how the battery

connections totally affect CO_2 emissions and costs.

Based on our model results, we find that Demand-side batteries result in the highest CO_2 emissions of the three uniform battery deployment strategies. However, in provinces which implement peak and valley electricity prices, the Demand-side battery strategy could help users reduce electricity bills and achieve peak-to-valley arbitrage. Also, in addition to fixed battery storage, electric vehicles could provide mobile battery storage. According to current projections (DRCCAT, 2019), the total number of pure electric vehicles in China's passenger car market will reach 230 million to 350 million vehicles (~ 50%-76% of total vehicle stock) in 2050. If these EV batteries can be integrated as Demand-side batteries, capital costs of regular battery storage could be further decreased.

Carbon pricing is a useful tool to guide investment decisions. It can help clean energy technologies compete with carbon-intensive alternatives and encourage more efficient energy use. Developing important decarbonization technologies such as carbon capture and storage, battery, and hydrogen storage, relies on long-term policies, such as carbon price signals. Our model does not include the potential effects of carbon prices on long-term renewable and battery costs.

Although our modeling results identify possible pathways to accelerate the decarbonization of China's power sector under the eighteen scenarios developed for this study, government policies, stakeholder interests, and capital market constraints, among other factors, will influence our results in the real world. Further research analyzing these factors would be of value.

In conclusion, we find that battery deployment strategies will affect national electricity transmission and provincial coal-fired power generation and CO_2 emissions. At the

national level, a rapid decrease of battery storage costs and high carbon prices play key roles in large-scale battery deployment and a rapid decarbonization of the power system. Uniform national RE-connected batteries can effectively reduce peak and total electricity transmission, even when they are optimally deployed. Optimally deployed uniform national Demand-side batteries will result in the highest national system costs and CO_2 emissions. RE- and Grid-connected batteries have similar national system costs and CO_2 emissions. At the provincial level, for supply provinces with abundant renewable resources, RE-connected batteries are the optimal strategy resulting in the lowest carbon emissions and system costs. For demand provinces with limited renewable resources, Demand-side batteries are the optimal strategy resulting in the lowest carbon emissions and system costs. Heterogeneous provincial battery deployment strategies should consider local renewable resources, the availability of transmission, and the characteristics of demand. Our findings provide valuable insights on optimal battery storage deployment policies for China that facilitate carbon neutrality of the power sector. In addition, our approach can help other countries identify optimal carbon prices and battery deployment strategies for their own power system decarbonization.

4. Methods

4.1 SWITCH-China model

We extend the SWITCH-China capacity expansion model (He G. et al., 2016) and use the extended model to conduct experiments. SWITCH-China is an optimization model which solves for the optimal installed capacities of generators and transmission line capacities to meet a specific demand. The optimal solution minimizes the cost of producing and

delivering the electricity while satisfying a set of operational constraints. In other words, given the electricity demand projection at a certain temporal and spatial resolution, SWITCH-China optimizes the number of each type of generator, energy storage, and transmission lines built each year in order to balance the projected demand with supply within each time step in each load zone. (Fripp M. 2012 and Johnston J., et al, 2019). The electricity demand projection at this resolution is detailed in Supplementary Note 2. The cost information for renewable power generators, such as wind and solar is detailed in Supplementary Note 3.

In our study, we choose an hour as a time step and a province as a load zone. To model power system dynamics, four levels of temporal resolution are employed by the SWITCH-China model: investment periods months, days, and hours. Our study divides the time span 2025-2050 into six five-year long investment periods: 2023-2028, 2028-2033, 2033-2038, 2038-2043, 2043-2048, 2048-2053. We use 12 months to characterize each investment period, one day to characterize each month (the median load day) and six hours to characterize each day. For each day, hourly sampling begins at midnight China Standard Time (CST) and includes the 0th, 4th, 8th, 12th, 16th, and 20th hours. This results in (6 investment periods) $\times$(12 months/investment period) $\times$ (1 day/month) $\times$ (6 hours/day) = 432 study hours over which the system is dispatched. The results of 2025, 2030, 2035, 2040, 2045 and 2050 are representative years for the six investment periods.

4.2 Objective function

The default objective function in SWITCH-China is the system cost. In other words, SWITCH-China outputs a power system plan that minimizes system cost by default. In

this study, we model the power system that is not only cost efficient, but environmentally friendly as well. Thus, we set up the objective function in SWITCH-China to be a weighted sum of system costs and CO_2 emissions.

$$\text{Minimize:} \quad \textit{System Costs} + w \times \textit{CO}_2 \textit{ Emissions}, \tag{3}$$

where the weight w can be interpreted as the carbon price, as more CO_2 emissions undesirably raise the total "cost". The carbon price w captures the trade-off between cost efficiency and environmental impact, as a higher w guides the model to output a system that prioritizes minimizing CO_2 emissions (and other detrimental emissions) with a greater tolerance of higher system cost, and vice versa. The carbon prices used in our study are detailed in Table S2.

The system costs in the objective function include (a) capital costs of new power plants, battery storage and transmission lines, (b) operation and maintenance (O&M) costs of existing and new power plants, battery storage and transmission lines, and (c) variable costs incurred by power plants, e.g. fuel costs of coal and gas. Variable costs of wind, solar, pumped-hydro storage, PGP and battery storage are assumed to be zero. In general, these costs depend on both installed capacities within each province, which are model variables to be solved, as well as the unit capital costs and O&M costs, which are model inputs. The unit costs of wind and solar are obtained from the annual technology baseline (ATB) 2021 and IRENA, 2020, and detailed in Supplementary Note 2.3. The capital costs of battery storage are detailed in the following section. The capital costs of PGP storage technologies are evaluated from the H2A model data compiled by the National Renewable Energy Laboratory (NREL) (Steward et al., 2009, Brian et al., 2013 and Pan et al, 2021). As for coal,

natural gas, oil, hydro and nuclear power plants, their unit costs are derived from He et al. (2020).

CO_2 emissions in the objective function come from burning coal, natural gas and oil in the process of power generation. We calculate CO_2 emissions using energy consumption, based on input CO_2 emission factors and the total power generation from coal and gas power generators (variables to be solved for in the optimization). In our study, the CO_2 emission factors are derived from the China Provincial GHG Emission Inventory Guideline (in Chinese) released by China's National Development and Reform Commission (NRDC). For fossil fuel power plants, we use average values for emission factors for coal-fired power plants of 25.41 kgC/GJ (93.2kgCO_2/GJ), for natural gas power plants of 15.32 kgC/GJ (56.2kgCO_2/GJ), and for oil power plants of 21.1 kgC/GJ (77.4kgCO_2/GJ).

4.3 Scenario design

In this study, we consider three factors - battery deployment strategies, carbon prices, and battery storage cost trajectories. In particular, we examine three battery deployment strategies (RE, Grid, and Demand), two carbon prices (Low, High), and three rates of battery storage cost decreases (Base, Moderate, Rapid). We then combine these three factors to set up eighteen scenarios (Table 1). The motivation and implementation of each factor are explained below.

Battery deployment strategy. Three primary types of battery deployment are considered – RE-connected (RE), Grid-connected (Grid), and Demand-side (Demand), as well as a mixed battery deployment option that includes RE, Grid and Demand batteries (Mixed).

Grid-connected batteries are the most flexible since they can be charged from any type of generator. In the SWITCH-China model, we attach grid-connected batteries to the central grid with no additional constraints. RE-connected batteries are co-located with renewables (solar PV and wind), in order to smooth intermittent renewable generation before transmitting it to the central grid. Since 2021, some provinces in China have required that new renewable power plants be equipped with energy storage devices to smooth intermittency before power is transmitted to the grid. This is exactly the RE-connected battery scenarios considered in this study. In addition to attaching RE-connected batteries to the central grid, we add a constraint in the SWITCH-China model for them - in each province and at each time step, the total electricity used to charge these batteries does not exceed the power generated by the renewables. This constraint does not prevent renewables from being transmitted to other provinces and does not prevent discharged battery electricity from being transmitted to other provinces. Demand-side batteries are attached to the local power grid and are co-located with end users such as industrial factories or commercial buildings. Due to existing infrastructure limitations in China, local power grids cannot transmit power back to the central power grid. Thus, in the SWITCH-China model, we attach Demand-side batteries to the local grid which allows them to be charged from the central grid but only discharged to the local grid. For Mixed battery deployment, we assume that each province can use any mix of battery deployment strategies that minimizes both national and provincial costs.

Carbon prices. Faster decarbonization leads to lower cumulative CO_2 emissions, potentially at a higher cost due to earlier expansion of renewable generation and storage

before their prices have decreased. He et al. (2021) showed that high carbon prices can significantly increase storage capacity and reduce CO_2 emissions (He et al., 2021), thus achieving rapid decarbonization. In our model, we assume that the decarbonization rates of the power system are driven by carbon prices.

This makes our results relevant to policy makers, since the role of carbon pricing in climate policies is widely acknowledged (Bertram et al., 2015; Baranzini et al., 2017; Bergh et al., 2020). We set up 1) low carbon prices, which allows the power sector to slowly transition away from fossil fuels to low carbon power generation; and 2) high carbon prices, which enables a fast transition to low carbon power generation.

Battery storage cost reduction trajectories. We assume the cost of battery storage will decrease over time as the technology advances. Chen et al. (2021) pointed out reductions in storage costs could effectively decrease the overall cost for carbon abatement and impact the scale of storage deployment. High uncertainties exist in current battery storage cost projections for the next few decades as the cost might decrease faster than expected (Ziegler and Trancik, 2021). Thus, we propose three battery cost trajectories to gain insight into how battery cost trajectories affect optimal battery storage deployment. The base trajectory (B) is constructed from the battery storage capital costs in NREL's ATB 2021 and storage futures study (2021). For the moderate trajectory (M), we assume projected battery costs are one-third of those in the base trajectory. For the rapid trajectory (R), we assume the projected battery costs are one-fifth of those in the base case. The cost trajectories for all types of batteries are illustrated in Figure S3.

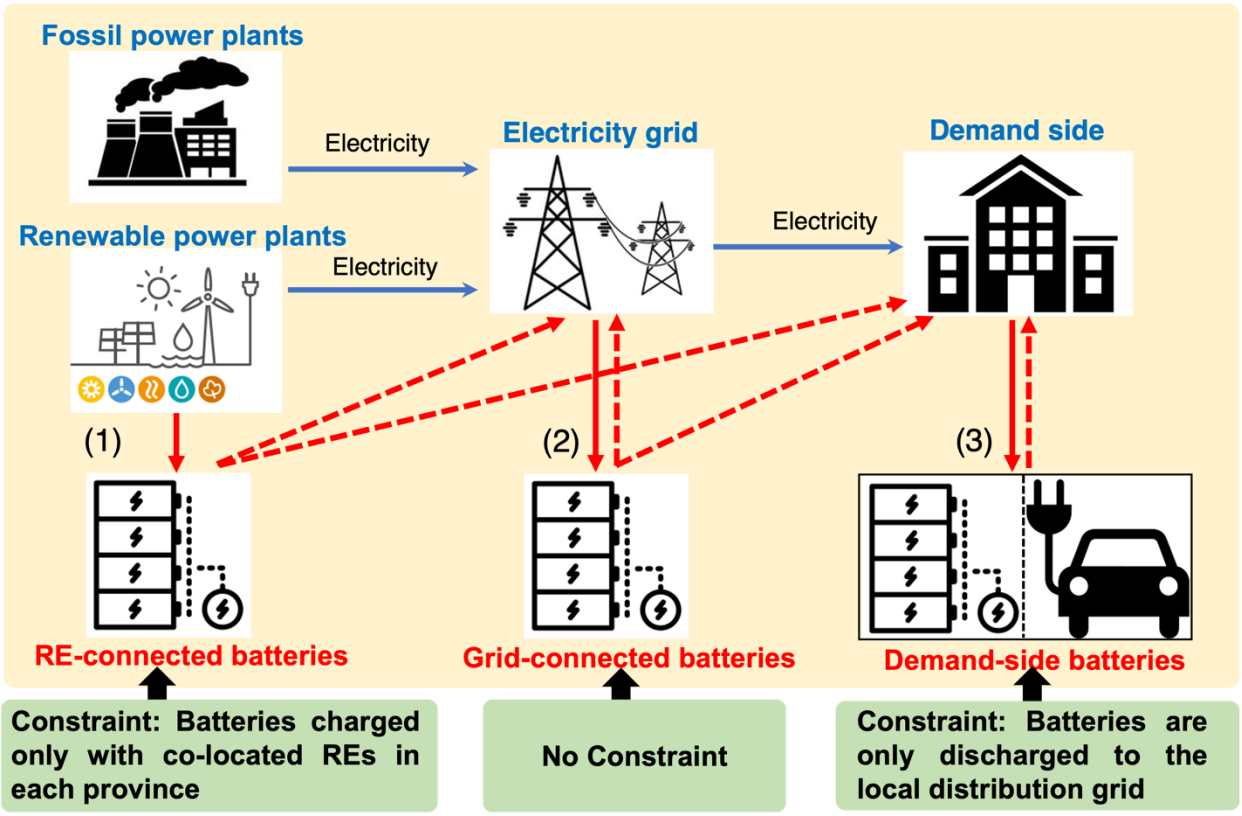

Figure 3.1. Three battery storage deployment strategies that can be deployed either uniformly nationally or individually within each province. (1) Renewable-connected (RE-connected) batteries: batteries that are co-located and only charged with RE; (2) Grid-connected batteries: batteries attached to the central grid with no additional constraints; and (3) Demand-side batteries: batteries co-located with demand loads and discharging only to the local grid.

Solid red arrows show the electricity used to charge batteries. Dashed red arrows show electricity discharged from batteries.

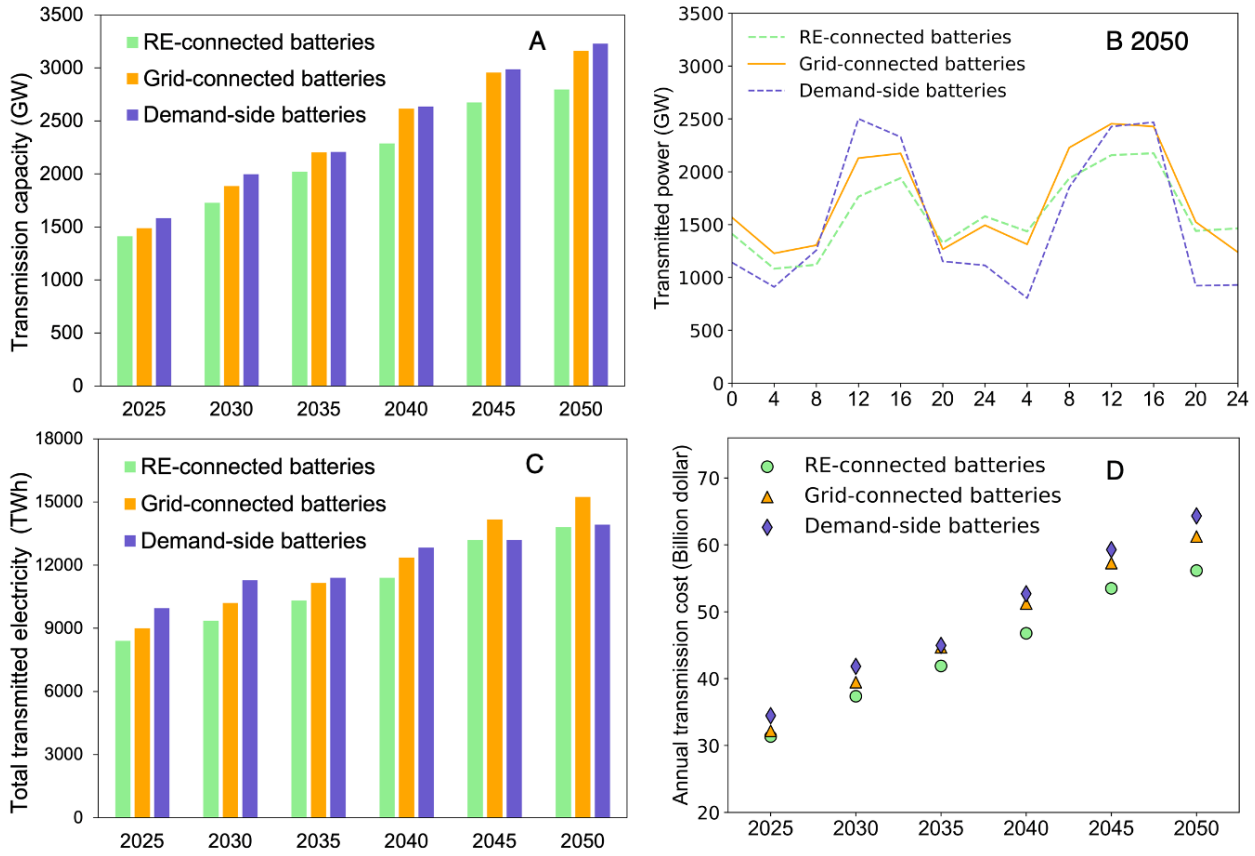

Figure 3.2. Transmitted power and transmission costs of RE-connected, Grid-connected, and Demand-side battery deployment strategies over time.

Comparison of (A) optimal transmission capacity, (B) a comparison of optimal transmission power profiles for the three deployment strategies for 2-days in 2050, (C) optimal total transmitted electricity and (D) optimal annual transmission costs for the three battery storage deployment strategies with low carbon prices and rapid battery cost decreases.

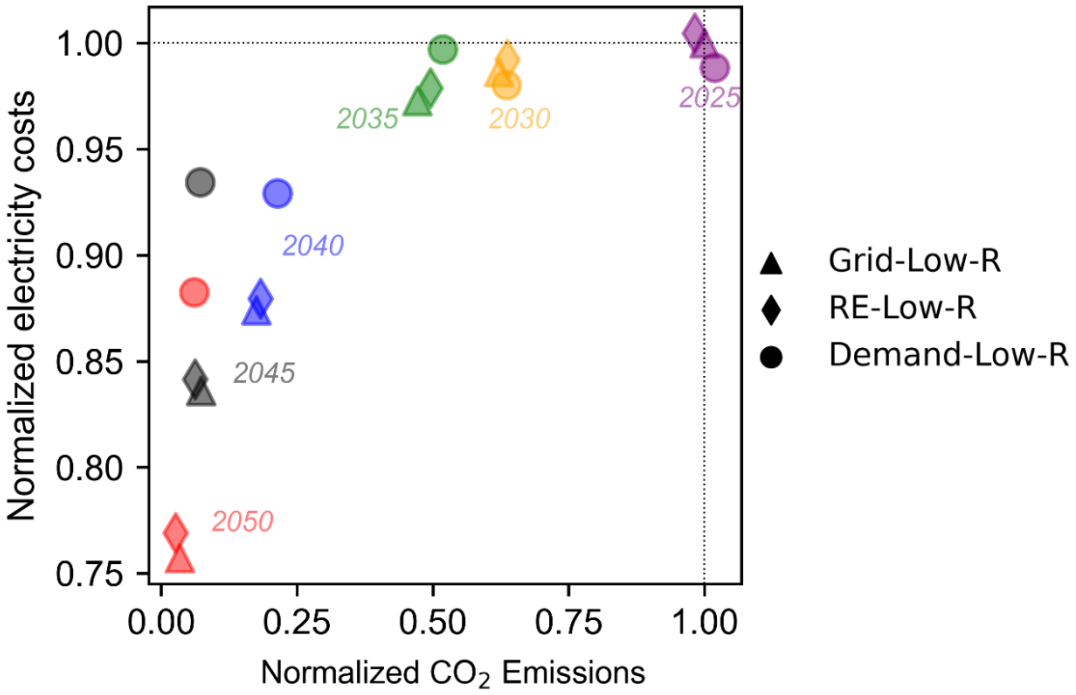

Figure 3.3. National average optimal CO_2 emissions and optimal electricity costs of three battery storage deployment strategies from 2025-2050. Different colors represent different years. Grid-Low-R, RE-low-R and Demand-Low-R are RE-connected, Grid-connected and Demand-side with low carbon prices and rapid decrease of battery costs.

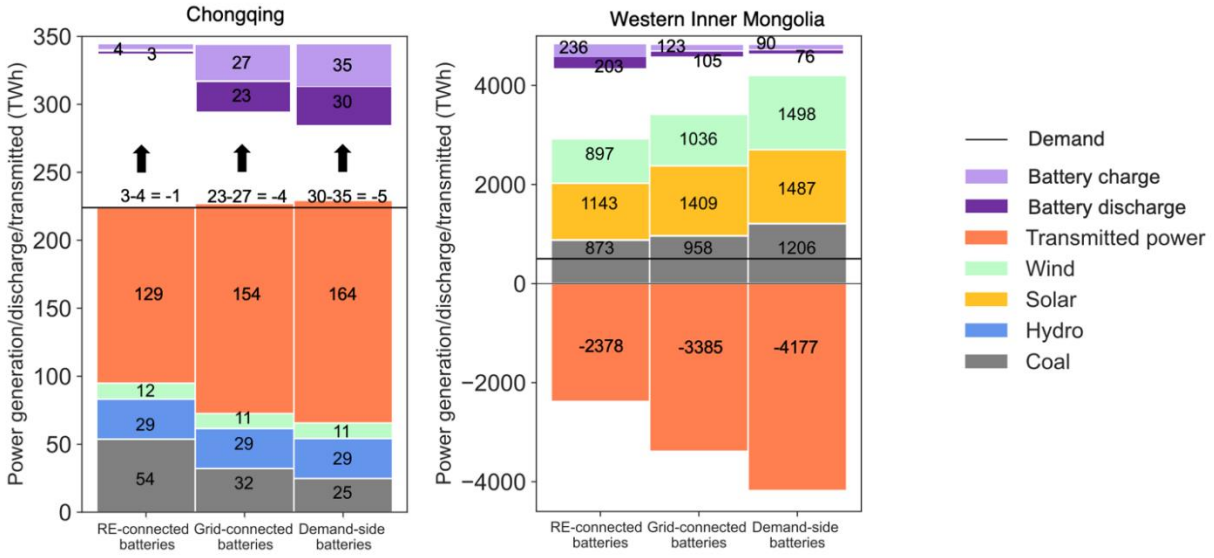

Figure 3.4. Energy balance of Chongqing province (relatively high local demand and low local electricity supply) and western Inner Mongolia (relatively low local demand and high local coal and RE supply) in 2040 using RE-connected batteries, Grid-connected batteries and Demand-side batteries with low carbon prices and accelerated battery cost decreases. Positive (Negative) values indicate local production or transmission into (out) of the province. Black line indicates provincial level electricity demand, colored bar segments indicate source of electricity supplied, and transmitted electricity into/out of province. For Chongqing province, numbers at the top of each column indicate battery charge/discharge with the difference between the two resulting from efficiency losses.

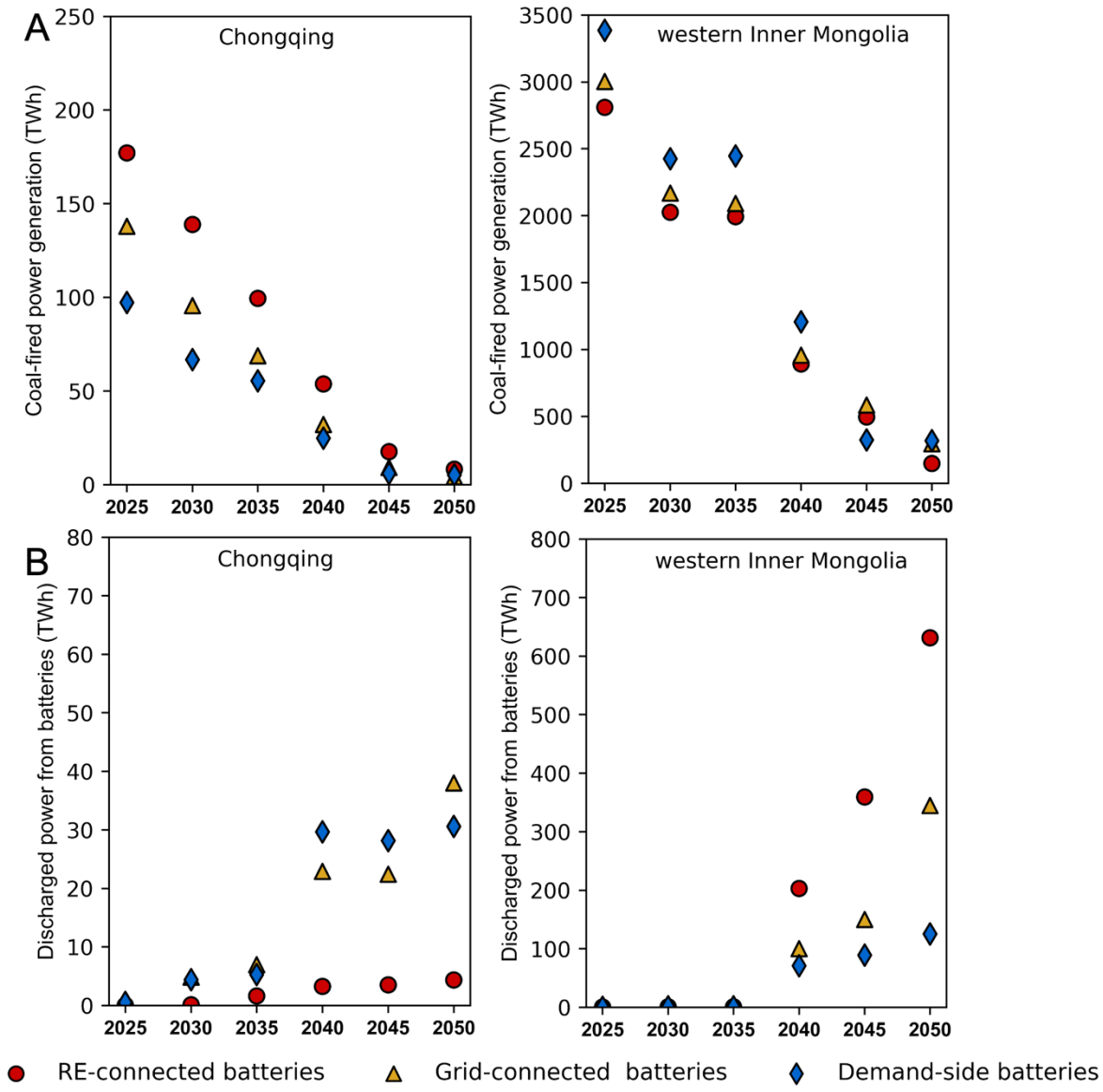

Figure 3.5. Coal-fired power generation and power discharged from batteries in a typical supply and demand province

Comparison of (A) coal-fired power generation and (B) power discharged from batteries in a supply province (western Inner Mongolia) and a demand province (Chongqing) for three battery storage deployment strategies with low carbon prices and rapid battery cost decreases. Effects of other scenarios are shown in the Figure S12-15.

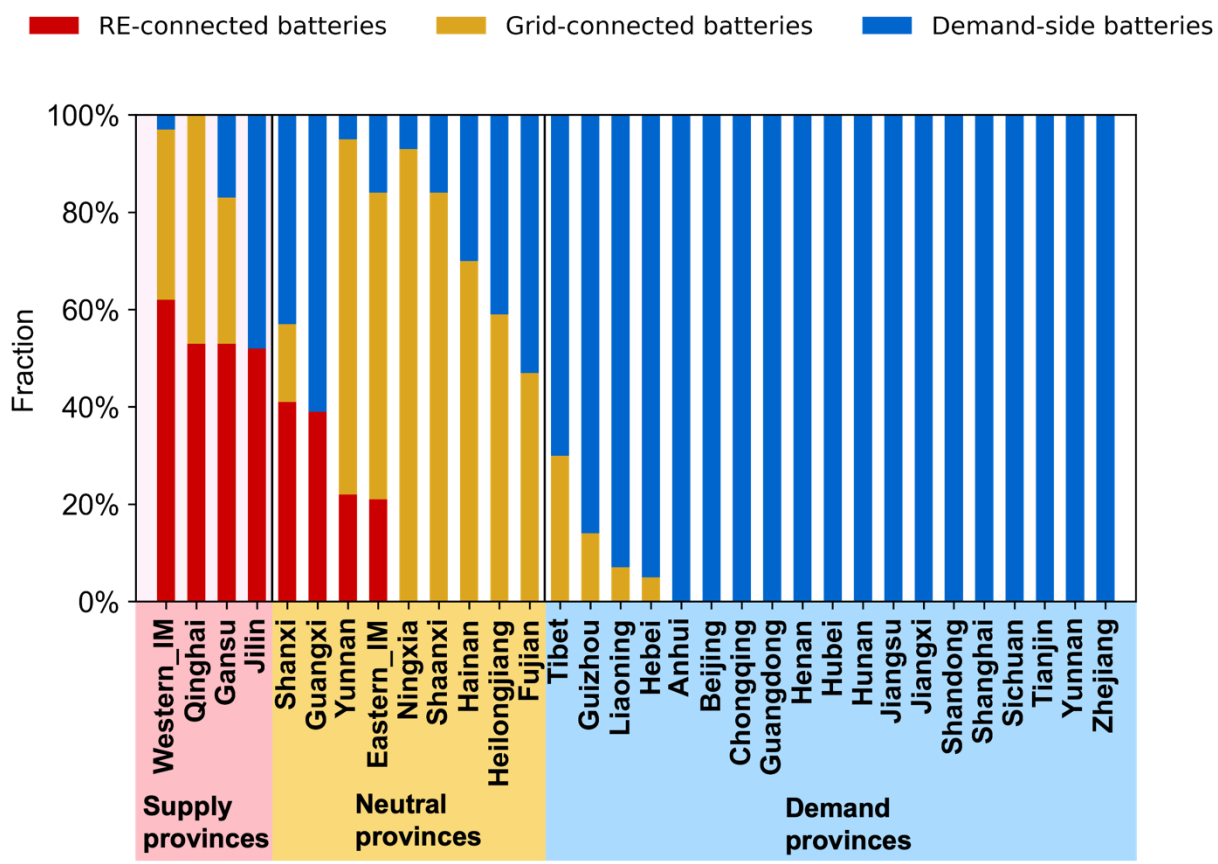

Figure 3.6. Share of discharged power from each type of battery in the Mixed-Low-R scenario (see Table 1b for scenario descriptions). Results for the Mixed-High-R scenario are shown in Figure S16.

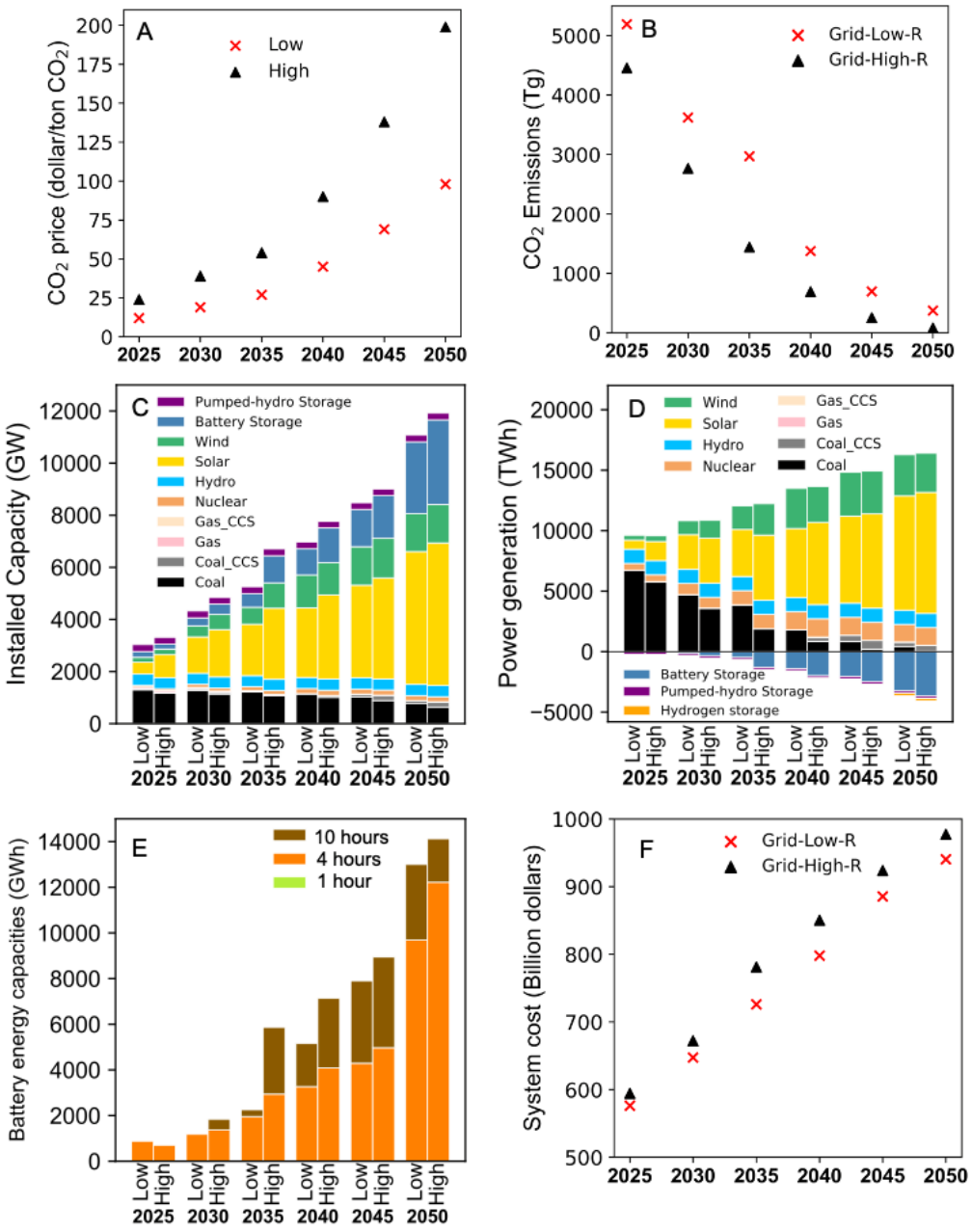

Figure 3.7. Implications of high and low carbon prices on the national power system

(A) CO_2 prices over time, (B) optimal national CO_2 emissions, (C) optimal installed capacity of each generation technology, (D) optimal power generation, (E) optimal installed battery energy capacities by storage duration (battery storage capacities of 1-hour storage duration are tiny compared to longer storage durations), and (F) Optimal system cost of the Grid-connected battery strategy with rapid battery cost decreases. Low and High in (A), (C), (D) and (E) represent low and high carbon prices. Grid-Low-R/Grid-High-R indicates batteries which are connected to the grid that have low or high carbon prices and rapid decreases in battery costs.

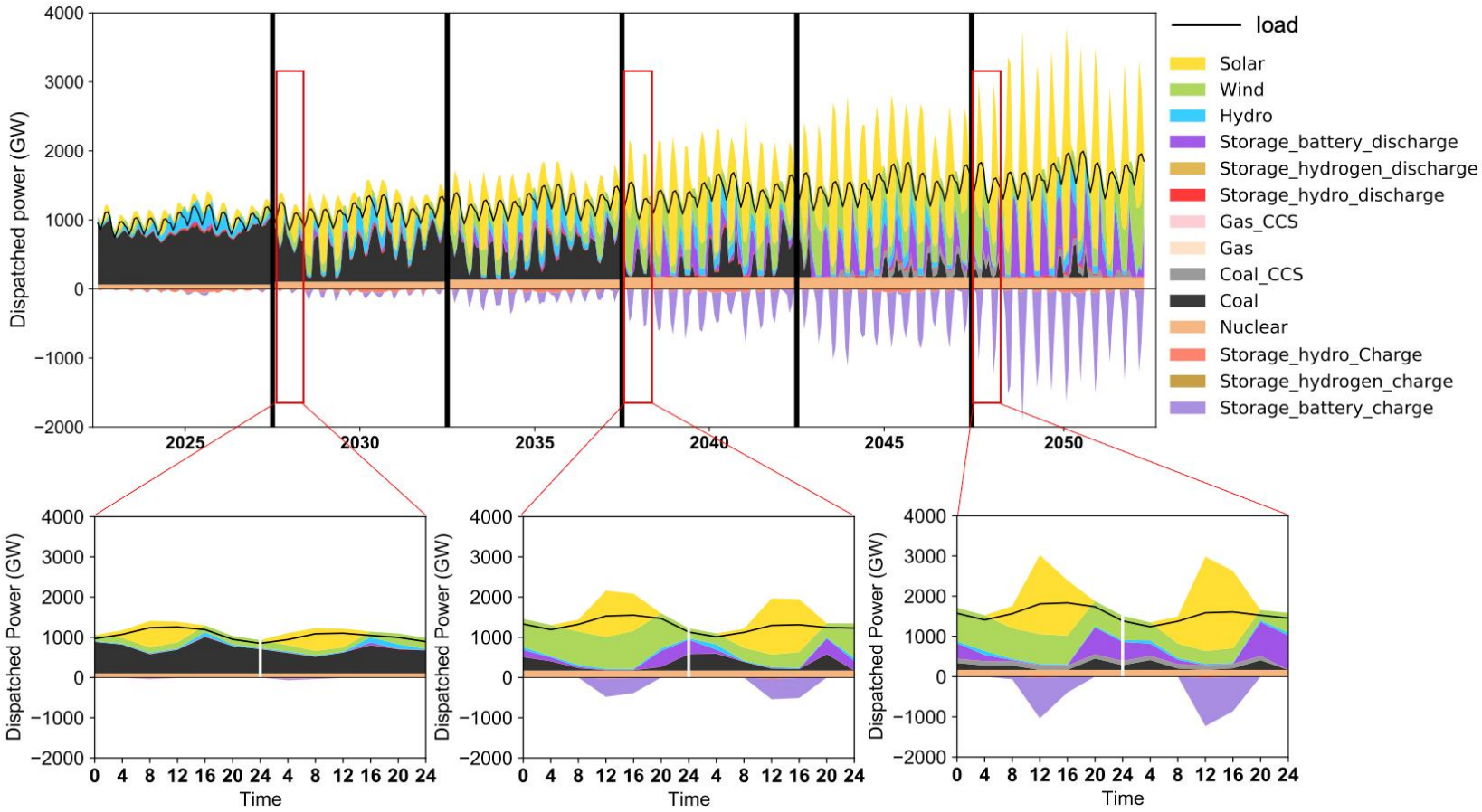

Figure 3.8. Dispatched power and load profiles from 2025 to 2050 under Grid-Low-R scenario (Grid connected batteries with low carbon prices and rapid decrease in battery storage costs)

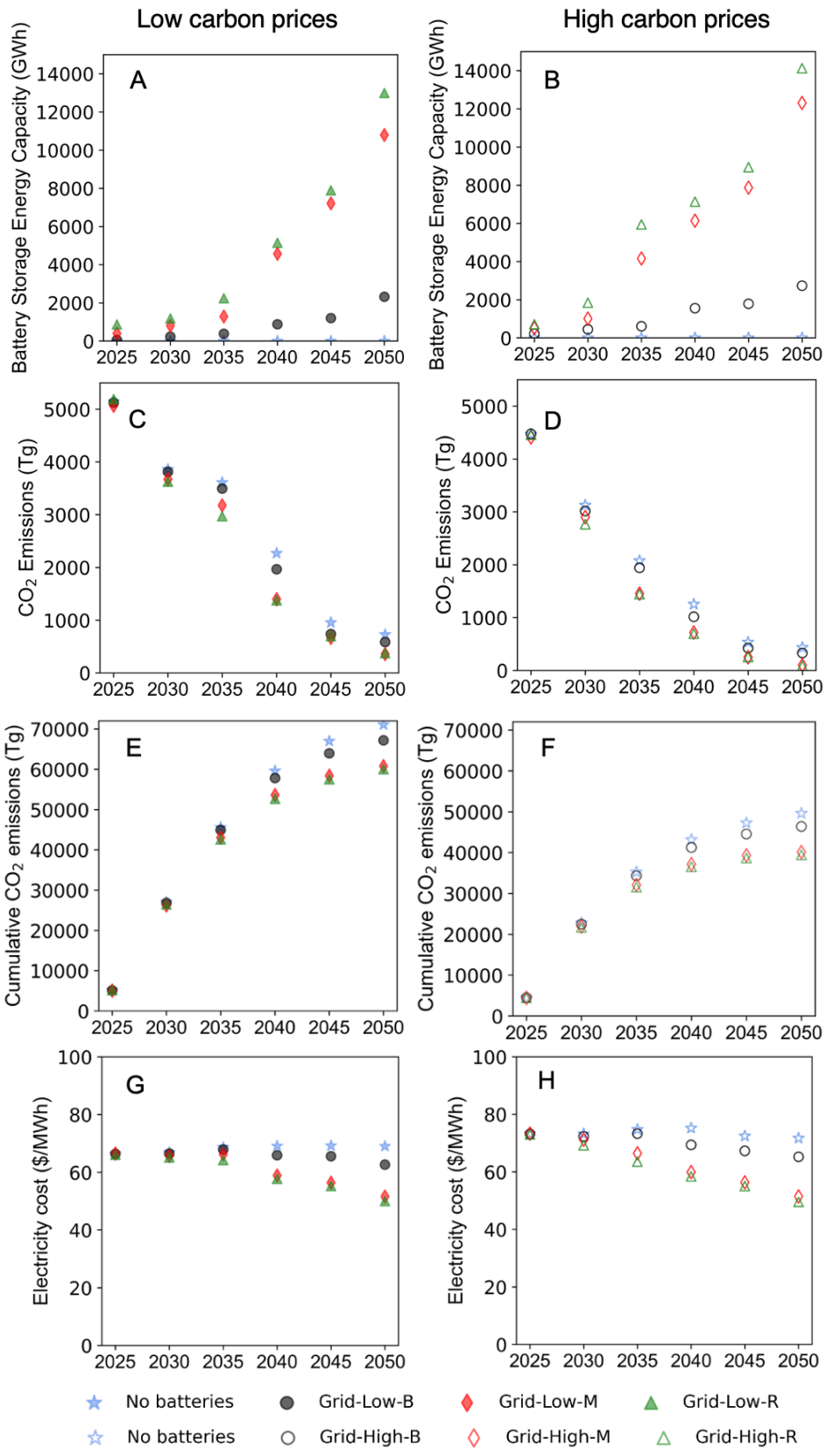
Low carbon prices
High carbon prices
A
B
C
D
E
F
G
H
Battery Storage Energy Capacity (GWh)
CO_2 Emissions (Tg)
Cumulative CO_2 emissions (Tg)
Electricity cost ($/MWh)
2025
2030
2035
2040
2045
2050
No batteries
Grid-Low-B
Grid-Low-M
Grid-Low-R
No batteries
Grid-High-B
Grid-High-M
Grid-High-R

Figure 3.9. Implications of low and high carbon prices and battery storage cost reductions on the national power system.

Under low (left column) and high (right column) carbon prices we show temporal pathways of (A) and (B) optimal battery storage energy capacity, (C) and (D) optimal CO_2 emissions, (E) and (F) optimal cumulative CO_2 emissions, and (G) and (H) optimal electricity costs with no batteries, base case (B, high battery costs), moderate (M, medium battery costs) and rapid (R, low battery costs).

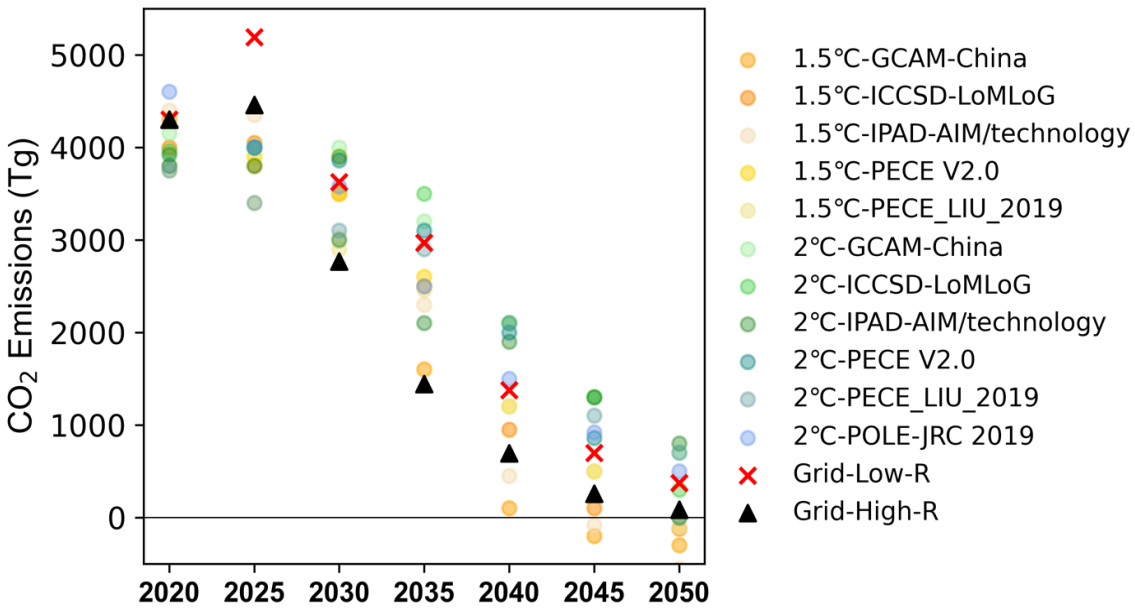

Figure 3.10. Comparison of CO_2 emissions in our study (Grid-Low-R and Grid-High-R) with other studies (Energy Foundation, China's New Growth Pathway, 2020)

1.5 ℃ and 2 ℃ represent under 1.5 ℃and 2 ℃ target, respectively.

Table 3.1A. Scenario designs – National homogenous battery deployment strategies

Scenarios	Battery storage deployment strategies	Carbon prices	Battery storage cost reduction trajectories
RE-Low-B	Batteries charged only with co-located RE in each province **(RE-connected batteries)**	**Low** carbon price	**B**ase case
RE-Low-M			**M**oderate battery cost decreases
RE-Low-R			**R**apid battery cost decreases
RE-High-B		**High** carbon price	**B**ase case
RE-High-M			**M**oderate battery cost decrease
RE-High-R			**R**apid battery cost decrease
Grid-Low-B	Batteries charged by and discharged to grid **(Grid-connected batteries)**	**Low** carbon price	**B**ase case
Grid-Low-M			**M**oderate battery cost decrease
Grid-Low-R			**R**apid battery cost decrease
Grid-High-B		**High** carbon price	**B**ase case
Grid-High-M			**M**oderate battery cost decrease
Grid-High-R			**R**apid battery cost decrease
Demand-Low-B	Batteries charged and discharged on demand side in each province **(Demand-side batteries)**	**Low** carbon price	**B**ase case
Demand-Low-M			**M**oderate battery cost decrease
Demand-Low-R			**R**apid battery cost decrease
Demand-High-B		**High** carbon price	**B**ase case
Demand-High-M			**M**oderate battery cost decrease
Demand-High-R			**R**apid battery cost decrease

Table 3.1B. Scenario designs – Provincial heterogenous battery storage deployment strategies*

Scenarios	Battery storage deployment strategies	Carbon prices	Battery storage cost reduction trajectories
Mixed-Low-R	A **mix** of RE-, Grid-connected, and Demand-side batteries	**Low** carbon price	**R**apid battery cost decrease
Mixed-High-R	A mix of RE-, Grid-connected, and Demand-side batteries	**High** carbon price	**R**apid battery cost decrease

*The results from RE-Low-R, Grid-Low-R, Demand-Low-R and Mixed-Low-R are presented in the main text. The results from other scenarios are presented in Supplementary note 3.3 and 3.4, Figure S3.9-S3.12 and Table S3.2 and S3.3.

Acknowledgements

This work was funded by the Princeton School of Public and International Affairs. I thank the following co-authors of this chapter: Yaofeng "Desmond" Zhong, Gang He and Denise L. Mauzerall. I thank Matthias Fripp for instructions and insights on SWITCH model updates. I thank Nicolas Choquette-Levy for constructive comments on our manuscript.

Reference

Arbabzadeh, M., Sioshansi, R., Johnson, J.X., and Keoleian, G.A. (2019). The role of energy storage in deep decarbonization of electricity production. Nature Communications 10, 1–11.

NREL. National Renewable Energy Laboratory. Annual Technology Baseline (ATB), 2021. https://atb.nrel.gov/electricity/2021/data

Baranzini, A.; Van den Bergh, J.C.; Carattini, S.; Howarth, R.B.; Padilla, E.; Roca, J. Carbon pricing in climate policy: Seven reasons, complementary instruments, and political economy considerations. Wiley Interdiscip. Rev. Clim. Chang. 2017, 8, e462

Bergh, J.V.D.; Botzen, W. Low-carbon transition is improbable without carbon pricing. Proc. Natl. Acad. Sci. USA 2020,117, 23219–23220.

Bertram, C.; Luderer, G.; Pietzcker, R.; Schmid, E.; Kriegler, E.; Edenhofer, O. Complementing carbon prices with technology policies to keep climate targets within reach. Nat. Clim. Chang. 2015, 5, 235–239

Bistline, J., Cole, W., Damato, G., DeCarolis, J., Frazier, W., Linga, V., Marcy, C., Namovicz, C., Podkaminer, K., Sims, R., et al. (2020). Energy storage in long-term system models: a review of considerations, best practices, and research needs. Prog. Energy 2, 032001.

Brian, J., Whitney, C., Jenni, M., Saur, G., and Ramsden, T. (2013). PEM electrolysis H2A production case study documentation (National Renewable Energy Lab (NREL)). https://doi.org/10.2172/1214980.

California Energy Commission (2020). GFO-19-308 - assessing long-duration energy storage deployment scenarios to meet California's energy goals, grant solicitation.

https://www.energy.ca.gov/solicitations/2020-01/gfo-19-308-assessing-long-durationenergy- storage-deployment-scenarios-meet.

Chen, X., Liu, Y., Wang, Q., Lv, J., Wen, J., Chen, X., Kang, C., Cheng, S., and McElroy, M.B. (2021). Pathway toward carbon-neutral electrical systems in China by mid-century with negative CO2 abatement costs informed by high-resolution modeling. Joule 5, 2715–2741.

China Energy & Electricity Outlook 2019 (State Grid Energy Research Institution, 2019); http://www.sgeri.sgcc.com.cn/html/files/2019-02/19/20190219111915944695018.pdf

Craig, M.T., Jaramillo, P., and Hodge, B.-M. (2018). Carbon dioxide emissions effects of grid-scale electricity storage in a decarbonizing power system. Environ. Res. Lett. 13, 014004.

de Sisternes, F.J., Jenkins, J.D., and Botterud, A. (2016). The value of energy storage in decarbonizing the electricity sector. Applied Energy 175, 368–379.

Dowling, J.A., Rinaldi, K.Z., Ruggles, T.H., Davis, S.J., Yuan, M., Tong, F., Lewis, N.S., and Caldeira, K. (2020). Role of Long-Duration Energy Storage in Variable Renewable Electricity Systems. Joule 4, 1907–1928.

DRCCAT. Data Resource Center of China Automotive Technology Research Center, 2019.

Fripp, M. Switch: a planning tool for power systems with large shares of intermittent renewable energy. Environ. Sci. Technol. 46, 6371–6378 (2012).

He, G. et al. SWITCH-China: a systems approach to decarbonizing China's power system. Environ. Sci. Technol. 50, 5467–5473 (2016).

He, G., Lin, J., Sifuentes, F., Liu, X., Abhyankar, N., and Phadke, A. (2020). Rapid cost decrease of renewables and storage accelerates the decarbonization of China's power system. Nature Communications 11, 2486.

Hittinger, E., and Azevedo, I.M.L. (2017). 5. Estimating the Quantity of Wind and Solar Required To Displace Storage-Induced Emissions. Environ. Sci. Technol. 51, 12988–12997.

IEA, 2021. An Energy Sector Roadmap to Carbon Neutrality in China.

IRENA. International Renewable Energy Agency. Renewable Power Generation Costs in 2020. https://www.irena.org/publications/2021/Jun/Renewable-Power-Costs-in-2020

Johnston, J., Henriquez-Auba, R., Maluenda, B. & Fripp, M. Switch 2.0: a modern platform for planning high-renewable power systems. SoftwareX 10, 100251 (2019).

Lilliestam, J., Patt, A., and Bersalli, G. (2021). The effect of carbon pricing on technological change for full energy decarbonization: A review of empirical ex-post evidence. WIREs Climate Change 12, e681.

NDRC, National Development and Reform Commission, 2021. Guidelines on accelerating the development of new energy storage. https://www.ndrc.gov.cn/xxgk/zcfb/ghxwj/202107/t20210723_1291321.html?code=&state=123

NDRC. National Development and Reform Commission, 2022. "14th Five-Year Plan" modern energy system planning. https://www.ndrc.gov.cn/xxgk/zcfb/ghwb/202203/t20220322_1320016.html?code

=&state=123

NEA. National Energy Administration. 2022. National electric Power industry statistics 2021. http://www.nea.gov.cn/2022-01/26/c_1310441589.htm

Pan, G., Gu, W., Hu, Q., Wang, J., Teng, F., and Strbac, G. (2021). Cost and low-carbon competitiveness of electrolytic hydrogen in China. Energy Environ. Sci. 14, 4868–4881.

Sepulveda, N.A., Jenkins, J.D., Edington, A., Mallapragada, D.S., and Lester, R.K. (2021). The design space for long-duration energy storage in decarbonized power systems. Nat Energy 6, 506–516.

Steward, D., Saur, G., Penev, M., and Ramsden, T. (2009). Lifecycle Cost analysis of hydrogen technologies for electrical energy storage, National Renewable Energy Lab (NREL). https://www.nrel.gov/docs/fy10osti/46719.pdf.

Zheng, B., Tong, D., Li, M., Liu, F., Hong, C., Geng, G., Li, H., Li, X., Peng, L., Qi, J., et al. (2018). 11. Trends in China's anthropogenic emissions since 2010 as the consequence of clean air actions. Atmospheric Chemistry and Physics 18, 14095–14111.

Ziegler, M.S., Mueller, J.M., Pereira, G.D., Song, J., Ferrara, M., Chiang, Y.-M., and Trancik, J.E. (2019). Storage Requirements and Costs of Shaping Renewable Energy Toward Grid Decarbonization. Joule 3, 2134–2153.

Ziegler, M.S., and Trancik, J.E. (2021). Re-examining rates of lithium-ion battery technology improvement and cost decline. Energy Environ. Sci. 14, 1635–1651.

Chapter 4: Subsidizing grid-based electrolytic hydrogen could increase GHG emissions

1. Introduction

Low-carbon hydrogen (H_2) is a critical fuel for the clean-energy transition, providing long-term energy storage in the power sector and offering ways to reduce emissions in industry and heavy transport sectors that will be difficult or expensive to electrify. H_2 can be produced from a diverse range of primary energy resources, including coal, natural gas, renewable and nuclear energy, and biomass (Moriarty, 2007).

Currently, nearly all hydrogen in China is either produced directly from fossil fuels (55% for coal gasification and 14% for stream methane reforming) or as a byproduct of petroleum refining (28%) with only 1% coming from water electrolysis (China EV100, 2020). Technologies are advancing rapidly for producing hydrogen with zero emissions using renewable electricity – "green" hydrogen, as opposed to hydrogen produced from coal gasification ("brown") and steam methane reforming (SMR) ("grey"). Blue hydrogen refers to hydrogen made either through coal gasification or SMR, but with carbon dioxide capture and storage (CCS). Production of 1kg of SMR-based or coal-based hydrogen is associated with an emission of ~10 and ~19kg of CO_2, respectively (Bartlett and Krupnick, 2020). Some studies indicate that greenhouse gas (GHG) emissions from blue hydrogen are greater than from directly burning fossil fuel for heat and only 18-25% less than SMR-based hydrogen (Howarth, 2021). This is because CCS is not 100% efficient and there is great uncertainty over the climate impacts of upstream methane leakage (Renssen, 2020). In 2020, hydrogen production from fossil fuel in China emitted ~322 Tg

CO2, which is equivalent to 25% of total CO_2 emission in industrial processes and will increase as hydrogen demand rises. Industrial processes in China include production of non-metallic mineral products, chemical production, production of metal products, production and consumption of halocarbons and sulphur hexafluoride (Zhu, 2021).

Depending on electricity sources, there are two types of electrolytic hydrogen – grid-based hydrogen, which is generated using electricity from the power grid; and renewable-based hydrogen, which is generated using renewable electricity directly. Grid-based hydrogen is cheaper than renewable-based hydrogen in some provinces, so lower subsidies are needed to develop the grid-based hydrogen industry. However, grid electricity can have substantial GHG emissions, making it less "green". Thus, subsidizing grid-based hydrogen could increase GHG emissions. In contrast, hydrogen directly generated from renewable energy has very low GHG emissions.

China has committed to peak carbon emissions by 2030 and reach net-zero carbon emission by 2060. However, the pathway to these targets will greatly influence total carbon emissions. To minimize cumulative emissions, decarbonizing hydrogen production and accelerating the transition to green hydrogen production is critical. However, production cost is a major barrier to the uptake of electrolytic hydrogen. Today, the cost of renewable-based hydrogen is 2-4 times higher than coal- or SMR-based hydrogen (China EV100, 2020 and IRENA, 2020) and the cost of grid-based hydrogen is 1.6-3 times higher than fossil-based hydrogen (Gunther et al., 2019; Nguyen T., et al., 2019). Before renewable-based hydrogen becomes cost competitive, large-scale development of hydrogen will likely expand fossil-based hydrogen production and

therefore increase GHG emissions. To rapidly decarbonize the hydrogen production process, it's necessary to accelerate the transition from fossil-based hydrogen to renewable-based hydrogen.

Subsidy policies play a significant role in developing emerging technologies. To accelerate the electrolytic hydrogen transition, subsidies on hydrogen-related devices and hydrogen used for the transportation are deployed in different regions as pilot projects (Jining city industry and information technology bureau, 2019; National Hydrogen Energy Standardization Technical Committee, 2018). Greater subsidies are required to make renewable hydrogen cost competitive and to commercialize its production.

Because availability of renewable resources varies dramatically by geographic location, the cost of renewable-based hydrogen production also varies greatly by location. Therefore, to minimize costs it could be advantageous to transport electrolytic hydrogen by pipeline from provinces with low to high-production costs. However, because hydrogen is an indirect GHG, leakage must be minimized. Some studies (Penev et al, 2019) show that pipeline transport becomes the lowest-cost option as hydrogen demand grows. Estimates show that the use of existing natural gas pipelines can reduce hydrogen transmission costs by more than 60% compared to building new pipelines (Cerniauskas et al., 2020). However, little research has examined hydrogen transport through pipelines on provincial $LCOH_2$ and life cycle GHG emissions.

This study strives to characterize provincial levelized costs of hydrogen ($LCOH_2$) and life cycle GHG emissions of electrolytic hydrogen from various sources. We investigate the trade-offs in GHG emissions resulting from various subsidies of both grid-based and

renewable-based hydrogen production. Our goal is to evaluate subsidies that make electrolytic hydrogen cost-competitive with fossil-based hydrogen while minimizing GHG emissions from 2025 to 2050. We focus on three questions. 1. When would either grid or renewable electrolytic hydrogen become cost competitive if no policy incentives are imposed to accelerate a hydrogen production transition? Which provinces would be among the first to have cost competitive electrolytic hydrogen and which would struggle to achieve this? 2. What are the GHG emission and subsidy cost trade-offs? Should renewable-based hydrogen and grid-based hydrogen production both be subsidized, or only the former? 3. If hydrogen is transported across provinces, how should the network of pipelines be designed to minimize GHG emissions (including CH_4, H_2 leakage and CO_2 emissions)?

We use an integrated assessment approach in conjunction with a life-cycle analysis to quantify the trade-offs between financial subsidies and life cycle GHG emissions in accelerating electrolytic hydrogen development in China. We develop two scenarios: The minimum-subsidy scenario sets subsidies equal to the difference between the lowest levelized cost of fossil-based hydrogen and the lowest levelized cost of electrolytic hydrogen. This scenario will encourage the development of the electrolytic hydrogen industry which will lead to GHG emissions from grid-based hydrogen produced electrolytically from grid-based electricity. The minimum-C-emissions scenario provides subsidies only for hydrogen generated from renewable energy and aims to minimize GHG emissions for hydrogen production and requires higher subsidies (See Methods, Scenario Design for details). For example, in a province with large coal-based hydrogen

production today (e.g., Xinjiang) subsidizing grid-based electrolytic hydrogen will result in minimum subsidies but will increase GHG emissions (minimum CO_{2e} emission scenario – minimum subsidy scenario). However, subsidizing solar- or wind-based hydrogen production will require large subsidies but will dramatically decrease GHG emissions. These results are obtained by subtracting our minimum subsidy scenario from our CO_{2e} emission scenario.

We compare provincial levelized costs of hydrogen ($LCOH_2$) and life cycle GHG emissions of grid-based and renewable-based hydrogen with fossil-based hydrogen generation from 2025-2050. We find that financial subsidies are necessary to accelerate all types of electrolytic hydrogen development as without subsidies it remains more costly than fossil-based hydrogen after 2040. However, subsidizing grid-based electrolytic hydrogen does not effectively reduce GHG emissions from 2025-2030 as the power system will remain heavily dependent on coal. When subsidies are placed on electrolytic hydrogen, the incremental subsidy necessary to support renewable-based hydrogen is small relative to the cost difference between coal-based and grid-based electrolytic hydrogen. Therefore, subsidies on renewable-based hydrogen provide very cost effective CO_{2e} emission reductions relative to grid-based hydrogen. Transporting hydrogen with pipelines leads to a 12-20% drop in $LCOH_2$ within individual provinces and a 24-31% increase in life cycle GHG emissions due to higher emissions from low hydrogen production cost provinces that use high coal grid electricity and hydrogen leakage.

2. Results

2.1 National analysis of levelized costs of hydrogen ($LCOH_2$) by generation technology

Figure 4.1 shows the national average results of $LCOH_2$ by each cost component (Capital expenditures, operational expenditures; fuel costs and battery costs) as well as life cycle GHG emissions (upstream and downstream) of each hydrogen production technology from 2025-2050. We find that electrolytic hydrogen will become cost competitive with coal-based hydrogen after 2040 (Figure 4.1). Coal-based hydrogen production will continue to have the lowest $LCOH_2$ from 2025-2040. Electrolytic hydrogen is more expensive than coal-based hydrogen not only due to its higher capital costs but also due to additional water electrolysis and battery costs. SMR-based hydrogen is more expensive than coal-based hydrogen in China due to the high cost of natural gas. Fossil-based hydrogen with CCS has higher $LCOH_2$ compared to both coal and SMR-based hydrogen because of CCS device costs. Thus, coal gasification is the mainstream hydrogen production method in China today.

Levelized costs of electrolytic hydrogen vary by the electricity's energy sources. Grid-based hydrogen has the lowest $LCOH_2$ in 2025 of electrolytic hydrogen types. However, solar- and onshore wind-based hydrogen have lower $LCOH_2$ than grid-based hydrogen starting in 2030. The proportion of $LCOH_2$ from each cost component differs by technology. For example, SMR-based hydrogen has a larger share of fuel costs compared to coal-based hydrogen because of the high price of natural gas in China. Offshore wind-based hydrogen has a larger share of operation and maintenance costs compared to solar and onshore wind-based hydrogen. This is because offshore wind turbines require more

maintenance due to the damage from sea waves and high wind speed. Offshore wind farms are difficult to access, further raising maintenance costs. In addition, renewable-based hydrogen requires on-site battery storage to maintain minimum electrolyzer operation during periods of low solar or wind electricity generation, so that additional battery costs are associated with each type of renewable-based hydrogen.

2.2 National analysis of life cycle GHG emissions

Although coal-based hydrogen has the lowest $LCOH_2$, it introduces the highest life cycle GHG emissions from 2025-2050 as shown in Figure 4.1. Life cycle GHG emissions from grid-based hydrogen production is the second highest in 2025 and 2030. This is because first, the power grid in 2025 is still dominated by coal (Figure 4.2) with more than 50% of China's electricity generation coming from coal-fired power generation. Second, energy efficiency of electrolytic hydrogen (12%-43%) is much lower than coal gasification and SMR-based hydrogen (60%-76%). With the decarbonization of the power system, GHG emissions from grid-based hydrogen production decrease dramatically from 20.8 to 1.6 kg/kg H_2 between 2025-2050.

The life cycle GHG emissions of renewable-based hydrogen are from upstream processes, including raw material extraction, module manufacture, device production and installation. With the development of renewable technologies, the GHG emissions decrease from 2025-2050. Upstream emissions of solar PV are about double those of onshore wind in China since wind farms utilize higher material recycling rates (20%) than solar PV facilities (Palmer et al., 2021; Zhu et al., 2022). Offshore wind has 70% higher upstream emissions than onshore wind (Yang et al., 2017 and 2018; Palmer et al., 2021;

Xiang et al., 2021; Xu et al., 2022) because of more complex deployment infrastructure requirements.

Fossil-based hydrogen with CCS achieves an 80-90% decrease of life cycle GHG emissions compared to fossil-based hydrogen (Figure 4.1). However, there are several obstacles and concerns surrounding the development of blue hydrogen in China. First, the feasibility and permanence of carbon storage has large uncertainties. The continental sedimentary low permeability reservoirs in China are characterized by strong heterogeneity, intertwined natural and artificial fractures, as well as large burial depth, which pose challenges to the success and benefits of CO_2 oil displacement and storage projects (Zhang, 2022). Second, carbon capture technologies in China have yet to achieve scale. China has not yet formed a CO_2 gas source market with a relatively reasonable price and stable supply for enhanced oil recovery (the application of CO_2 oil displacement and storage technology). Furthermore, large-scale CCUS projects require construction of CO_2 transport pipelines. The research on CO_2 pipeline technology started late in China and is currently in the stage of theoretical research and demonstration (Zhang, 2022). Third, 45% of natural gas demand in China is dependent on imports. Long distance transport increases the risk of methane leakage (Lauvaux et al., 2022) and imports from other countries pose national energy security risks.

2.3 Trade-offs between subsidies and GHG emissions in provincial electrolytic hydrogen production

The electrolytic hydrogen technology with the lowest levelized cost in most provinces change from 2025-2050. We compare the provincial $LCOH_2$ of grid-based electrolytic

hydrogen and renewable-based electrolytic hydrogen production to identify the province with the lowest cost of electrolytic hydrogen production before any policy incentives are applied (Figure 4.3A). We find that the lowest $LCOH_2$ changes from grid-based hydrogen to renewable-based hydrogen over time because of the decrease in costs of renewable energy. For two thirds of provinces in 2025, grid-based hydrogen has the lowest $LCOH_2$. The lowest cost for electrolytic hydrogen in 13 provinces (e.g., Anhui, Hubei) changes from grid-based hydrogen to solar-based hydrogen over time. For most coastal provinces (e.g., Hebei, Shandong, Jiangsu, Zhejiang, Fujian, Guangdong and Guangxi) as well as Chongqing and Heilongjiang provinces, wind-based hydrogen always has the lowest $LCOH_2$ while for Beijing, Gansu, Shanxi and Tianjin provinces, solar-based hydrogen always has the lowest $LCOH_2$ from 2025-2050.

The differences between the highest and the lowest $LCOH_2$ decrease over time. The provincial discrepancy decreases from 85% difference in 2025 to 47% difference in 2050. Hunan has the highest $LCOH_2$ from 2030 to 2050 because neither solar nor wind resources are abundant in Hunan province. Xinjiang has the lowest $LCOH_2$ in 2025 and 2030.

However, subsidizing grid-based electrolytic hydrogen in certain provinces and regions will increase life cycle GHG emissions compared to coal-based hydrogen because of high coal fired power generation in the power grid. Figure 4.3B shows that the life cycle GHG emissions of the lowest $LCOH_2$ is very high in Xinjiang (~30 kg/kg H_2) compared to ~20 kg/kg H_2 for coal-based hydrogen. Coal-fired power generation has a high penetration (65% in 2025) of the power grid of Xinjiang based on the SWITCH-China model results. Therefore, subsidizing grid-based hydrogen in provinces and regions, such

as Xinjiang, western and eastern Inner Mongolia, Ningxia, Shaanxi, Chongqing, Hunan, Jiangxi, and Anhui will increase GHG emissions compared to coal-based hydrogen.

Figure 4.4 shows trade-offs between financial subsidies and life cycle GHG emissions in accelerating grid-based and renewable-based electrolytic hydrogen development by province. The minimum-C-emission scenario can reduce 12 kg CO_{2e} per kg H_2 compared to the minimum-subsidy scenario with only a \$0.6 per kg H_2 subsidy increase in 2025. The cost of CO_{2e} emission reductions is \$0.28/kg CO_{2e} in the minimum-C-emission scenario. The benefits of high subsidies will depend on local renewable resources. For example, a subsidy increase of only \$0.5 per kg H_2 in the minimum-C-emission scenario can reduce 31 kg CO_{2e} per kg H_2 production compared to the minimum-subsidy scenario in western Inner Mongolia in 2025. In the same year in Sichuan province, subsidizing an additional \$1.45 per kg H_2 would only reduce 2.57 kg CO_{2e} per kg H_2 production.

2.4 Potential hydrogen pipeline network and impacts on subsidies and life cycle GHG emissions of electrolytic hydrogen

As hydrogen demand increases in the future, there will likely be a corresponding need to transport hydrogen across provinces. Transporting gaseous hydrogen via pipelines is likely to be the most cost-effective long-term delivery option for distances of 200-1500km (The future of hydrogen, 2021) though care to minimize leakage will be crucial. Figure 4.5 shows all cost-effective pipelines between the capital cities of any two provinces under the minimum-subsidy and minimum-C-emission scenarios. To better understand the impacts of hydrogen pipeline costs on potential pipeline network, we conduct sensitivity analyses of hydrogen pipeline costs as shown in Figure 4.6.

We find that western Inner Mongolia, Hebei, and Fujian are main hydrogen export regions. Western Inner Mongolia has the most cost-competitive grid-based hydrogen in the minimum-subsidy scenario. We will achieve a 12-14% reduction in national average $LCOH_2$ when grid-based hydrogen is transported from Western Inner Mongolia to center provinces with higher electrolytic hydrogen costs, however, this will cause an increase in H_2 GHG emissions of electrolytic hydrogen by 5.2kg/kg H_2, 2.2 kg/kg H_2 and 0.4 kg/kg in 2025, 2030 and 2040, respectively. This is because western Inner Mongolia has grid-based hydrogen with high GHG emissions and high hydrogen leakage emissions in long distance transport. In the minimum-C-emission scenario, Hebei and Fujian provinces have the most cost-competitive wind-based hydrogen. Transporting hydrogen from Hebei, Fujian and Inner Mongolia will reduce 14-21% of national average $LCOH_2$ with an increase of 0.4-0.5 kg/kg H_2 from 2025-2040 due to hydrogen leakage via pipeline transport.

2.5 Trade-offs between $LCOH_2$ and GHG emissions across four scenarios from 2025-2040

Electrolytic hydrogen has higher $LCOH_2$ in most scenarios from 2025-2040 compared with fossil-based hydrogen today (Figure 4.6A). This is due to projected high costs of electricity and capital costs of water electrolysis. Subsidies are effective policy incentives to increase cost competitiveness of electrolytic hydrogen. Our results indicate that national average US2020$1.5/kg H_2 subsidies can make electrolytic hydrogen cost-competitive with coal-based hydrogen in most provinces (using the lowest cost type of electrolytic hydrogen production in each province) in 2025.

To minimize carbon emissions, greater subsides are required for renewable- than grid-

based hydrogen. We find that higher subsidies result in lower costs of CO_{2e} /kg H_2 emission reductions (Figure 4.6B). The costs of 1kg CO_{2e} emission reduction in the Minimum-subsidy scenario and the Minimum-C-emission scenario are $0.18 and $0.10 in 2025, $0.06 and $0.04 in 2030, respectively. From 2025-2040 the Minimum-C-emission scenario reduces life cycle GHG emissions by 30-88% with a 5%-19% increase in $LCOH_2$, compared to the Minimum-subsidy scenario

Transporting electrolytic hydrogen with pipelines, rather than having each province supply its' own hydrogen, leads to a national 12-21% drop in $LCOH_2$ and a 20-38% increase in life cycle GHG emissions due to hydrogen leakage as well as to higher emissions from low hydrogen production cost provinces that use high coal grid electricity.

3. Discussion and policy implications

Hydrogen as an energy carrier will play an important role in decarbonizing energy systems, especially in heavy industry. hydrogen produced from renewably generated electricity is critical to nearly eliminate CO_2 emissions from hydrogen production and hence is a vital component of achieving net-zero emission economies. However, 99% of H_2 is currently produced from fossil fuels and is currently limited to a few selected industrial applications. Electrolytic hydrogen is more costly than fossil fuel alternatives but maximizing use of electrolytic hydrogen from renewably generated electricity is critical in the transition to a decarbonized energy system.

In this study, we first examine the $LCOH_2$ and life cycle GHG emissions from all hydrogen production technology from 2025-2050. We estimate the cost difference between coal-based hydrogen and electrolytic hydrogen using both grid electricity and

renewably generated electricity for each year. We then quantify the GHG mitigation benefits of providing subsidies which make grid-based hydrogen cost-competitive with coal-based hydrogen vs. those which minimize GHG emissions for each year. The overarching goal is to determine the best option to accelerate the development of cost-competitive electrolytic hydrogen which minimizes GHG emissions per kg H_2 over this period in China. We find that development of electrolytic hydrogen will be slow without financial subsidies since we project it to only become cost-competitive with fossil-based hydrogen after 2040. Subsidizing grid-based electrolytic hydrogen will increase GHG emissions in some provinces from 2025-2030 because of their remaining heavy dependence on coal power; national average emissions may not significantly decrease before 2040 when grid-based electrolytic hydrogen production is used. Larger subsidies for renewable- rather than grid-based electrolytic hydrogen result in lower costs for CO_2 emission reductions. We also examine the role that optimized inter-provincial hydrogen transport pipelines can provide in decreasing the lowest levelized cost of electrolytic hydrogen. We find that although transporting hydrogen with pipelines leads to a national 12-21% drop in LCOH2, it increases national life cycle GHG emissions by 20-38% due to higher emissions from low hydrogen production cost provinces that use high coal grid electricity and increased hydrogen leakage.

Hydrogen leakage

Hydrogen has indirect warming impacts (Derwent, 2018; Paulot et al., 2021; Field and Derwent, 2021; Ocko and Hamburg, 2022). Fugitive hydrogen in the troposphere is oxidized by the naturally occurring hydroxyl radical (OH) leaving less OH available to

react with methane, a strong greenhouse gas, leading to a longer atmospheric lifetime for methane. In addition, the production of atomic hydrogen from H_2 oxidation in the troposphere increases the formation of tropospheric ozone which is also a GHG (Paulot et al., 2021).

Transport of hydrogen can increase hydrogen leakage (van Rujiven et al., 2011; Cooper et al., 2022; Frazer-Nash Consultancy, 2022). To estimate potential hydrogen leakage through the hydrogen life cycle of production, compression, storage, and transport, we conduct a sensitivity analysis of hydrogen leakage emissions based on existing studies (IEA, 2021; China Hydrogen Energy Industry Development Report 2020; Ocko and Hamburg, 2022) (Table 2). Table S4.3 shows the hydrogen leakage for best- and worst-case leakage rates determined from the literature and based on potential future hydrogen demand in China. Cumulative future hydrogen leakage is very uncertain depending on total demand as well as leakage rates. We project it could reach ~150-4300 Mt CO_{2e} (GWP100 =11 and GWP_{20} = 33), accounting for between 1.3%-39% of total CO_2 emissions from China in 2020.

Policy implications

China currently encourages coal-based hydrogen production, which increases GHG emissions compared with the direct use of fossil fuels unless carbon capture and storage technology is used. For example, Shanxi province proposed to increase coal-based hydrogen production in the near term in its hydrogen energy industry development plan from 2022-2035. In Inner Mongolia and Shaanxi provinces, several coal-based hydrogen projects are planned, and one project is in operation in Sep 2022. In these provinces'

hydrogen production plans, electrolytic hydrogen production is mentioned but hydrogen production coupled with renewable generation is not explicitly discussed and coal-based hydrogen projects dominate.

China's national government is now supporting the development of concentrated renewable power generation in some northern and northwestern provinces, such as Inner Mongolia and Hebei provinces, which are referred to as renewable energy bases. Because these provinces have abundant renewable resources and are less developed regions in China, developing a renewable energy industry can also facilitate their economic development. This provides an opportunity to co-locate renewable energy generation with hydrogen production. We find that producing hydrogen with renewable electricity can reduce GHG emissions by 90% relative to coal-based hydrogen, 87% in 2025 using a still heavily coal base grid, and 30% in 2040 using a substantially decarbonized grid.

Renewable-based hydrogen production, deployed in these renewable energy bases, would help smooth intermittent renewable generation, and decrease production costs. Hydrogen can be used for long-duration energy storage and when redeployed in power generation can shift loads to balance the electricity supply and demand. hydrogen can also increase grid resilience to climate change-driven extreme weather. Because extreme high or low temperature require higher peak load and hydrogen can supply electricity to fill the gaps between supply and demand. Costs of renewable-based hydrogen largely depend on the costs of renewable energy generation which are rapidly decreasing. High capacity factors for renewables in "base" locations result in relatively low costs of renewable-based hydrogen production. Co-located renewable energy with hydrogen

production maximizes GHG mitigation and power grid stability at lowest cost per unit renewable based hydrogen production. However, we find renewably generated hydrogen remains more costly than grid-based hydrogen in the near term and higher than coal-based hydrogen after 2040.

Thus, subsidies for renewable-based hydrogen deployment are critical for low carbon hydrogen utilization. Financial incentives have been implemented in other countries, such as Australia (production cost below AUD 2/kg of hydrogen), and the United States (the highest tier is \$3/kg H_2 with less than 0.45kg CO_{2e}/kg H_2). We find a subsidy of 2022\$2/kg H_2 nationally (depending on the province the subsidy needs to range from 2022\$1-3/kg H_2) can make renewable-based electrolytic hydrogen cost-competitive with coal-based hydrogen in 2025. This subsidy is less than the highest tier tax credit in the 2022 US Inflation Reduction Act (IRA) (\$3/kg H_2). The IRA's clean hydrogen production tax credits begin at \$0.60/kg H_2 for hydrogen produced in a manner that captures slightly more than half of SMR process carbon emissions. Incentives rises to \$0.75/kg H_2 and \$1.00/kg H_2 with higher carbon capture rates.

Sensitivity Analyses

We conduct sensitivity analyses to better understand how the uncertainties of a range of capital and operational costs of renewable energy, water electrolysis and hydrogen pipeline costs, as well as discount rates, influence our results.

In the main text, we estimate the electrolytic $LCOH_2$ with rapid cost decreases of renewable energy and water electrolysis. In addition, we also estimate $LCOH_2$ of electrolytic hydrogen with medium and slow cost decreases of renewable energy and

water electrolysis in Note 1, Note 2, Figure S4.4 and S4.5. Policy incentives are needed to further accelerate the development of renewable energy, which will decrease the costs of renewable energy rapidly.

The costs of hydrogen pipelines are mainly determined by transport distances and capacity usage rates. High hydrogen demand increases pipeline capacity usage rates and decreases transport costs. In this study, we set up a 26%-300% uncertainty range of pipeline costs based on the existing literature (Hao., 2022; Miao et al., 2021; Huang et al., 2020; Li et al., 2020), as shown in Figure 4.5.

Discount rates also influence $LCOH_2$ estimates. We estimate the $LCOH_2$ of each H_2production technology with medium (4%) discount rate (ATB 2022). We then test low (half of medium scenario -2%) and high discount rates (double of medium scenario- 8%) on $LCOH_2$. High and low discount rates result in 4%-24% higher $LCOH_2$ and 3-12% lower $LCOH_2$ compared to the medium discount rate, as shown in Table S4.5. Discount rates are used to discount future costs and energy to a net present value (reflecting the financing cost of charging station operators where applicable) (%). A higher discount rate reduces the value of the future stream of net benefits or costs compared with a lower rate.

Limitations and Future Research

We have advanced understanding of provincial variations of $LCOH_2$ and life cycle GHG emissions and the impacts of electrolytic hydrogen subsidies. However, although we include the life-cycle energy requirements of building solar and wind power, in our estimation, we do not include GHG emissions from hydrogen and fossil fuel power plant infrastructure build-out，because these emissions are relatively small in their life cycle

emissions, these data are very limited and there are large variations of emissions due to scale, location, age, and raw material of devices. Second, the existing natural gas pipeline network could be used to transport and distribute hydrogen. However, this will increase hydrogen leakage risks. New infrastructure could also be developed. However, costs of transporting hydrogen will vary according to the type of pipeline used or built, geography, distance, scale, and the required end use of the hydrogen. Further research analyzing these factors would be of value. Third, there is very limited hydrogen leakage measurement data. Improvements in quantification of hydrogen leakage rates and development and deployment of leakage mitigation measures are needed before hydrogen infrastructure is widely built.

4. Methods

The essential methodology included in the main text consists of a detailed description of scenario design, estimates of $LCOH_2$ and life cycle GHG emissions for each hydrogen production technology, power system model- SWITCH-China, as well as hydrogen pipeline network selection. A more comprehensive methodology section including an explanation of the cost assumptions of renewable power generation, a description of water electrolyze selection, storage system can be found in the Supporting Information.

4.1 Scenario design

We design two key scenarios for driving electrolytic hydrogen development which have different objectives: (1) Minimum-subsidy scenario, designed to achieve cost-competitive electrolytic hydrogen production as soon as possible. (2) Minimum-C-emissions scenario, designed to minimize carbon emissions.

Our study estimates the $LCOH_2$ and life cycle GHG emissions of eight hydrogen production technologies. We divide the eight technologies into two categories. The first category is electrolytic hydrogen (EH_2), which uses electricity to split water into hydrogen and oxygen. Electricity comes from either the power grid or from renewable energy, such as solar PV, onshore wind, and offshore wind. The second category is fossil-based hydrogen (FFH_2) which includes hydrogen produced from coal gasification, from steam methane reforming and from coal and methane with CCS.

Minimum-subsidy scenario. We first calculate the lowest $LCOH_2$ from fossil fuel ($LCOH_2$-FF) and next calculate the lowest $LCOH_2$ from electrolytic H_2 ($LCOH_2$-EH_2). We then calculate the difference between $LCOH_2$-FF and $LCOH_2$-EH_2 as the smallest subsidy

required to develop electrolytic hydrogen. We estimate the differences in life cycle GHG emissions between the lowest levelized cost of electrolytic hydrogen and the lowest levelized cost of fossil-based hydrogen in each province from 2025-2050.

Minimum-C-emissions scenario. Instead of calculating the $LCOH_2$-EH_2, we calculate the lowest levelized cost of renewable-based hydrogen. We then estimate differences in both $LCOH_2$ and life cycle GHG emissions between the lowest levelized costs of renewable-based hydrogen and fossil-based hydrogen in each province over 2025-2050.

In addition, we test two additional scenarios using potential inter-provincial pipeline networks: (3) Minimum-subsidy-pipeline scenario, designed to achieve electrolytic hydrogen production that is cost-competitive with fossil-based hydrogen and that includes inter-provincial hydrogen transport through pipelines. (4) Minimum-C-emissions-pipeline scenario, designed to achieve renewable-based hydrogen production that is cost-competitive with fossil-based hydrogen while minimizing carbon emissions and that includes hydrogen transport through pipelines.

4.2 Levelized Cost of Hydrogen Production

The $LCOH_2$ is determined by many factors, such as electricity costs, fuel costs, capital costs and operation and maintenance (O&M) costs of water electrolysis, conversion efficiency and the interest rate. Here, we divide our $LCOH_2$ estimates into three categories: (1) Fossil-based hydrogen (coal, SMR-based and coal, SMR-based hydrogen with CCS): the levelized cost of hydrogen production is estimated as follows:

$$LCOH_2 = \frac{\sum_{t=1}^{n} \frac{I_t + O_t + F_t}{(1+r)^t}}{\sum_{t=1}^{n} \frac{H_t}{(1+r)^t}} \quad (1)$$

Here, n is lifespan of the system; I_t represents capital costs of hydrogen producing devices in year t (including financing); O_t represents operations and maintenance expenditures of power plants in year t; F_t represents fuel expenditures in year t, H_t represents hydrogen production in year t, and r is discount rate of 2.5%.

(2) Grid-based electrolytic hydrogen: the levelized cost of hydrogen production is estimated as follows:

$$LCOH_2 = \frac{\sum_{t=1}^{n} \frac{G_t + EC_t + EO_t}{(1+r)^t}}{\sum_{t=1}^{n} \frac{H_t}{(1+r)^t}} \quad (2)$$

Here, n is lifespan of the system; G_t represent capital and operational expenditures of grid electricity in year t (including financing); EC_t represents capital costs of water electrolyzers; EO_t represents operations and maintenance expenditures of water electrolyzers in year t, and H_t represents hydrogen production in year t, and r is discount rate of 2.5%.

(3) Renewable-based electrolytic hydrogen: the levelized cost of hydrogen production is estimated as follows:

$$LCOH_2 = \frac{\sum_{t=1}^{n} \frac{RC_t + RO_t + EC_t + EO_t + B_t}{(1+r)^t}}{\sum_{t=1}^{n} \frac{H_t}{(1+r)^t}} \quad (3)$$

Here, n is lifespan of the system; RC_t and RO_t represent capital costs and operational & maintenance expenditures for renewable energy (i.e. solar, onshore wind and offshore wind) in year t (including financing); EC_t and EO_t represent capital costs and operations and maintenance expenditures of water electrolyzers in year t; B_t represents capital and

operational costs of battery storage; H_t represents hydrogen production in year t, and r is a discount rate of 2.5%.

As for coal, natural gas, oil, hydro and nuclear power plants, their capital costs, and operational & maintenance expenditures are derived from He et al. 2020. The costs of wind energy, solar energy, and batteries are obtained from the annual technology baseline (ATB) 2021 and IRENA, 2020 (See details in Figure S4.1-3). This study does not include the cost of water because its cost is tiny compared to the other hydrogen production costs (ACIL, 2018).

4.3 Life cycle GHG emission estimation

Life cycle assessments (LCA) quantify cradle-to-grave environmental and net-energy impacts of the energy supply system (Palmer G., et al., 2021), which facilitates more consistent comparisons of energy technologies. In our study, we use LCA to estimate provincial GHG emissions from upstream processes (e.g., module manufacture, installation, raw material extraction) and operational processes (e.g., fuel transport and combustion, plant operation and maintenance) of hydrogen production. The proportion of GHG emissions from each lifecycle stage differs by technology. For fossil-fueled technologies, fuel combustion during operation of the facility emits the vast majority of GHGs. For renewable energy technologies, most GHG emissions occur upstream of operation (NREL, 2021).

We collect the emission factors for various stages of each technology (IKE, 2014; IEA, 2019; Zhu et al., 2022; Xu et al., 2022; Yang et al., 2018; Palmer et al., 2021; Ocko et al., 2022; Xiang et al., 2021 and Yang et al., 2017) as shown in Table S4.4. LCA studies find that

electrolysis powered by solar PV is less GHG emission intensive than SMR, but higher than wind powered electrolysis (Bhandari, R., et al.,2014; Cetinkaya, E., et al., 2012 and Dufour, J., et al., 2012). This is because reuse of materials following decommissioning can offset ~20% of a wind farm's lifetime emissions, while only ~3% solar PV facility's emissions can be offset through reuse of materials (Nugent and Sovacool, 2014).

Methane leakage occurs in each stage of natural gas production & gathering, processing, transmission & storage, and distribution, as well as in end use combustion. For both SMR-based and SMR-based with CCS hydrogen, we also include the methane emissions from natural gas operations and use a range of values in a sensitivity analysis. The existing measurements have large lower and upper bounds of methane leakage rates (Jiang et al., 2011; Alvarez et al., 2018; Miller et al., 2019; Weller et al., 2020; Schneising et al., 2020). In table S4.3, we summarize the methane leakage rates from the existing literature. We use 3.5% as the mean methane leakage rate.

Many studies compare methane with CO_2 for an integrated period of 100 years. However, this estimate underestimates the shorter-term role of methane in global warming as methane lifetime in the atmosphere is only about 12 years (IPCC, 2013). An increasing number of studies are using a 20-year integrated period instead of or in addition to the 100-year period (Howarth RW et al., 2014; Ocko IB, et al., 2017, Fesenfeld LP et al., 2018 and Howarth RW et al., 2021; Qin et al., 2018). Also, a 20-year period is more appropriate than a 100-year time frame given the urgency of rapidly reducing methane emissions globally (UNEP, 2021). Therefore, our analysis uses the 20-year Global Warming Potentials (GWP-20) of methane to estimate CO_{2e} emissions.

Hydrogen is also an indirect greenhouse gas which increases the lifetime of methane and other reactive GHG. It is a small volatile molecule which easily leaks into the atmosphere. In our life cycle emission estimations, we also include hydrogen leakage during the process of production and transport. However, there are large uncertainties involved with how much hydrogen will be deployed in the future, how much hydrogen will ultimately be emitted from hydrogen systems and how hydrogen's warming impacts are calculated and reported. There is very little confidence in any published estimates of hydrogen emissions from a future hydrogen economy in the absence of empirical data. Some studies have made assumptions on total value-chain emissions, typically using a range of 1% to 10% (Prather, 2003; Petipas et al., 2018; Derwent et al., 2001, 2020; Paulot et al., 2021; Warwick et al., 2022). We follow the published literature and Ocko and Hamburg (2022) and assume three hydrogen leakage rates: 1% (best case), 5% (medium case) and 10% (worst case) per 1 kg hydrogen transported in our estimation and uncertainty analysis.

4.4 SWITCH-China model

We extend the SWITCH-China capacity expansion model (He et al., 2016) and use the extended model to conduct experiments. SWITCH-China is an optimization model which solves for the optimal installed capacities of generators and transmission line capacities to meet a specific demand. The optimal solution minimizes the cost of producing and delivering electricity while satisfying a set of operational constraints. In other words, given the electricity demand projection at a certain temporal and spatial resolution, SWITCH-China optimizes the number of each type of generator, energy storage, and

transmission lines built each year to balance the projected demand with supply within each time step in each load zone at minimum cost (Fripp M. 2012 and Johnston J., et al, 2019). The specific parameters used in the model are as same as in Peng et al. (under review).

The objective function is to minimize the total costs of meeting the load demand at each time step. Total costs include (1) capital costs of existing and new power plants and storage projects; (2) fixed O&M costs incurred by all active power plants and storage projects; (3) fuel costs incurred by each plant; (4) capital costs of new and existing transmission lines and distribution infrastructure; and (5) annual O&M costs for new and existing transmission lines and distribution infrastructure (He et al., 2021).

We set a decreasing carbon emission cap as a constraint in the SWITCH-China model. Here, we set up three carbon emission cap scenarios based on Zhuo et al.'s study. They are 1) high carbon cap scenario: Nationally Determined Contribution (NDC) scenario, 2) Medium carbon cap scenario: Global Warming of 2.0 °C (GM2.0) scenario and 3) Low carbon cap scenario: Carbon neutrality by 2050 (CN2050) scenario. See detailed description of these three scenarios in Table 1 from Zhuo et al., 2022. The carbon emission cap for every five years from 2025-2050 is shown in Table S4.2. The main text consists of medium carbon cap scenario results, and the results from other two scenario can be found in the support information.

4.5 Hydrogen pipeline network selection model

We develop a simple model to design a hydrogen pipeline network to achieve the lowest $LCOH_2$ for each province in China.

$$AC_{i,t} = \min(C_{j,t} + D_{i,j,t} \times p) \qquad \forall j \tag{4}$$

$$i_s = \arg\min_j (C_{j,t} + D_{i,j,t} \times p) \tag{5}$$

$$AE_{i,t} = E_{i_s,t} + D_{i,i_s,t} \times r \tag{6}$$

Here, $C_{j,t}$ represents levelized cost of hydrogen production in province j in year t (including financing); $D_{i,j,t}$ represents the distance between two capital cities of province i and j in year t; and p represents per kilometer cost of hydrogen pipelines (2021USD/km). We compute $AC_{i,t}$, the adjusted levelized cost of hydrogen of province i, by taking the minimum of potential cost of hydrogen transported from each province to province i. The potential cost of hydrogen transported from province j is the sum of the hydrogen $LCOH_2$ in province j, (i.e., $C_{j,t}$) and the cost of pipelines from province j to i, (i.e., $D_{i,j,t} \times p$). The source province that results in the lowest potential cost of transported hydrogen for province i is denoted as i_s. The pipeline from province i_s to i is the most cost-effective pipeline to build to transport hydrogen. Note that if no transported hydrogen is more economic than local hydrogen, local hydrogen will be used and no in-bound pipeline will be built, so that $AC_{i,t} = C_{i,t}$ and $i_s = i$. This case is considered in Eqn. (4) and (5) since $D_{i,i,t}$.

$E_{i,t}$ represents the life cycle GHG emissions of hydrogen production in province i in year t. The life cycle GHG emissions of hydrogen consumption in each province will be affected by hydrogen pipelines and we use $AE_{i,t}$ to denote the adjusted life cycle GHG emissions of hydrogen in province i. This is calculated by Eqn. (6), which is the sum of emissions from the source province, (i.e., $E_{i_s,t}$), and the leakage along the pipeline,

$(D_{i,i_s,t} \times r)$, where r represents hydrogen leakage rate. We choose $r = 1\%, 5\% \; and \; 10\%$ in this study based on a review of the literature (Kobayashi et al., 2018; Najjar et al., 2019; Ocko et al., 2022). The main text shows the results with 5% hydrogen leakage rate. Other results can be found in the Supporting Information.

The cost of hydrogen pipelines plays a significant role in the total $LCOH_2$ for each province. Cost of pipeline projects may vary with construction year, location, topographic features along the line. However, the capital cost in this study is simply calculated by taking the average of publicly available data of long-distance gas pipeline projects. Hydrogen pipeline costs was assumed to be close to that of natural gas pipelines with an additional 10% increase (Saadi et al., 2018). This may be an underestimate for hydrogen as piping hydrogen without leakage may be more costly than piping natural gas. Also, we assume that capital costs are linearly related to the transport distance (Miao et al, 2021). This assumption may underestimate the capital cost of short-distance pipelines and over-estimate the capital cost of long-distance pipelines. We assume that hydrogen transport through pipelines has a fixed cost $\$0.56 kg\ H_2 \cdot 1000 km$ (red line in Figure 4.6) in our estimate. We also estimate an uncertainty cost estimate of \$0.15-\$1.68$kg\ H_2 \cdot 1000 km$ hydrogen pipelines based on the existing studies (Hao., 2022; Miao et al., 2021; Huang et al., 2020; Li et al., 2020).

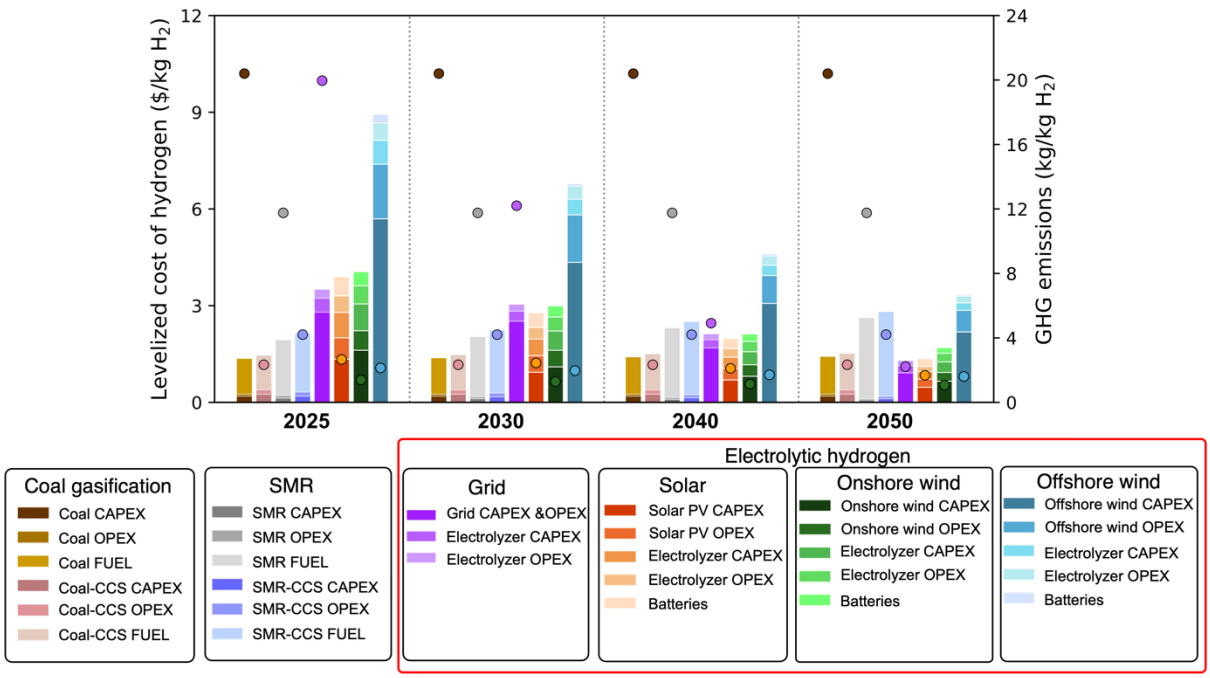

Figure 4.1. National average $LCOH_2$ and GHG emissions by hydrogen production technologies (coal gasification, steam methane reforming, electrolytic hydrogen from grid-based, solar, onshore wind and offshore wind) with rapid cost decrease of renewable energy in 2025, 2030, 2040 and 2050. Results for slow and medium cost decrease of renewable energy are shown in Figure S4.4 and S4.5.

Bars and dots represent $LCOH_2$ and GHG emissions respectively for each technology. (Lifecycle GHG emissions under GWP_{20}, assuming mean methane and hydrogen leakage rates). CAPEX: Capital expenditures; OPEX: Operational expenditures; Fuel: fuel costs.

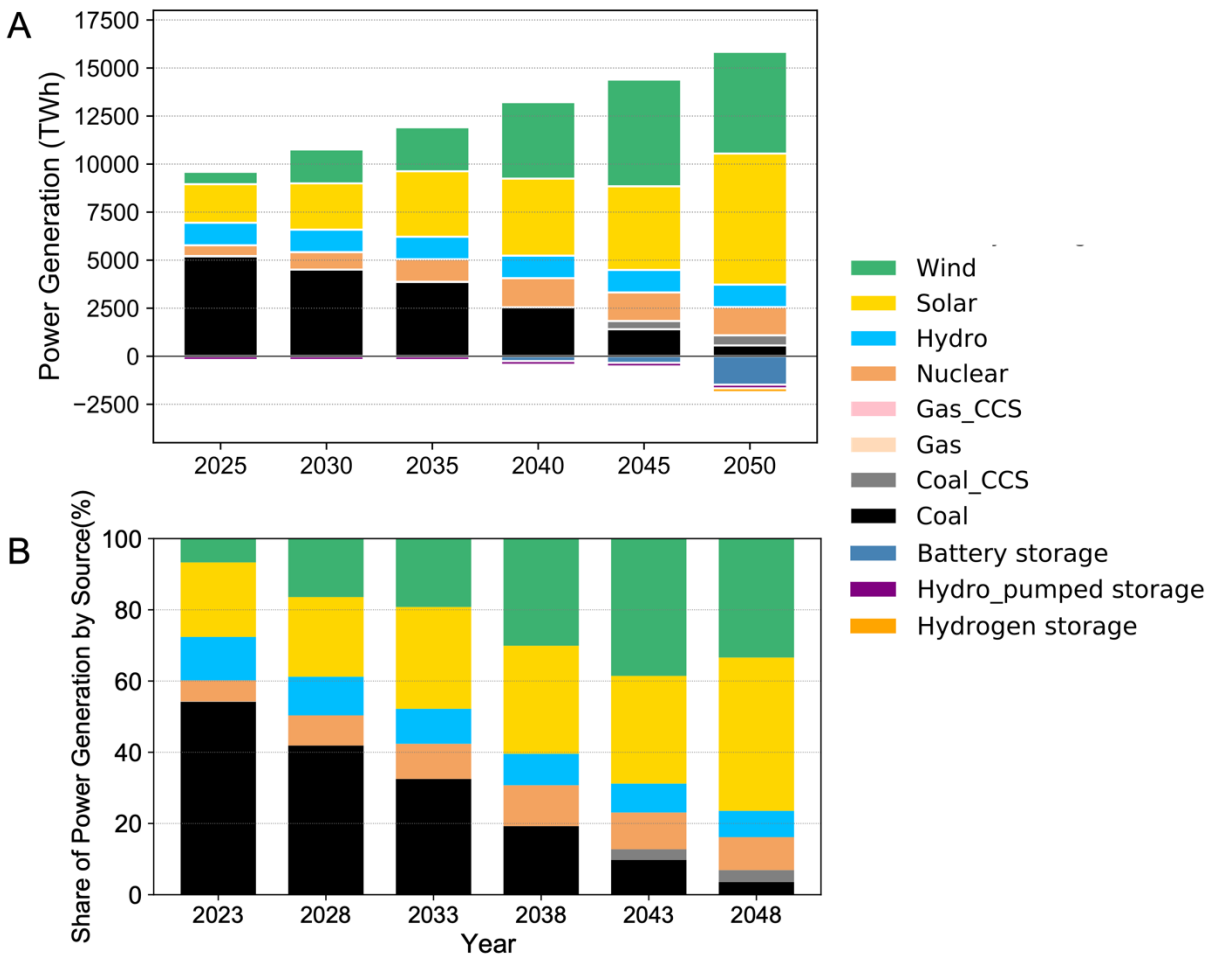

Figure 4.2. SWITCH model (A) generated electricity generation/discharge and (B) share of power generation by energy source from 2025-2050.

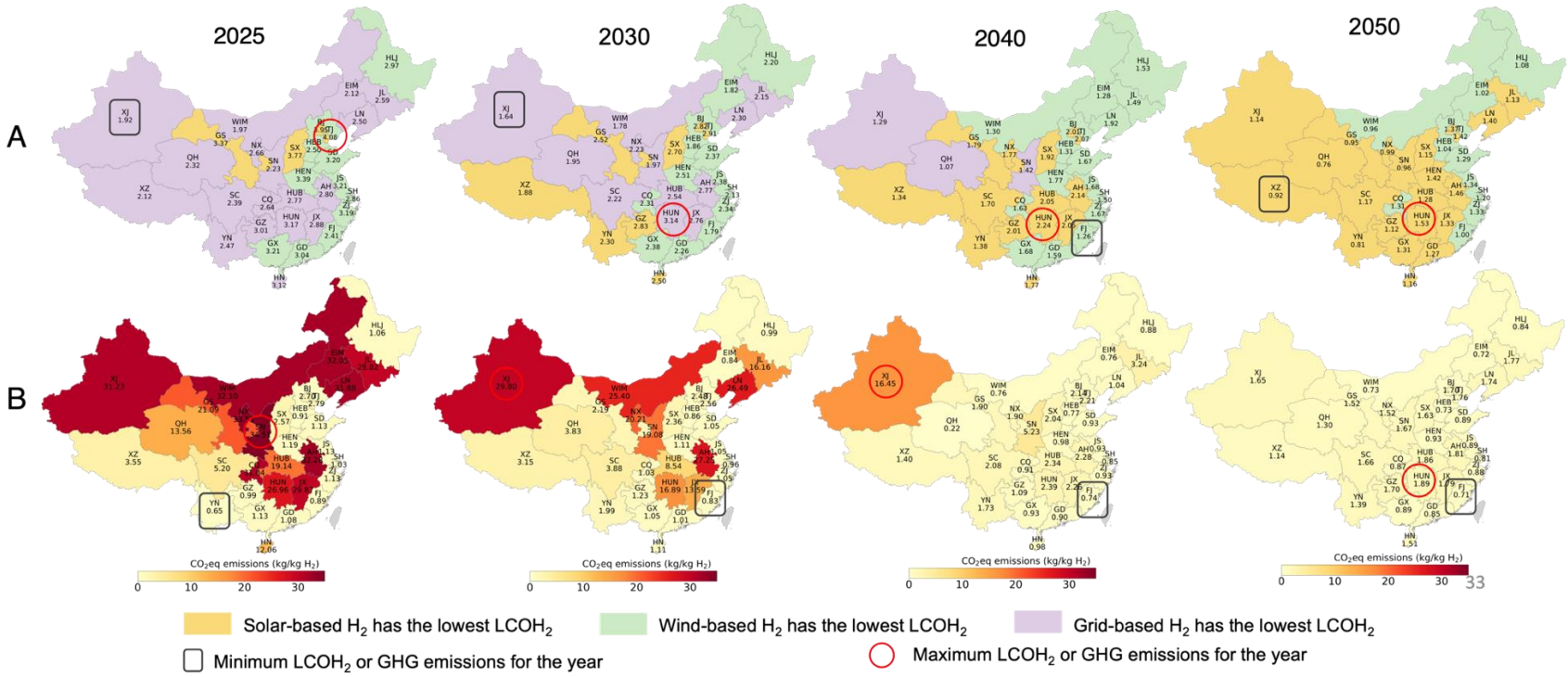

Figure 4.3. (A) Lowest levelized cost and (B) corresponding life cycle GHG emissions of electrolytic hydrogen production by province without subsidies from 2025-2050. Top row (A): Colors represent the technology with the lowest $LCOH_2$ in each province and numbers provide the actual cost (2021USD/kg H_2). Black rectangles and red circles represent the province with the minimum and maximum $LCOH_2$ in each year. Bottom row (B): Colors represent the lowest GHG emissions in each province using the lowest cost technology and numbers provide the actual GHG emissions (CO_{2e} kg/kgH_2). Black rectangles and red circles represent the province with the resulting minimum and maximum GHG emissions each year. Hydrogen production from coal gasification results in 20kgCO_2/kgH_2 without CCS and 2kgCO_2/kgH_2 with CCS. Thus, any provinces with CO_2 eq emissions above 20kgCO_2/kgH_2 are an increase in GHG emissions from coal gasification hydrogen.

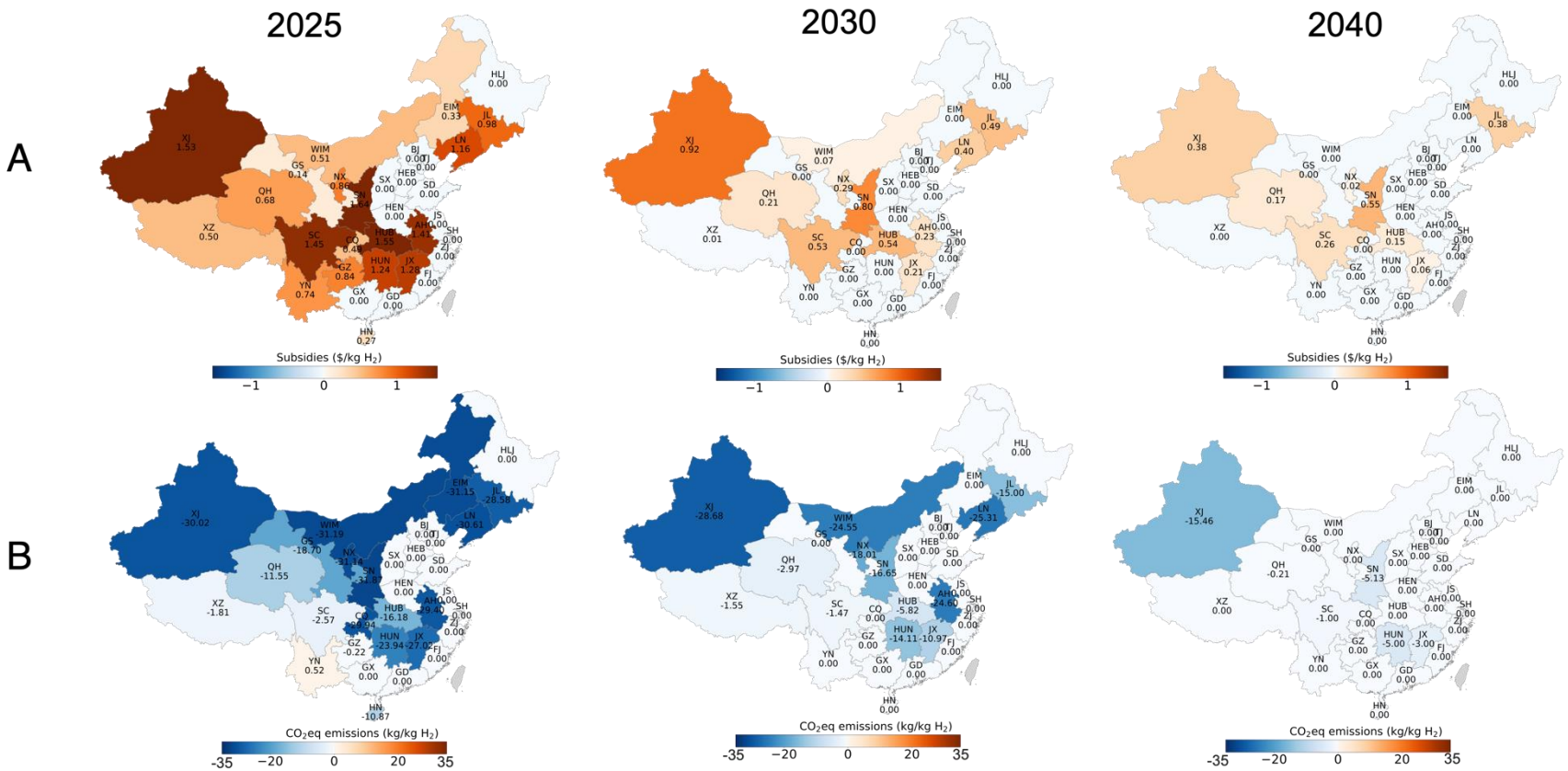

Figure 4.4. Provincial differences in (A) subsidies and (B) life cycle GHG emissions for 2025, 2030 and 2040. Top row (A): Increase in necessary subsidies when renewable-based hydrogen is subsidized rather than grid-based hydrogen (i.e. Subsidies for the minimum-C-emission scenario minus subsidies for the minimum-subsidy scenario); Bottom row (B): Reduction in GHG emissions when renewable based H_2 is subsidized rather than grid-based hydrogen (i.e. GHG emissions of minimum-C-emission scenario minus minimum-subsidy scenario). This shows that if C emissions are the focus of policy, far greater emission reductions will occur than if electrolytic subsidies are minimized and grid-based power is used instead of directly coupling renewable energy to hydrogen production.

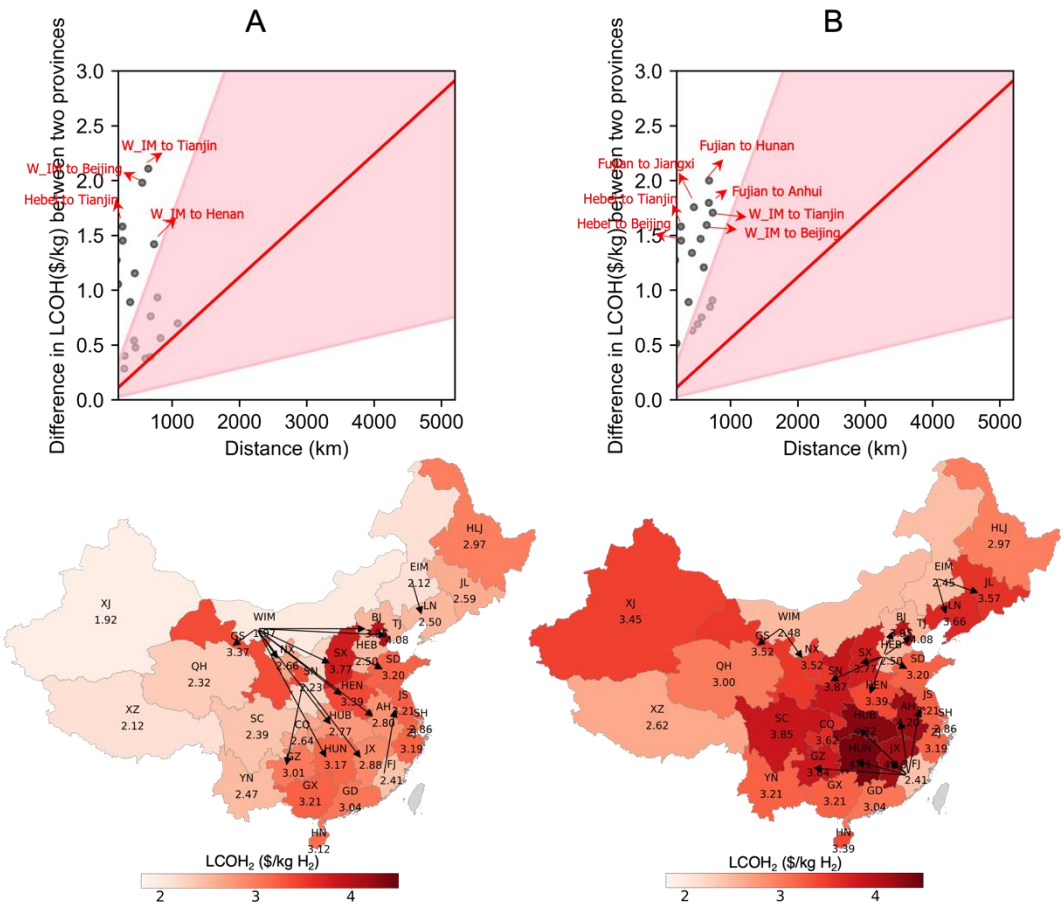

Figure 4.5. Potential hydrogen pipelines between any two provinces in China. A) shows results for the minimum subsidy scenario and (B) shows results for the minimum-C-emission scenario.

Top row: Red lines represent our estimate of the cost of hydrogen pipelines as a function of distance. Dots represent the cost of a pipeline between the capital cities of two provinces. Dots above (below) the red line indicate pipelines that lead to lower (higher) $LCOH_2$ in the recipient province than locally produced electrolytic hydrogen. Pink shading represents the uncertainty of pipeline costs. Bottom row: Black arrows show hydrogen pipelines from one province to another. Colors from pink to dark red indicate the $LCOH_2$ of (A) grid-based electrolytic hydrogen and (B) renewable-based electrolytic hydrogen in 2025.

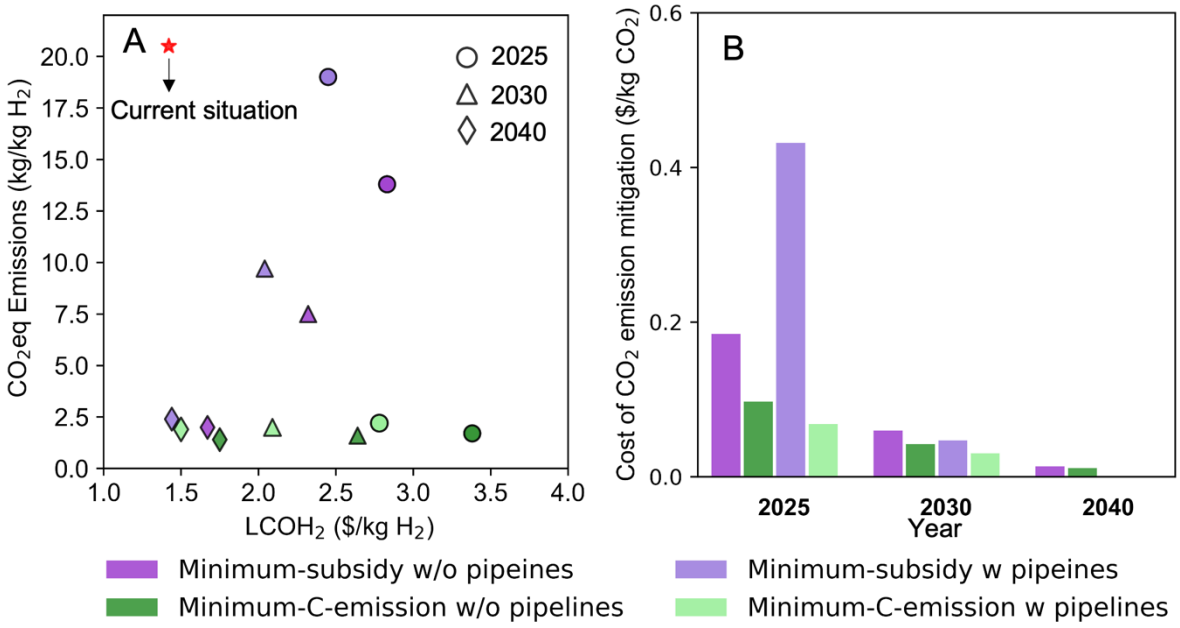

Figure 4.6. Comparison of $LCOH_2$, CO_{2e} emissions and cost of per kg CO_{2e} emission reduction under minimum subsidies – with and without pipeline transport of hydrogen and minimum carbon emissions – with and without pipeline transport of hydrogen. (A) National average $LCOH_2$ and life cycle GHG emissions for the four scenarios for 2025, 2030, 2035 and 2040 compared with 2021. (B) Cost of 1kg CO_{2e} emission reduction for the four scenarios from 2025-2040. The red star indicates the $LCOH_2$ and CO_{2e} of national average hydrogen production (99% from coal, gas, and industrial byproducts) in 2021.

Acknowledgements

I thank the following co-authors of this chapter: Yang Guo, Shangwei Liu, Gang He and Denise L. Mauzerall.

Reference

ACIL Allen Consulting for ARENA, 2018. Opportunities for Australia from hydrogen exports, https://apo.org.au/orga nisation/187246.

Alvarez, R. A. et al. Assessment of methane emissions from the U.S. oil and gas supply chain. Science 361, 186–188 (2018).

Akar, S. et al. 2021 Annual technology baseline (ATB) cost and performance data for electricity generation technologies. (National Renewable Energy Lab (NREL), 2021).

Bartlett J. and Krupnick A. 2020. Decarbonized Hydrogen in the US Power and Industrial Sectors: Identifying and Incentivizing Opportunities to Lower Emissions.

BloombergNEF. New Energy Outlook 2019. https://about.bnef.com/new-energy-outlook/#toc-download (2019).

Bloomberg Finance L.P. Hydrogen Economy Outlook: Key Messages (2020).

Blue Book of Infrastructure Development of China's Hydrogen Energy Industry, China National Institute of Standardization, National Hydrogen Energy Standardization Technical Committee, 2018, https://item.jd.com/69646953883.html.

Bhandari R., C. A. Trudewind and P. Zapp, Life Cycle Assessment of Hydrogen Production via Electrolysis - A Review, J. Clean. Prod., 2014, 85, 151–163.

Buttler, A. & Spliethoff, H. Current status of water electrolysis for energy storage, grid balancing and sector coupling via power-to-gas and power-toliquids: a review. Renew. Sustain. Energy Rev. 82, 2440–2454 (2018).

Cetinkaya E., I. Dincer and G. F. Naterer, Life Cycle Assessment of Various Hydrogen Production Methods, Int. J. Hydrogen Energy, 2012, 37(3), 2071–2080.

Cerniauskas S, Jose Chavez Junco A, Grube T, Robinius M, Stolten D. Options of natural gas pipeline reassignment for hydrogen: cost assessment for a Germany case study. Int J Hydrogen Energy 2020;45:12095e107. https://doi.org/10.1016/j.ijhydene.2020.02.12.

China EV100. China Hydrogen Energy Industry Development Report. 2020.

Cooper, J., Dubey, L., Bakkaloglu, S., and Hawkes, A.: Hydrogen emissions from the hydrogen value chain-emissions profile and impact to global warming, Sci. Total Environ., 830, 15624, https://doi.org/10.1016/j.scitotenv.2022.154624, 2022.

Derwent, R. G.: Hydrogen for Heating: Atmospheric Impacts, Department for Business, Energy & Industrial Strategy, (last access: 12 May 2012), 2018.

Derwent, R. G., Collins, W. J., Johnson, C. E., and Stevenson, D. S.: Transient behaviour of tropospheric ozone precursors in a global 3-D CTM and their indirect greenhouse effects, Climatic Change, 49, 463–487, https://doi.org/10.1023/A:1010648913655, 2001.

Derwent, R. G., Stevenson, D. S., Utembe, S. R., Jenkin, M. E., Khan, A. H., and Shallcross, D. E.: Global modelling studies of hydrogen and its isotopomers using STOCHEMCRI: Likely radiative forcing consequences of a future hydrogen economy, Int. J. Hydrogen Energ., 45, 9211–9221, https://doi.org/10.1016/j.ijhydene.2020.01.125, 2020.

Dufour J., D. P. Serrano, J. L. Ga ́lvez, A. Gonza ́lez, E. Soria and J. L. G. Fierro, Life Cycle Assessment of Alternatives for Hydrogen Production from Renewable and Fossil Sources, Int. J. Hydrogen Energy, 2012, 37(2), 1173–1183.

Erb Tom. The Social Cost of Carbon – Going Nowhere But Up.

https://www.c2es.org/2021/03/the-social-cost-of-carbon-going-nowhere-but-up/

Fesenfeld LP, Schmidt TS, Schrode A. Climate policy for shortand long-lived pollutants. Nat Clim Change. 2018;8:933-936. https://doi.org/10.1038/s41558-018-0328-1

Field, R. A. and Derwent, R. G.: Global warming consequences of replacing natural gas with hydrogen in the domestic energy sectors of future low-carbon economies in the United Kingdom and the United States of America, Int. J. Hydrogen Energ., 46, 30190–30203, 2021.

Frazer-Nash Consultancy: Fugitive Hydrogen Emissions in a Future Hydrogen Economy, Department for Business, Energy & Industrial Strategy, https://www.gov.uk/government/publications/ fugitive-hydrogen-emissions-in-a-future-hydrogen-economy (last access: 14 April 2022), 2022.

Howarth, R.W., and Jacobson, M.Z. How green is blue hydrogen? Energy Science & Engineering 9, 1676–1687. (2021).

Howarth RW. A bridge to nowhere: Methane emissions and the greenhouse gas footprint of natural gas. Energy Sci Eng. 2014; 2:4760. https://doi.org/10.1002/ese3.35

International Renewable Energy Agency (IRENA). Renewable power generation costs in 2019 (2020).

International Energy Agency (IEA). The future of hydrogen. www.iea.org/ reports/the-future-of-hydrogen (2019).

IPCC. Climate Change 2013: The Physical Science Basis. Contribution of Working Group I to the Fifth Assessment Report of the Intergovernmental Panel on Climate Change. Intergovernmental Panel on Climate Change; 2013.

https://www.ipcc.ch/report/ar5/ wg1/. Accessed October 15, 2020.

IPCC SR15 Ch4 2018, p. 374

IPCC. Carbon Dioxide Capture and Storage. Intergovernmental Panel on Climate Change; 2005. https://www.ipcc.ch/report/carbo n-dioxide-capture-and-storage/. Accessed April 1, 2021.

IRENA, 2021. Renewable Power Generation Costs in 2021.

ITP Renewables, Lithium-Ion Battery Testing, ACT, Australia, 2020.

IWG. The Interagency Working Group on social cost of greenhouse gases. Technical Support Document: Social Cost of Carbon, Methane, and Nitrous Oxide Interim Estimates under Executive Order 13990. https://www.whitehouse.gov/wp-content/uploads/2021/02/TechnicalSupportDocument_SocialCostofCarbonMethaneNitrousOxide.pdf

Kikstra, J. S. et al. The social cost of carbon dioxide under climate-economy feedbacks and temperature variability. Environ. Res. Lett. 16, 094037 (2021).

Lauvaux, T. et al. Global assessment of oil and gas methane ultra-emitters. Science 375, 557–561 (2022).

Liu Q, Tian C (2017) Status evaluation of carbon capture, utilization and storage in China and development suggestions [J]. Strategic Research on Climate Change 24(24):1–14

Miao B., Giordano, L. and Chan S.H. Long-distance renewable hydrogen transmission via cables and pipelines. International Journal of Hydrogen Energy, 2021, 46, 18699-18718.

Notice on the public solicitation of opinions on the ‘‘Opinions on Supporting the Development of the Hydrogen Energy Industry’’, Jining City Industry and

Information Technology Bureau, 2019, http://www.jining.gov.cn/art/2019/10/18/art_33400_2203009.html.

Nugent, D., and Sovacool, B.K. (2014). Assessing the lifecycle greenhouse gas emissions from solar PV and wind energy: A critical meta-survey. Energy Policy 65, 229–244. 10.1016/j.enpol.2013.10.048.

NREL. 2021. Life Cycle Greenhouse Gas Emissions from Electricity Generation: Update. https://www.nrel.gov/docs/fy21osti/80580.pdf

Ocko IB, Hamburg SP, Jacob DJ, et al. Unmask temporal trade-offs in climate policy debates. Science. 2017;356:492-493. https://doi. org/10.1126/science.aaj2350 28-1.

Ocko, I.B., and Hamburg, S.P. (2022). Climate consequences of hydrogen emissions. Atmospheric Chemistry and Physics 22, 9349–9368.

Palmer G., Robers A., Hoadley A., Dargaville R and Honnery D. Life-cycle greenhouse gas emissions and net energy assessment of large-scale hydrogen production via electrolysis and solar PV. Energy Environ. Sci., 2021, 14, 5113.

Pan CEER. European cost-efficiency benchmark for gas transmission system operators. 2018.

Paulot, F., Paynter, D., Naik, V., Malyshev, S., Menzel, R., and Horowitz, L. W.: Global modeling of hydrogen using GFDL-AM4.1: Sensitivity of soil removal and radiative forcing, Int. J. Hydrogen Energ., 46, 13446–13460, 2021.

Pellow M. A.; Ambrose H.; Mulvaney D.; Betita R. and Shaw S., Research Gaps in Environmental Life Cycle Assessments of Lithium ion Batteries for Grid-Scale Stationary Energy Storage Systems: End-of-Life Options and Other Issues, Sustainable

Materials and Technologies, Elsevier B.V., 2020.

Penev M, Zuboy J, Hunter C. Economic analysis of a high-pressure urban pipeline concept (HyLine) for delivering hydrogen to retail fueling stations. Transport Res Transport Environ. 2019;77:92e105. https://doi.org/10.1016/j.trd.2019.10.005.

Pingan Securities Research Institute. Special report on power industry equipment. (2019).

P. Moriarty and D. Honnery, Intermittent Renewable Energy: The Only Future Source of Hydrogen?, Int. J. Hydrogen Energy, 2007, 32(12), 1616–1624.

Prather, M. J.: An Environmental Experiment with H2?, Science, 302, 581–582, https://doi.org/10.1126/science.1091060, 2003.

Renssen, S.V. The hydrogen solution? Nat. Clim. Chang. 10, 799–801 (2020).

Saadi FH, Lewis NS, McFarland EW. Relative costs of transporting electrical and chemical energy. Energy Environ Sci 2018; 11:469-475.

Sgouridis S, Carbajales-Dale M, Csala D, Chiesa M, Bardi U. Comparative net energy analysis of renewable electricity and carbon capture and storage. Nat Energy. 2019;4:456-465. https://doi. org/10.1038/s41560-019-0365-7

UNEP. Global Methane Assessment: Benefits and Costs of Mitigating Methane Emissions. United Nations Environment Programme and Climate and Clean Air Coalition; 2021. ISBN: 978-92-807-3854-4. https://www.unep.org/resources/report/globa l-methane-assessment-benefits-and-costs-mitigating-methaneemissions. Accessed July 15, 2021.

van Ruijven, B., Lamarque, J. F., van Vuuren, D. P., Kram, T., and Eerens, H.: Emission scenarios for a global hydrogen economy and the consequences for global air

pollution, Glo. Env. Change, 21, 983–994, https://doi.org/10.1016/j.gloenvcha.2011.03.013, 2011.

Wang qinyi. 2021. Energy data 2020. Energy foundation. In Chinese. https://www.efchina.org/Attachments/Report/report-lceg-20210430-3/2020%E8%83%BD%E6%BA%90%E6%95%B0%E6%8D%AE.pdf

Warwick, N., Griffiths, P., Keeble, J., Archibald, A., Pyle, J., and Shine, K.: Atmospheric implications of increased Hydrogen use, Department for Business, Energy and Industrial Strategy, 75 pp., https://www.gov.uk/government/publications/atmospheric-implications-of-increased-hydrogen-use (last access: 15 April 2022), 2022.

Wei, N., Jiao, Z., Ellett, K., Ku, A.Y., Liu, S., Middleton, R., and Li, X. (2021). Decarbonizing the Coal-Fired Power Sector in China via Carbon Capture, Geological Utilization, and Storage Technology. Environ. Sci. Technol. 55, 13164–13173. 10.1021/acs.est.1c01144.

Wiser, R. et al. Expert elicitation survey on future wind energy costs. Nat. Energy 1, 16135 (2016).

The Oxford Institute For Energy Studies. Power-to-Gas: linking electricity and gas in a decarbonizing world. 2018.

Jiutian, Z., Zhiyong, W., Jia-Ning, K., Xiangjing, S., and Dong, X. (2022). Several key issues for CCUS development in China targeting carbon neutrality. Carb Neutrality 1, 17. 10.1007/s43979-022-00019-3. Zhu, 2021. The Characteristics, Problems and Positioning of hydrogen energy industry in China. China Development Observation. https://cdo.develpress.com/?p=12270

Chapter 5: Conclusion

China is facing challenges of both air pollution and climate change. Decarbonization of energy system is critical to mitigating climate change, improving air quality, protecting human health, and bringing economic benefits simultaneously. To facilitate the clean energy transition and achieve carbon neutrality by 2060, China's government has implemented various deployment policies to accelerate the adoption of low carbon energy technologies. This dissertation advances the understanding of (1) the impacts of alternative-energy-vehicles on air quality, health, and climate (Chapter 2) (2) how battery storage deployment strategies influence the system costs and carbon emissions of China's power system (Chapter 3) and (3) trade-offs between financial subsidies and life cycle GHG emissions in accelerating electrolytic hydrogen development (Chapter 4).

Chapter 2 indicates that a clean energy transition in China's transport sector offers increasing benefits as the power sector decarbonizes. Our study provides a plausible strategy to largely reduce $PM_{2.5}$ and O_3 concentrations in urban areas and achieve carbon neutrality for the on-road transport sector by 2050 through replacing all vehicles with alternative energy vehicles (e.g., electric vehicles, natural gas vehicles and hydrogen fuel cell vehicles), as well as powering those vehicles with primarily non-fossil fuel electricity (91%). We find that increased AEV penetration alone increases $PM_{2.5}$, SO_2, and CO_{2e} emissions when AEVs are powered using electricity generated with the mix of technologies and hydrogen derived from coal or natural gas rather than via water electrolysis using non-fossil electricity. The results highlight the importance of decarbonizing power sector while transforming the transport sector from internal

combustion engine vehicles to alternative energy vehicles simultaneously.

Chapter 3 shows that impacts of battery storage deployment strategies on system costs and carbon emissions depend on provincial resources. When nationally uniform battery deployment takes place, Demand-side and RE-connected batteries have opposite effects on provincial coal-fired power generation and national transmission when they are compared with Grid-connected batteries. Coal-fired power generation is increased by up to 26% in provinces with abundant renewable resources that use Demand-side batteries. However, coal-fired power generation is decreased by up to 22% in provinces with limited renewable resources since more power is transmitted into these provinces and less local power generation is needed. Provincial heterogenous battery storage deployment results in the lowest system costs. Supply provinces with abundant renewable resources can minimize costs by having more RE-connected batteries and fewer Demand-side batteries while demand provinces with limited renewable resources can minimize costs by deploying more Demand-side batteries. Although the cumulative CO_2 emissions in the Mixed battery strategy is not the lowest, the gaps of CO_2 emissions become smaller between the Mixed battery strategy and the RE-connected strategy with the growth of carbon prices. My results provide a method for policymakers to better evaluate the impacts of battery storage strategies on CO_2 emissions and system costs by taking local characteristics of solar radiation, wind resources and fossil fuel prices into consideration.

Chapter 4 reveals that subsidizing grid-based electrolytic hydrogen could increase life cycle GHG emissions. To minimize carbon emissions, more subsides are required to

subsidize renewable-based electrolytic hydrogen rather than grid-based electrolytic hydrogen. Also, larger subsidies for renewable- rather than grid-based electrolytic hydrogen result in lower costs for CO_2 emission reductions. The Minimum-C-emission scenario reduce life cycle GHG emissions by 30%-87% with a 4%-23% increase of $LCOH_2$, compared to the Minimum-subsidy scenario. Transporting hydrogen with pipelines can effectively reduce $LCOH_2$ within individual provinces, however, it will induce increase in life cycle GHG emissions because some provinces have low levelized cost of grid-based hydrogen with high life cycle GHG emissions.

Building on my dissertation that focuses on the decarbonization of China's energy system. To further improved the understanding of the low carbon technology policy deployment and its impacts on China's energy system and economic investments, I make the following suggestions for future studies:

1. **Sector-coupling in facilitating the integration of variable renewable energy**

   Sector coupling technologies and strategies will play a key role in the transition. For example, on the one hand, low carbon hydrogen can be used as a medium to store excess energy generated by intermittent renewable electricity sources, as a source of domestic and industrial heat, and as a feedstock for industrial processes, such as refining, steel production and fertilizer production. On the other hand, low carbon hydrogen produced from renewables, will increase the electricity demand for power sector. Sector coupling can help match hydrogen production and electricity consumption and optimize the energy system. Quantifying the sector-coupling opportunities requires an integrated approach to model the increasing complexity and

interconnectedness of energy systems. The development of these model tools will be helpful to estimate the cross-sector synergies and trade-offs of different low carbon technologies.

2. **Impacts of climate change and extreme climate events on energy systems**

   Climate change and extreme climate events will influence energy system from both supply side and demand side. On the supply side, renewable resources like solar and wind energy vary depending on the weather and the time of day or year, so in these extreme weather events, the cloudiness and wind density will change. Reduced rainfall and dry weather conditions are raising concerns about hydropower's electricity output. Also, thermal power plants face temperature-related impacts on cooling systems. On the demand side, climate change influences energy demand by affecting the duration and magnitude of diurnal and seasonal heating and cooling requirements in these end-use sectors, like building, transport, and industry. Those extreme weather events, like storms, snowstorms, summer heat waves will increase electricity demand as people turn on air conditioning and as some machines work harder to maintain cool temperatures. Therefore, evaluating the impacts of climate change on energy system is very valuable to make the decarbonized energy system more resilient.

3. **Low carbon technology deployment policy impacts on other developing countries**

   To achieve Paris Agreement global temperature 2℃ increase limitation, developing countries have to move toward a greener future and net-zero emissions. Insights from this China-focused dissertation may have important value for other developing

countries to tackle similar challenges in the decarbonization of their energy system and take one step closer to carbon neutrality. Deployment policies should be adapted to reflect specific national and local circumstances and further improve integration of renewables into the energy system.

Appendix for Chapter 2

Supplementary Note S2.1. Alternative energy vehicles

The State Council of China set a new energy vehicle goal for the production and sale of at least 500,000 BEVs and PHEVs by 2015, and cumulative sales of BEVs and PHEVs of 5 million by the end of 2020[9]. The stock of EVs reached 58,000 at the end of 2015[10], which achieved the stated 2015 target. By the end of 2019, the stock of EVs had increased to 3.8 million[11]. Some Chinese government consumer subsidies for EVs can be up to 50% of the purchase price[12]. China has the largest electric vehicle (EV) market (2.3 million)in the world, with almost half of the global EV stock in 2018, followed by Europe (1.2 million) and the US (1.1 million)[5]. The China Renewable Energy Outlook report[2] predicts that the EV market share in China could reach 80% of all passenger vehicles by 2050.

The development of hydrogen fuel cell vehicles (HFCVs) started more recently in China. China's government plans to introduce 5,000 HFCVs as buses and taxis into public service by 2020, and 50,000 HFCVs by 2025. By 2030, the stock of HFCVs is projected to reach 1 million, with more than 1000 hydrogen fueling stations established across the country. The China Renewable Energy Outlook predicts that in 2050, almost 50% of trucks will be HFCVs.

In contrast to HFCVs, the development of both compressed natural gas/liquid natural gas (CNG/LNG) vehicles and fueling stations for CNG/LNG vehicles increased rapidly between 2011 and 2019 in China. Natural gas vehicles (NGVs) with ultra-low NO_x engines can produce near-zero NO_x emissions[13]. Compared with diesel, CNG/LNG emits less CO_2 per vehicle mile travelled. CNG/LNG vehicles are a viable low-carbon

alternative to conventional vehicles. However, most studies[14,15] remain concerned about future CNG/LNG deployment because natural gas use frequently results in methane leakage, results in CO_2 emissions during combustion, and it is a nonrenewable fossil fuel.

Electric vehicles (EVs) can reduce the emissions that contribute to climate change and regional air pollution, improving public health. However, they are not currently good options for long distance travel because of limitations in battery technology and refueling constraints. HFCVs are good alternative options for medium and heavy-duty trucks for long distance travel due to their relatively high energy density and fast refueling. However, currently most H_2 is produced by natural gas[16,17], which results in air pollutant and greenhouse gas (GHG) emissions. In the future, if H_2 is increasingly produced by hydrolysis of water using renewably generated electricity, air pollutant and GHG emissions will decrease. Compressed natural gas/liquid natural gas (CNG/LNG) vehicles are suitable options to reduce air pollutant emissions in the short-term but are not well-suited to address long-term goals of decarbonizing the transport sector and eliminating the sector's dependence on fossil fuels.

Table S2.1. Pros and cons of alternative energy vehicles

Types	Pros	Cons
Electric vehicles (Including EMCs)	1. Zero emissions during vehicle operation 2. Reduced cost of purchase compared with ICEVs 3. Vehicle batteries potentially used as energy storage for vehicle to grid infrastructure	1. Limited charging infrastructure 2. Range limitation 3. Slow charging
Hydrogen fuel cell vehicles	1. Zero emissions during vehicle operation 2. Long driving range 3. Fast refueling 4. Renewable energy storage if H_2 is derived from hydrolysis using non-fossil electricity.	1. Limited refueling infrastructure 2. High cost of hydrogen production 3. Source of H_2 is typically from natural gas but could come from renewable electricity. 3. Uncertainty regarding future costs.
Compressed natural gas/Liquid natural gas vehicles	1. Low cost of refueling infrastructure 2. Low cost of fuel 3. Low air pollutant emissions	1. GHG emissions 2. Natural gas is a nonrenewable fossil fuel 3. Limited natural gas supply in China.

Table S2.2. Alternative energy vehicle penetration scenarios for 2050

Scenarios	EV-PVs	EV-Trucks	EV-Buses &Taxies	HFCVs-Trucks	CNG/LNG-HDPV & Trucks	EMC-MC
Low penetration (LP)	10%	2%	50%	2%	3%	30%
Intermediate penetration (IP)	50%	5%	80%	10%	6%	50%
High penetration (HP)	80%	9%	100%	18%	10%	80%
Maximum penetration (MP)	100%	50%	100%	50%	/	100%

Notes:
PV: Passenger vehicle (Including light-duty, medium-duty, and heavy-duty passenger vehicle)
HDPV: Heavy-duty passenger vehicle
EMC: Electric motorcycles
MC: Motorcycles

Table S2.3. Electric power generation scenarios for 2050

Scenarios	Coal	Renewables	Nuclear	NG
2015 national average	70%	25%	3%	2%
Low Renewable (LR)	38%	40%	15%	7%
High Renewable (HR)	8%	85%	6%	1%

Supplementary Note S2.2. Electric vehicle deployment strategy

The rapid increase in China's EV sales has been broadly driven by strong purchase subsidies, which favor battery electric vehicles (BEVs) over plug-in hybrid electric vehicles (PHEVs) and do not extend to internal combustion engine vehicles (ICEVs). The Chinese government has announced that the these purchase subsides will cease after 2020, while new subsidies will switch to the charging infrastructure[18]. Liang et al.[4] employed a normalized influential scoring method based on collected survey data on LDPVs during 2015-2018 to analyze EV purchase intentions. We adopt the ratio of BEVs to PHEVs determined by Liang et al. (1.7:1 for passenger vehicles, 9:1 for trucks and 23:1 for taxies and buses) for the total EV population in LP scenario (Table S2.5). The ratio of BEV to PHEVs gradually increases in IP, HP and MP scenarios. In MP scenario, we assume 100% of EVs are BEVs, which allow a total decarbonization of on-road transport sector.

Table S2.4. The proportion of BEVs and PHEVs in various vehicle fleets under four scenarios

Scenarios	EV- PVs		EV-Trucks		EV-Buses &Taxies	
	BEVs	PHEVs	BEVs	PHEVs	BEVs	PHEVs
Low penetration (LP)	6.3%	3.7%	1.8%	0.2%	47.8%	2.2%
Intermediate penetration (IP)	40%	10%	4.5%	0.5%	78%	2%
High penetration (HP)	65%	15%	8.5%	0.5%	98%	2%
Maximum penetration (MP)	100%	0%	50%	0%	100%	0%

Table S2.5. Four hydrogen source scenarios[19]

Scenarios	Fossil fuel		Renewables		Chlor alkali-by product	Others
	Methane reforming	Coal gasification	Wind power	Solar power		
Low Penetration (LP)	54%	6%	5%	5%	30%	2%
Intermediate penetration (IP)	36%	4%	25%	25%	15%	7%
High Penetration (HP)	18%	2%	35%	35%	6%	1%
Maximum penetration (MP)	9%	1%	45%	45%		

Supplementary Figures

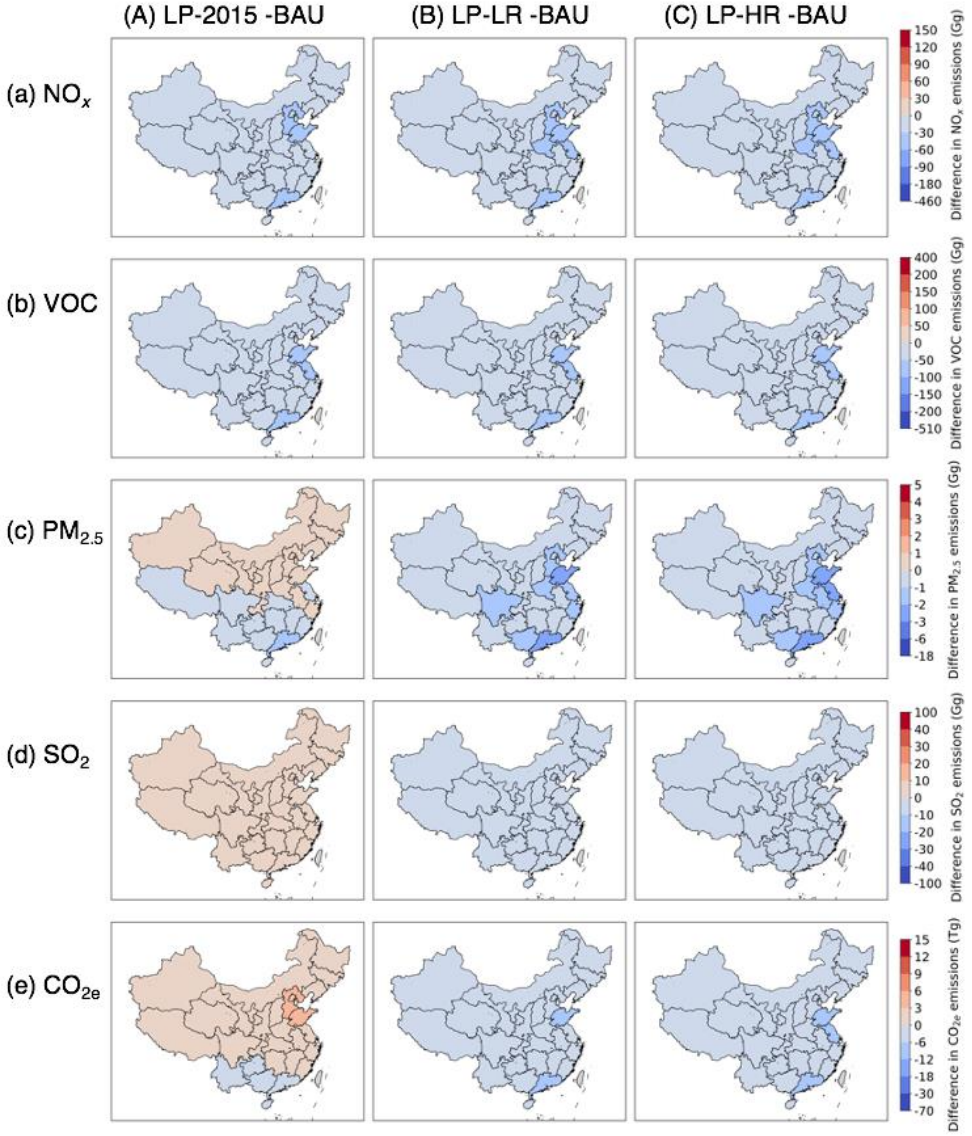

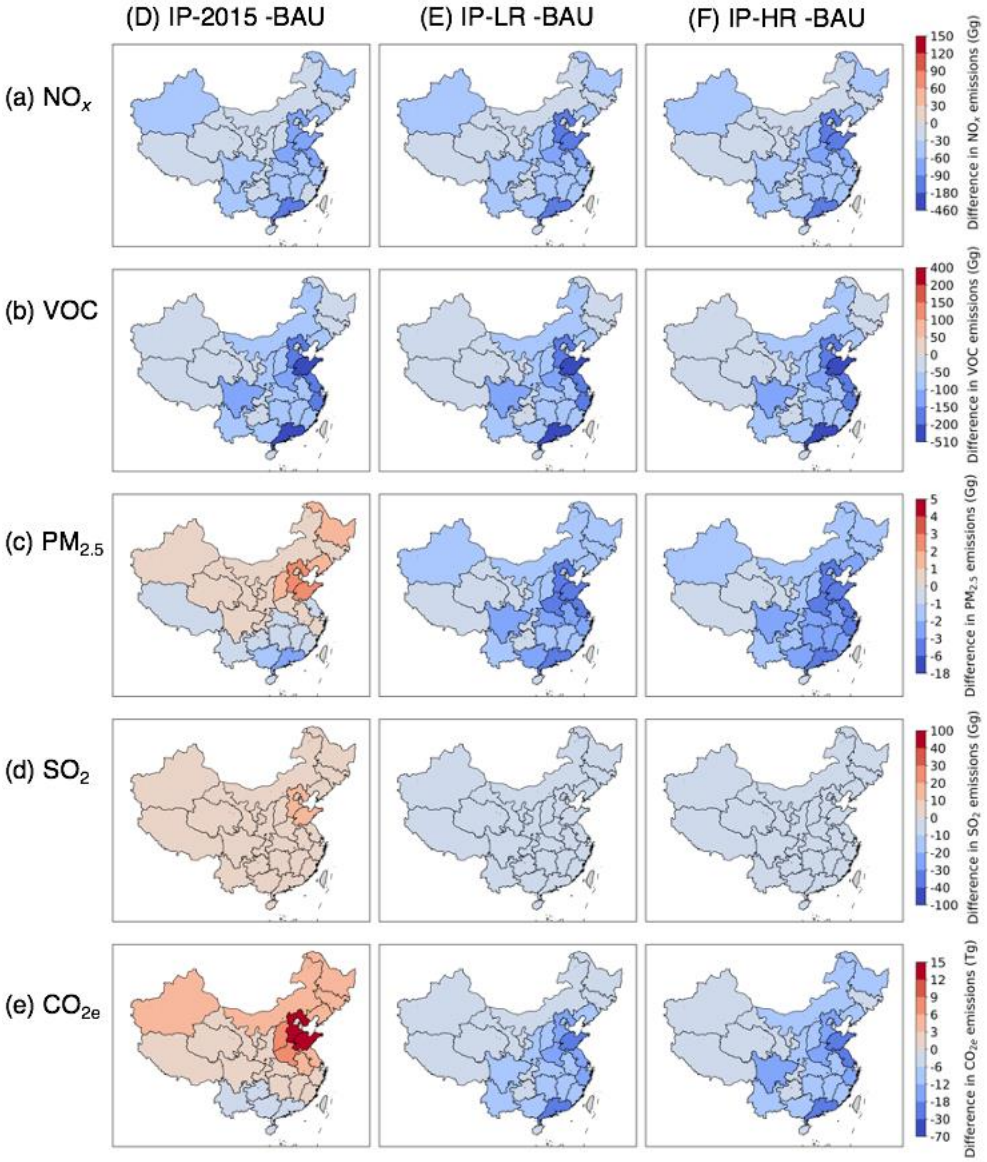
(D) IP-2015 -BAU
(E) IP-LR -BAU
(F) IP-HR -BAU
(a) NO_x
(b) VOC
(c) $PM_{2.5}$
(d) SO_2
(e) CO_{2e}
Difference in NO_x emissions (Gg)
150 120 90 60 30 0 -30 -60 -90 -180 -460
Difference in VOC emissions (Gg)
400 200 150 100 50 0 -50 -100 -150 -200 -510
Difference in $PM_{2.5}$ emissions (Gg)
5 4 3 2 1 0 -1 -2 -3 -6 -18
Difference in SO_2 emissions (Gg)
100 40 30 20 10 0 -10 -20 -30 -40 -100
Difference in CO_{2e} emissions (Tg)
15 12 9 6 3 0 -6 -12 -18 -30 -70

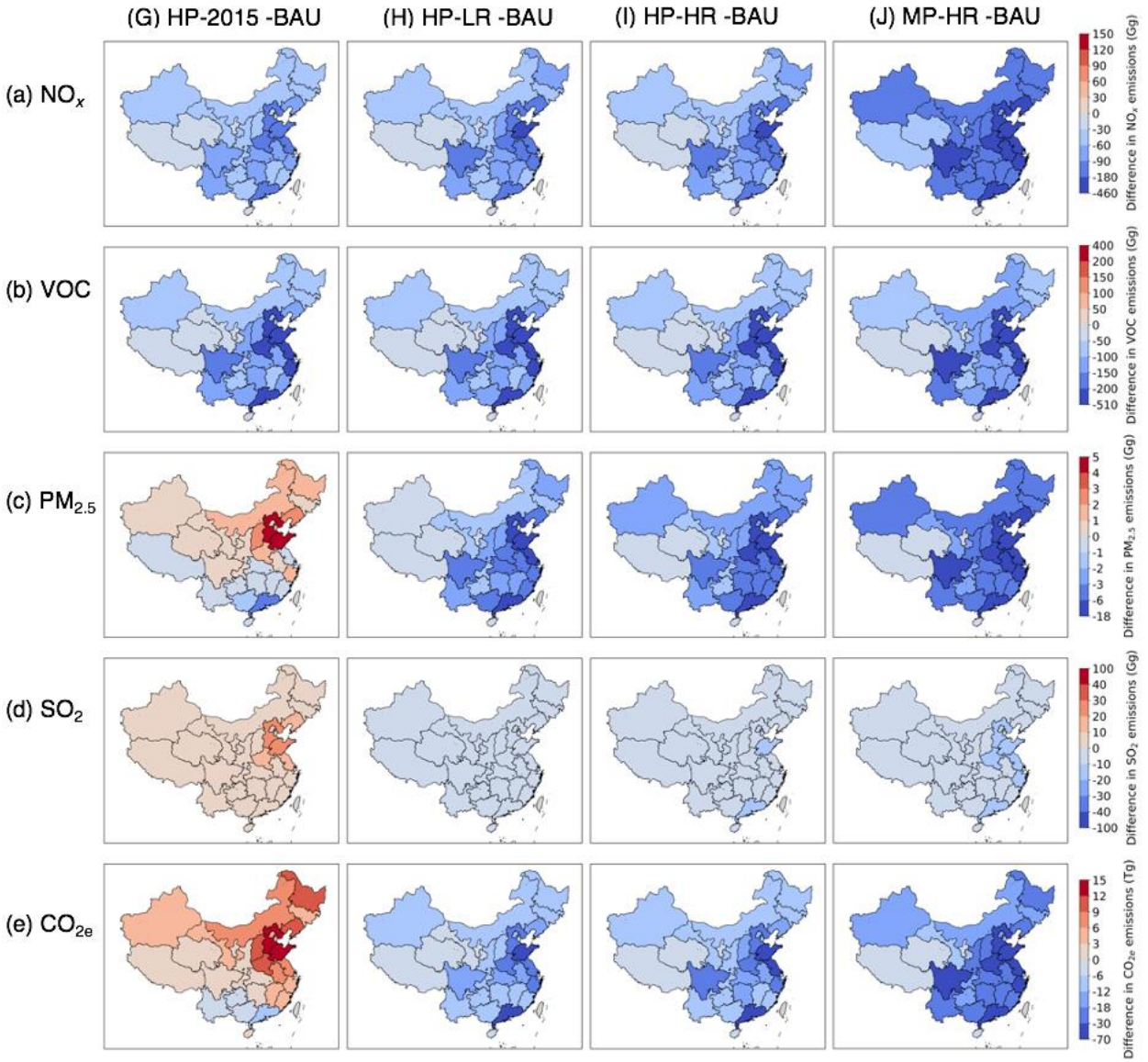

Figure S2.1. Provincial changes in air pollutant and CO_{2e} emissions

Provincial changes in (a) NO_x, (b) VOC, (c) $PM_{2.5}$, (d) SO_2 and (e) CO_{2e} emissions under (A) LP-2015 scenario (low AEV penetration with 2015 power mix), (B) LP-LR scenario (low AEV penetration with low renewable penetration), (C) LP-HR scenario (low AEV penetration with high renewable penetration), (D) IP-2015 scenario (intermedium AEV penetration with 2015 power mix), (E) IP-LR scenario (intermedium AEV penetration with low RE penetration), (F) IP-HR scenario (intermedium AEV penetration with high RE penetration) , (G) HP-2015 scenario (high AEV penetration with 2015 power mix), (H) HP-LR scenario (high AEV penetration with low RE penetration), (I) HP-HR scenario (high AEV penetration with high RE penetration) and (J) MP-HR scenario (maximum AEV penetration with high RE penetration) compared to the base case.

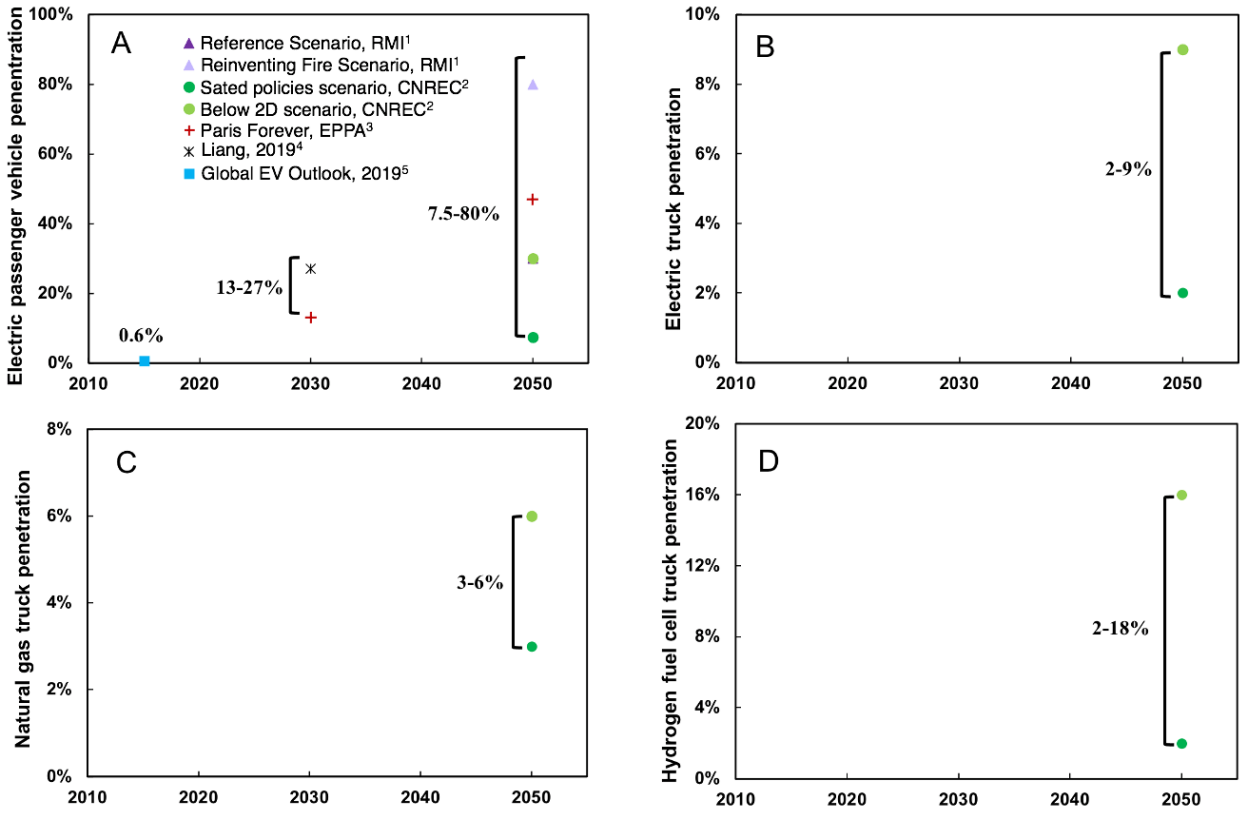

Figure S2.2. Summary of literature indicating possible ranges of penetration in China

(A-D) represent penetration of (A) Electric passenger vehicles, (B) EV trucks, (C) CNG/LNG trucks and (D) HFCV trucks in total vehicle population from 2015-2050. The data are from projections by the Rocky Mountain Institute[1] (Reference Scenario and Reinventing Fire China Scenario, 2017), the Chinese Energy Research Institute[2] (Stated policies and Below two degree Scenario in the China Renewable Energy Outlook 2018), a MIT report based on economic projection and policy analysis (EPPA) model[3], Liang et al (2019) [4]and Global EV outlook 2019[5].

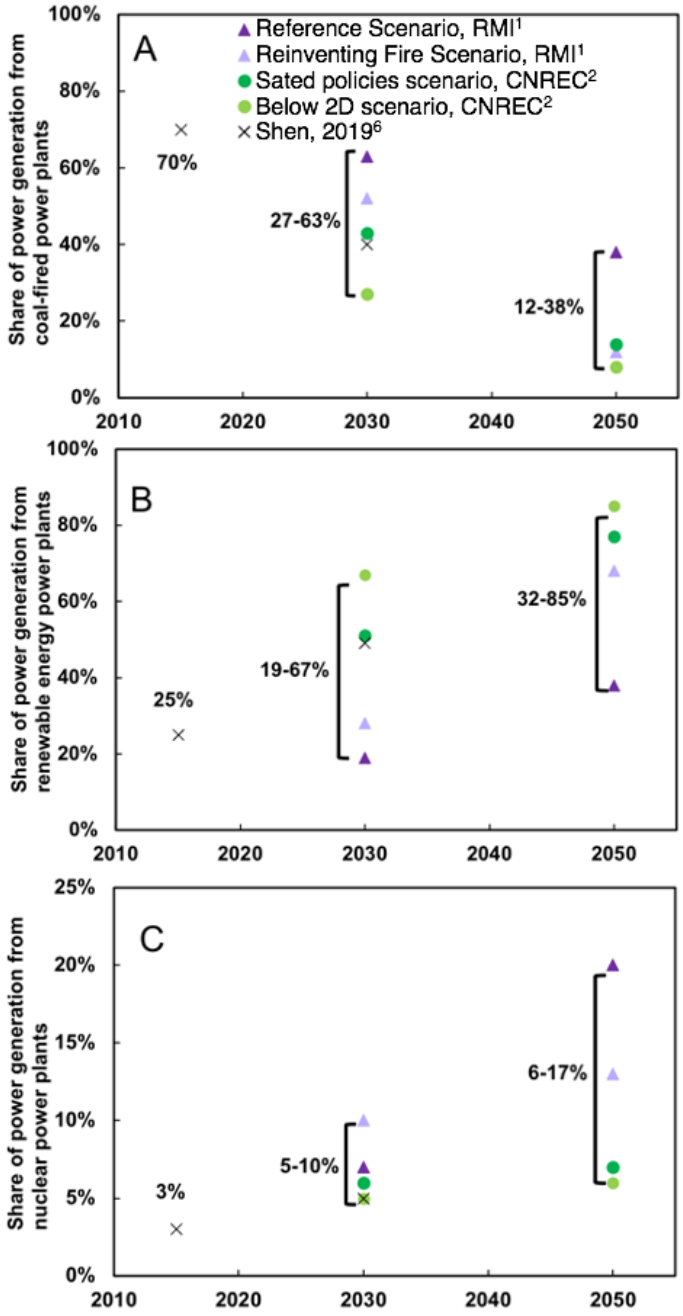

Figure S2.3. Literature review of fraction of power generation in China

(A-C) represent share of power generation from (A) coal-fired, (B) renewable energy, and (C) nuclear power plants compared to total power generation from 2015-2050. The data are from projections by the Rocky Mountain Institute[1] (Reference Scenario and Reinventing Fire China Scenario, 2017), the Chinese Energy Research Institute[2] and Shen et al., (2019)[6] .

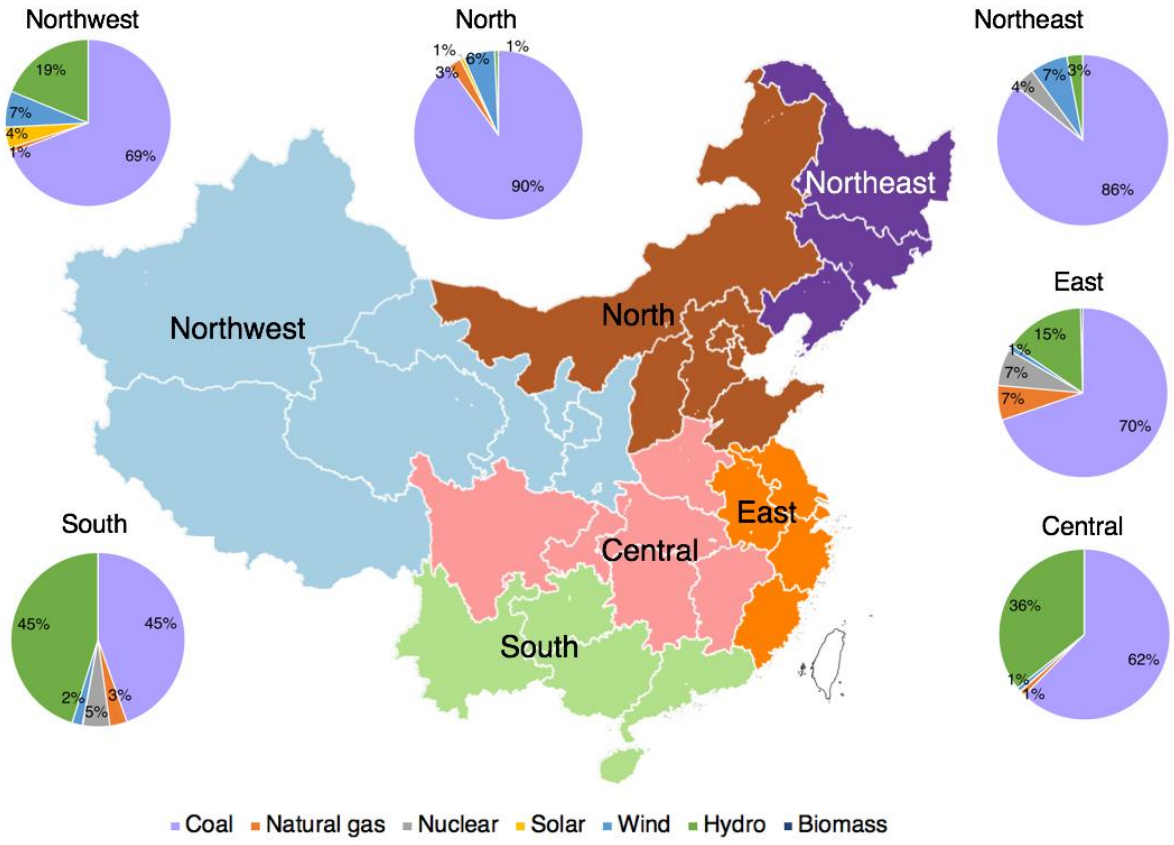

Figure S2.4. Power mix of each power grid in 2015[6]

Pie charts indicate the power mix in the northeast, north, northwest, east, central and south grid, respectively.

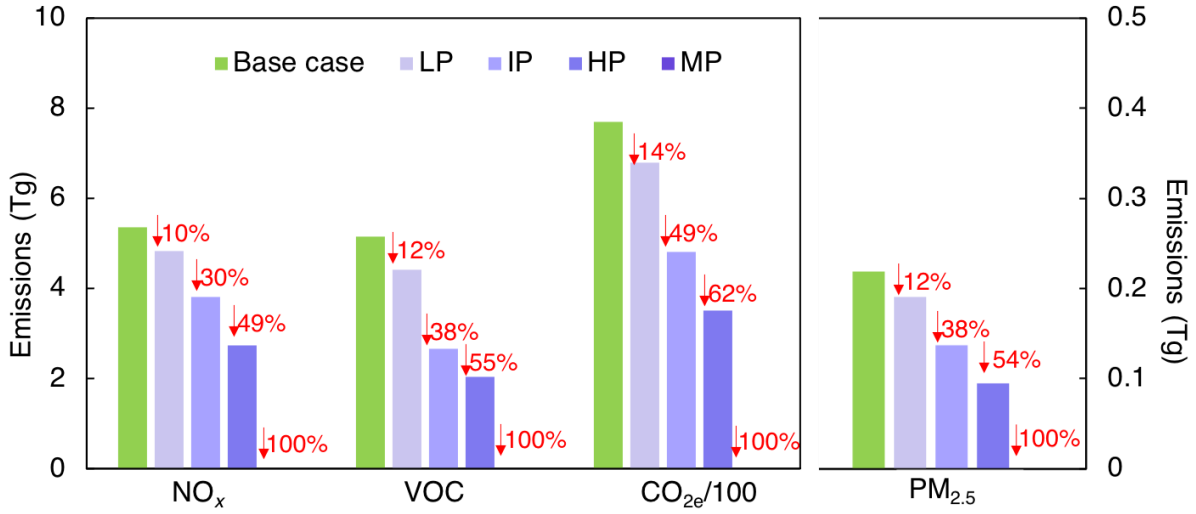

Figure S2.5. Tailpipe emissions of the on-road transport sector in four AEV scenarios

Bars indicate the tailpipe emissions in the base case and each scenario. Red arrows and numbers indicate the percent reduction of tailpipe emissions in LP, IP, HP and MP scenarios compared to the Base case.

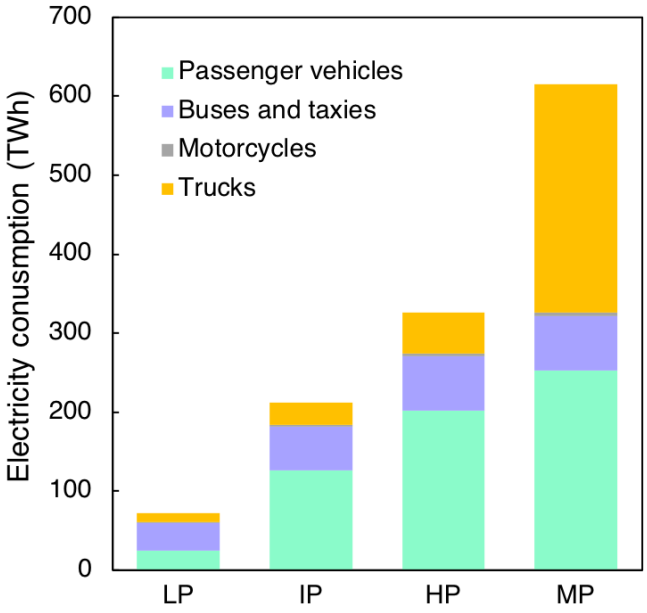

Figure S2.6. Electricity consumption of four alternative energy vehicle scenarios

Electricity consumption from passenger vehicles, buses and taxies, motorcycles and trucks in low AEV penetration (LP), intermediate AEV penetration (IP), high AEV penetration (HP) and maximum AEV penetration (MP) scenario.

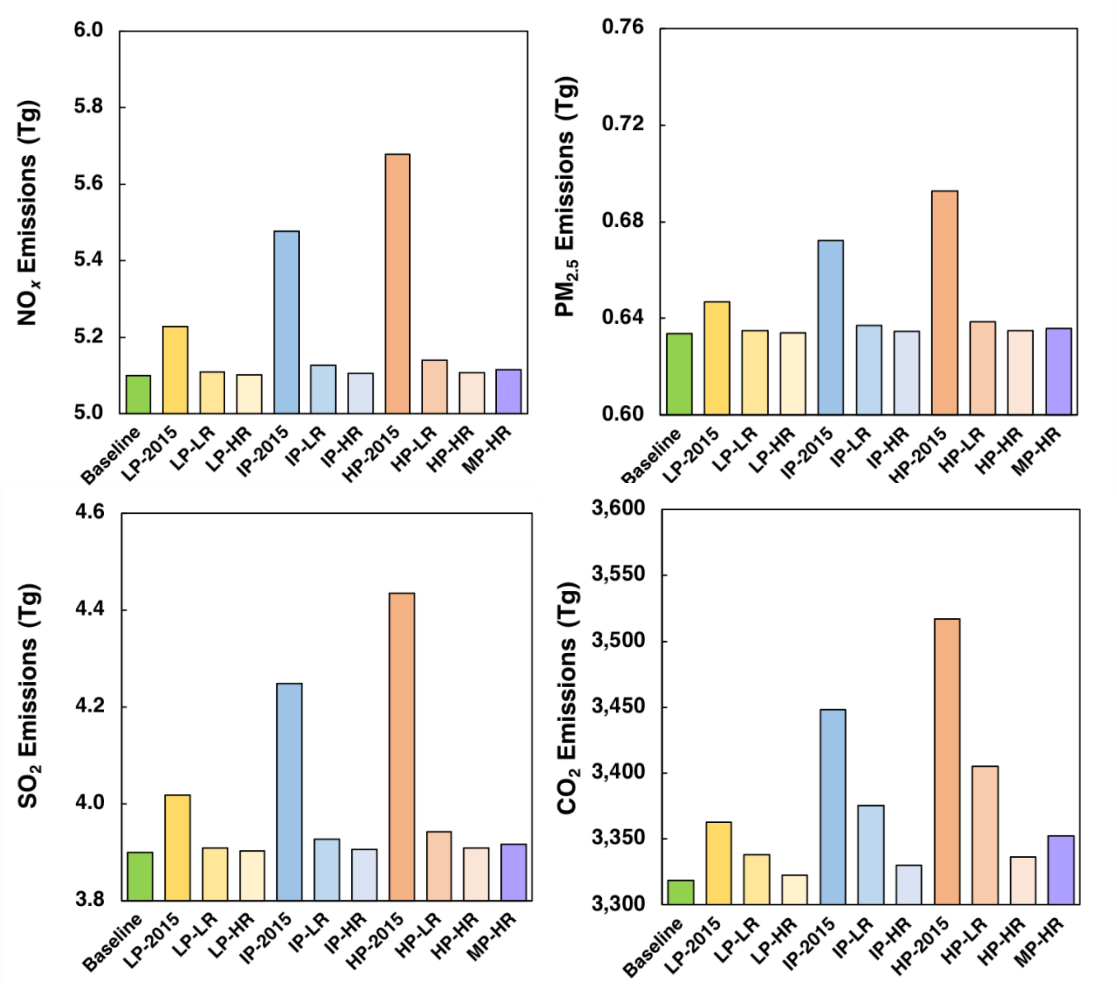

Figure S2.7. Emissions from the power sector resulting from AEV penetration under various scenarios

Electricity production for charging electric vehicles increases air pollutant and CO_{2e} emissions from power generation in each scenario compared to the base case. Changes in emissions are obtained by subtracting the Baseline quantity from the emissions for each scenario.

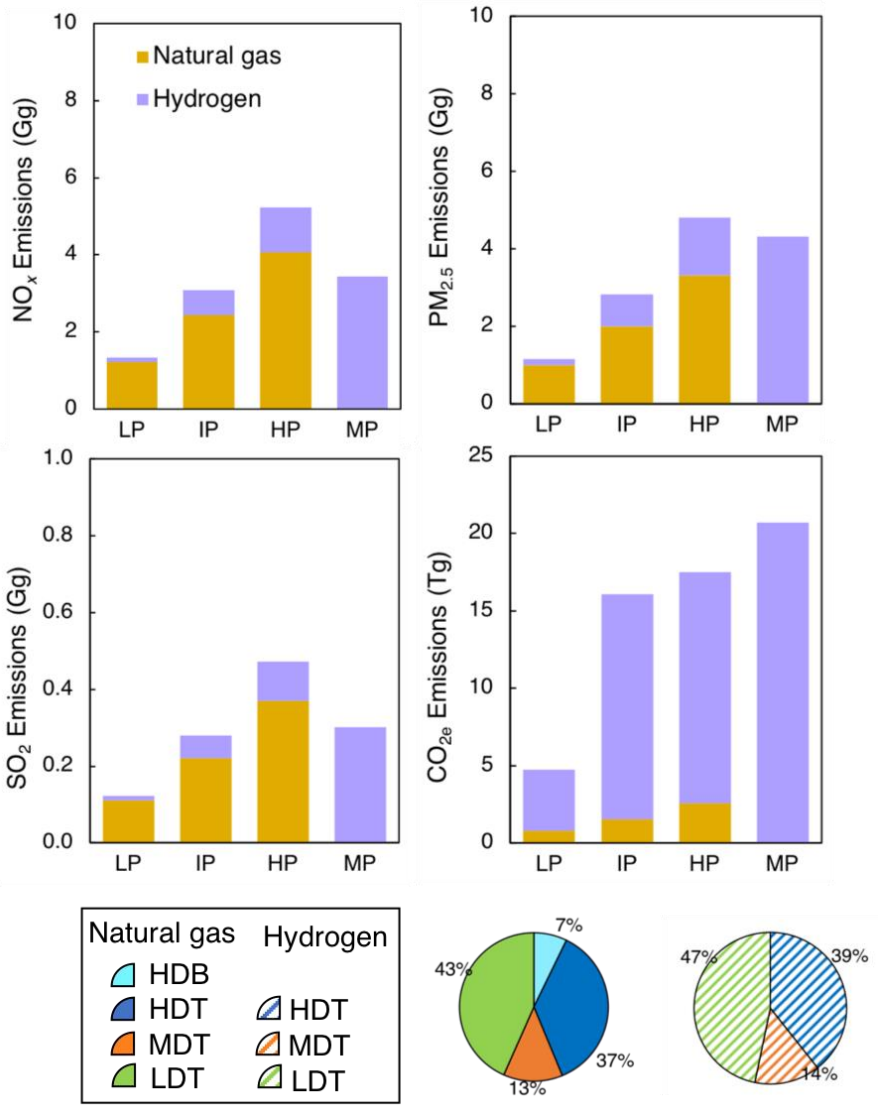

Figure S2.8. Air pollutants and CO_{2e} emissions from natural gas and hydrogen upstream production

Brown and purple bars indicate the increase emissions from natural gas and hydrogen production, respectively, under LP, IP, HP and MP scenario. The pie charts indicate the share of natural gas (solid color) and hydrogen (colored diagonal lines) upstream emissions from different vehicle types.

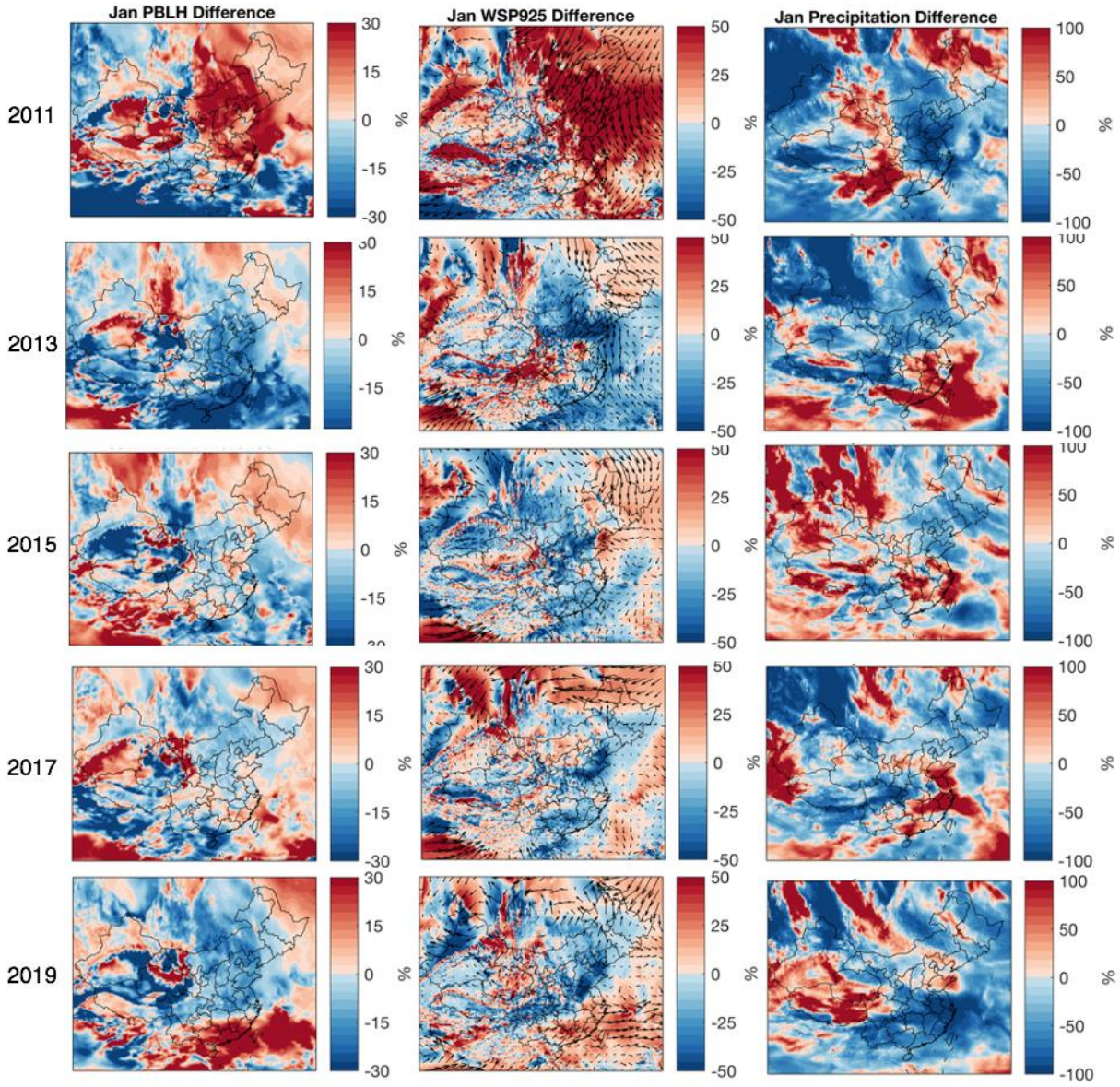

Figure S2.9. Percentage changes in meteorology of January

Percentage difference of average (A) planetary boundary layer height, (B) wind speed at 925-hPa and (C) total precipitation in January 2011, 2013, 2015, 2017 and 2019 compared with the average of 2011-2020.

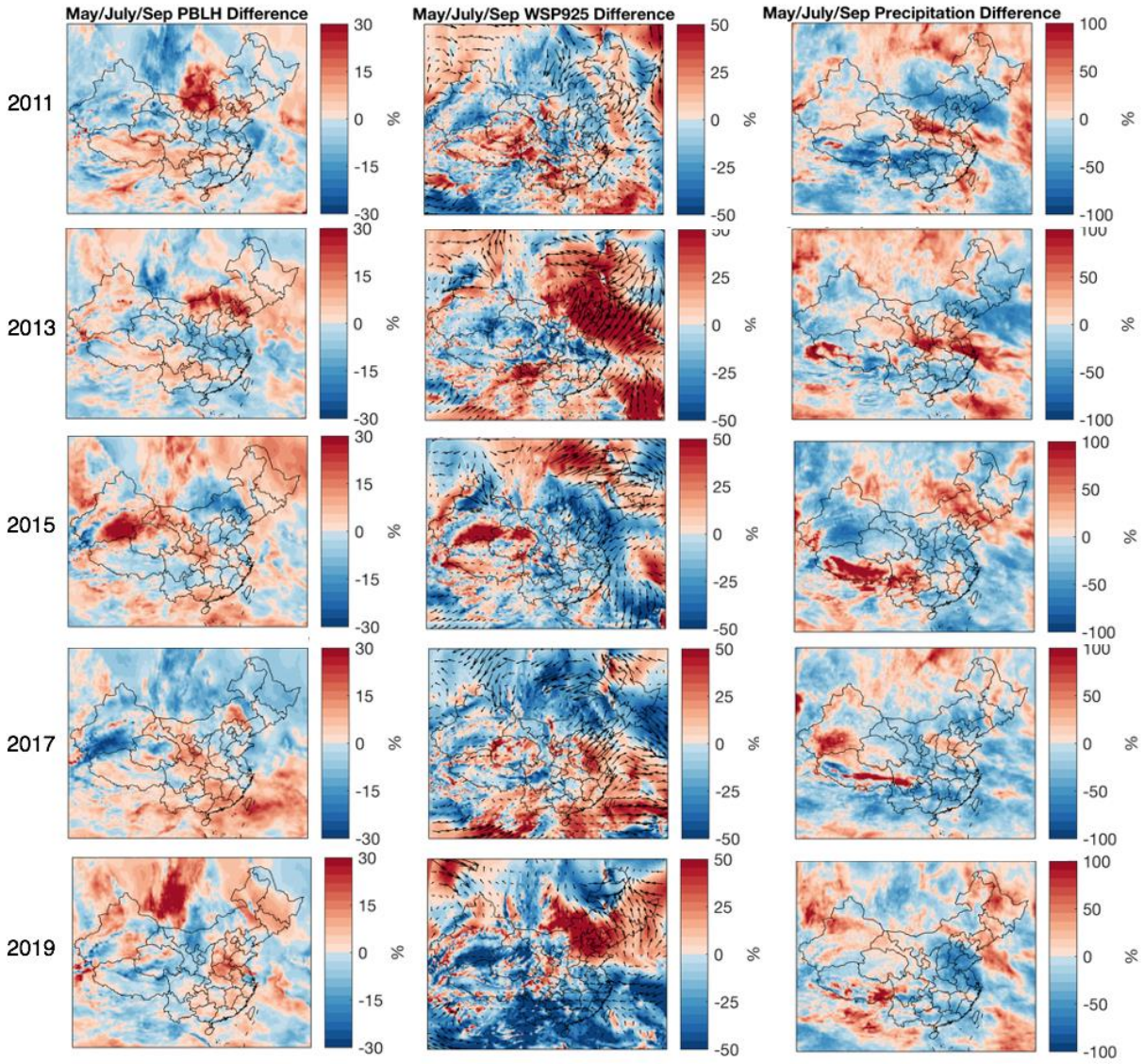

Figure S2.10. Percentage changes in meteorology of average of May, July and September. Percentage difference of average (A) planetary boundary layer height, (B) wind speed at 925-hPa and (C) total precipitation during May, July and September 2011, 2013, 2015, 2017 and 2019 compared with the average of 2011-2020.

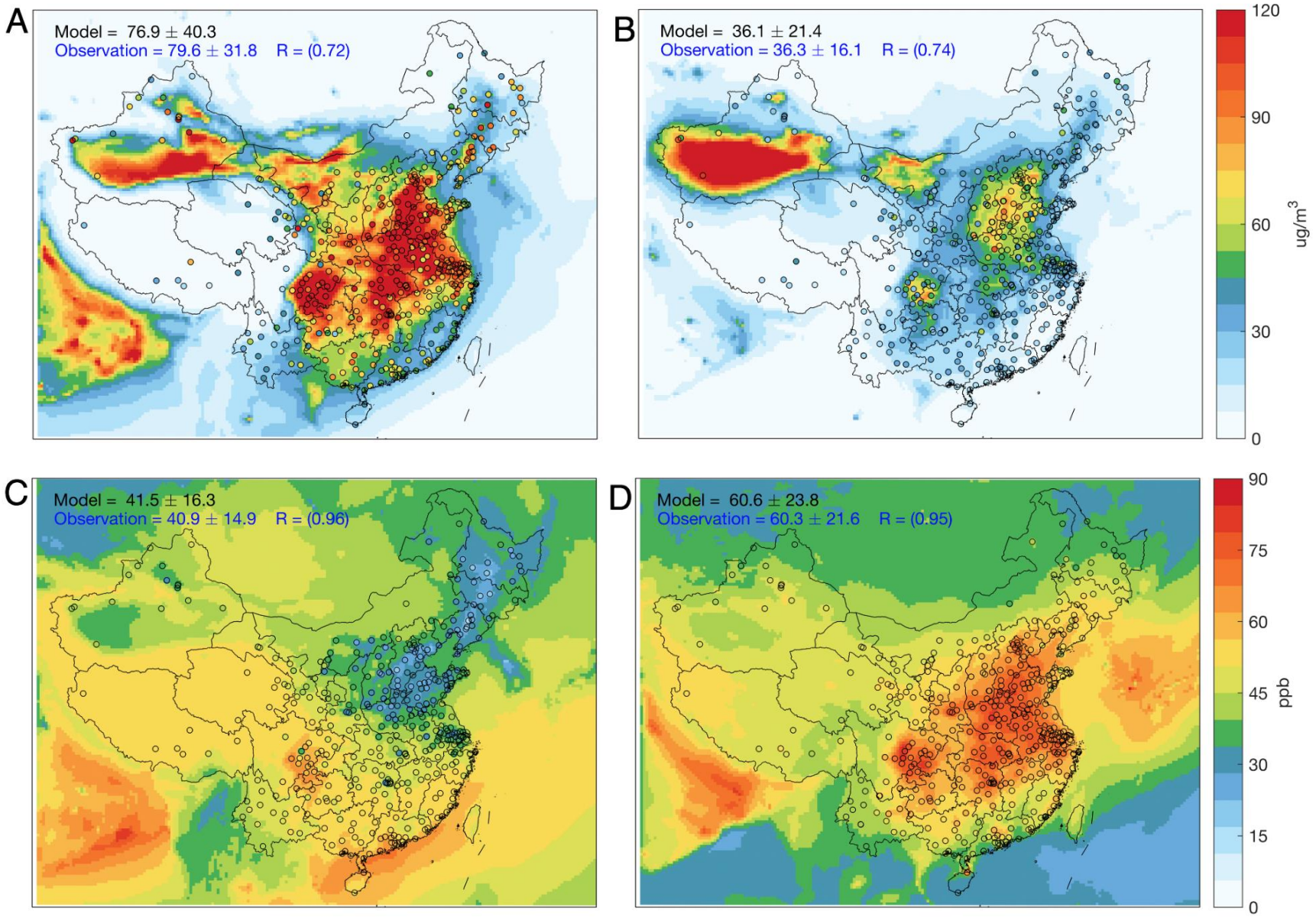
A
Model = 76.9 ± 40.3
Observation = 79.6 ± 31.8 R = (0.72)
B
Model = 36.1 ± 21.4
Observation = 36.3 ± 16.1 R = (0.74)
120
90
60
30
0
ug/m3
C
Model = 41.5 ± 16.3
Observation = 40.9 ± 14.9 R = (0.96)
D
Model = 60.6 ± 23.8
Observation = 60.3 ± 21.6 R = (0.95)
90
75
60
45
30
15
0
ppb

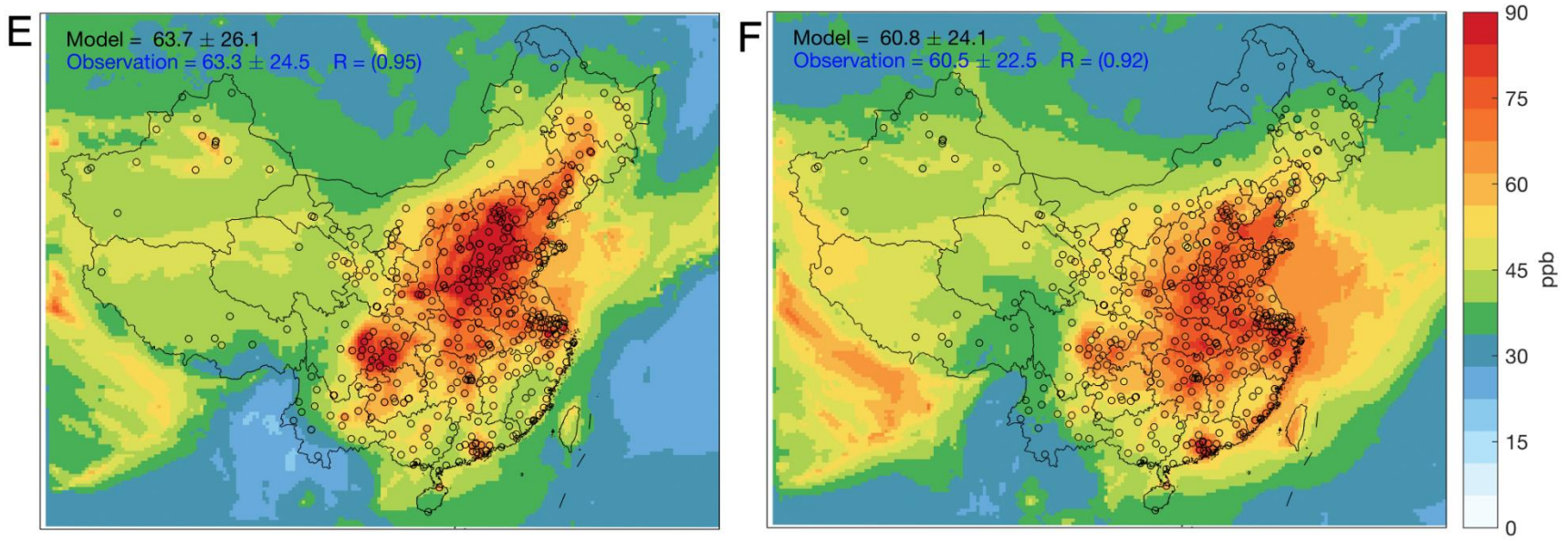

Figure S2.11. Comparison of observed and simulated monthly mean $PM_{2.5}$ and MDA8 O_3 concentration

Comparison of observed (dots) and simulated (map) monthly mean $PM_{2.5}$ concentrations are shown in (A) January, (B) July, and MDA8 O_3 concentrations in (C) January, (D) May, (E) July and (F) September 2015. Monitoring sites with less than 5% missing data per month are used. Numbers inset are mean values and standard deviations of observations (black) and simulations (red) averaged over all the sites and their spatial correlation coefficient (R) for each month.

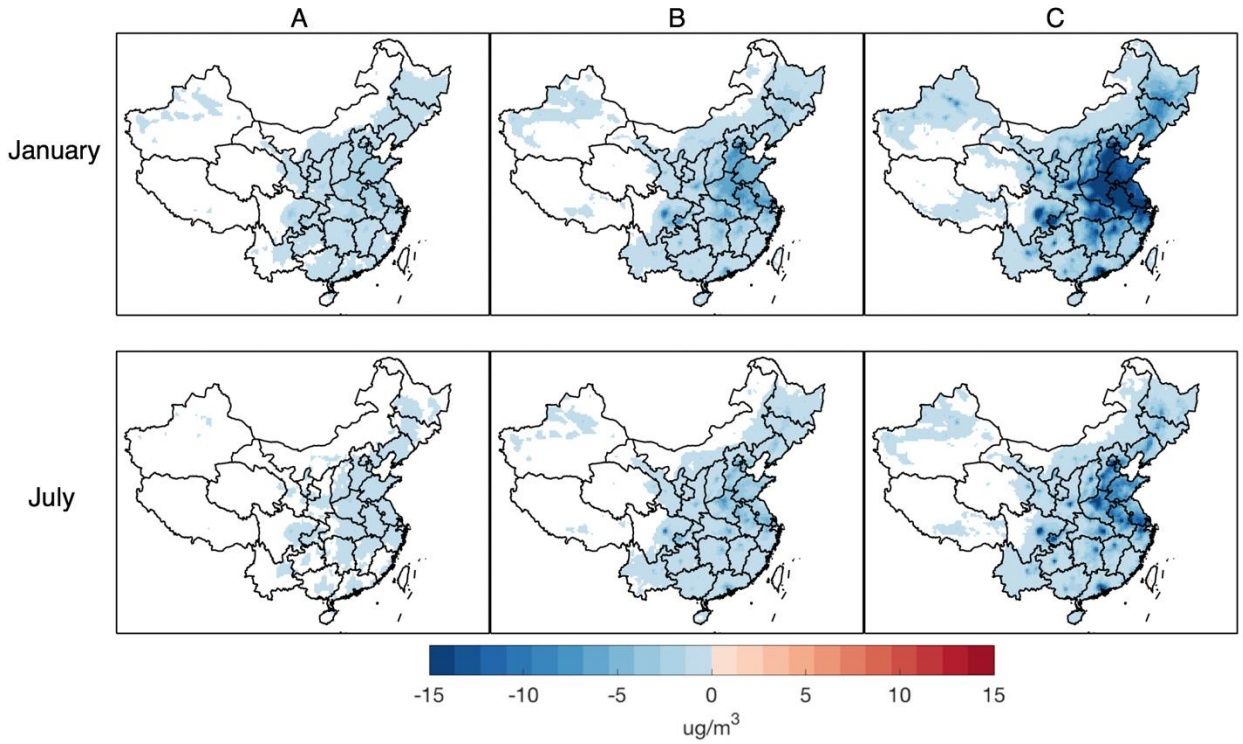

Figure S2.12. Reductions in January and July of mean NO_2 concentrations

Reductions in January and July of mean NO_2 concentrations are shown in (A) LP-LR, (B) HP-HR and (C) MP-HR scenario compared with the base case.

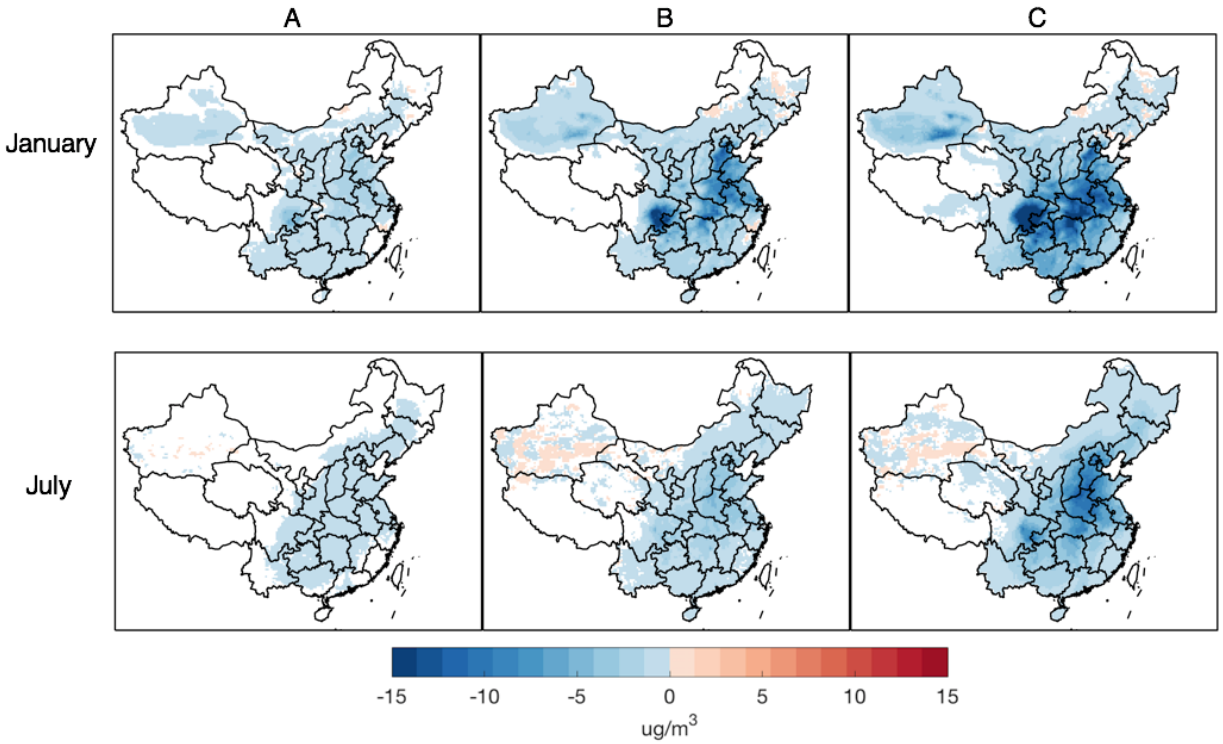

Figure S2.13. Reductions in January and July of mean $PM_{2.5}$ concentrations

Reductions in January and July of mean NO_2 concentrations are shown in (A) LP-LR , (B) HP-HR and (C) MP-HR scenario compared with the base case.

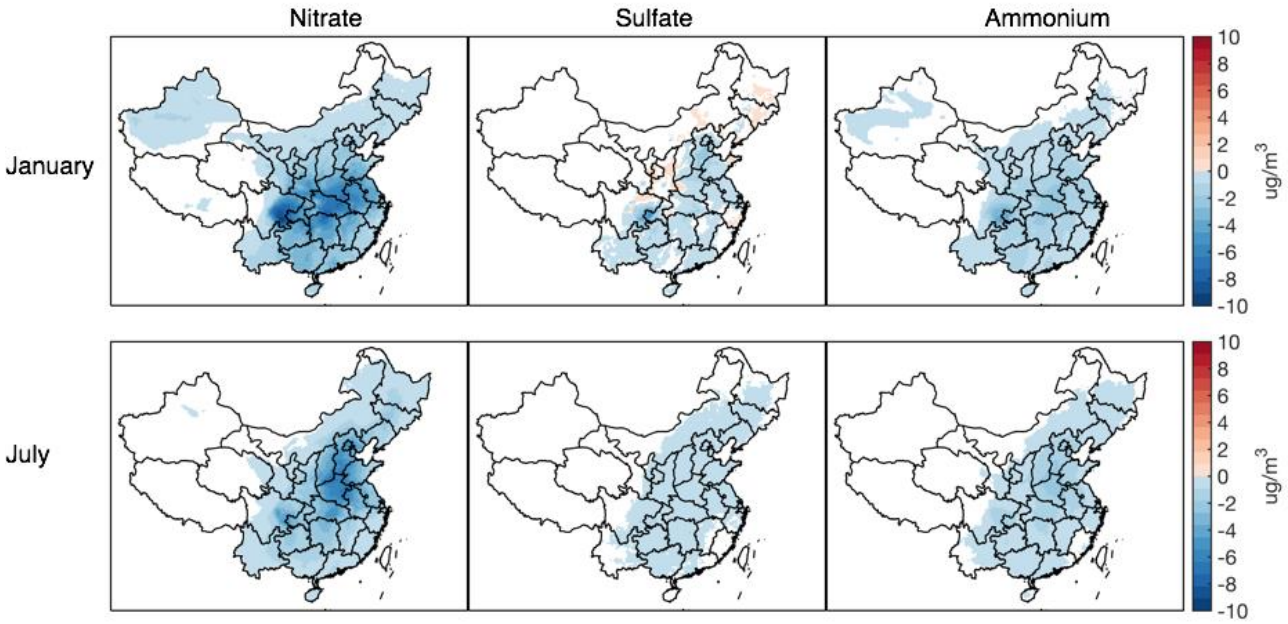

Figure S2.14A. Reductions in January and July of nitrite, sulfate and ammonia concentrations relative to the base case in MP-HR scenario

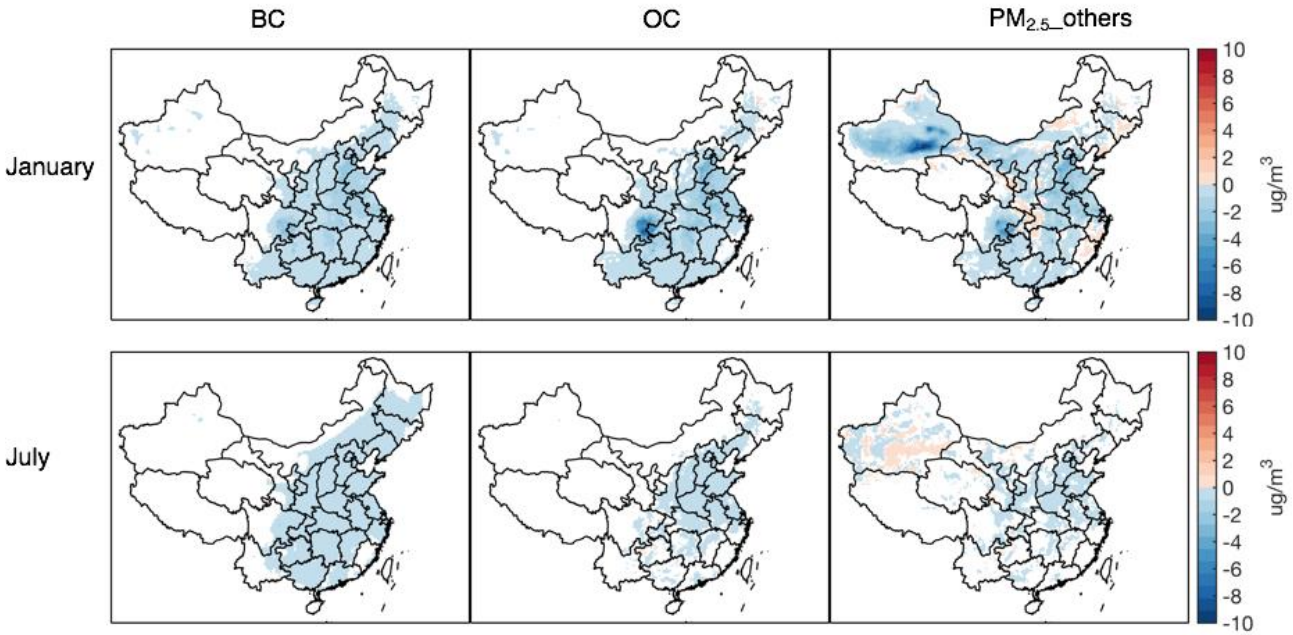

Figure S2.14B. Reductions in January and July of BC, OC and $PM_{2.5}$_others concentrations relative to the base case in the MP-HR scenario

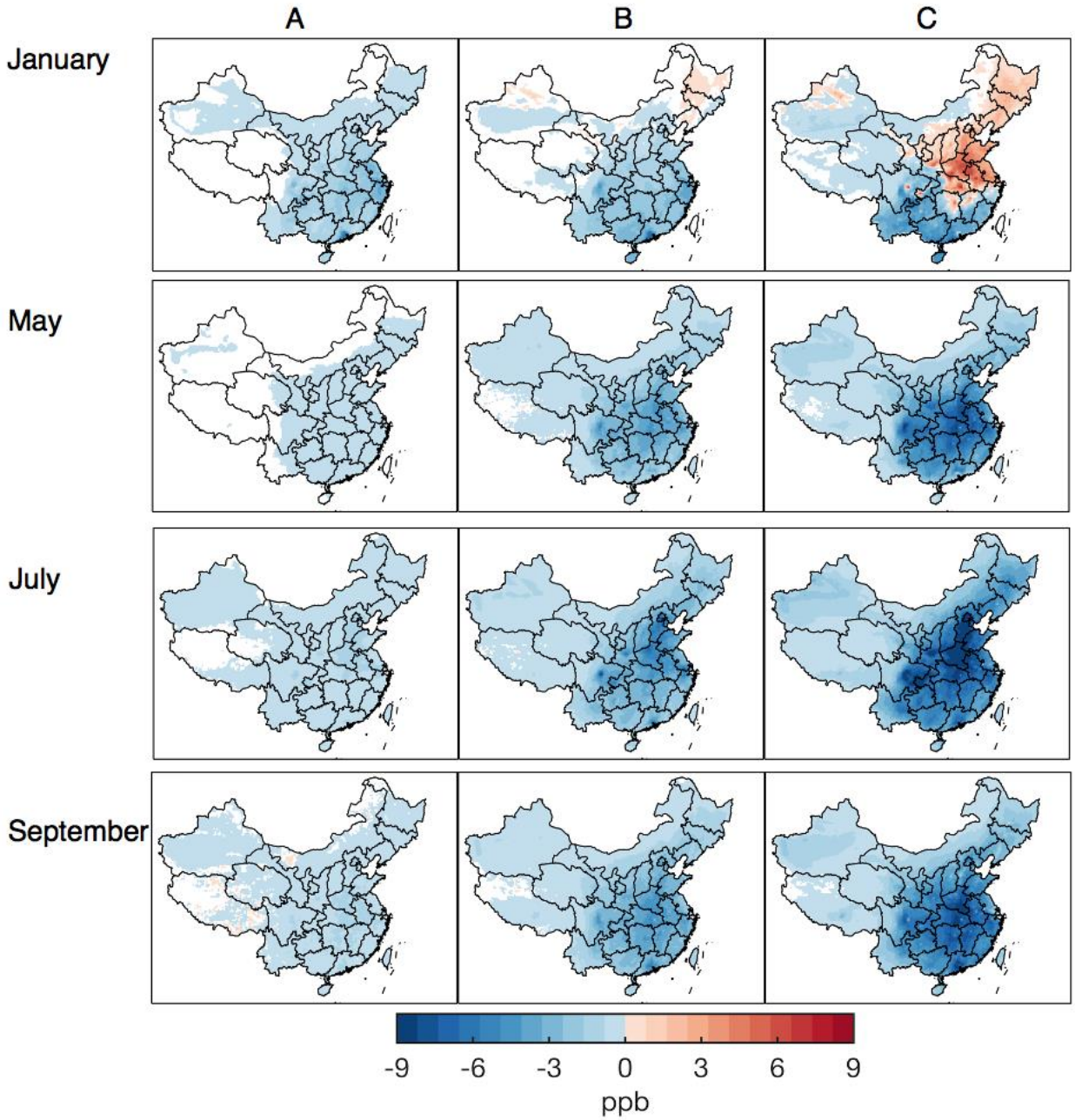

Figure S2.15. Reductions in January, May, July and September of MDA8 O_3 concentrations

Reductions in January, May, July and September of MDA8 O_3 concentrations are shown in (A) LP-LR, (B) HP-HR and (C) MP-HR scenario compared with the base case.

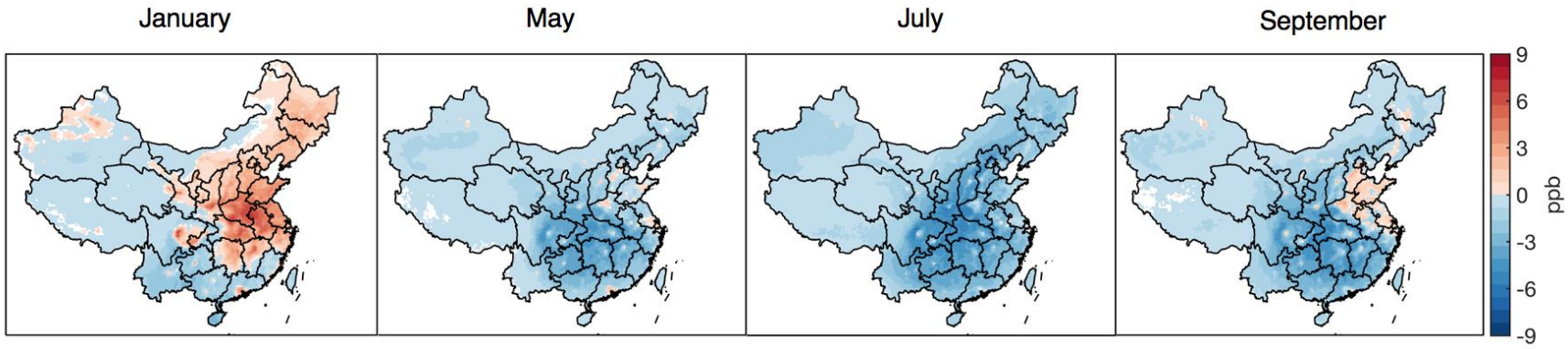

Figure S2.16. Reductions in January, May, July and September average ozone concentrations in the MP-HR scenario compared with the base case.

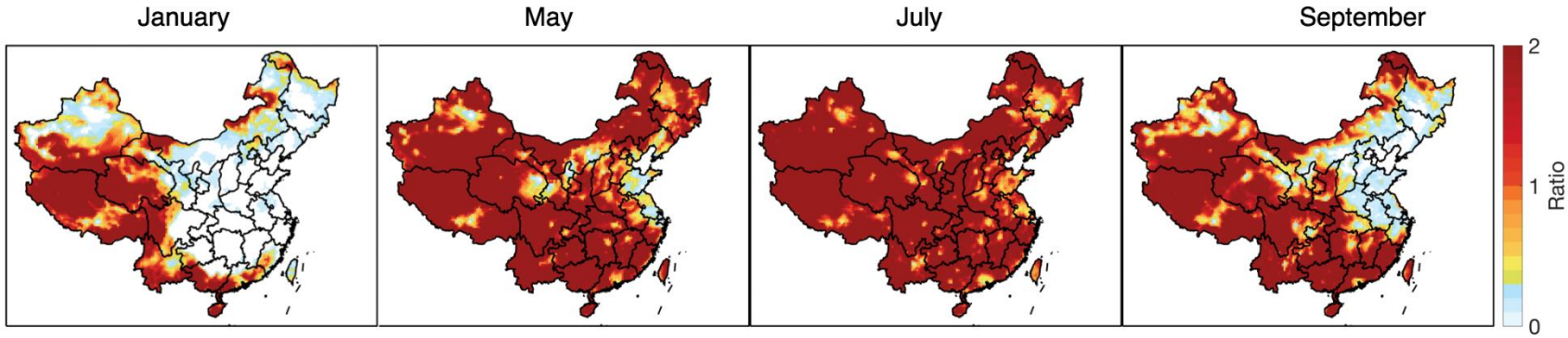

Figure S2.17. Distribution of the ratio for O_3 chemistry

The regime indicator (estimated based on formaldehyde (HCHO)×hydrogen peroxide (H_2O_2)/nitrogen dioxide (NO_2)) successfully captured the strong VOC-limited regime in January (ratio < 1) and the NOx-limited (ratio > 1) regime in July.

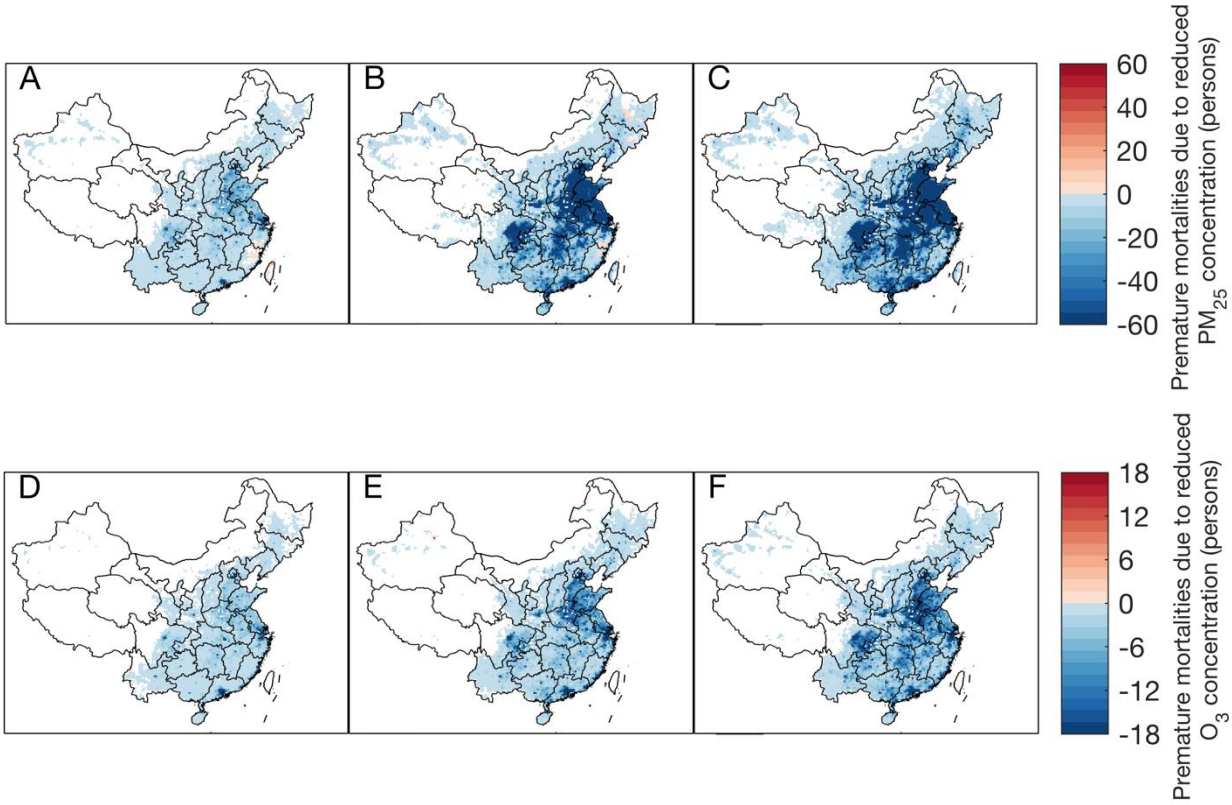

Figure S2.18. Distribution of avoided premature mortalities

Avoided premature mortalities attributed to reduced annual average $PM_{2.5}$ (A-C) and MDA8 O_3 (D-F) concentrations are shown in the LP-LR, HP-HR, and MP-HR scenario, respectively, compared with the base case.

Supplementary Tables

Table S2.6. 2015 population of various vehicle types

Vehicle types in MEIC	Vehicle types in this study	Stock (Million)	Fraction of vehicle fleet
Heavy-duty bus (HDB)/Medium-duty bus (MDB)	Buses	0.6[a]	0.2%
	Large commercial passenger vehicles	2.3[b]	0.9%
Light-duty bus (LDB)	Taxies	1.4[a]	0.6%
	Private passenger vehicles	134.6[b]	53.5%
Heavy-duty truck (HDT)	Trucks	6[c]	2.4%
Medium-duty truck (MDT)		2.1[b]	0.8%
Light-duty truck (LDT)		15.8[b]	6.3%
Motorcycle (MC)	Motorcycles	88.4[b]	35.3%
Total		250.6	100%

a: Chen, et al., 2018[7].
b: MEIC. http://www.meicmodel.org/about.html.
c: Song, et al., 2017[8].

Table S2.7. Summary of baseline air pollutants and CO2e emissions from all sectors in China and the corresponding changes (percentage in parentheses) resulting from implementation of each scenario.

	$PM_{2.5}$	SO_2	NO_x	VOC	CO	$CO_{2e}(GWP_{100})$
	Gg/year (%)				Tg/year (%)	
Base case	9134	16900	23795	19100	155	10347
LP-2015	2 (0.02)	37 (0.2)	-447 (-1.9)	-610 (-3.2)	-2 (-1.3)	23 (0.2)
LP-LR	-24 (-0.3)	-20 (-0.1)	-508 (-2.1)	-610 (-3.2)	-2 (-1.5)	-87 (-0.8)
LP-HR	-27 (-0.3)	-23 (-0.1)	-512 (-2.2)	-610 (-3.2)	-3 (-1.9)	-95 (-0.9)
IP-2015	8 (0.1)	128 (0.8)	-1098 (-4.6)	-2366 (-12.4)	-10 (-6.6)	86 (0.8)
IP-LR	-61 (-0.7)	-81 (-0.5)	-1309 (-5.6)	-2370 (-12.4)	-11 (-7.1)	-246 (-2.4)
IP-HR	-66 (-0.7)	-85 (-0.5)	-1329 (-5.6)	-2377 (-12.4)	-12 (-7.8)	-274 (-2.6)
HP-2015	15 (0.2)	194 (1.1)	-1883 (-7.9)	-3817 (-19.9)	-14 (-9.0)	149 (1.5)
HP-LR	-101 (-1.1)	-111 (-0.7)	-2200 (-9.2)	-3822 (-20.0)	-16 (-10.3)	-388 (-3.7)
HP-HR	-104 (-1.1)	-130 (-0.8)	-2242 (-9.4)	-3828 (-20.0)	-16 (-10.7)	-420 (-4.1)
MP-HR	-171 (-1.9)	-224 (-1.3)	-5332 (-22.4)	-4598 (-24.1)	-26 (-16.4)	-708 (-6.8)

Table S2.8. Vehicle kilometers travelled (VKT) and fuel economy by each vehicle type

	VKT (km)	Fuel economy (kWh/100km)
LDPV	11,000[a]	17[c,d]
MDPV	24,000[a]	54[d]
HDPV	29,800[b]	104[e]
LDT	29,699[c]	40[f]
MDT	29,699[c]	87[c]
HDT	39,500[b]	146[c]
Taxi	126,000[b]	31[c]
Bus	58,000[b]	100[c,e]

Note:
[a] Data from Ministry of Commerce of The People's Republic of China.
[b] Data from Chen et al, 2018[7].
[c] Data from Global EV outlook 2019[5].
[d] Data from Ke et al., 2017[20].
[e] Data from Wang et al., 2015[21].
[f] We assume the fuel economy of LDT is 50% of that of LDPV based on their oil economy share.

Table S2.9. Emission factors of coal and natural gas power units in the Global Power Emissions Database (g/kWh)

		NO_x	SO_2	CO_2	$PM_{2.5}$	VOC	Data sources
2015	Coal	1.1	1	795	0.2	0.012	Wu et al., 2019[22]; MEIC
	NG	0.57	0	455	0.01	0.007	Tong et al., 2018[23], MEIC
2030	Coal	0.31	0.34	622	0.04	0.012	Wu et al., 2019[22], Shen, 2019[6]
	NG	0.12	0	455	0	0.007	Tong et al., 2018[23]

Table S2.10. Evaluation of meteorological variables simulated by WRF-Chem in 2015

	Month of 2015	Pairs of data	R	Simulation Mean	Observation Mean	Mean Bias	Mean Error
2-m temperature (°C)	Jan	391281	0.95	1.76	1.81	-0.05	2.86
	May	381870	0.92	18.86	18.40	0.47	2.36
	Jul	393764	0.88	24.18	23.52	0.66	2.14
	Sep	380284	0.92	20.20	19.77	0.42	2.06
Dewpoint temperature (°C)	Jan	390896	0.94	-4.30	-3.01	-1.29	3.33
	May	380970	0.92	10.68	10.75	-0.07	2.57
	Jul	392908	0.92	18.55	18.59	-0.04	1.75
	Sep	379126	0.93	14.88	14.88	-0.01	1.96
10-m wind speed (m/s)	Jan	367563	0.59	3.02	5.00	-1.98	2.51
	May	369551	0.49	3.04	4.43	-1.39	2.12
	Jul	377322	0.55	2.82	4.14	-1.32	2.02
	Sep	365086	0.48	2.62	4.05	-1.43	2.02
Sea level pressure (hPa)	Jan	274689	0.96	1022.52	1022.44	0.08	1.67
	May	267192	0.94	1008.72	1008.25	0.47	1.44
	Jul	275282	0.94	1006.25	1005.11	1.14	1.58
	Sep	267579	0.95	1012.91	1012.09	0.81	1.43

Table S2.11. Premature mortalities by province attributed to ambient PM2.5 exposure by 2050 assuming an age distribution reflecting the evolution of the population from 2015 to 2050 for various scenarios.

	Premature mortalities (unit: hundreds of people)			
Province	Base case	Base case - LP-LR	Base case - HP-HR	Base case - MP-HR
Beijing	1300	7 (95% CI: 6 - 9)	43 (95% CI: 34 - 54)	54 (95% CI: 43 - 68)
Tianjin	823	4 (95% CI: 4 - 6)	29 (95% CI: 23 - 36)	32 (95% CI: 25 - 40)
Hebei	4481	25 (95% CI: 20 - 31)	148 (95% CI: 119 - 185)	187 (95% CI: 150 - 234)
Shanxi	1481	8 (95% CI: 6 - 9)	41 (95% CI: 33 - 52)	73 (95% CI: 59 - 91)
Inner Mongolia	512	2 (95% CI: 2 - 3)	14 (95% CI: 11 - 18)	25 (95% CI: 20 - 32)
Liaoning	926	5 (95% CI: 4 - 6)	25 (95% CI: 20 - 31)	47 (95% CI: 38 - 59)
Jilin	507	3 (95% CI: 2 - 3)	13 (95% CI: 10 - 16)	27 (95% CI: 22 - 34)
Heilongjiang	596	3 (95% CI: 3 - 4)	13 (95% CI: 10 - 16)	35 (95% CI: 28 - 44)
Shanghai	1057	6 (95% CI: 5 - 8)	36 (95% CI: 29 - 45)	43 (95% CI: 34 - 54)
Jiangsu	5249	29 (95% CI: 23 - 37)	171 (95% CI: 137 - 214)	223 (95% CI: 178 - 279)
Zhejiang	1893	10 (95% CI: 8 - 12)	56 (95% CI: 44 - 69)	90 (95% CI: 72 - 112)
Anhui	4284	22 (95% CI: 18 - 28)	138 (95% CI: 110 - 172)	185 (95% CI: 148 - 232)
Fujian	608	1 (95% CI: 1 - 1)	14 (95% CI: 11 - 17)	35 (95% CI: 28 - 43)
Jiangxi	2018	8 (95% CI: 7 - 10)	61 (95% CI: 48 - 76)	93 (95% CI: 75 - 117)
Shandong	6528	36 (95% CI: 28 - 44)	215 (95% CI: 172 - 268)	275 (95% CI: 220 - 344)
Henan	6568	33 (95% CI: 27 - 42)	204 (95% CI: 164 - 256)	294 (95% CI: 235 - 367)
Hubei	3303	16 (95% CI: 13 - 20)	99 (95% CI: 80 - 124)	153 (95% CI: 122 - 191)
Hunan	3747	16 (95% CI: 13 - 21)	111 (95% CI: 89 - 139)	176 (95% CI: 141 - 220)
Guangdong	4898	19 (95% CI: 15 - 23)	149 (95% CI: 120 - 187)	223 (95% CI: 179 - 279)
Guangxi	2145	7 (95% CI: 5 - 8)	60 (95% CI: 48 - 75)	105 (95% CI: 84 - 132)
Hainan	266	1 (95% CI: 1 - 1)	9 (95% CI: 7 - 11)	11 (95% CI: 9 - 14)
Chongqing	1438	7 (95% CI: 6 - 9)	44 (95% CI: 35 - 55)	66 (95% CI: 53 - 82)
Sichuan	5130	25 (95% CI: 20 - 31)	160 (95% CI: 128 - 200)	229 (95% CI: 183 - 287)
Guizhou	1856	9 (95% CI: 7 - 11)	55 (95% CI: 44 - 69)	87 (95% CI: 70 - 109)
Yunnan	1571	8 (95% CI: 6 - 10)	43 (95% CI: 35 - 54)	79 (95% CI: 63 - 98)
Tibet	16	0 (95% CI: 0 - 0)	0 (95% CI: 0 - 1)	1 (95% CI: 1 - 1)
Shaanxi	1608	7 (95% CI: 6 - 9)	47 (95% CI: 38 - 59)	76 (95% CI: 61 - 95)
Gansu	655	2 (95% CI: 2 - 3)	20 (95% CI: 16 - 25)	30 (95% CI: 24 - 37)
Qinghai	73	0 (95% CI: 0 - 0)	2 (95% CI: 2 - 2)	4 (95% CI: 3 - 5)
Ningxia	104	0 (95% CI: 0 - 1)	3 (95% CI: 3 - 4)	5 (95% CI: 4 - 6)
Xinjiang	279	1 (95% CI: 1 - 1)	9 (95% CI: 8 - 12)	11 (95% CI: 9 - 14)
Total	65920	321 (95% CI: 257 - 482)	2033 (95% CI: 1626 - 2397)	2975 (95% CI: 2380 - 3249)

Table S2.12. Premature mortalities by province attributed to ambient O3 exposure by 2050

assuming an age distribution reflecting the evolution of the population from 2015 to 2050 for various scenarios.

	Premature mortalities (unit: hundreds of people)			
Province	Base case	Base case - LP-LR	Base case - HP-HR	Base case - MP-HR
Beijing	51	1 (95% CI: 1 - 3)	5 (95% CI: 2 - 8)	5 (95% CI: 3 - 10)
Tianjin	27	1 (95% CI: 0 - 1)	2 (95% CI: 1 - 4)	2 (95% CI: 1 - 5)
Hebei	173	4 (95% CI: 2 - 7)	13 (95% CI: 7 - 24)	16 (95% CI: 9 - 30)
Shanxi	74	1 (95% CI: 1 - 2)	4 (95% CI: 2 - 8)	7 (95% CI: 3 - 12)
Inner Mongolia	38	0 (95% CI: 0 - 1)	2 (95% CI: 1 - 3)	3 (95% CI: 1 - 5)
Liaoning	63	1 (95% CI: 1 - 2)	4 (95% CI: 2 - 7)	5 (95% CI: 3 - 9)
Jilin	30	1 (95% CI: 0 - 1)	2 (95% CI: 1 - 4)	3 (95% CI: 1 - 5)
Heilongjiang	37	1 (95% CI: 0 - 1)	2 (95% CI: 1 - 4)	4 (95% CI: 2 - 8)
Shanghai	31	1 (95% CI: 1 - 2)	2 (95% CI: 1 - 4)	1 (95% CI: 0 - 1)
Jiangsu	176	8 (95% CI: 4 - 14)	15 (95% CI: 8 - 28)	14 (95% CI: 7 - 25)
Zhejiang	108	6 (95% CI: 3 - 11)	11 (95% CI: 6 - 20)	13 (95% CI: 7 - 24)
Anhui	150	5 (95% CI: 3 - 10)	12 (95% CI: 6 - 23)	18 (95% CI: 9 - 32)
Fujian	54	2 (95% CI: 1 - 4)	6 (95% CI: 3 - 10)	8 (95% CI: 4 - 15)
Jiangxi	73	3 (95% CI: 2 - 6)	7 (95% CI: 4 - 13)	13 (95% CI: 7 - 24)
Shandong	242	6 (95% CI: 3 - 12)	19 (95% CI: 10 - 35)	23 (95% CI: 12 - 43)
Henan	227	6 (95% CI: 3 - 11)	19 (95% CI: 10 - 34)	28 (95% CI: 14 - 51)
Hubei	125	4 (95% CI: 2 - 7)	8 (95% CI: 4 - 15)	16 (95% CI: 8 - 30)
Hunan	136	5 (95% CI: 2 - 8)	9 (95% CI: 5 - 17)	21 (95% CI: 11 - 39)
Guangdong	169	10 (95% CI: 5 - 18)	23 (95% CI: 12 - 43)	27 (95% CI: 14 - 51)
Guangxi	71	2 (95% CI: 1 - 4)	9 (95% CI: 5 - 17)	15 (95% CI: 7 - 28)
Hainan	9	0 (95% CI: 0 - 1)	1 (95% CI: 0 - 2)	1 (95% CI: 1 - 3)
Chongqing	60	1 (95% CI: 1 - 2)	4 (95% CI: 2 - 8)	8 (95% CI: 4 - 14)
Sichuan	191	5 (95% CI: 3 - 9)	16 (95% CI: 8 - 29)	26 (95% CI: 14 - 48)
Guizhou	63	2 (95% CI: 1 - 4)	6 (95% CI: 3 - 11)	11 (95% CI: 6 - 20)
Yunnan	61	2 (95% CI: 1 - 4)	6 (95% CI: 3 - 12)	11 (95% CI: 5 - 20)
Tibet	3	0 (95% CI: 0 - 0)	0 (95% CI: 0 - 0)	0 (95% CI: 0 - 0)
Shaanxi	72	2 (95% CI: 1 - 3)	6 (95% CI: 3 - 10)	9 (95% CI: 5 - 17)
Gansu	40	1 (95% CI: 0 - 1)	2 (95% CI: 1 - 4)	4 (95% CI: 2 - 8)
Qinghai	10	0 (95% CI: 0 - 0)	0 (95% CI: 0 - 1)	1 (95% CI: 0 - 1)
Ningxia	9	0 (95% CI: 0 - 0)	0 (95% CI: 0 - 1)	1 (95% CI: 0 - 1)
Xinjiang	29	0 (95% CI: 0 - 0)	0 (95% CI: 0 - 0)	1 (95% CI: 1 - 2)
Total	2604	81 (95% CI: 41 - 150)	214 (95% CI: 111 - 397)	313 (95% CI: 162 - 582)

Table S2.13. Premature mortalities and years of life lost attributed to ambient PM2.5 exposure by 2050 assuming an 80-year life expectancy and a constant age distribution from 2015 to 2050 for various scenarios.

	Premature mortalities (unit: hundreds of people)			
Age	Base case	Base case - LP-LR	Base case - HP-HR	Base case - MP-HR
25-29	135	1 (95% CI: 1 - 1)	4 (95% CI: 3 - 4)	6 (95% CI: 5 - 6)
30-34	167	1 (95% CI: 1 - 2)	5 (95% CI: 4 - 6)	7 (95% CI: 6 - 7)
35-39	207	1 (95% CI: 1 - 2)	6 (95% CI: 5 - 7)	9 (95% CI: 8 - 9)
40-44	434	2 (95% CI: 2 - 5)	13 (95% CI: 11 - 15)	19 (95% CI: 16 - 19)
45-49	999	5 (95% CI: 4 - 11)	29 (95% CI: 25 - 33)	43 (95% CI: 37 - 44)
50-54	1,417	7 (95% CI: 6 - 16)	42 (95% CI: 36 - 48)	62 (95% CI: 52 - 62)
55-59	1,231	6 (95% CI: 5 - 14)	37 (95% CI: 31 - 42)	54 (95% CI: 46 - 55)
60-64	2,765	13 (95% CI: 11 - 32)	83 (95% CI: 71 - 95)	122 (95% CI: 103 - 123)
65-69	3,403	16 (95% CI: 14 - 40)	103 (95% CI: 88 - 117)	150 (95% CI: 127 - 153)
70-74	3,175	15 (95% CI: 13 - 38)	97 (95% CI: 83 - 111)	142 (95% CI: 119 - 144)
75-79	3,811	19 (95% CI: 16 - 47)	117 (95% CI: 100 - 134)	172 (95% CI: 143 - 175)
80 plus	8,002	40 (95% CI: 33 - 103)	251 (95% CI: 214 - 288)	367 (95% CI: 303 - 373)
Total	25,745	124 (95% CI: 105 - 311)	785 (95% CI: 672 - 899)	1,151 (95% CI: 964 – 1,170)

	Years of life lost (YLL) at 80 years age limit (unit: hundreds of years)			
Age	Base case	Base case - LP-LR	Base case - HP-HR	Base case - MP-HR
25-29	6,422	29 (95% CI: 26 - 69)	187 (95% CI: 161 - 213)	275 (95% CI: 236 - 279)
30-34	7,917	36 (95% CI: 31 - 86)	230 (95% CI: 197 - 263)	340 (95% CI: 290 - 345)
35-39	8,797	40 (95% CI: 35 - 95)	256 (95% CI: 220 - 292)	377 (95% CI: 323 - 383)
40-44	16,291	75 (95% CI: 65 - 177)	477 (95% CI: 409 - 544)	701 (95% CI: 600 - 711)
45-49	32,475	150 (95% CI: 129 - 355)	952 (95% CI: 818 - 1087)	1,402 (95% CI: 1,197 – 1,423)
50-54	38,959	182 (95% CI: 156 - 434)	1150 (95% CI: 987 - 1312)	1,691 (95% CI: 1,439 – 1,716)
55-59	27,702	131 (95% CI: 112 - 315)	821 (95% CI: 703 - 939)	1,211 (95% CI: 1,026 – 1,229)
60-64	48,389	228 (95% CI: 194 - 556)	1447 (95% CI: 1241 - 1654)	2,126 (95% CI: 1,798 – 2,160)
65-69	42,534	201 (95% CI: 171 - 495)	1281 (95% CI: 1099 - 1463)	1,880 (95% CI: 1,586 – 1,910)
70-74	23,811	115 (95% CI: 97 - 287)	725 (95% CI: 621 - 830)	1,063 (95% CI: 891 – 1,080)
75-79	9,526	46 (95% CI: 39 - 118)	293 (95% CI: 250 - 336)	429 (95% CI: 357 - 437)
80 plus	0	0 (95% CI: 0 - 0)	0 (95% CI: 0 - 0)	0 (95% CI: 0 - 0)
Total	262,823	1,233 (95% CI: 1055 - 2985)	7,820 (95% CI: 6,706 – 8,934)	11,496 (95% CI: 9,743 – 11,674)

Table S2.14. Premature mortalities and potential years of life lost attributed to ambient O3 exposure by 2050 assuming an 80-year life expectancy and a constant age distribution from 2015 to 2050 for various scenarios.

	Premature mortalities (unit: hundreds of people)			
Age	Base case	Base case - LP-LR	Base case - HP-HR	Base case - MP-HR
30-34	2	0 (95% CI: 0 - 0)	0 (95% CI: 0 - 0)	0 (95% CI: 0 - 0)
35-39	3	0 (95% CI: 0 - 0)	0 (95% CI: 0 - 0)	0 (95% CI: 0 - 1)
40-44	8	0 (95% CI: 0 - 0)	1 (95% CI: 0 - 1)	1 (95% CI: 0 - 2)
45-49	21	1 (95% CI: 0 - 1)	2 (95% CI: 1 - 3)	2 (95% CI: 1 - 4)
50-54	38	1 (95% CI: 1 - 2)	3 (95% CI: 1 - 5)	4 (95% CI: 2 - 7)
55-59	38	1 (95% CI: 1 - 2)	3 (95% CI: 1 - 5)	4 (95% CI: 2 - 8)
60-64	99	3 (95% CI: 1 - 5)	7 (95% CI: 4 - 13)	11 (95% CI: 6 - 20)
65-69	131	4 (95% CI: 2 - 7)	10 (95% CI: 5 - 18)	14 (95% CI: 7 - 26)
70-74	136	4 (95% CI: 2 - 7)	10 (95% CI: 5 - 19)	15 (95% CI: 8 - 27)
75-79	173	5 (95% CI: 3 - 9)	13 (95% CI: 7 - 24)	19 (95% CI: 10 - 35)
80 plus	386	11 (95% CI: 6 - 20)	28 (95% CI: 15 - 53)	41 (95% CI: 22 - 77)
Total	1035	29 (95% CI: 15 - 53)	76 (95% CI: 40 - 141)	111 (95% CI: 58 - 207)

	Years of life lost (YLL) at 80 years age limit (unit: hundreds of years)			
Age	Base case	Base case - LP-LR	Base case - HP-HR	Base case - MP-HR
30-34	106	3 (95% CI: 2 - 5)	8 (95% CI: 4 - 14)	11 (95% CI: 2 - 21)
35-39	129	4 (95% CI: 2 - 7)	9 (95% CI: 5 - 18)	14 (95% CI: 2 - 26)
40-44	287	8 (95% CI: 4 - 15)	21 (95% CI: 11 - 39)	31 (95% CI: 4 - 57)
45-49	698	19 (95% CI: 10 - 36)	51 (95% CI: 27 - 95)	75 (95% CI: 10 - 140)
50-54	1031	29 (95% CI: 15 - 53)	76 (95% CI: 39 - 141)	111 (95% CI: 15 - 206)
55-59	850	24 (95% CI: 12 - 44)	63 (95% CI: 32 - 116)	91 (95% CI: 12 - 170)
60-64	1729	48 (95% CI: 25 - 89)	127 (95% CI: 66 - 236)	186 (95% CI: 25 - 346)
65-69	1641	46 (95% CI: 24 - 85)	121 (95% CI: 63 - 224)	177 (95% CI: 24 - 328)
70-74	1022	29 (95% CI: 15 - 53)	75 (95% CI: 39 - 139)	110 (95% CI: 15 - 204)
75-79	434	12 (95% CI: 6 - 22)	32 (95% CI: 17 - 59)	47 (95% CI: 6 - 87)
80 plus	0	0 (95% CI: 0 - 0)	0 (95% CI: 0 - 0)	0 (95% CI: 0 - 0)
Total	7927	221 (95% CI: 115 - 409)	583 (95% CI: 303 - 1081)	853 (95% CI: 115 - 1585)

Table S2.15. Premature mortalities and years of life lost attributed to ambient PM2.5 exposure by 2050 assuming an 80-year life expectancy and an age distribution reflecting the evolution of the population from 2015 to 2050 for various scenarios.

	Premature mortalities (unit: hundreds of people)			
Age	Base case	Base case - LP-LR	Base case - HP-HR	Base case - MP-HR
25-29	76	0 (95% CI: 0 - 1)	2 (95% CI: 2 - 3)	3 (95% CI: 3 - 3)
30-34	131	1 (95% CI: 1 - 1)	4 (95% CI: 3 - 4)	6 (95% CI: 5 - 6)
35-39	173	1 (95% CI: 1 - 2)	5 (95% CI: 4 - 6)	7 (95% CI: 6 - 8)
40-44	296	1 (95% CI: 1 - 3)	9 (95% CI: 7 - 10)	13 (95% CI: 11 - 13)
45-49	624	3 (95% CI: 2 - 7)	18 (95% CI: 16 - 21)	27 (95% CI: 23 - 27)
50-54	1,110	10 (95% CI: 9 - 17)	30 (95% CI: 25 - 35)	50 (95% CI: 43 - 51)
55-59	1,460	12 (95% CI: 10 - 20)	40 (95% CI: 34 - 46)	60 (95% CI: 50 - 61)
60-64	4,150	20 (95% CI: 17 - 48)	120 (95% CI: 102 - 138)	190 (95% CI: 162 - 193)
65-69	5,460	30 (95% CI: 26 - 69)	155 (95% CI: 136 - 184)	235 (95% CI: 201 - 244)
70-74	6,740	30 (95% CI: 25 - 79)	200 (95% CI: 180 - 240)	290 (95% CI: 251 - 305)
75-79	11,600	100 (95% CI: 91 - 187)	380 (95% CI: 349 - 451)	600 (95% CI: 513 - 609)
80 plus	34,100	150 (95% CI: 101 - 376)	1,070 (95% CI: 941 - 1259)	1,490 (95% CI: 1224 - 1529)
Total	65,920	321 (95% CI: 254 - 609)	2,033 (95% CI: 1800 - 2396)	2,975 (95% CI: 2493 - 3048)

	Years of life lost (YLL) at 80 years age limit (unit: hundreds of years)			
Age	Base case	Base case - LP-LR	Base case - HP-HR	Base case - MP-HR
25-29	3,627	17 (95% CI: 14 - 39)	105 (95% CI: 91 - 120)	155 (95% CI: 133 - 158)
30-34	6,204	29 (95% CI: 25 - 66)	181 (95% CI: 155 - 206)	266 (95% CI: 228 - 270)
35-39	7,372	34 (95% CI: 30 - 79)	215 (95% CI: 185 - 245)	317 (95% CI: 271 - 321)
40-44	11,109	51 (95% CI: 44 - 119)	324 (95% CI: 279 - 370)	478 (95% CI: 410 - 485)
45-49	20,272	94 (95% CI: 81 - 221)	595 (95% CI: 512 - 678)	876 (95% CI: 749 - 888)
50-54	30,525	275 (95% CI: 255 - 470)	825 (95% CI: 699 - 951)	1,375 (95% CI: 1,180 – 1,395)
55-59	32,850	225 (95% CI: 202 - 443)	900 (95% CI: 761 – 1,039)	1,350 (95% CI: 1,132 – 1,373)
60-64	72,625	350 (95% CI: 300 - 844)	2,100 (95% CI: 1,789 – 2,411)	3,325 (95% CI: 2,831 – 3,375)
65-69	68,250	375 (95% CI: 325 - 861)	2,000 (95% CI: 1,699 – 2,301)	3,000 (95% CI: 2,514 – 3,050)
70-74	50,550	225 (95% CI: 188 - 590)	1,575 (95% CI: 1,353 – 1,797)	2,250 (95% CI: 1,885 – 2,287)
75-79	29,000	250 (95% CI: 228 - 466)	1,000 (95% CI: 871 – 1.129)	1,500 (95% CI: 1,284 - 1522)
80 plus	0	0 (95% CI: 0 - 0)	0 (95% CI: 0 - 0)	0 (95% CI: 0 - 0)
Total	332,384	1924 (95% CI: 1692 - 4199)	9,820 (95% CI: 8.393 – 11,247)	14,892 (95% CI: 12,617 – 15,123)

Table S2.16. Premature mortalities and potential years of life lost attributed to ambient O3 exposure by 2050 assuming an 80-year life expectancy and an age distribution reflecting the evolution of the population from 2015 to 2050 for various scenarios.

	Premature mortalities (unit: hundreds of people)			
Age	Base case	Base case - LP-LR	Base case - HP-HR	Base case - MP-HR
30-34	2	0 (95% CI: 0 - 0)	0 (95% CI: 0 - 0)	0 (95% CI: 0 - 0)
35-39	3	0 (95% CI: 0 - 0)	0 (95% CI: 0 - 0)	0 (95% CI: 0 - 1)
40-44	5	0 (95% CI: 0 - 0)	0 (95% CI: 0 - 1)	1 (95% CI: 0 - 1)
45-49	13	0 (95% CI: 0 - 1)	1 (95% CI: 1 - 2)	1 (95% CI: 1 - 3)
50-54	29	1 (95% CI: 0 - 2)	2 (95% CI: 1 - 4)	3 (95% CI: 2 - 6)
55-59	45	1 (95% CI: 1 - 2)	3 (95% CI: 2 - 6)	5 (95% CI: 3 - 9)
60-64	148	4 (95% CI: 2 - 8)	11 (95% CI: 6 - 20)	16 (95% CI: 8 - 30)
65-69	211	6 (95% CI: 3 - 11)	16 (95% CI: 8 - 29)	23 (95% CI: 12 - 42)
70-74	289	8 (95% CI: 4 - 15)	21 (95% CI: 11 - 39)	31 (95% CI: 16 - 58)
75-79	522	15 (95% CI: 8 - 27)	39 (95% CI: 20 - 72)	57 (95% CI: 29 - 105)
80 plus	1641	46 (95% CI: 24 - 85)	121 (95% CI: 63 - 225)	177 (95% CI: 92 - 329)
Total	2604	81 (95% CI: 66 - 151)	214 (95% CI: 174 - 398)	313 (95% CI: 270 - 583)

	Years of life lost (YLL) at 80 years age limit (unit: hundreds of years)			
Age	Base case	Base case - LP-LR	Base case - HP-HR	Base case - MP-HR
30-34	83	2 (95% CI: 1 - 4)	6 (95% CI: 3 - 11)	9 (95% CI: 5 - 17)
35-39	108	3 (95% CI: 2 - 6)	8 (95% CI: 4 - 15)	12 (95% CI: 6 - 22)
40-44	196	5 (95% CI: 3 - 10)	14 (95% CI: 7 - 27)	21 (95% CI: 11 - 39)
45-49	436	12 (95% CI: 6 - 22)	32 (95% CI: 17 - 59)	47 (95% CI: 24 - 87)
50-54	808	23 (95% CI: 12 - 42)	59 (95% CI: 31 - 110)	87 (95% CI: 45 - 162)
55-59	1008	28 (95% CI: 15 - 52)	74 (95% CI: 38 - 137)	108 (95% CI: 56 - 201)
60-64	2588	72 (95% CI: 38 - 134)	190 (95% CI: 99 - 353)	278 (95% CI: 144 - 518)
65-69	2638	74 (95% CI: 38 - 136)	194 (95% CI: 101 - 360)	284 (95% CI: 147 - 527)
70-74	2166	60 (95% CI: 31 - 112)	159 (95% CI: 83 - 295)	233 (95% CI: 121 - 433)
75-79	1316	37 (95% CI: 19 - 68)	97 (95% CI: 50 - 179)	142 (95% CI: 73 - 263)
80 plus	0	0 (95% CI: 0 - 0)	0 (95% CI: 0 - 0)	0 (95% CI: 0 - 0)
Total	11346	316 (95% CI: 165 - 586)	834 (95% CI: 433 - 1547)	1220 (95% CI: 633 - 2269)

Supplementary Reference:

1. Reinventing Fire: China. A roadmap for China's Revolution in Energy Consumption and Production to 2050. (2019).

2. China National Renewable Energy Centre (2018). China Renewable Energy Outlook 2018.

3. Chen, H., Paltsev, S., Reilly, J., Mottis, J., and Karplus, V. (2017). The MIT Economic Projection and Policy Analysis (EPPA) Model: Version 5.

4. Liang, X., Zhang, S., Wu, Y., Xing, J., He, X., Zhang, K.M., Wang, S., and Hao, J. (2019). Air quality and health benefits from fleet electrification in China. Nature Sustainability 2, 962–971.

5. International Energy Agency (2019). Global EV Outlook 2019: Scaling-up the transition to electric mobility (OECD).

6. Shen, W., Han, W., Wallington, T.J., and Winkler, S.L. (2019). China Electricity Generation Greenhouse Gas Emission Intensity in 2030: Implications for Electric Vehicles. Environ. Sci. Technol. 53, 6063–6072.

7. Chen, X., Zhang, H., Xu, Z., Nielsen, C.P., McElroy, M.B., and Lv, J. (2018). 30. Impacts of fleet types and charging modes for electric vehicles on emissions under different penetrations of wind power. Nature Energy 3, 413–421.

8. Song, H., Ou, X., Yuan, J., Yu, M., and Wang, C. (2017). Energy consumption and greenhouse gas emissions of diesel/LNG heavy-duty vehicle fleets in China based on a bottom-up model analysis. Energy 140, 966–978.

9. State Council of China (2012). Energy-Saving and New Energy Vehicle Industry

Development Plan (2012–2020).

10. National Bureau of Statistics. (2016). China Statistical Yearbook 2016. (China Statistics Press).

11. National Bureau of Statistics (2020). China Energy Statistical Yearbook 2020 (China Statistical Press).

12. Qiao, Q., and Lee, H. (2019). The Role of Electric Vehicles in Decarbonizing China's Transportation Sector. 46.

13. U.S Department of Energy Alternative fuels Data Center. https://afdc.energy.gov/vehicles/natural_gas_emissions.html.

14. China Renewable Energy Outlook 2017 (2017). (Energy Research Institute of Academy of Macroeconomic Research).

15. Chris, L.F. (2019). A review of prospects for natural gas as a fuel in road transport (The Oxford Insititue for Energy Studies).

16. Wang, D., Zamel, N., Jiao, K., Zhou, Y., Yu, S., Du, Q., and Yin, Y. (2013). Life cycle analysis of internal combustion engine, electric and fuel cell vehicles for China. Energy 59, 402–412.

17. Hao, H., Mu, Z., Liu, Z., and Zhao, F. (2018). Abating transport GHG emissions by hydrogen fuel cell vehicles: Chances for the developing world. Front. Energy 12, 466–480.

18. National Development and Reform Commission (2015). Electric vehicle charging infrastructure development guidelines(2015-2020).

19. Liu, F., Mauzerall, D.L., Zhao, F., and Hao, H. (2021). Deployment of fuel cell vehicles in China: Greenhouse gas emission reductions from converting the heavy-duty truck fleet

from diesel and natural gas to hydrogen. International Journal of Hydrogen Energy 46, 17982–17997.

20. Ke, W., Zhang, S., Wu, Y., Zhao, B., Wang, S., and Hao, J. (2017). Assessing the Future Vehicle Fleet Electrification: The Impacts on Regional and Urban Air Quality. Environmental Science & Technology 51, 1007–1016.

21. Wang, R., Wu, Y., Ke, W., Zhang, S., Zhou, B., and Hao, J. (2015). Can propulsion and fuel diversity for the bus fleet achieve the win–win strategy of energy conservation and environmental protection? Applied Energy 147, 92–103.

22. Wu, R., Liu, F., Tong, D., Zheng, Y., Lei, Y., Hong, C., Li, M., Liu, J., Zheng, B., Bo, Y., et al. (2019). Air quality and health benefits of China's emission control policies on coal-fired power plants during 2005–2020. Environ. Res. Lett. 14, 094016.

23. Tong, D., Zhang, Q., Davis, S.J., Liu, F., Zheng, B., Geng, G., Xue, T., Li, M., Hong, C., Lu, Z., et al. (2018). Targeted emission reductions from global super-polluting power plant units. Nature Sustainability 1, 59–68.

Appendix for Chapter 3

Supplementary Information

Supplementary Note 1: Electricity demand projections

The total electricity demand projection is derived from below 2-degree scenario of China National Renewable Energy Outlook 2020 which assumes an electrification of an increasing portion of the economy. We allocate total electricity demand into provinces based on Hu's presentation. The total electricity demand projection is derived from below 2-degree scenario of China National Renewable Energy Outlook 2020. We allocate total electricity demand into provinces based on Hu's presentation. In 2050, Hebei, Shandong, Jiangsu, and Guangdong provinces have the highest electricity demand. Next, we gather the monthly and daily profile of power load by province and estimate the hourly electricity demand by province.

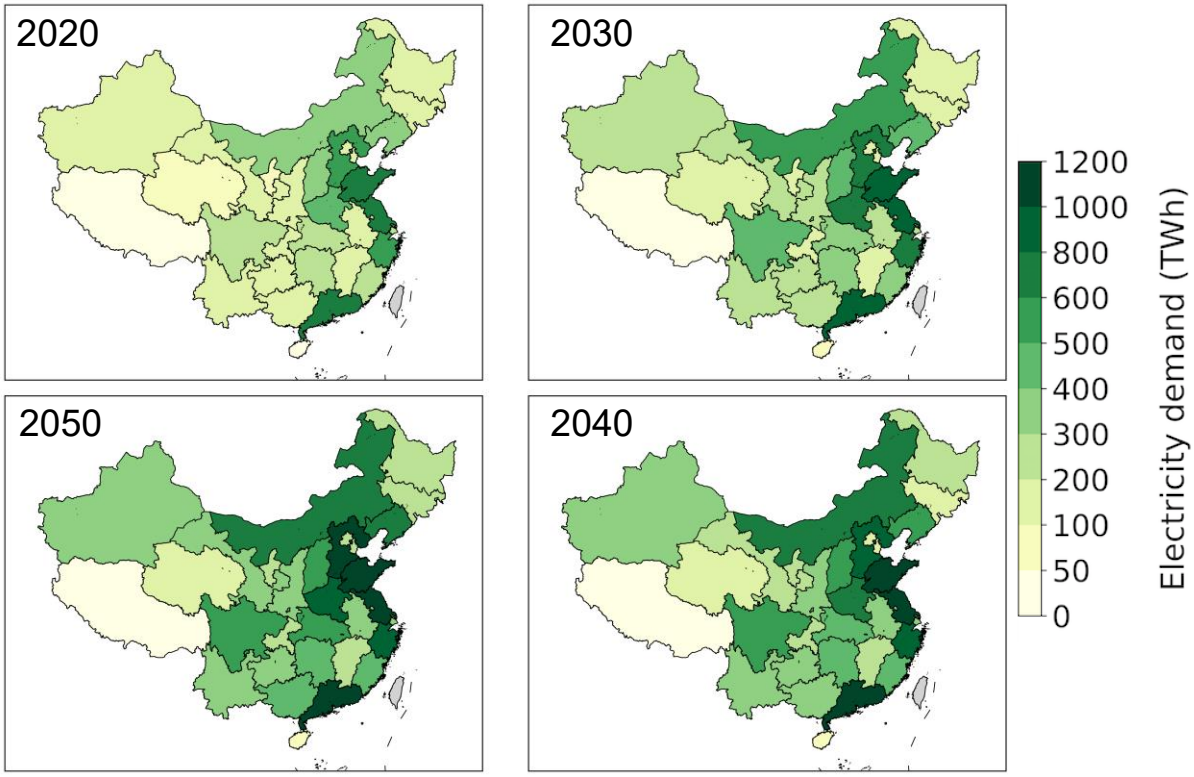

Figure S3.1. Distribution of electricity demand by province from 2020-2050.

Supplementary Note 2: Cost information

Capital costs are amortized over the expected lifetime of each generator or transmission line. Only those payments that occur during the period covered by the study are included in the SWITCH-China objective function. We set up three cost trajectories for solar PV, wind and battery storage. Technology adoption, learning-by-doing, economies of scale, and manufacturing localization are driving the cost decease of solar PV, wind and battery storage.

Figure S3.2, S3.3 and S3.4 show the capital costs assumptions of renewables and storage. Our estimates for the O&M costs for these three technologies in our model are equal to 1% of the capital costs of that given technology for that given scenario.

Charging and discharging batteries results in a "roundtrip" loss of energy. In our model, we assume a roundtrip energy loss of 12%, 15% and 20% for 1h batteries, 4h batteries and 10h batteries during battery charge and discharge (NREL, 2021).) The hourly based wind and solar capacity factors used in this study are estimated using the model in He et al. 2016.

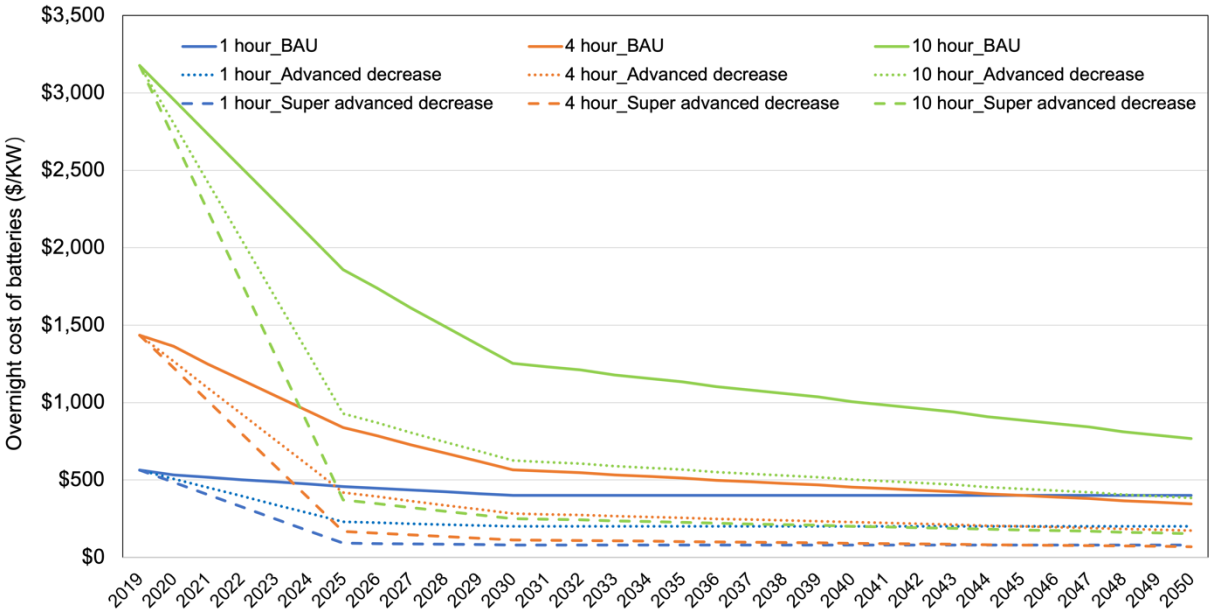

Figure S3.2. Capital cost of batteries in the model

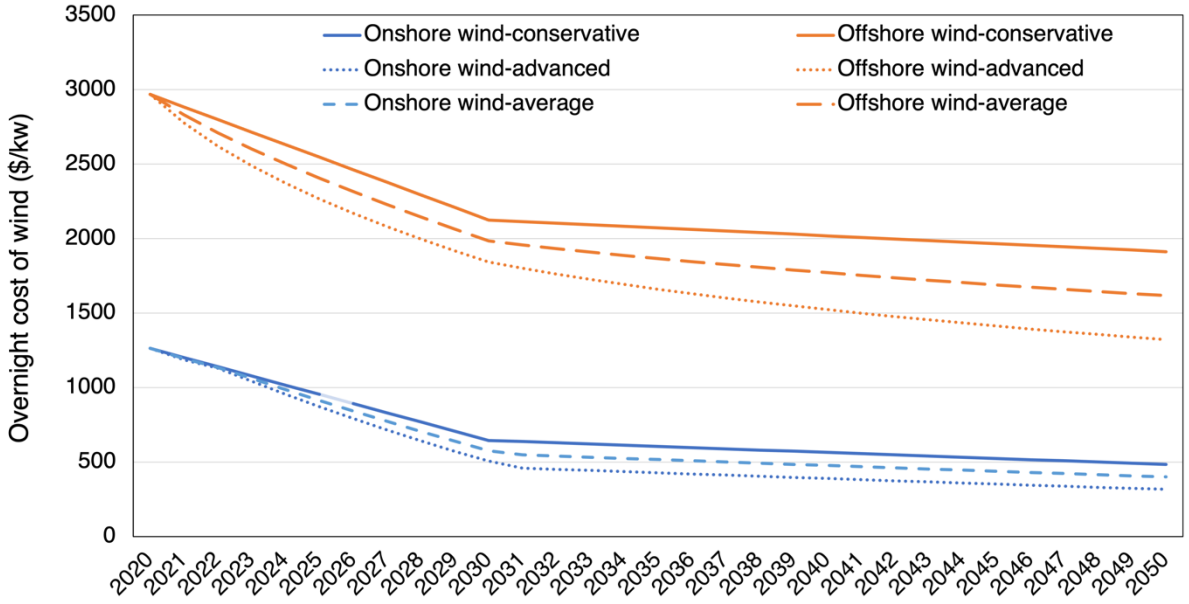

Figure S3.3. Capital cost of solar PV in the model

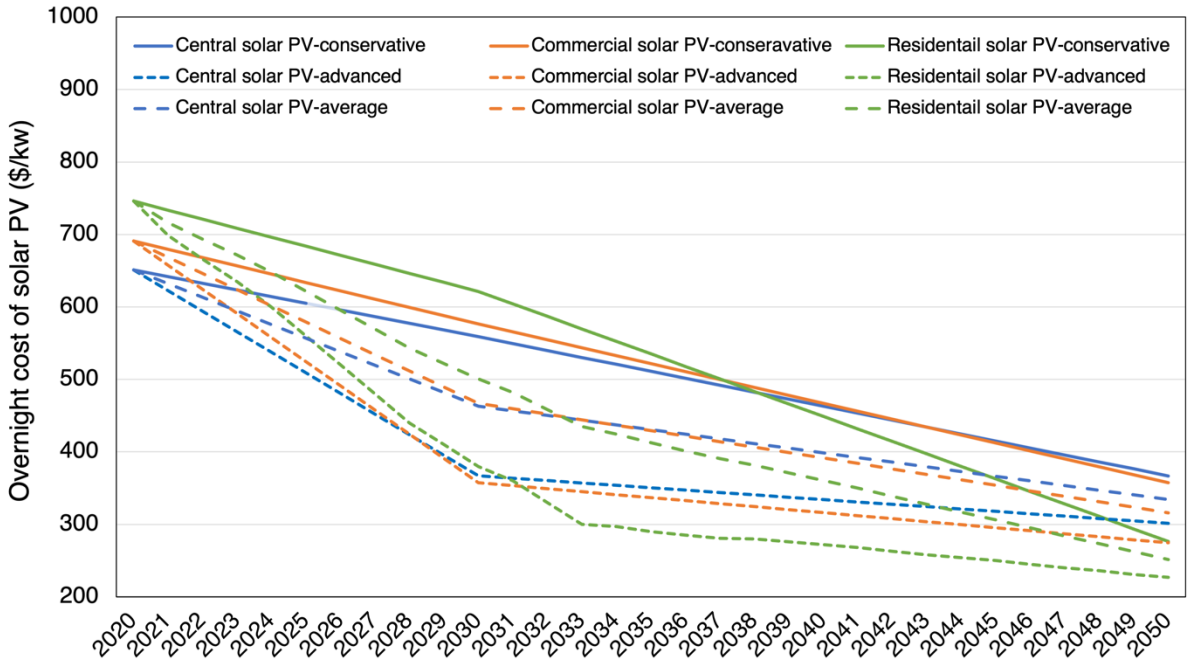

Figure S3.4. Capital cost of wind in the model

Supplementary Figures

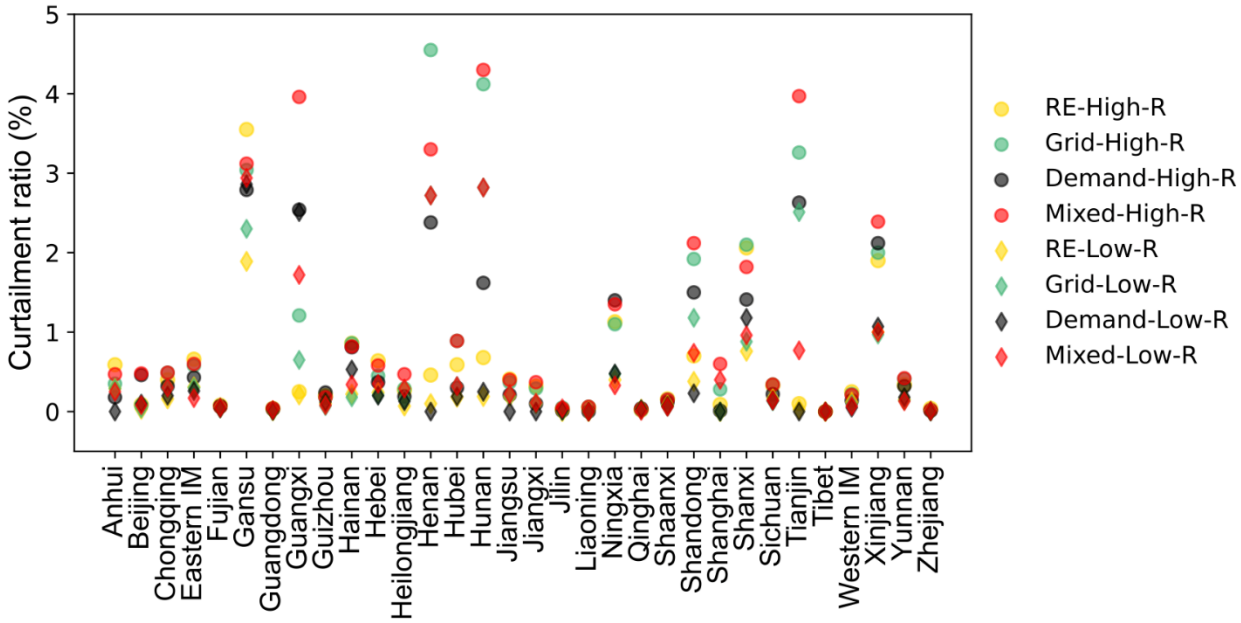

Figure S3.5. Comparison of average curtailment ratio of renewables (both solar PV and wind) in each province under eight scenarios

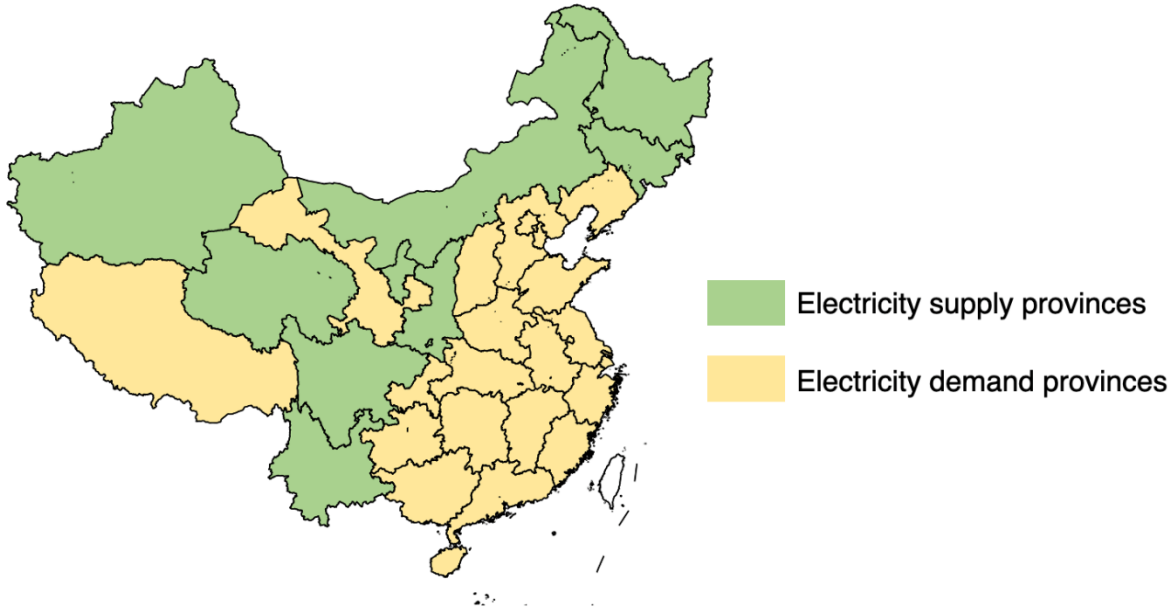

Figure S3.6. Distribution of electricity supply and demand provinces.

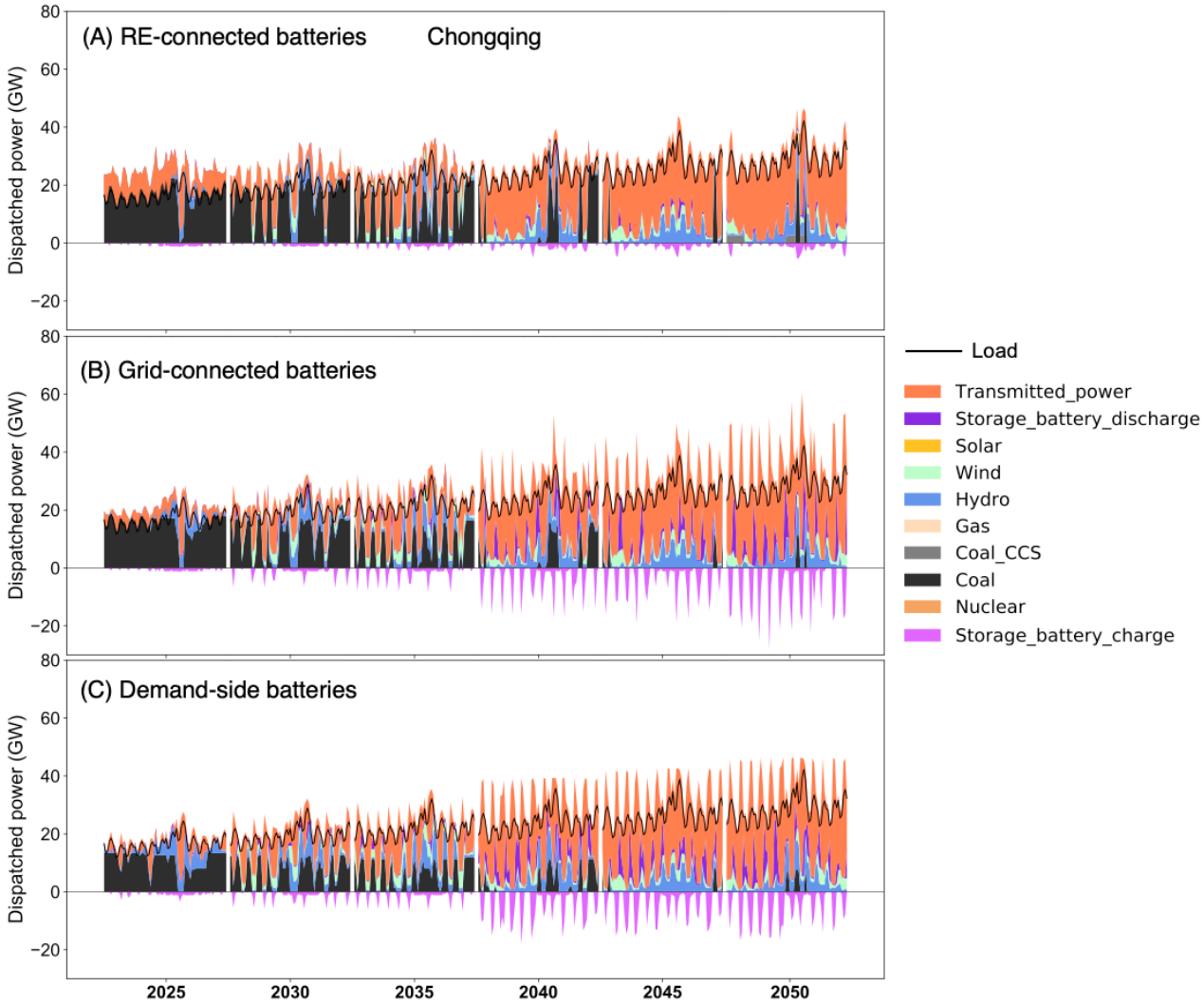

Figure S3.7. Dispatched power under three battery deployment strategies in Chongqing province

Dispatched power from various power generators, transmission, and battery discharges in (A) RE-connected battery, (B) Grid-connected battery and (C) Demand-side strategy with low carbon and rapid decreases in battery costs.

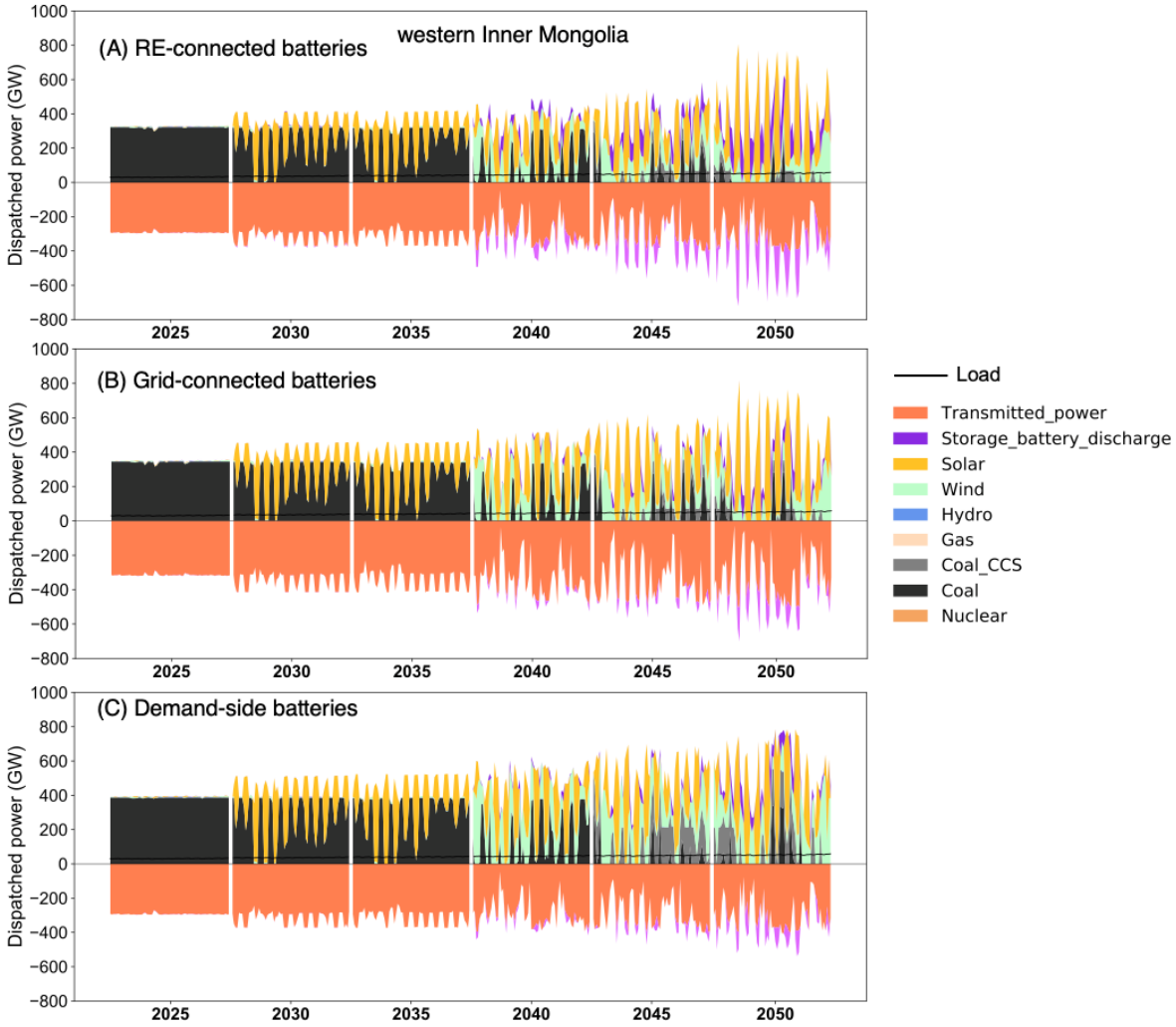

Figure S3.8. Dispatched power under three battery deployment strategies in western Inner Mongolia

(A) RE-connected battery, (B) Grid-connected battery and (C) Demand-side strategy with low carbon and rapid decreases in battery costs

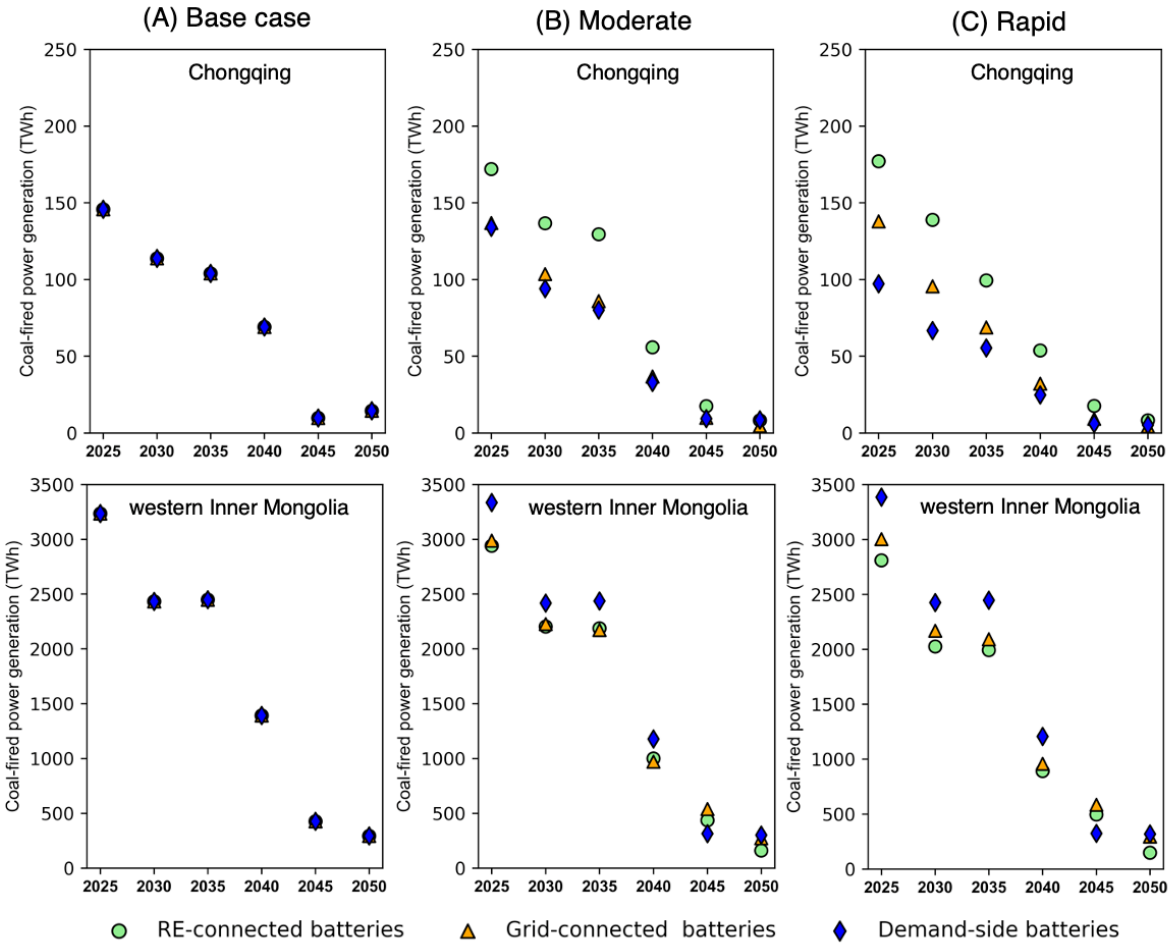

Figure S3.9. Comparison of provincial coal-fired power generation among three battery storage deployment strategies under low carbon prices with (A) Base case, (B) moderate and (C) rapid battery cost decreases

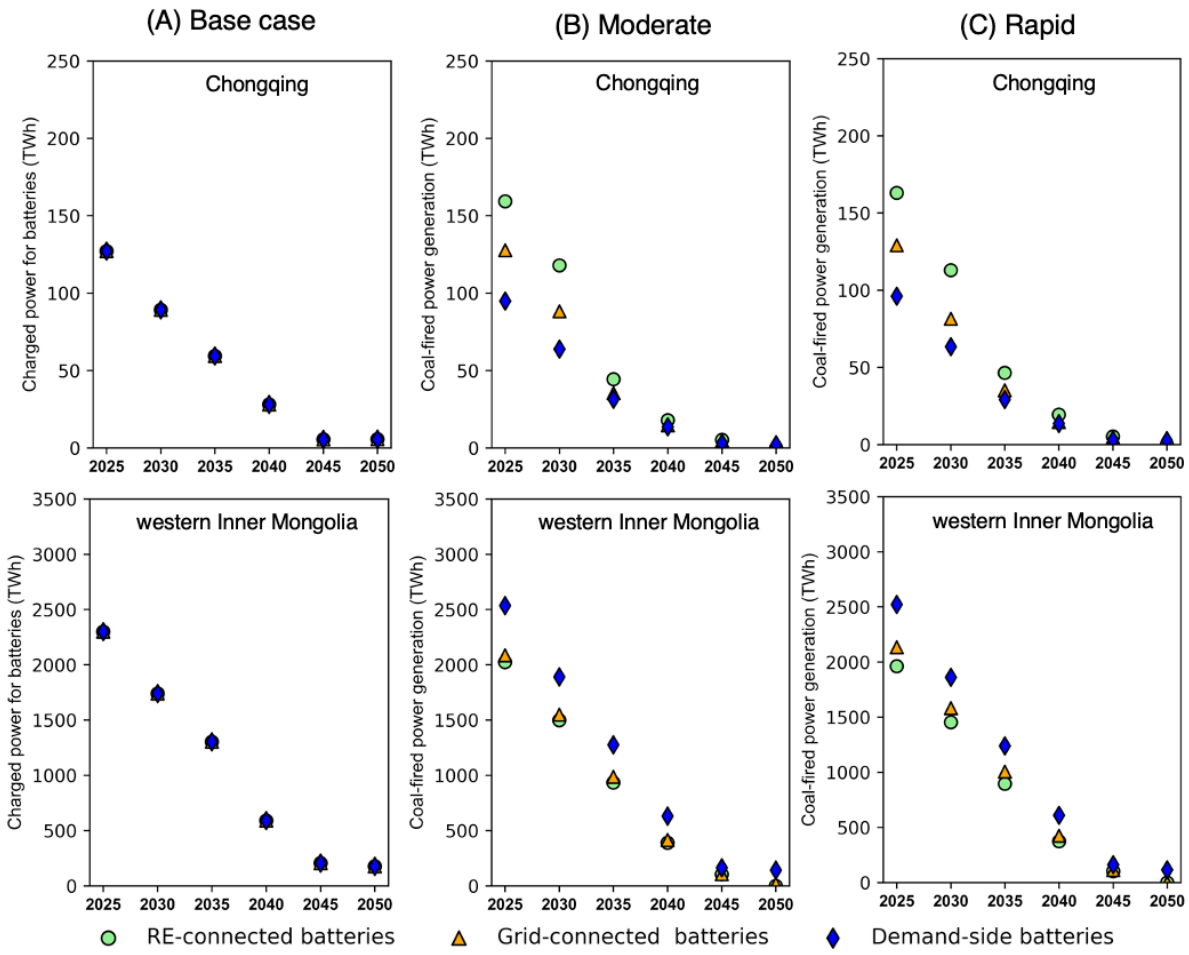

Figure S3.10. Comparison of provincial coal-fired power generation among three battery storage deployment strategies under high carbon prices with (A) Base case, (B) moderate and (C) rapid battery cost decreases

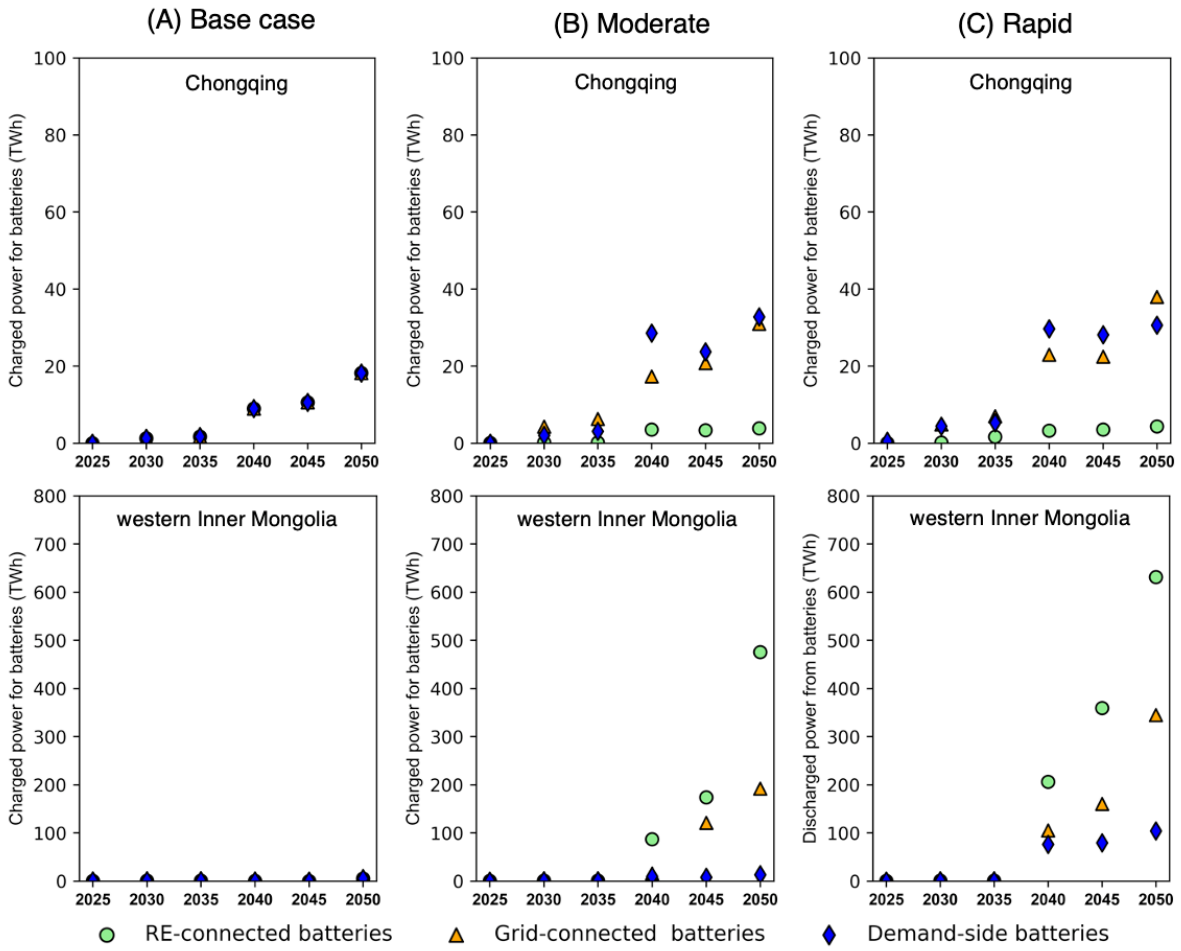

Figure S3.11. Comparison of provincial power discharged from batteries among three battery storage deployment strategies under low carbon prices with (A) Base case, (B) moderate and (C) rapid battery cost decrease

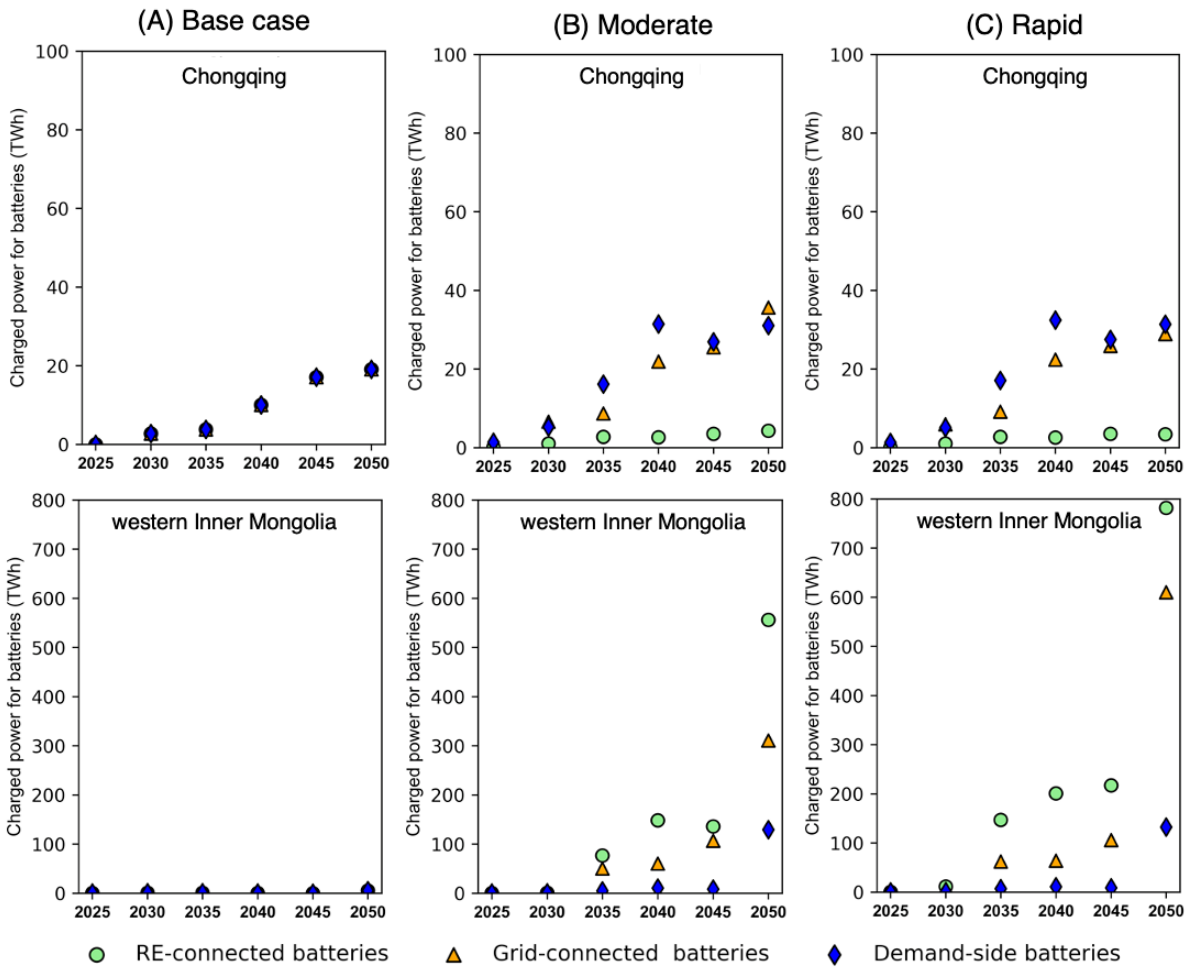

Figure S3.12. Comparison of provincial charged power for batteries among three battery storage deployment strategies under high carbon prices with three battery cost decrease (A) Base case, (B) moderate and (C) rapid battery cost decrease

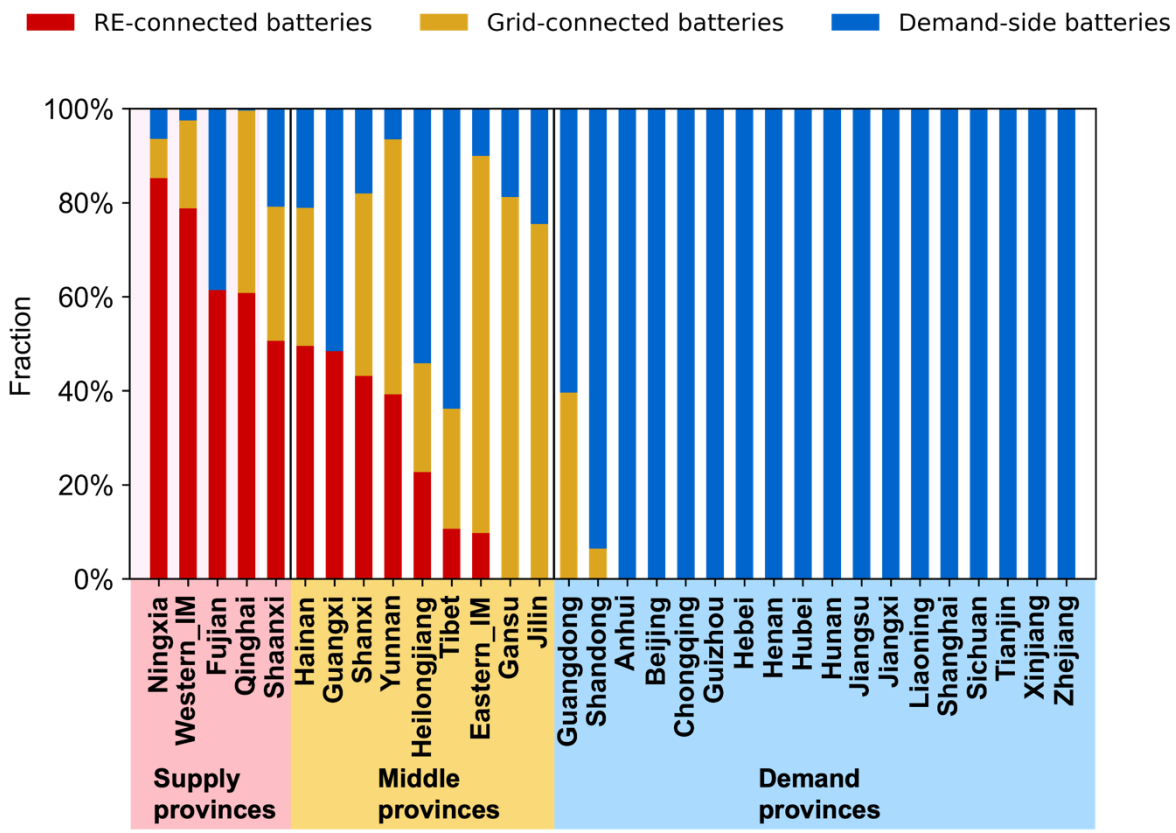

Figure S3.13. Share of each battery storage deployment strategy in the Mixed-High -R scenario

Supplementary Tables

Table S3.1 Carbon emissions of each scenario (Unit: Tg)

Scenario	2025	2030	2035	2040	2045	2050
RE-Low-B	5644	4235	3750	1536	605	302
RE-Low-M	5084	3747	3336	1471	567	281
RE-Low-R	**5153**	**3637**	**3023**	**1365**	**641**	**286**
RE-High-B	4523	3097	1578	698	268	104
RE-High-M	4425	2964	1443	682	237	81
RE-High-R	**4419**	**2803**	**1411**	**652**	**241**	**80**
Grid-Low-B	5536	4112	3644	1700	698	321
Grid-Low-M	5064	3671	3176	1398	664	358
Grid-Low-R	**5191**	**3626**	**2971**	**1377**	**696**	**374**
Grid-High-B	4502	3011	1634	734	287	128
Grid-High-M	4408	2900	1452	717	249	98
Grid-High-R	**4460**	**2766**	**1445**	**695**	**257**	**86**
Demand-Low-B	5896	4334	3843	1878	835	498
Demand-Low-M	5293	3747	3392	1618	796	561
Demand-Low-R	**5368**	**3751**	**3370**	**1668**	**582**	**559**
Demand-High-B	4798	3109	1703	812	345	198
Demand-High-M	4617	3038	1716	937	350	257
Demand-High-R	**4602**	**3002**	**1653**	**917**	**335**	**226**

Table S3.2 System costs of each scenario (Unit: Billion dollars)

Scenario	2025	2030	2035	2040	2045	2050
RE-Low-B	940	721	556	414	306	221
RE-Low-M	940	720	554	406	298	216
RE-Low-R	**939**	**717**	**550**	**403**	**297**	**212**
RE-High-B	1032	786	603	444	318	233
RE-High-M	1032	783	591	431	308	220
RE-High-R	**1031**	**779**	**586**	**427**	**306**	**216**
Grid-Low-B	939	721	556	414	306	221
Grid-Low-M	940	719	553	402	296	213
Grid-Low-R	**936**	**716**	**548**	**398**	**294**	**209**
Grid-High-B	1033	786	603	444	318	234
Grid-High-M	1033	782	591	427	305	218
Grid-High-R	**1029**	**776**	**584**	**423**	**302**	**213**
Demand-Low-B	939	721	556	414	306	221
Demand-Low-M	930	712	547	401	302	216
Demand-Low-R	**927**	**709**	**545**	**399**	**301**	**215**
Demand-High-B	1032	786	603	444	318	234
Demand-High-M	1026	776	591	431	312	227
Demand-High-R	**1022**	**773**	**587**	**429**	**310**	**225**

Table S3.3. Summary of national results by each battery storage deployment strategy with high carbon prices and rapid battery costs decrease from 2025-2050

		RE-connected batteries	Grid-connected batteries	Demand-side batteries	Mixed batteries
Total cost (Billion dollars)		3344.4	3328.4	3347.7	3308.1
	Emission costs	367.5	371.4	411.7	378.8
	Gen fixed costs	1787.5	1765.4	1687.3	1733.5
	Gen variable costs	76.3	76.4	84.7	77
	Fuel costs	533.4	522.7	559.9	529
	Transmission costs	578.3	591.0	602.2	588.3
	Others	1.4	1.5	1.9	1.5
Cumulative emission (Mt)		9607.4	9710.2	10735.1	9903.1
Cumulative renewable capacities (GW)		24248.9	24007.3	21148.9	23912.4
Cumulative battery capacities (GW)		7128.8	7838.8	3857.2	7034.4

Table S3.4. Summary of national results by each battery storage deployment strategy with low carbon prices and rapid battery costs decrease from 2025-2050

		RE-connected batteries	Grid-connected batteries	Demand-side batteries	Mixed batteries
Total cost (Billion dollars)		3118.9	3102.1	3197.6	3075.3
	Emission costs	269.6	272.4	292.9	280.1
	Gen fixed costs	1563.1	1540.4	1458.9	1494.3
	Gen variable costs	86.9	87.2	93.8	88.5
	Fuel costs	623.3	616.5	656.1	625.7
	Transmission costs	574.7	584.9	593.9	585.6
	Others	1.3	1.3	1.2	1.1
Cumulative emissions (Mt)		14104.7	14235.3	15301.4	14544.1
Cumulative renewable capacities (GW)		20921.7	20607.6	17513.3	20357.5
Cumulative battery capacities (GW)		5639.1	6253.7	4808.2	5493

Table S3.5. Carbon price in the model

Scenarios (RMB/t CO_2)	2025	2030	2035	2040	2045	2050
Low carbon price	75[a]	120[a]	165[a]	280	430	610
High carbon price	150	240	330	550	860	1220

a CO_2 price is obtained from the projection by the State Grid Energy Research Institution (China Energy & Electricity Outlook 2019).
*CO_2 price in slow decarbonization scenario after 2035 is based on our own assumptions.
*CO_2 price in rapid decarbonization scenario is set twice the value of that in slow decarbonization scenario

Supplementary Reference:

China Southern Power Grid. 2018 Corporate Social Responsibility Report. http://eng.csg.cn/Social_Responsibility/Social_Responsibility_Report/201905/P020190523361009432864.pdf (2019).

State Grid. 2017 Corporate Social Responsibility Report. http://www.sgcc.com.cn/html/files/2018-08/29/20180829165036376453337.pdf (2018).

Geng, Q., Lu, Y., Fan, H. & Zhang, P. Comparative analysis of the system operation losses between UHV AC and EHV AC transmission systems. Power System Protection and Control 72–77 (2016).

EPPEI & CREEI. Grid Project Construction Cost Analysis in the 12th Five-year Period (in Chinese). (2017).

NREL. National Renewable Energy Laboratory. Annual Technology Baseline (ATB), 2021. https://atb.nrel.gov/electricity/2021/data

Appendix for Chapter 4

Supplementary Information

Supplementary Note 1. Renewable power generation

The average capital costs of solar PV, onshore wind, and offshore wind power farms in China in 2021 was around $658/kW, $1157/kW, and $2857/kW (IRENA, 2021). In this study, we set up three scenarios of capital cost reduction rates (slow, medium, and rapid cost decrease scenarios) for solar PV, onshore and offshore wind from 2025-2050 based on three technology innovation scenarios (conservative, moderate ad advanced) discussed by the National Renewable Energy Laboratory (NREL) in its 2021 Annual Technology Baseline (ATB) (Akar, S. et al. 2022). The annual O&M costs of solar PV, onshore wind, and offshore wind were assumed to be 2% of their capital costs (IRENA, 2021), and the lifetimes of all renewable projects were assumed to be 20 years (Wiser, R. et al., 2016). The capital costs of solar PV, onshore wind, and offshore wind in slow, medium, and rapid cost decrease scenarios are presented in Figure S1, S2 and S3.

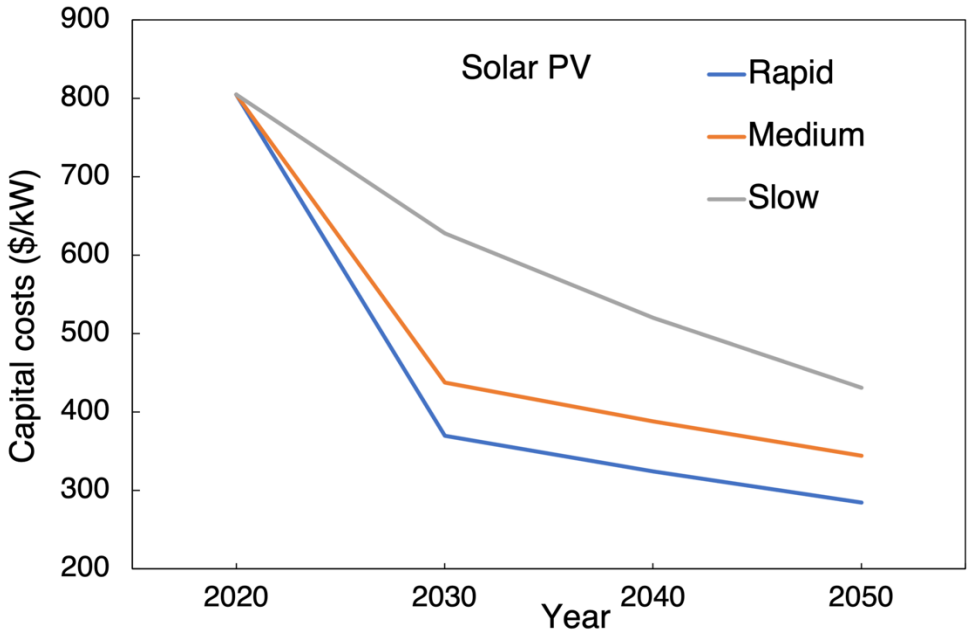

Figure S4.1. Capital costs of solar PV in slow, medium, and rapid cost decrease scenarios from 2020-2050.

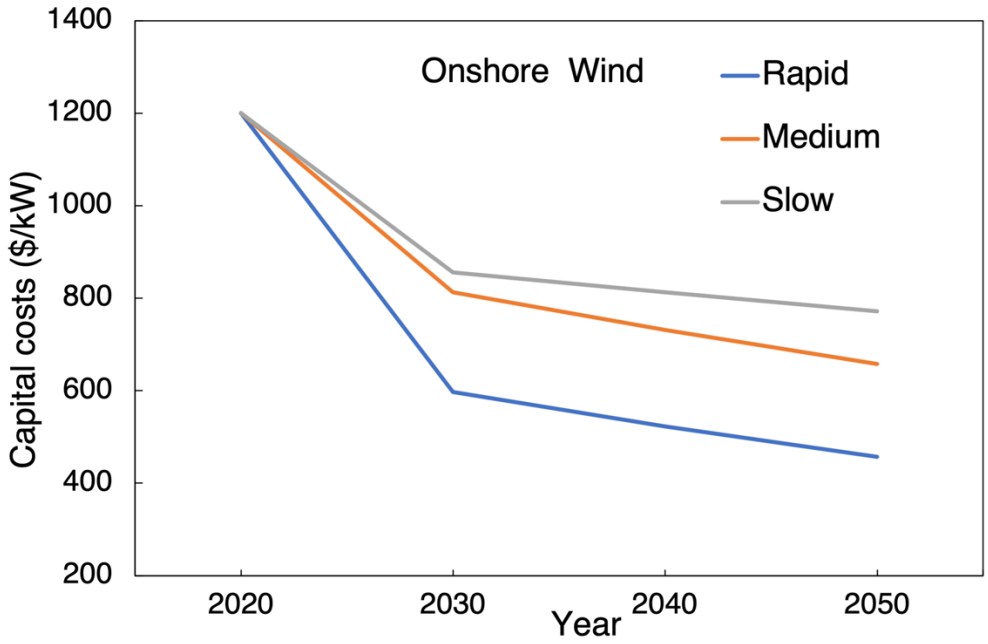

Figure S4.2. Capital costs of onshore wind in slow, medium, and rapid cost decrease scenarios from 2020-2050.

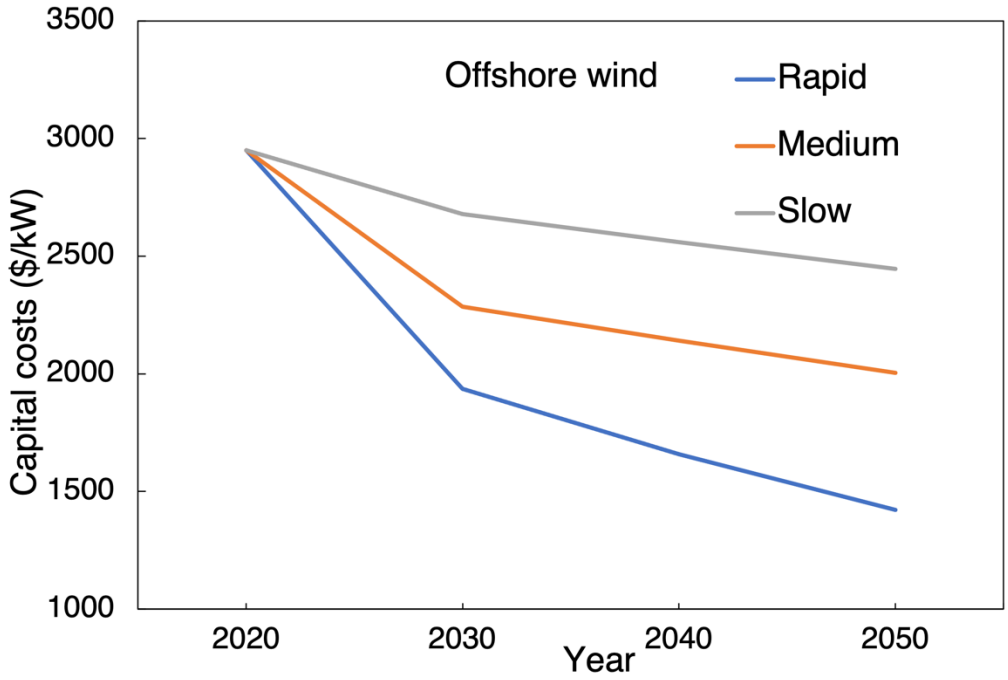

Figure S4.3. Capital costs of offshore wind in slow, medium, and rapid cost decrease scenarios from 2020-2050.

Supplementary Note 2. Water electrolysis

The techno-economic characteristics of the three specific technology options, alkaline (AEC), proton exchange membrane (PEMEC), and solid oxide electrolysis cell (SOEC), are summarized in Table S1. Capital costs include expenses for electrolyzer, foundation, turn-key installation, and all necessary auxiliary systems such as feed water treatment and devices for cooling and purification. Annual O&M expenses include maintenance, stack replacement, and labor costs are expressed as a percentage of initial capital investments (Buttler, et al., 2018). The AEC system is currently the most mature and durable among these three options. Given this advantage, the cost for selection of AEC is particularly favorable for China. PEMEC has ability to operate at high current densities (Carmo et al., 2013). This can result in reduced operational costs, especially for systems coupled with very dynamic energy sources such as wind and solar. The SOEC system is the least developed and has not yet been extensively commercialized. In this study, we only include centralized electrolysis using AEC and PEMEC electrolyzers. The data on the capital cost and electrical efficiency were obtained from projections by the International Energy Agency (IEA) (2019) and Bloomberg New Energy Finance (2020).

Table S4.1. Main characteristics of AEC, PEMEC and SOEC systems. (Yang et al., 2022; Bloomberg New Energy Finance, 2020; IEA, 2019; Schmidt et al., 2017)

Technology description	Capital cost [$/kW]				Fixed O&M cost [$/kW]				Efficiency (LHV) [%]				Lifetime	System Response	Technology Maturity
	2020	2030	2040	2050	2020	2030	2040	2050	2020	2030	2040	2050	Years		
AEC electrolysis, centralized	719	659	629	599	36	33	32	30	64%	66%	67%	69%	25	Seconds	Mature
PEMEC electrolysis, centralized	1318	719	599	479	66	34	29	24	58%	62%	64%	67%	15	Milliseconds	Commercial
SOEC electrolysis, centralized	4552	2636	719	479	228	79	22	14	68%	76%	79%	79%	20	seconds	Lab-scale

Supplementary Figures

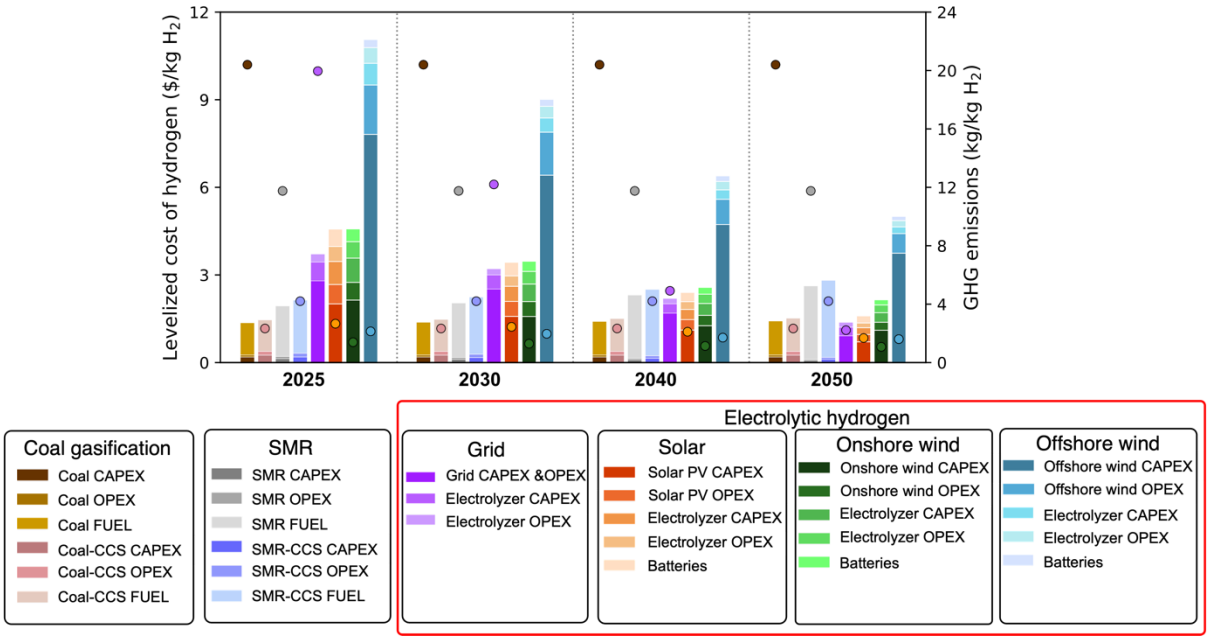

Figure S4.4. National average $LCOH_2$ and GHG emissions by hydrogen production technologies with slow cost decrease of renewable energy in 2025, 2030, 2040 and 2050.

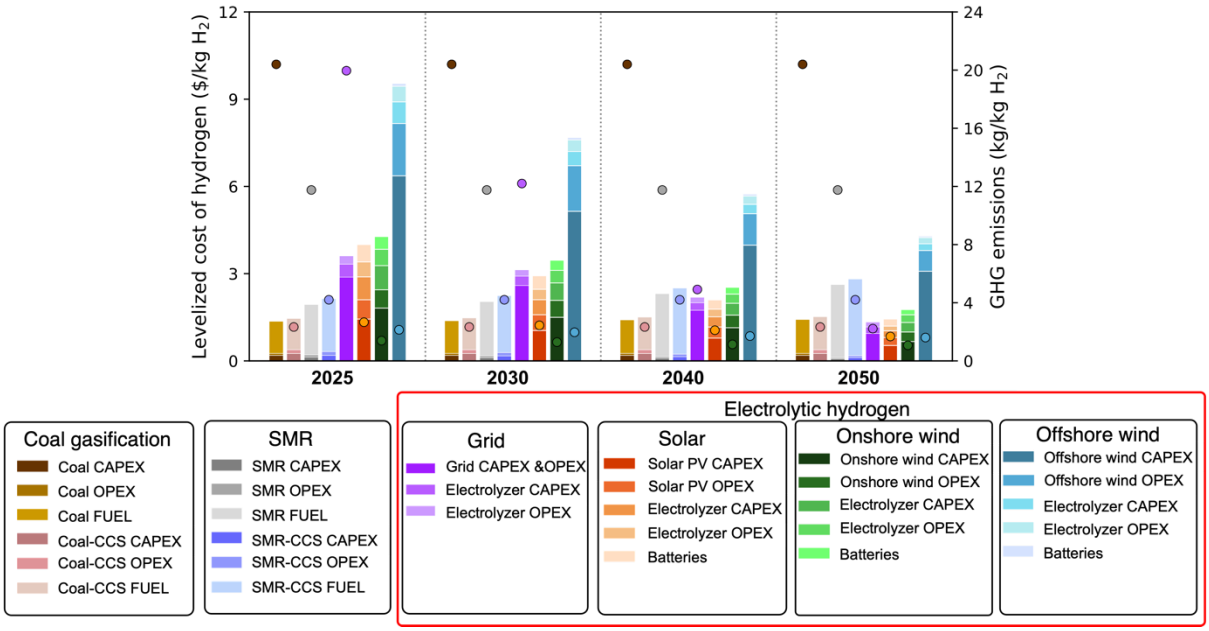

Figure S4.5. National average $LCOH_2$ and GHG emissions by hydrogen production technologies with medium cost decrease of renewable energy in 2025, 2030, 2040 and 2050.

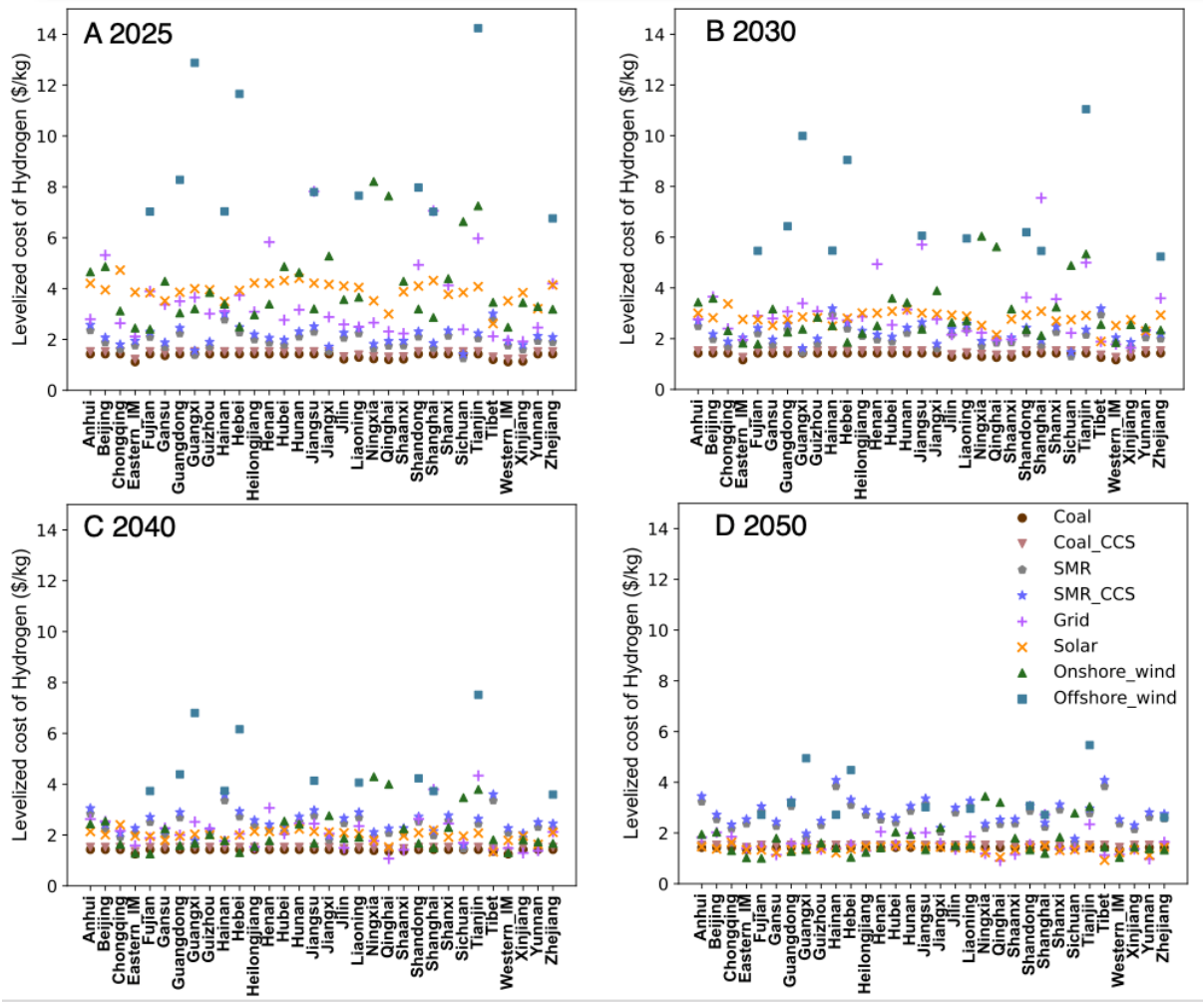

Figure S4.6. $LCOH_2$ for each hydrogen production technology by province in (A) 2025, (B) 2030, (C) 2040 and (D) 2050.

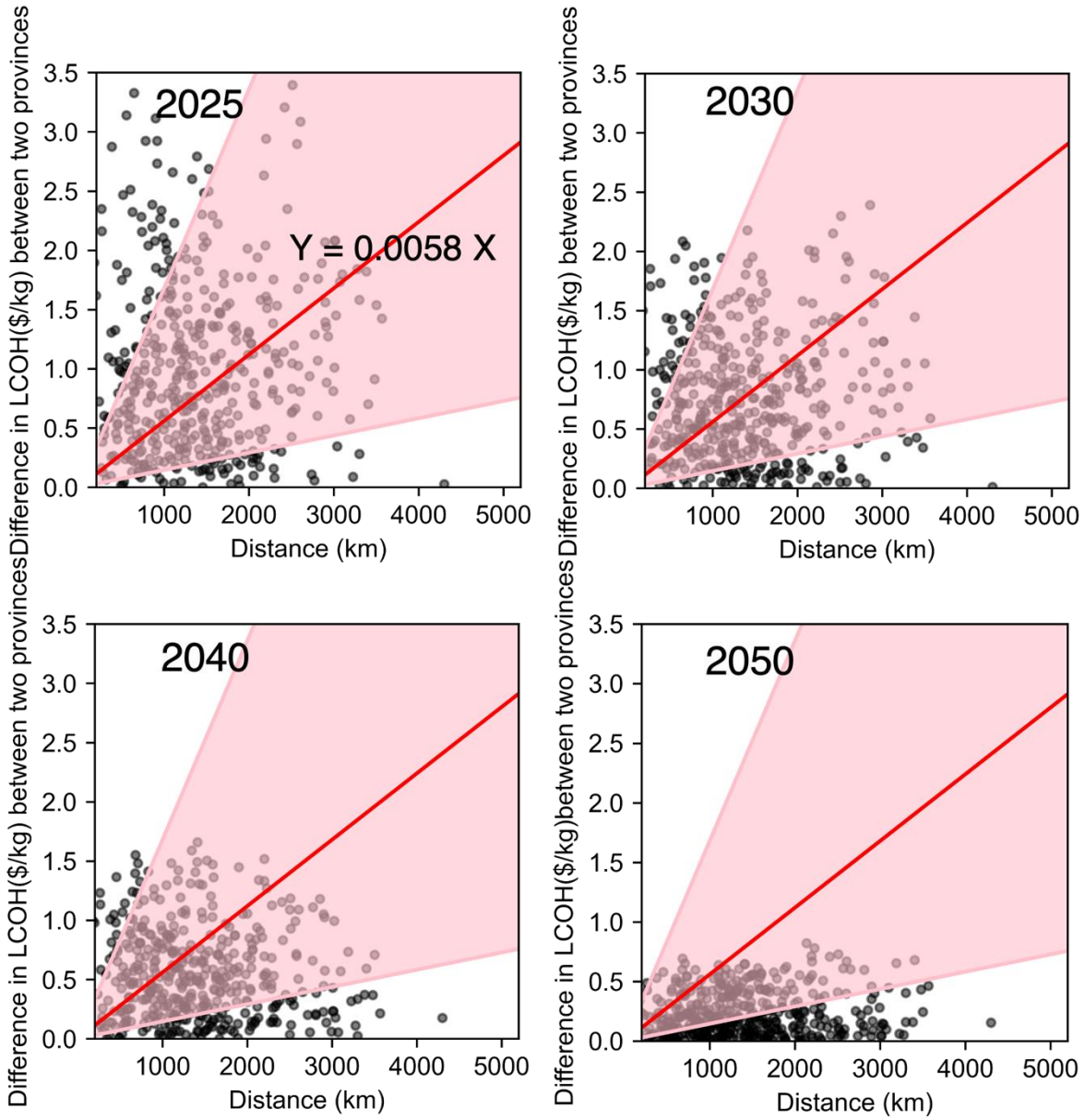

Figure S4.7. Comparison of $LCOH_2$ in difference of two provinces and the cost of hydrogen pipelines under the Minimum-subsidy scenario from 2025-2050.

Dots represent the cost of a pipeline between the capital cities of two provinces. Dots above (below) the red line indicate pipelines that lead to lower (higher) $LCOH_2$ in the recipient province than locally produced electrolytic H_2. Pink shading represents the uncertainty of pipeline costs.

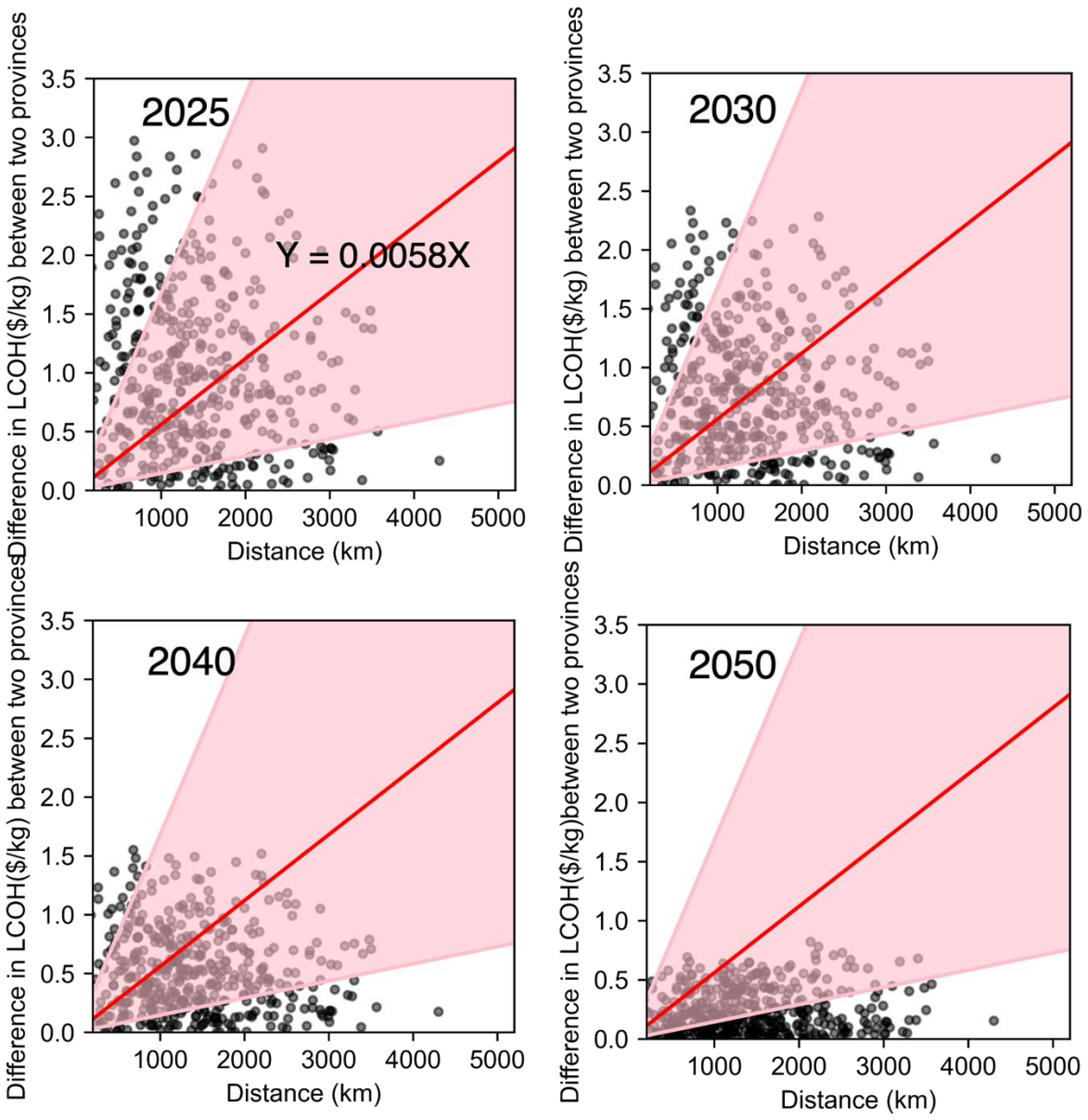

Figure S4.8. Comparison of $LCOH_2$ in difference of two provinces and the cost of hydrogen pipelines under the Minimum-C-emission scenario from 2025-2050.

Dots represent the cost of a pipeline between the capital cities of two provinces. Dots above (below) the red line indicate pipelines that lead to lower (higher) $LCOH_2$ in the recipient province than locally produced electrolytic H_2. Pink shading represents the uncertainty of pipeline costs.

Supplementary Tables

Table S4.2. CO_2 emission cap from 2025-2050 in the SWITCH-China model (unit: Gt) (Zhuo et al., 2022)

Scenarios		2025	2030	2035	2040	2045	2050
High carbon emissions	NDC	4.59	4.27	3.72	2.94	2.27	1.64
Medium carbon emissions	GM2.0	4.39	3.82	2.91	2.01	1.20	0.48
Low carbon emissions	CN2050	4.36	3.48	2.19	0.76	0.17	0.00

Table S4.3. Cumulative hydrogen leakage emissions under 1%, 5% and 10% leakage rate

Year	Hydrogen consumption (Mt)	1%	5%	10%
2020	28[a]	0.28	1.4	2.8
2030	32[a, b]	0.32	1.6	3.2
2040	48[a, b]	0.48	2.4	4.8
2050	66[a, b]	0.66	3.3	6.6
Cumulative emissions (CO_2eq Mt) (GWP100)		145	723	1447
Cumulative emissions (CO_2eq Mt) (GWP20)		435	2169	4341
Percentage of CO_2 emissions in 2020 (%)		1-4	7-20	13-39

a. An energy sector roadmap to carbon neutrality in China, IEA, 2021

b. China Hydrogen Energy Industry Development Report 2020

Table S4.4 Life cycle GHG emissions by each stage

Technology	Fuel Upstream (kg/kgcoal) or (kg/m^3 NG)	Device upstream (kg/MWh)	Operational process	Water electrolysis upstream	Battery upstream (kg/kg H_2)	Fugitive CH_4 (leakage rate %)	Fugitive H_2 (leakage rate %)
Coal	0.18[a]		20.2[b]				
Coal w/ CCS	0.18[a]		2.1[b]				
SMR	0.28[a]		8.9[b]			3.5%[g]	
SMR w/ CCS	0.28[a]		1[b]			3.5%[g]	
Grid	Mix of fuels	Mix of technologies	Mix of technologies	0.1[f]			
Solar		36.2[c]	0	0.1[f]	0.18[f]		
Onshore wind		30.5[c], 19.88[d], 3.62[i], 26.5[j]	0	0.1[f]	0.18[f]		
Offshore wind		7.65[e], 1.49[i]	0	0.1[f]	0.18[f]		
H2 transport							1-10%[h]

a IKE Environmental Technology Co., Ltd, Sichuan University.

b IEA, The future of Hydrogen. 2019.

c Zhu XN., Wang SR and Wang L. 2022.

d Xu K., Chang JF., et al. 2022.

e Yang JH., Chang Y., et al. 2018.

e Onshore wind has 32% of life cycle GHG emissions from offshore wind.

f Palmer, G., Roberts, A., Hoadley, A., Dargaville, R., and Honnery, D. (2021).

g Ocko, I.B., and Hamburg, S.P. (2022).

h Ocko, I.B., and Hamburg, S.P. (2022).

i Xiang N,Wang L M, Qu Q S, et al. 2021.

j Yang J H, Zhang L X, Wang C B, et al. 2017.

Table S4.5. National average $LCOH_2$ with low (2%), medium (4%), and high (8%) discount rate

Hydrogen production type	Year	Low (2%)	Medium (4%)	High (8%)
Solar	2025	3.51	3.9	4.78
Solar	2030	2.52	2.79	3.39
Solar	2040	1.79	1.98	2.42
Solar	2050	1.23	1.36	1.64
Onshore wind	2025	3.58	4.05	5.04
Onshore wind	2030	2.66	2.99	3.68
Onshore wind	2040	1.88	2.12	2.61
Onshore wind	2050	1.5	1.7	2.09
Offshore wind	2025	8.05	9.2	11.22
Offshore wind	2030	6.31	6.9	8.46
Offshore wind	2040	4.36	4.2	5.11
Offshore wind	2050	3.3	3.45	4.26
Grid	2025	3.32	3.51	3.66
Grid	2030	2.78	3.04	3.19
Grid	2040	1.87	2.12	2.26
Grid	2050	1.15	1.3	1.47
Coal	2025	1.41	1.46	1.56
Coal	2030	1.43	1.48	1.58
Coal	2040	1.46	1.51	1.61
Coal	2050	1.47	1.52	1.62
SMR	2025	1.89	1.94	2.12
SMR	2030	1.98	2.04	2.13
SMR	2040	2.2	2.31	2.47
SMR	2050	2.5	2.62	2.77
Coal-CCS	2025	1.35	1.36	1.48
Coal-CCS	2030	1.37	1.38	1.5
Coal-CCS	2040	1.4	1.41	1.53
Coal-CCS	2050	1.41	1.42	1.54
SMR-CCS	2025	2.1	2.14	2.22
SMR-CCS	2030	2.21	2.24	2.34
SMR-CCS	2040	2.38	2.5	2.61
SMR-CCS	2050	2.71	2.81	2.96

Supplementary Reference:

Akar, S. et al. 2021 Annual technology baseline (ATB) cost and performance data for electricity generation technologies. (National Renewable Energy Lab (NREL), 2021).

Buttler, A. & Spliethoff, H. Current status of water electrolysis for energy storage, grid balancing and sector coupling via power-to-gas and power-toliquids: a review. Renew. Sustain. Energy Rev. 82, 2440–2454 (2018).

Carmo, M; Fritz D; Mergel J; Stolten D (2013). "A comprehensive review on PEM water electrolysis". International Journal of Hydrogen Energy. 38 (12): 4901–4934. doi:10.1016/j.ijhydene.2013.01.151.

China EV100. China Hydrogen Energy Industry Development Report. 2020.

IRENA, 2021. Renewable Power Generation Costs in 2021.

Wiser, R. et al. Expert elicitation survey on future wind energy costs. Nat. Energy 1, 16135 (2016).

International Energy Agency (IEA). The future of hydrogen. www.iea.org/ reports/the-future-of-hydrogen (2019).

Ocko, I. B. & Hamburg, S. P. Climate consequences of hydrogen emissions. Atmospheric Chemistry and Physics 22, 9349–9368 (2022).

Yang, X., Nielsen, C. P., Song, S. & McElroy, M. B. Breaking the hard-to-abate bottleneck in China's path to carbon neutrality with clean hydrogen. Nat Energy 7, 955–965 (2022).

Zhuo, Z. et al. Cost increase in the electricity supply to achieve carbon neutrality in China. Nat Commun 13, 3172 (2022).

Palmer, G., Roberts, A., Hoadley, A., Dargaville, R. & Honnery, D. Life-cycle greenhouse gas emissions and net energy assessment of large-scale hydrogen production via electrolysis and solar PV. Energy Environ. Sci. 14, 5113–5131 (2021).

Xiang N, Wang L.M., Qu Q.S., et al. 2021. Comparison of emissions from offshore and onshore wind power systems based on life cycle assessment. http://www.resci.cn/EN/10.18402/resci.2021.04.09.